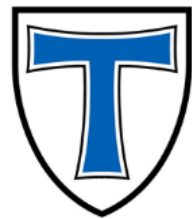


Aus dem Institut für Insektenbiotechnologie
Professur für Naturstoffforschung mit Schwerpunkt Insektenbiotechnologie
der

JUSTUS-LIEBIG-



**UNIVERSITÄT
GIESSEN**

**High-throughput approaches for bioprospection to
leverage natural product discovery
and for single-cell persister phenotyping**

Inaugural - Dissertation

zur Erlangung des Doktorgrades (Dr. rer. nat.)
im Fachbereich Agrarwissenschaften, Ökotoxikologie und
Umweltmanagement der Justus-Liebig-Universität Gießen

vorgelegt von

Markus Oberpaul
aus München

Gießen, April 2022

Mit Genehmigung des Fachbereichs 09
Agrarwissenschaften, Ökotrophologie und Umweltmanagement
der Justus-Liebig-Universität Gießen

Prüfungskommission:

Disputationsvorsitz: Prof. Dr. Marc Schetelig

1. Gutachter: Prof. Dr. Till F. Schäberle

2. Gutachter: Prof. Dr. Andreas Vilcinskas

3. Prüfer: Prof. Dr. Kai M. Thormann

4. Prüfer: PD Dr. Bork A. Berghoff

Teile der nachfolgenden Arbeiten wurden bis April 2021 im Rahmen des LOEWE-geförderten Public-Private-Partnerships (PPP) „Sanofi-Fraunhofer Natural Product Center of Excellence“ (SFNPCE, 2016-2018), danach „Fraunhofer-Evotec Natural Product Excellence Center for Infectious Diseases“ (FENPEC-ID, 2018-2019) unter der wissenschaftlichen Leitung von PD Dr. Jens Glaeser und unter der administrativen Leitung von Prof. Dr. Till Schäberle angefertigt. Für die Initiierung und Gesamtleitung des Projekts am Standort Gießen waren Prof. Dr. Peter Hammann und Prof. Dr. Andreas Vilcinskas verantwortlich. Bis 2018 unterstützte Dr. Luigi Toti die wissenschaftliche Leitung der Abteilung „Mikrobiologie/Screening“, die der „Chemie/Analytik“ Dr. Armin Bauer. Von 10/2018 bis 12/2019 war Dr. Sören Schuler für die Abteilung „Chemie/Analytik“ verantwortlich. Nach Projekt- und Finanzierungsende - ab 2020 - wurden Nachfolgearbeiten und die Promotion in der Arbeitsgruppe „Fraunhofer Naturstoffforschung“ fortgeführt und von Prof. Dr. Till Schäberle betreut.

Eigenständigkeitserklärung

**Erklärung gemäß der Promotionsordnung des Fachbereichs 09 vom 07. Juli 2004 § 17 (2),
geändert am 29.05.2019**

Ich erkläre: Ich habe die vorgelegte Dissertation selbständig und ohne unerlaubte fremde Hilfe und nur mit den Hilfen angefertigt, die ich in der Dissertation angegeben habe. Alle Textstellen, die wörtlich oder sinngemäß aus veröffentlichten Schriften entnommen sind, und alle Angaben, die auf mündlichen Auskünften beruhen, sind als solche kenntlich gemacht. Bei den von mir durchgeführten und in der Dissertation erwähnten Untersuchungen habe ich die Grundsätze guter wissenschaftlicher Praxis, wie sie in der „Satzung der Justus-Liebig-Universität Gießen zur Sicherung guter wissenschaftlicher Praxis“ niedergelegt sind, eingehalten.

Gießen, 13.04.2022

Ort, Datum

Markus Oberpaul

Für meine Liebsten

-

Julia

&

Theodora

TABLE OF CONTENTS

Summary	i
Zusammenfassung	iii
1. Introduction	1
1.1. The antibiotic crisis	1
1.2. The golden era of antibiotics	3
1.3. Techniques for Natural product discovery – past, present and future.....	3
1.3.1. Novel cultivation strategies	5
1.3.2. Underexplored bioresources and bacterial phyla	10
1.3.3. Computational approaches.....	12
1.4. Antibiotic targets and bacterial evasion strategies.....	15
1.4.1. Resistance transmission, tolerance and persistence	17
1.4.2. Toxin-antitoxin-dependent persister in <i>E. coli</i>	19
Chapter 1: Implementation of high-throughput techniques to bioprospect for Natural products in underexplored bioresources	22
3. Aims of Chapter 1	23
Manuscript 1: High-Throughput Cultivation for the Selective Isolation of Acidobacteria From Termite Nests	25
Manuscript 2: Combination of high-throughput microfluidics and FACS technologies to leverage the numbers game in NP discovery	42
Manuscript 3: Novel Glycerophospholipid, Lipo- and N-acyl Amino Acids from Bacteroidetes: Isolation, Structure Elucidation and Bioactivity.....	79
Manuscript 4: <i>Trichoderma</i> -derived pentapeptides isolated from the mycobiome of <i>Coptotermes testaceus</i>	98
Manuscript 5: Two-step generation of monodisperse agarose-solidified double emulsions (w/w/o) excluding an inner oil barrier	110
4. Summary of Chapter 1	121
Chapter 2: High-throughput <i>E.coli</i> persister phenotyping	124
6. Aims of Chapter 2	125
Manuscript 6: Post-transcriptional deregulation of the <i>tisB/istR-1</i> toxin-antitoxin system promotes SOS-independent persister formation in <i>Escherichia coli</i>	127
Manuscript 7: Elevated Expression of Toxin TisB Protects Persister Cells against Ciprofloxacin but Enhances Susceptibility to Mitomycin C.....	138
7. Summary of Chapter 2	155
8. Discussion	156
2.1.1 Ultrahigh-throughput microfluidics expands the cultivability of microbial dark matter	156
2.1.2 High-throughput persister phenotyping	162
9. Future perspective	164
10. References	166
11. Supporting Information	172
13. Danksagungen	175
14. Liste ausgewählter wissenschaftlicher Beiträge	177
15. Curriculum vitae	179

SUMMARY

Due to multifactorial causes, e.g. the spread of antimicrobial resistances, it is hypothesized that we may face a post-antibiotic era in the upcoming decades. Although pharmaceutical industry stopped or outsourced natural products research and development of antibiotics in the recent past, fresh inspirations have to be discovered steadily. One option to outpace this issue to aim on dismantling the 'microbial dark matter', which offer a vast and largely untapped chemical space that is ready to be investigated. To this end, the implementation of innovative high-throughput cultivation techniques is critical, which also facilitates the comprehensive exploration of diverse untapped bioresources and meet the needs of fastidious hitherto uncultured microorganisms. Thus, the imperative of an adaptive, and cost-effective high-throughput pipeline that is ready to uncover novel natural products from environmental microorganisms, was converted into an entire process 'from bioresources to bioactive compounds' within the framework of Fraunhofer IME-BR and Sanofi (later Evotec) Public-Private-Partnership (PPP).

Social insects display an example for underexplored bioresources. Due to longtime evolutionary effects, a homeostasis of microbial symbionts was established, which supports defense mechanisms of nest inhabitants against invaders. It is known that lower subterranean termites lack of a great arsenal of antimicrobial peptides compared to numerous other insects. Thus, in the first chapter of this work, the focus was on the implementation of selective and adaptive cultivation techniques in order to make this untapped chemical space available. As a case study, the microbiota at different nest levels and in specimens of three subterranean termites (*Coptotermes testaceus*, *C. gestroi* and *C. formosanus*), which have been reared since decades before, were analyzed over a timeframe of 2 years. A stable core microbiome was determined, which was further confirmed by comparison to a nest suffering from a fungal infection. The analysis of the microbiome revealed a high abundance and diversity of Acidobacteria. They are interesting in terms of natural product research, however, few representatives are currently available. Therefore, a high-throughput microplate-based cultivation pipeline was applied to successfully integrate new Acidobacteria species in the Fraunhofer strain collection.

This was brought to the next level by a prior cultivation step using droplet microfluidics in combination with fluorescence-associated cell sorting. Furthermore, the workload was rapidly minimized due to the identification of cultivated redundancy. This was facilitated by applying sophisticated metabolomic studies and UHPLC-HRMS/MS bioactivity-guided screening for chemical novelty, which sets new benchmarks for the utilization of microfluidics cultivation techniques combined with bioactivity-guided screenings.

The pipeline facilitated the cultivation of a broad diversity of microbes from a common forest soil sample, including three new species in each genus *Edaphobacter*, *Acidobacterium* and *Olivibacter*, respectively. The integrated downstream metabolomics and screening pipeline led to the discovery of new bioactive derivatives of macrotetrolides, massetolides and cyclic lipopeptides in other species. Moreover, axenic cultures of *Trichoderma* sp. FHG000531 isolated from the nest of *C. testaceus* facing the fungal infection, and *Olivibacter* sp. FHG000416 isolated from the carton nest of *C. gestroi* were analyzed to characterize their chemical repertoire. This led to the identification of a novel pentapeptide (FE011) and five derivatives thereof, additionally three novel *N*-acyl-amino acids (NAAAs) two lipoamino acids (LAAs) and one lysophosphatidylethanolamine (LPE). Two of the LAAs showed a valuable bioactivity with a minimal inhibitory concentration (MIC) of 8-16 µg/mL and the LPE 16 µg/mL against the Gram-negative pathogenic bacterium *Moraxella catarrhalis* ATCC 25238.

Relapsing nosocomial infections aggravate the spread of antimicrobial resistance. Thus, in the second chapter of this work, drug-induced persister formation of the model organism *E. coli*, which are facing phenotypic consequences, were analyzed in high-throughput fashion. To this end, a stationary-phase model to detail TisB-dependent persistence in *E. coli* was established (*E. coli* Δ 1-41 Δ *ist-R*), and a comprehensive single-cell persister phenotyping was achieved. This contributes to the understanding of drug-induced persister formation, which is urgent to develop approaches to overcome persister formation in e.g. wound infections.

The high-throughput microfluidics-based cultivation pipeline and persister phenotyping supported by flow cytometry methods, which is presented in this work, will significantly contribute to natural product discovery. Thus, ultimately increasing the chances to combat the threat of the antimicrobial resistance crisis.

ZUSAMMENFASSUNG

Aufgrund multifaktorieller Ursachen u.a. der Verbreitung von Antibiotikaresistenzen wird bereits in den nächsten Dekaden eine post-antibiotische Zeit prognostiziert. Trotz dem Ausscheiden von großen Pharmaunternehmen aus der Naturstoffforschung und Entwicklung von Antibiotika, müssen stets neue Inspirationen gefunden werden. Eine Möglichkeit dafür bietet die Erschließung der sog. „mikrobiellen dunklen Materie“, damit einhergehend mannigfache, bisher unbekannte strukturelle chemische Neuheiten, welche für die Naturstoffentwicklung zugänglich gemacht werden müssen. Um dieses hoch gesteckte Ziel zu erreichen, ist bspw. Implementierung innovativer Hochdurchsatz-Kultivierungstechniken von entscheidender Bedeutung. Diese müssen die umfassende Erforschung verschiedener unerschlossener Bioressourcen erleichtern und auf die Bedürfnisse anspruchsvoller, bisher nicht kultivierter Mikroorganismen eingehen können. Deshalb fokussierte diese Arbeit auf die Implementierung eines vollumfassenden Prozesses „von Bioressourcen zu bioaktiven Verbindungen“ im Rahmen des Public-Private-Partnerships (PPP) von Fraunhofer IME-BR und Sanofi (später Evotec).

Eine Bioressource mit viel Potential findet sich bei staatenbildenden Insekten. Durch langjährige Evolution hat sich eine Homöostase von mikrobiellen Helfern im Nest etabliert und gegenüber der Abwehr von Pathogenen bewährt. Von einer niederen Termitenart ist bekannt, dass ihr Arsenal an antimikrobiellen Peptiden im Vergleich zu zahlreichen andren Insekten sehr klein ausfällt. Aus diesen Gründen stechen die Nester von Termiten als besonders spannende Bioressource hervor. Daher wurden in dieser Arbeit exemplarisch die Mikrobiome von drei Termitennestern der Spezies *Coptotermes* und deren Individuen, sowie zusätzlich das Mycobiom eines mit einem Pilz infizierten Nests untersucht. Dadurch wurde die beste Quelle für unkultivierte mikrobielle Vielfalt ermittelt. Durch die kultivierungsunabhängige Analyse der Nestebenen und der Individuen aus einem Zeitraum von zwei Jahren, konnte ein stabiles Kernmikrobiom bestimmt werden, was durch den Vergleich mit dessen Verschiebung des Pilz-infizierten Nest untermauert wurde. In allen Nestern, aber besonders im Kartonnest, wurde im gesamten erfassten Zeitraum eine Fülle von potentiellen Naturstoffproduzenten nachgewiesen. Insbesondere wurde eine hohe Abundanz von Acidobacteria detektiert, die für die Naturstoffforschung von Interesse sind, wohingegen bisher

nur sehr wenige Reinkulturen in Stammsammlungen hinterlegt sind. Daher wurde eine mikrotiterplatten-basierte Hochdurchsatzkultivierungsmethode, für die industrielle Routineanwendung etabliert und zur selektiven Kultivierung von *Acidobacteria* genutzt. Später wurde diese Technik sowohl mit einer vorgeschalteten Tröpfchen-Mikrofluidik als auch mit einer fluoreszenz-assoziierten Zellsortierung kombiniert. Durch diese Hochdurchsatztechnologie wurden rund 500.000 Einzelzellen pro Stunde in agarose-verfestigte mikrometergroße Tröpfchen in unterschiedlichen Bedingungen verkapselt. Durch nicht-invasive Fluoreszenzfarbstoffe wurde mittels Durchflusszytometrie mikrobielles Koloniewachstum im Tröpfchen detektiert und deren Separierung in Mikrotiterplatten ermöglicht. Durch die Hochskalierung in standardisierten Plattenformaten konnte die gesamte gewonnene mikrobielle Diversität in eine eigens aufgebaute semi-automatisierte Plattform zur Entdeckung neuer Naturstoffe eingespeist werden.

Beide Anwendungen ermöglichten die Kultivierung einer breiten Vielfalt von Mikroben, darunter neue Arten der Gattungen *Edaphobacter*, *Acidobacterium* und *Olivibacter*. Des Weiteren führte die Applikation der Technologien zur Entdeckung neuer bioaktiver Derivate. Darüber hinaus wurden Reinkulturen von *Trichoderma* sp. FHG000531 (isoliert aus dem infizierten Nest von *C. testaceus*) und die neue Spezies innerhalb der Gattung *Olivibacter* (FHG000416 aus dem Kartonnest von *C. gestroi*) hinsichtlich ihres chemischen Repertoires genauer untersucht. Dies führte zur Identifizierung eines neuartigen Pentapeptids (FE011) und fünf Derivaten davon, sowie zu drei neuen *N*-Acyl-Aminosäuren (NAAAs), zwei neuartigen Lipoaminosäuren (LAAs) und ein Lysophosphatidylethanolamin (LPE). Bei zwei der LAAs wurde eine nennenswerte Bioaktivität mit einer minimalen inhibitorischen Konzentration (MIC) von 8-16 µg/mL und bei dem neuen LPE eine MIC von 16 µg/mL gegen das Gram-negative pathogene Bakterium *Moraxella catarrhalis* ATCC 25238 beobachtet.

Persistierende nosokomiale Infektionen intensivieren die Ausbreitung von Antibiotikaresistenzen. Daher wurde im zweiten Teil dieser Arbeit ein Modell zur detaillierten Untersuchung der Kaskade zur Bildung von persistierenden *E. coli* Zellen etabliert, welche abhängig vom antibiotikainduzierbaren Toxin TisB sind. Mittels Durchflußzytometrie und fluoreszierenden Erkennungsmarkern von vitalen Zellen wurde eine umfassende Persistierphänotypisierung durchgeführt. Aus den erzielten Ergebnissen konnte eine Phänotypisierung des „stationären-Phasen

Persistenzmodells“ (*E. coli* $\Delta 1-41$ $\Delta ist-R$) abgeleitet werden. Diese Methodik unterstützt im Allgemeinen das Verständnis der antibiotikainduzierten Persistenzbildung und unterstützt folglich Therapieansätze und deren Entwicklung. Alles in allem werden die hier vorgestellten, flexibel einsetzbaren state-of-the-art Hochdurchsatzmikrofluidik-Kultivierungstechnologien und die Methodik zur Persistenzphänotypisierung die Naturstoffforschung in vielerlei Hinsicht nachhaltig beeinflussen. Das wiederum wird auf der Suche nach neuartigen Inspirationen helfen, um die voranschreitende Antibiotikakrise in Schach zu halten.

1. INTRODUCTION

1.1. The antibiotic crisis

Since 2019, the world has been kept in thrall by a pandemic caused by Severe acute respiratory syndrome coronavirus type 2 (SARS-CoV-2). This infectious disease has influenced humanity significantly, e.g. by requiring the imposition of several lockdowns, but has also exacerbated existing problems concerning human health by pushing them into the margins (Laxminarayan, 2021). For decades, one of these arising problems is the so-called **antimicrobial resistance (AMR) crisis** (Ventola, 2015; Laxminarayan, 2021). AMR has even become worse since the SARS-CoV-2 pandemic, e.g. due to clinical uncertainty towards superinfections that led to increased consumption antibiotics and due to the understandable focus on fighting the pandemic (Lucien *et al.*, 2021; Rawson *et al.*, 2021; Pintado *et al.*,

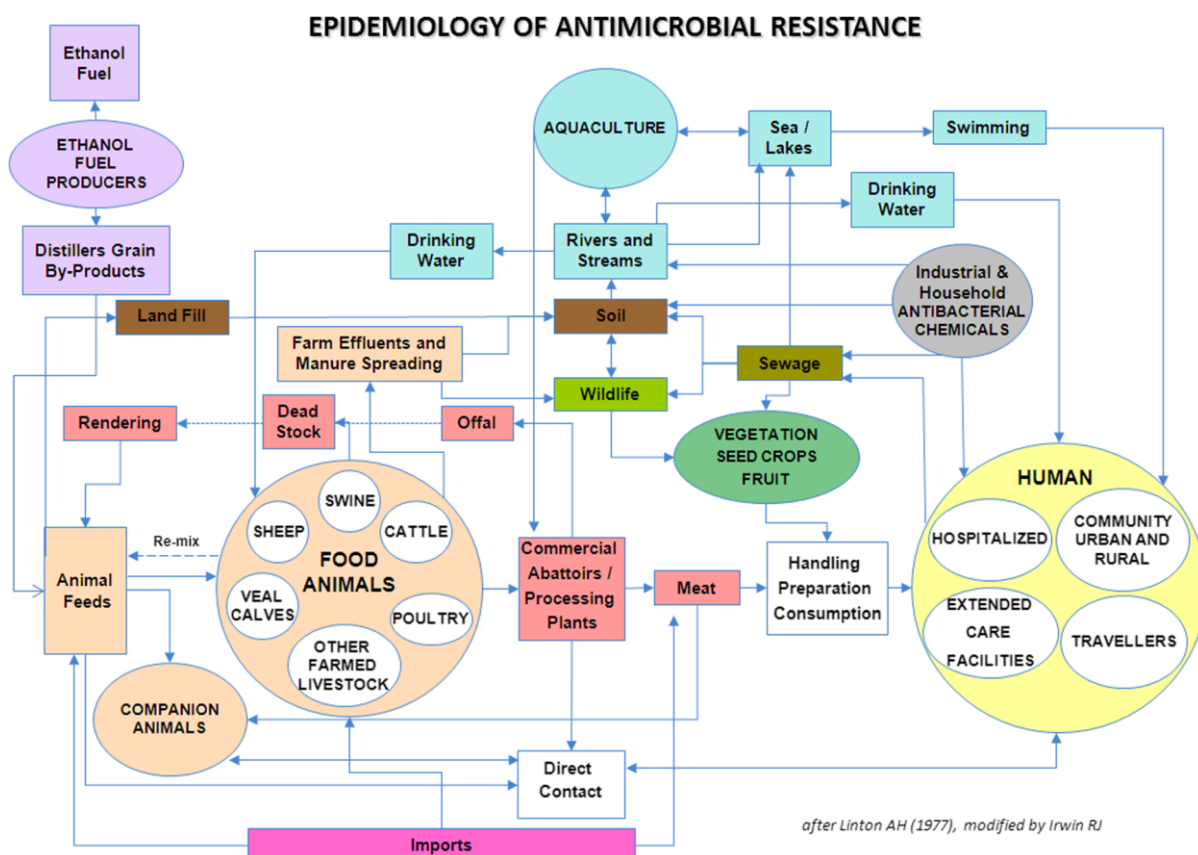


Figure 1: The epidemiology of antimicrobial resistance shows the potential transfer points of resistant bacteria and resistance genes.

Modified from Morel *et al.* *Antimicrob Resist Infect Control.* 2020 Nov 26;9(1):187.

2022). This is leading to the rapid spread of bacterial infections, which are listed in the top ten of major causes of death globally (World Health Organization 2019; U.S. Centers for Disease Control and Prevention, 2019). The AMR crisis is based on a complex network of interrelated issues from an epidemiological point of view (Figure 1). One problem is the transfer of AMR among gram-negative bacteria, and another is the exchange of AMR bacteria to animals and humans and *vice versa*, which is nearly impossible to prevent (Mølbak, 2004; Ma *et al.*, 2021). AMR transfer is not solely limited to the animal-human interface, but also occurs globally in wildlife, natural soil, limnic habitats and agriculture (Figure 1) (Sanseverino *et al.*, 2019). In the recent past, the use of antibiotics in livestock, the overuse and misuse of reserve antibiotics in humans, has increased the prevalence of AMR bacteria and promoted the spread of the associated infections (van Boeckel *et al.*, 2015). In 2017, the amount of antibiotics administered to livestock exceeded medical use in humans for the first time (ECDC/EFSA/EMA 2021), which rapidly aggravates the AMR issue globally.

Recent initiatives to combat the AMR crisis in humans include vaccination campaigns, which reduced the number of fatalities caused by drug-resistant bacteria e.g. *Streptococcus pneumoniae*, *Mycobacterium tuberculosis* and *Salmonella typhi* (Klugman *et al.*, 2003; Klugman and Black, 2018), however, this could not completely stop the spread of AMR bacteria (Vekemans *et al.*, 2021). Furthermore, global frameworks such as the 'One Health Framework' have achieved certain action points, suggesting that the improved handling and control of nosocomial infections combined with vaccination (wherever possible) is a successful approach (Morel *et al.*, 2020; Frost *et al.*, 2021). Although, in 2019 the number of deaths caused by AMR declined compared to earlier years, even so in the United States more than 2.8 million AMR infections were reported, ~35,900 of which are fatal and are ascending annually (U.S. Centers for Disease Control and Prevention, 2019). Despite the measures discussed above, there is still an urgent need to find and develop new antimicrobials to overcome the growing AMR crisis.

1.2. The golden era of antibiotics

Where do antibiotics come from? The antibiotic era began in 1910 when Hoechst AG introduced salvarsan, which was developed by Paul Ehrlich and Sahachiro Hata to treat syphilis and other spirochetal infections. The subsequent discovery of penicillin by Alexander Fleming in 1928 rang in the **golden era of antibiotics** (Hutchings *et al.*, 2019). Since 1907, ~200 antibiotics have reached the market, but more than 90% were introduced before 1970 (Lakemeyer *et al.*, 2018). The 1960s brought key insights into the mechanism of antibiotics, as the first cases of penicillin and methicillin resistant *Staphylococcus aureus* (MRSA) were discovered (Figure 2). From here on, the discovery of AMR following the market introduction of the corresponding antibiotics diminished steadily (Clatworthy *et al.*, 2007; U.S. Centers for Disease Control and Prevention, 2013). Since 2010, only 18 systemic, 'recycled' antibiotics have been approved by the FDA! (Chahine *et al.*, 2021). This in turn dramatically highlights the demand for novel antibiotics, but where might these novel antibiotics originate from?

1.3. Techniques for Natural product discovery – past, present and future

Antibiotics can be assigned to **21 different classes** (Butler, 2004; Butler and Buss, 2006), 17 of which are derived from **bacterial natural products (NPs)** or at least inspired by them (Table S1). The best-known bioresource for new chemical entities are microbial NPs (Figure 2), most frequently derived from **Actinomycetes** (Newman and Cragg, 2020). Although an astonishing number of NPs with antibacterial activity (~23,000) was estimated in 2016 (Katz and Baltz, 2016), only ~1% of Actinomycetes, and bacteria in general, have been cultured thus far (Wohlleben *et al.*, 2016). This highlights the gap between the immense number of **uncultured microorganisms** and the correspondingly enormous **untapped chemical space** (Lok, 2015; Lakemeyer *et al.*, 2018). The rediscovery rate of known antibiotics is high, and the finding of new antibiotics is unlikely (Wang *et al.*, 2006; Lewis, 2020). Therefore, it is reasonable to extend the search to **underexplored bioresources** and **hitherto uncultivated microorganisms** (Butler, 2004; Schneider, 2021). However, since the 1980s, the rediscovery rate

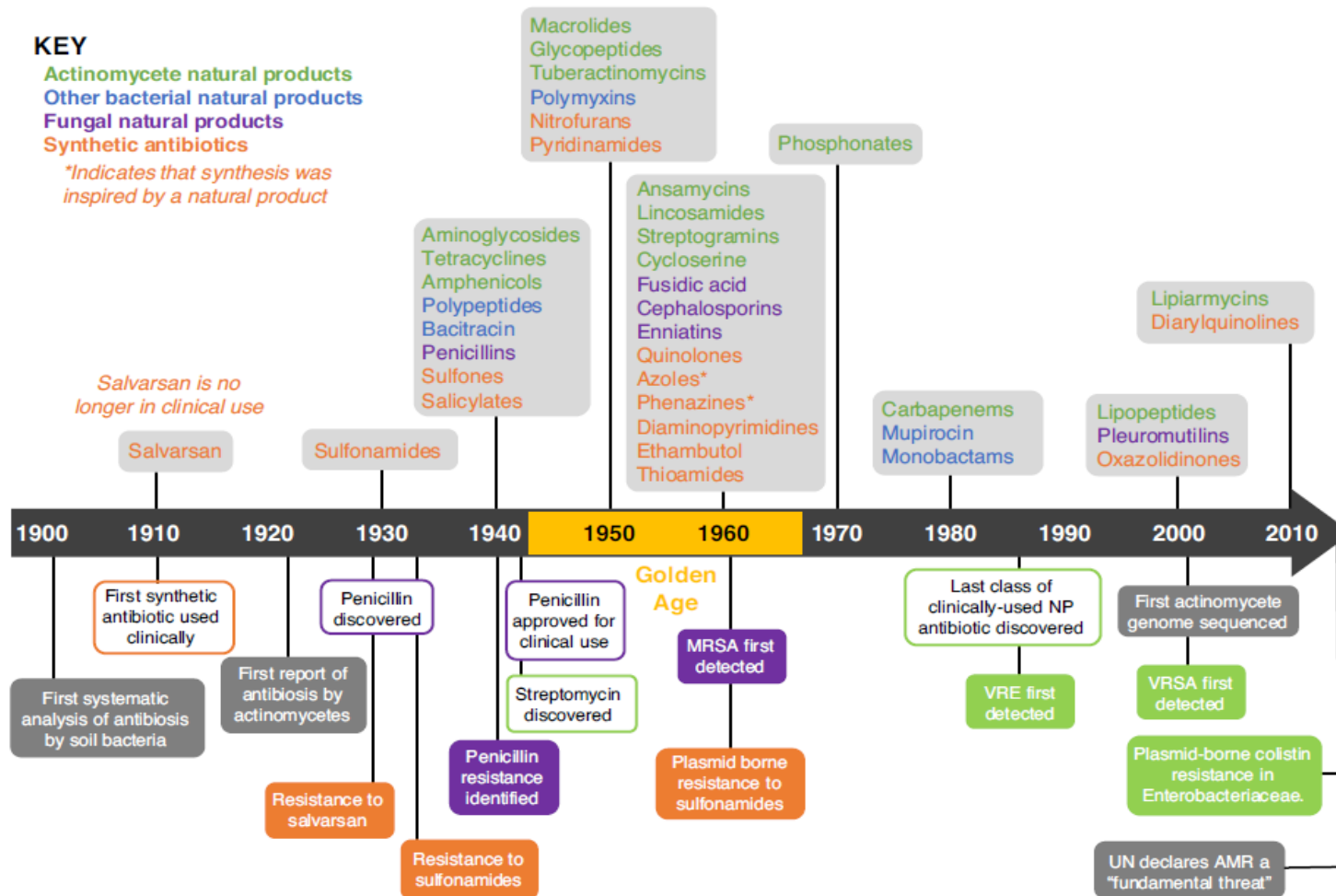


Figure 2: Timeline showing the clinical approval of new classes of antibiotics and the emergence of resistance.

Most antibiotics were retrieved or inspired by NPs from the bacterial group of Actinomycetes (indicated in green). Other bacterial NPs are indicated in blue, fungal NPs in purple, and synthetic antibiotics in orange. Below the timescale, examples of momentous events are shown, such as the first reports of methicillin-resistant *Staphylococcus aureus* (MRSA), vancomycin-resistant enterococci (VRE), vancomycin-resistant *S. aureus* (VRSA) and plasmid-borne colistin resistance in the *Enterobacteriaceae*. Since 2010 no novel class of antibiotics was approved, only synthetic derivatives of antibiotics e.g. tigecycline - a tetracycline derivative (Zha *et al.*, 2020), ceftaroline fosamile a 5th generation cephalosporin (Eckmann, 2014), beta-lactamase inhibitors e.g. avibactam (Nichols *et al.*, 2018) or combinatorial drugs e.g. pretomanid/bedaquiline/linezolid (Andrei *et al.*, 2019) and ceftazidime/avibactam (Zavicefta) (Shirley, 2018) were approved for treatment of infections. Adapted from Hutchings *et al.* *Curr Opin Microbiol.* 2019; 51:72–80.

of antibiotics has increased, whereas the introduction of novel antibiotics has declined dramatically (Schäberle and Hack, 2014). Since 2010 no novel class of antibiotics was approved (Figure 2), thus other solutions were introduced due to the lack of novelty from NPs. For example synthetic derivatives of antibiotics e.g. tigecycline - a tetracycline derivative (Zha *et al.*, 2020), ceftaroline fosamil a 5th generation cephalosporin (Eckmann, 2014), β -lactamase inhibitors e.g. avibactam (Nichols *et al.*, 2018) or combinatorial drugs e.g. pretomanid/bedaquiline/linezolid (Andrei *et al.*, 2019) and ceftazidime/avibactam (Shirley, 2018) were approved for treatment of infections. Due to these reasons, novel cultivation techniques that grant access to the so-called '**microbial dark matter**' have drawn attention to NP research (Lok, 2015) in order to mine for inspirations for new antibiotics in this untapped chemical space (Baltz, 2008; Lewis, 2020).

It can be hypothesized that the chance of finding novel NPs increases significantly by applying cultivation techniques that promote the growth underexplored bioresources and microorganisms in laboratories.

1.3.1. Novel cultivation strategies

Besides purely synthetic approaches, one strategy is to create lead structures on the basis of inspirations from natural products derived from bacteria. The first streamlined experimental platform for bacteria-derived antibiotics was implemented by Selman Waksman and co-workers (Schatz *et al.*, 1944). The term '**grind-and-find**' was coined to describe the testing of antagonistic effects of soil-borne microorganisms, or the corresponding filtrates, on solid or in liquid media against pathogenic bacteria (Waksman and Lechevalier, 1949; Lechevalier and Corke, 1953). This work led to several discoveries, including actinomycin, clavacin, streptothricin, streptomycin, and neomycin (Waksman *et al.*, 1942; Waksman, 1943, 1947, 1950, 1960; Sakula, 1988). Thus, the **Waksman platform** built the basis for the golden era of antibiotic research.

Later, due to the high rediscovery rates of already known antibiotics new cultivation and screening strategies were implemented (Lewis, 2020). For example, automated drug discovery by standardized microplate-based **high-throughput screening (HTS)** in the American National Standards Institute

(ANSI) format, was widely used in the 1990s. The obvious advantages include the increased throughput and lower costs (Auld *et al.*, 2020). Furthermore, improved cultivation techniques in the ANSI microplate format facilitated automation and robotics. This was intended to overcome the issues of the '**great plate count anomaly**' (Staley and Konopka, 1985), whereby methods for the cultivation of marine microorganisms using the concept of '**extinction culturing**' in microplate format were implemented (Connon and Giovannoni, 2002; Bruns *et al.*, 2003). This concept facilitated the targeted high-throughput cultivation of e.g. slow-growing and low-nutrient favoring marine microorganisms.

In the same year, Kaeberlein, Lewis and Epstein introduced the '**diffusion growth chamber for *in situ* cultivation**' (Kaeberlein *et al.*, 2002). This facilitated the diffusion of e.g. proteins or molecules with a greater size than 0.2 μM and trapped everything with a greater size than 0.03 μM due to size exclusion among the compartments where microorganisms were grown, mimicking the regular exchange of substances in the environmental habitat. Therefore, this chamber improved the success of cultivation by bypassing the limitations of unfamiliar environments such as agar plates. The experimental outcome underlined the hypothesis that microorganisms need growth factors produced by their neighbors or even by themselves, which is now described as quorum sensing (Dunny and Winans, 1999; D'Onofrio *et al.*, 2010; Scherlach and Hertweck, 2021).

This concept was subsequently converted into the so-called '**iChip**', which increased the growth recovery rate of soil microorganisms up to 50% compared to 1% on a nutrient agar plate (Nichols *et al.*, 2010; Ling *et al.*, 2015). In contrast to known methods thus far, the iChip enabled arraying of single cells in the diffusion growth chambers, which were placed back into their natural habitat to promote cultivation by *in situ* growth. This innovation led to the isolation of the erstwhile uncultivable bacteria, e.g. *Eleftheria terrae*, producing the first novel antibiotic since the 1980s, namely teixobactin (Wright, 2015). This cyclic depsipeptide acts against Gram-positive bacteria by binding to lipid II, a precursor peptidoglycan and lipid III, a precursor of teichoic acid, therefore supposed to overcome development of resistance (Ling *et al.*, 2015). Moreover, the application of the iChip cultivation led to the discovery of several NPs that effectively kill Mycobacteria (Gavrish *et al.*, 2014; Quigley *et al.*, 2020). These examples

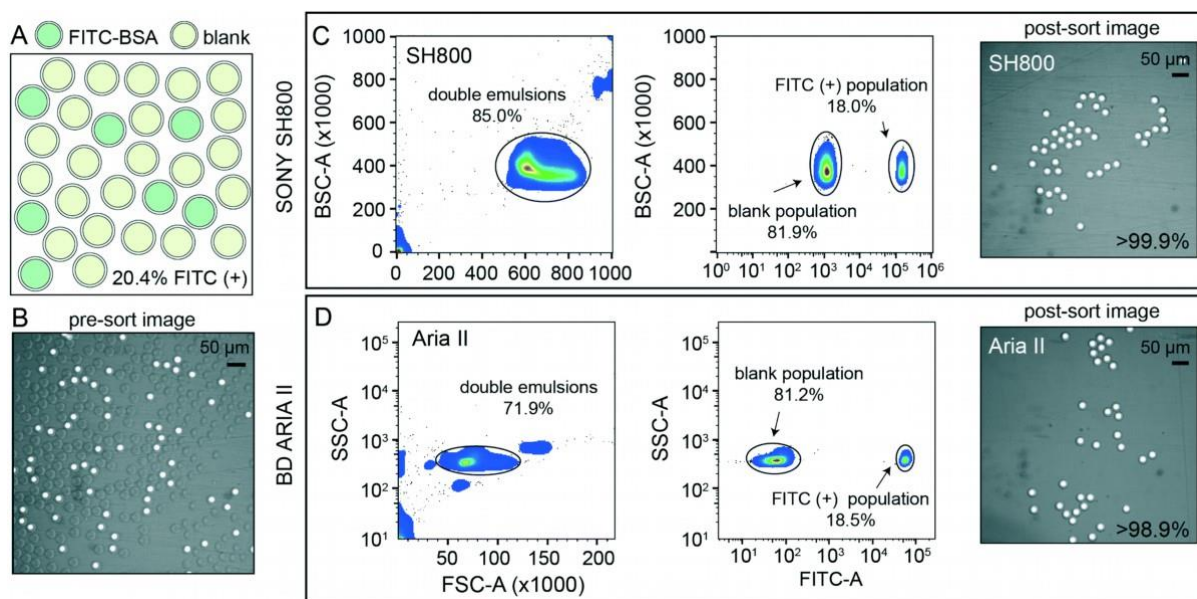


Figure 3: Enrichment of rare populations of interest using fluorescence-activated cell sorting (FACS). **A:** Scheme of pre-sort droplet populations containing FITC-positive droplets as determined by manual count. **B:** Image of droplet population before sorting containing wanted and unwanted events. **C:** Sony SH800 gates and post-sort image of 100 droplets arrayed in a microplate well with 99.9% target specificity. **D:** BD Aria II gates and post-sort image of 100 droplets arrayed in a microplate well with 98.9% target specificity. Parental FACS gate shows 10 000 events per condition, randomly sampled, for both sorters. Adapted from Brower et al. *Lab Chip*. 2020 Jun 21;20(12):2062-2074.

emphasize the importance of novel high-throughput cultivation strategies, which mimic the isolation source, to cultivate hitherto uncultivable bacteria, thus supporting new findings in NP research.

In 2002, which saw the introduction of the diffusion growth chamber and extinction culturing, Zengler and colleagues developed an miniaturized ultrahigh-throughput cultivation technique (Zengler *et al.*, 2002). By using '**microfluidics cultivation**', bacteria were encapsulated in agarose-solidified picoliter droplets functioning as miniaturized compartments, even smaller than in the iChip. Microfluidics cultivation leverages the **numbers game** by applying massive parallelization to improve the probability of success in regard to the cultivation of besides also considering the microbial metabolic requirements (Lok, 2015). Advantageously, it also allows the arranged diffusion of certain molecules among droplets (e.g. signaling factors), which can be adjusted by controlling the droplet size and surfactant concentrations (Skhiri *et al.*, 2012; Etienne *et al.*, 2018). Droplet microfluidics is built on the principle of emulsions consisting of aqueous and oil phases containing stabilizing surfactants in a laminar flow regime.

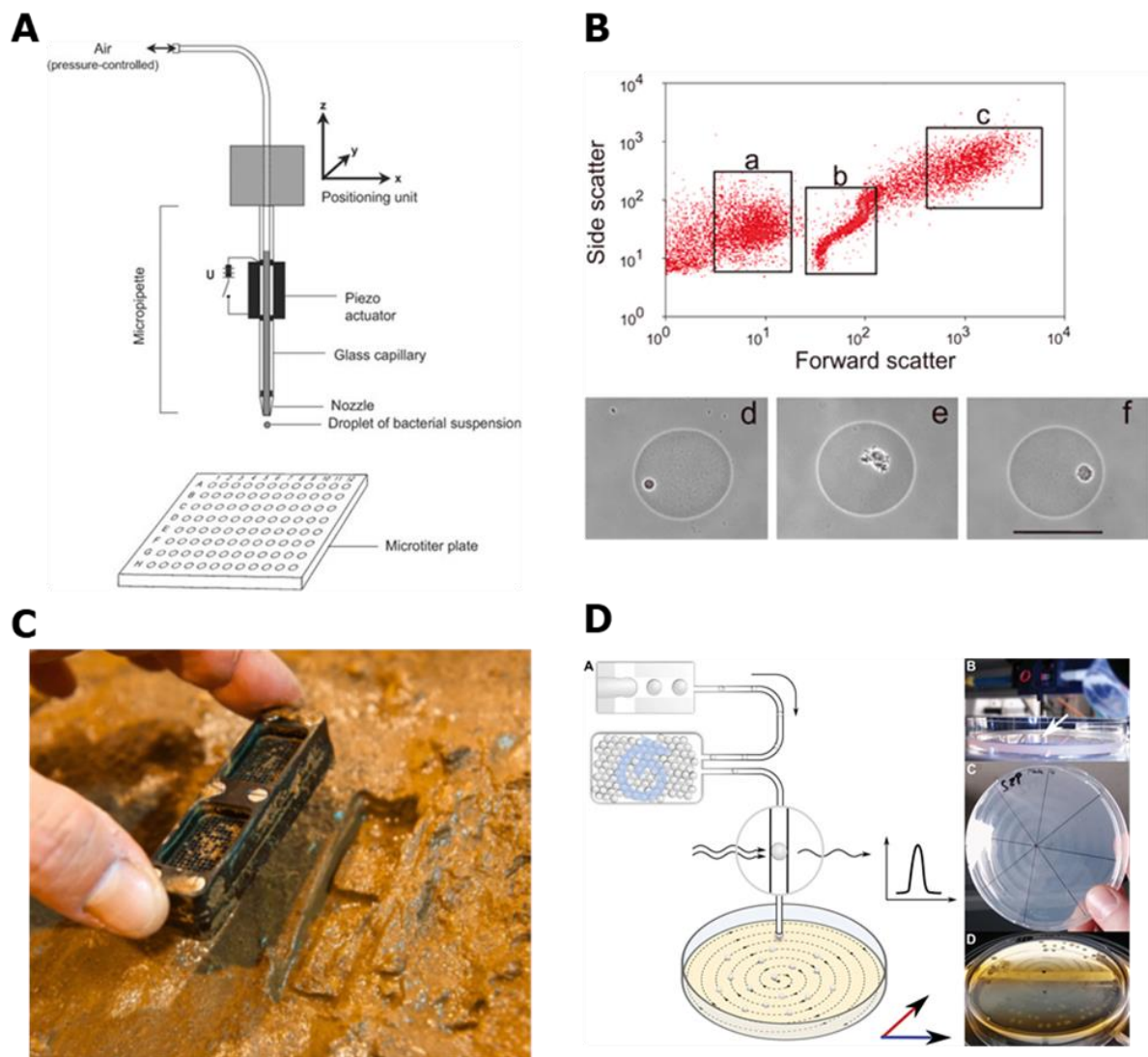


Figure 4: Cultivation strategies to obtain axenic cultures from the microbial dark matter.

A: The MicroDrop® for high-throughput cultivation assays and the isolation of planktonic bacteria allows the inoculation of a 96-well microplate within less than 1 min, thus accelerating the extinction culturing method. Adapted from Bruns et al. *FEMS Microb Ecol.* (2003) Jul 1;45(2):161-71.

B: Encapsulation of environmental microorganisms in gel microdroplets and subsequent flow cytometry analysis facilitated the massively parallel cultivation. Thus far uncultured bacteria were obtained by its application.

Adapted from Zengler et al. *Proc Natl Acad Sci USA* (2002) Nov 26;99(24):15681-6. Copyright © 2002, The National Academy of Sciences.

C: The iChip developed by Slava Epstein to enrich single-cell arrayed microorganisms in their respective habitat e.g. soil. This resulted for instance in the cultivation of *Eleftheria terrae*, from which teixobactin was isolated.

Adapted from Ledford, H. *Nature* (2015) doi: 10.1038/nature.2015.16675. Credit to: Slava Epstein.

D: A droplet-based microscale cultivation system was directly coupled to a high-throughput screening for the prospection of antimicrobial activity prior to strain isolation from environmental cells isolated from soil. This system enabled the cultivation of thus far uncultured bacterial species and uncovered its ability to produce bioactive substances.

Adapted from Mahler et al. *eLife* 2021;10:e64774.

Pressurized in small array channels at the nanometer or micrometer scale, this led to monodisperse aqueous femtoliter to picoliter droplets (Leman *et al.*, 2015). Droplet microfluidics was steadily improved in terms of cost-efficiency, droplet stability, biocompatibility, and throughput (Baret *et al.*, 2009). Today's simplified ready-to-use systems are easy accessible (Nge *et al.*, 2013; Volpatti and Yetisen, 2014). The implementation of subsequent screening and sorting devices, such as fluorescence-activated cell sorting (FACS) (Figure 3), facilitated the targeted analysis of events of interest and their separation into microarrays and microplates (Baret *et al.*, 2009; Zinchenko *et al.*, 2014; Brower *et al.*, 2020). These micrometer-scale compartments are intended to mimic the natural habitat, specifically the low nutrient availability and self-mediating growth factors, better than an agar plate and even better than a microplate well or iChip compartments. Once microcolonies have formed within the droplets, they are sorted by flow cytometry into high-nutrient liquid medium (Akselband *et al.*, 2006). This again facilitated the cultivation of thus far uncultured bacteria representing the '*Planctomycetes* and *Bacteroides* clade' (Zengler *et al.*, 2002). Microfluidic cultivation techniques were subsequently adapted for soil microbes and human oral microbiota (Gao *et al.*, 2013; Zinchenko *et al.*, 2014; Boitard *et al.*, 2015; Jiang *et al.*, 2016; Cao *et al.*, 2017). Furthermore, screening systems to prospect for NPs with activity against human pathogens were tested (Terekhov *et al.*, 2017; Mahler *et al.*, 2018). Recent improvements enabled the modulation of certain abiotic and biotic factors to meet the specific needs of microorganisms (Hengoju *et al.*, 2020; Kästner *et al.*, 2021). This resulted in the cultivation of thus far uncultured bacteria, but have not yet yielded any novel NP scaffolds (Mahler *et al.*, 2021).

In summary, these developments constitute state-of-the-art techniques to prospect for NPs within microbial dark matter (summarized in Figure 4). The further improvement of microfluidics techniques, suitable for cultivation and screening for antibiotics, poses an ideal strategy for future bioprospecting campaigns of e.g. underexplored bioresources in order to leverage the numbers game (Wohlleben *et al.*, 2016; Lewis, 2020; Matilla, 2021).

1.3.2. Underexplored bioresources and bacterial phyla

There is continuous competitive pressure among microorganisms in all bioresources. Microbes have therefore evolved to produce substances, such as antimicrobials, to outcompete surrounding species. Most of the antibiotics on the market are derived from soil-borne microorganisms, especially from Actinobacteria (Table S1). Therefore, as well as novel cultivation techniques, the investigation of **underexplored bioresources** (e.g. deep sea, endophytes, insects, and the human microbiome) is another driver in the search for new NPs (Tortorella *et al.*, 2018; Rangseekaew and Pathom-Aree, 2019; Quinn *et al.*, 2020). Bacteria isolated from marine habitats, are a good source of new chemical entities (Corinaldesi, 2015; Wink *et al.*, 2017). One example is the genus *Verrucosispora*, which contains only 10 validly published representatives (<https://lpsn.dsmz.de/genus/verrucosispora>); last access date 10.10.2021). They were later reclassified as *Micromonospora* (Nouioui *et al.*, 2018), which produce the so-called abyssomicins. Abyssomicins are tetronates, more exactly spirotetronates, which have been studied due to their peculiar structural moieties and e.g. anti-influenza and antibacterial properties (Sadaka *et al.*, 2018; Zhang *et al.*, 2020). They may be suitable for further development as drug candidates because they target folate biosynthesis, which is exclusively limited to prokaryotes (Iglesias *et al.*, 2020; Fiedler, 2021).

Another genus of marine bacteria with a large and distinct metabolic repertoire is the candidate genus *Entotheonella* (candidate phylum 'Tectomicrobia'), closely related to Myxobacteria (Schmidt *et al.*, 2000). *Entotheonella* spp. are associated with sponges (*Theonella swinhoei*) and are proposed as symbionts. They possess diverse type III polyketide synthase (PKS) clusters that predictably lack identified NPs (Reiter *et al.*, 2020). The resulting unique compounds may also provide opportunities for drug discovery (Wilson *et al.*, 2014; Lackner *et al.*, 2017). Although no candidate of the genus *Entotheonella* has been cultured in the laboratory thus far, successful cultivation would open the way for the in-depth analysis of their full repertoire of NPs.

From a genetic perspective, there are many more interesting phyla such as **Acidobacteria** (Kielak *et al.*, 2016), which could also provide a good source of

new chemical entities (Crits-Christoph *et al.*, 2018). Recent *in silico* analysis of the genetic repertoire of the candidate genus *Angelobacter* and others shed light on the overall potential of this ubiquitous phylum (Zhang *et al.*, 2019; Crits-Christoph *et al.*, 2021). However, few representatives have been isolated thus far because most species in this phylum are difficult to cultivate, and they are poorly represented in public collections of microorganisms (Bryant *et al.*, 2007; Lee *et al.*, 2008; Da Rocha *et al.*, 2009; Navarrete *et al.*, 2013). Accessibility of more representatives will support unraveling the potential of Acidobacteria. To this end, cultivation techniques have to be adapted in the respect of their growth pace and specific metabolic needs (Kielak *et al.*, 2017).

Insect-associated microorganisms also possess an underexplored bioresource (Challinor and Bode, 2015; Benndorf *et al.*, 2018; Heise *et al.*, 2019; Hirsch *et al.*, 2019). The evolutionary success of insects in terms of biodiversity is partially mediated by host-interactions with beneficial microbes. Thus, they have been recognized as promising bioresource for NP research (Chevrette *et al.*, 2019; van Moll *et al.*, 2021). **Social insects** in particular are known to harbor **bacterial symbionts**, which can produce many NPs (Beemelmans *et al.*, 2016; van Moll *et al.*, 2021). One well-known example is the association of *Lactobacillales* with the honeybee *Apis mellifera mellifera*. *Lactobacillus* spp. produces the pore-forming lantibiotic nisin and derivatives thereof, which supports the survival of honey bees during infections with the pathogen *Melisococcus plutonius* (Janashia *et al.*, 2016; Nakamura *et al.*, 2016; Zendo *et al.*, 2020). A further example is the association of several Actinomycetes with leaf-cutting ants (Goldstein and Klassen, 2020). Actinomycetes produce many secondary metabolites (Chevrette and Currie, 2019), most of which are antifungal agents used to inhibit invasive fungi to protect the ant colony (van Arnem *et al.*, 2016; Heine *et al.*, 2018). Fungus-growing higher termites are also a good source of insect-associated microbes (Benndorf *et al.*, 2018; Schmidt *et al.*, 2021). In contrast, the nest symbionts of lower subterranean termites such as **Coptotermes spp.** are not well characterized thus far. Little is known about termite-associated Actinobacteria and their influence on colony fitness during interactions with fungi (Chouvenc *et al.*, 2013), thus providing a good example of an underexplored bioresources worth an exploration. Solitary insects also harbor gut bacteria, which are beneficial for the life cycle of the host and/or their offspring. For example, the burying beetle

Nicrophorus vespilloides and the black soldier fly *Hermetia illucens* both offer an untapped resource for NPs by outsourcing defense mechanisms to their microbiome or mycobiome (Heise *et al.*, 2019; Brinkrolf *et al.*, 2021; Tegtmeier *et al.*, 2021). Approximately one million insects have been described, leading to the assumption that 80% of insects remain to be discovered (Stork, 2018). In summary, insects itself and their associated microorganisms constitute a great untapped source for NP-producing microorganisms which may lead to new chemical scaffolds for drug discovery.

Interestingly, the human microbiome, especially in the nasal passage and gut, also provide a rich source of antimicrobial substances (Kumpitsch *et al.*, 2019). This was exemplified by the discovery of the cyclic peptide lugdunin produced by *S. lugdunensis*, which was isolated from the human nose (Zipperer *et al.*, 2016). Besides its antimicrobial properties against *S. aureus*, intranasal application also stimulates the immune system by activating CXCL8, thus inhibiting skin colonization by *S. aureus* (Bitschar *et al.*, 2019). Another example is Ruminococcin C, an anti-colostridial, novel ribosomally synthesized and posttranslationally modified peptide (RiPP), produced by the human gut commensal *Ruminococcus gnavus* (Balty *et al.*, 2019; Balty *et al.*, 2020). These recent discoveries point out that also 'obvious' bioresources should receive more attention to uncover novel useful antimicrobials.

In conclusion, new cultivation strategies paired with the bioprospection of underexplored bioresources are key drivers for the identification of novel NPs to meet the high demand for antimicrobials to combat AMR.

1.3.3. Computational approaches

Finding novel antibiotics in bacteria suitable as lead structures has become less likely since the 'golden era' of antibiotics, but is not impossible thanks to novel cultivation techniques, untapped bioresources and also computational approaches such as **genome mining and metabolomics** (Bachmann *et al.*, 2014; Wohlleben *et al.*, 2017; Medema *et al.*, 2021; Panter *et al.*, 2021).

Furthermore, by coupling certain approaches, the discovery of new molecules becomes even more likely: for example, **multi-omics approaches** such as the coupling of bacterial genomics and metabolomics (Palazzotto and

Weber, 2018), or **'one strain - many compounds (OSMAC)** approaches (Bode *et al.*, 2002). These in turn, coupled with strong downstream analytical toolboxes based on **high-resolution liquid chromatography tandem mass spectrometry (HR-LC/MS/MS)**, has facilitated the detection of new compounds in the resulting multitude of extracts (Krug and Müller, 2014). The development of compound isolation and structure dereplication improved significantly, leading to yearly ~1600 numbers of published structures from nature, which is steadily increasing (Pye *et al.*, 2017). Further improvement of robust statistical tools facilitate semi-automated extract prioritization to explore the extensive scientific

benefits of metabolic clusters (Marner *et al.*, 2020; Riyanti *et al.*, 2020). The combination of a **bioactivity-guided approach** with **metabolomics** is capable of preventing the re-isolation of already known NPs (Figure 5) (Demarque *et al.*, 2020). Combinations of these streamlined comprehensive techniques are now the state-of-the-art for the discovery of new NPs, exemplified by the description of new cyclic lipopeptides known as chitinopeptins isolated from *Chitinophaga* spp. (Brinkmann *et al.*, 2021a).

These combined computational approaches will advance NP research to a higher level (Tommasi *et al.*, 2015; Cully, 2018; Brogi, 2019), but type strains

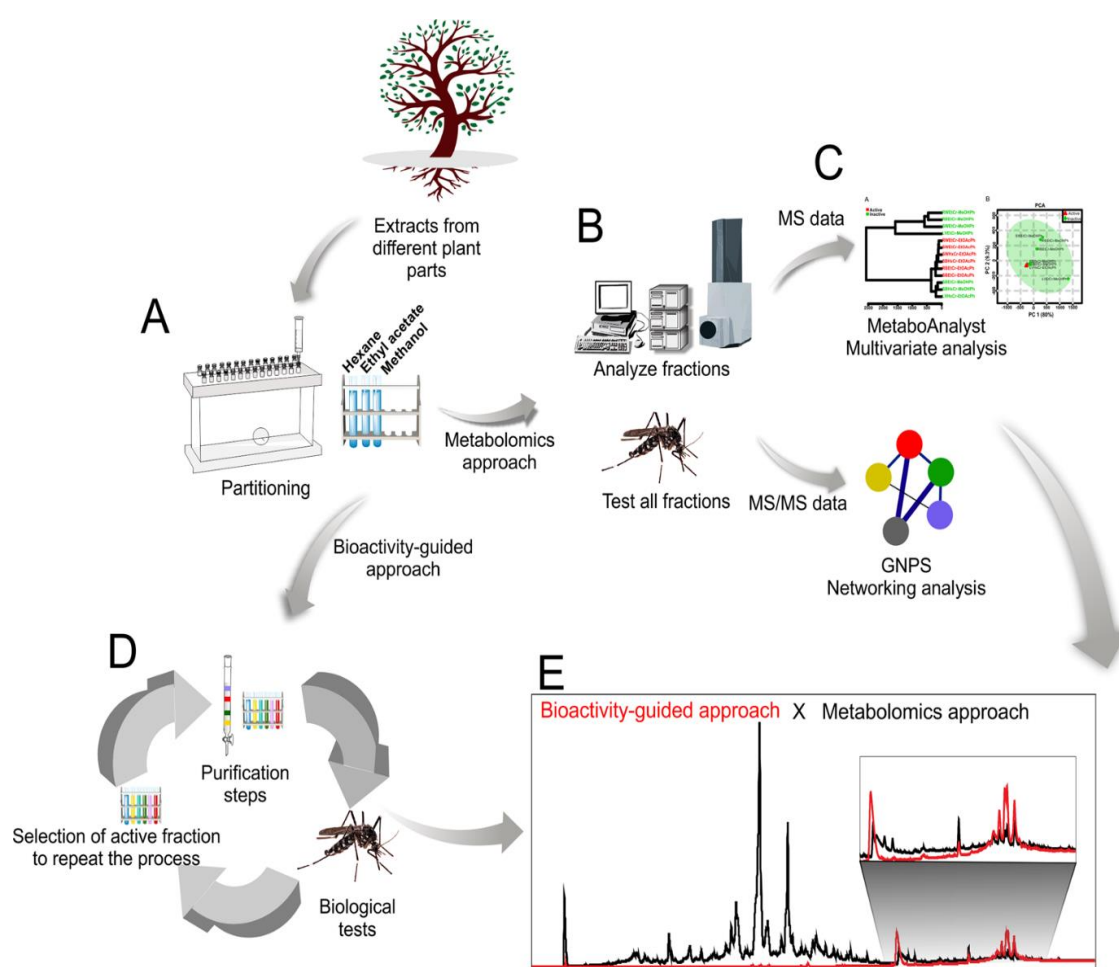


Figure 5: The comparative potential of the bioactivity-guided approach and metabolomics. **A:** The first step of both approaches involves crude extract pre-fractionation. **B:** In the metabolomics approach, all fractions from the crude extracts are analyzed by LC-MS/MS and biological testing. **C:** The data are then analyzed in metabolomics platforms such as GNPS indicating the active compounds. **D:** This represents the cycle of purification steps, where fractions are recovered by chromatography before testing. When the active fraction is identified, repeated purification steps are applied until an enriched fraction is obtained containing the active compounds. **E:** The black chromatogram represents one active fraction, where the active compounds are highlighted (RT 28.0–32.0 min), whereas the red chromatogram, obtained after earlier purification steps, indicates the same active compounds previously revealed by the metabolomics approach. Adapted from Demarque *et al.* *Sci Rep* 2020 Jan 23;10(1):1051.

should nevertheless be made accessible in the laboratory to prospect the complete chemical repertoire of the microbial diversity.

1.4. Antibiotic targets and bacterial evasion strategies

So far, antibiotics aim only a limited number of targets, encompassing **few different general MoAs**: **i) alteration of cell membranes** (e.g. transpeptidase, muramyl ligase, BamA, LipidII), **ii) protein biosynthesis** (e.g. ribosomal 30 and 50S subunits), **iii) nucleic acid synthesis** (e.g. DNA- and RNA polymerase, topoisomerase), **iv) metabolic pathways** (e.g. fatty acid synthesis, folate pathway) and **v) depolarization** (ATP-synthase) (Figure 6). The requirements of NPs underlay chemical as well as biological rules that define criteria for exclusion of molecules that can be developed as drugs. For instance, a molecular weight not more than 500 dalton (Da), partition coefficient ($\log P$), and a number of atoms from 20 to 70 in -0.4 to $+5.6$ range (Ghose *et al.*, 1999; Lipinski *et al.*, 2001). The ultimate goal is to find molecules, that meet these criteria, possess a potential novel **mechanism of action (MoA)**, low **frequency of resistance** and define a new structural class of antibiotics (Tacconelli *et al.*, 2018), given by the examples of the synthetic peptidomimetic compound Murepavadin (Srinivas *et al.*, 2010; Díez-Aguilar *et al.*, 2021), and the NPs teixobactin (Ling *et al.*, 2015) and darobactin (Imai *et al.*, 2019). Bacteria possess numerous survival strategies to overcome susceptibility to antibiotics. They can be categorized into **i) resistance**, **ii) tolerance** and **iii) persistence** mechanisms (Brauner *et al.*, 2016), whereby the latter will be introduced in more detail later. Generally, bacteria exhibit a physical barrier, their cell wall and an extracellular matrix, which passively decreases the cell permeability of drugs. Another mechanism is that bacteria undergo certain mutations that change the target

For example, only one **random single point mutations** in ribosomal subunits can lead to a resistance towards the respective antibiotic by lowering the possibility to bind to the target. Additionally, enzymes can be produced to **deactivate the target** and/or for the **destruction the antibiotic** exemplified by the secretion of penicillin-binding proteins such as β -lactamases, which cleave of β -lactams. A similar resistance mechanism is the production of **antibiotic chelating agents**. In answer to the recognition of antibiotics, bacteria augment their **efflux pumps**, which enable the selective export of compounds out of the cell (Lakemeyer *et al.*, 2018). Augmentation of drug targets within the cell is also possible; the higher the amount of drug targets, the less effective the antibiotics. Bacteria possess the ability to **bypass metabolic pathways**, which are targeted by certain antibiotics such as the folate synthesis by sulfonamides.

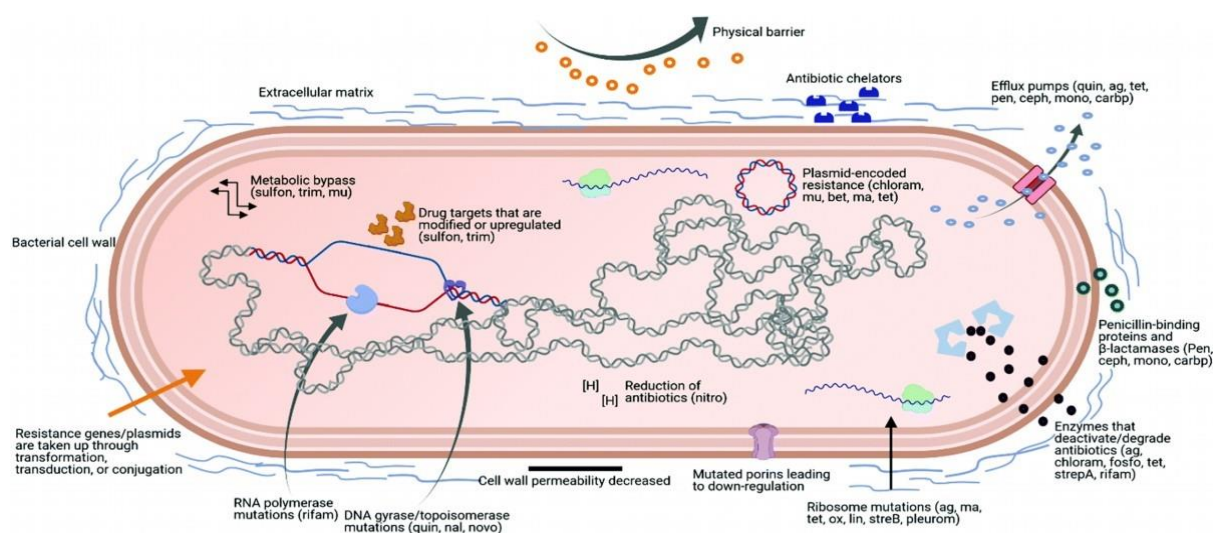


Figure 6: Bacterial drug targets and their resistance mechanisms towards corresponding antibiotics.

Examples of known mechanisms of resistances towards specific antibiotics are shown (depicted in brackets). ag: aminoglycosides, ma: macrolides, tet: tetracyclines, ox: oxazolidinones, lin: lincosamides, strepA: streptogramin A, strepB: streptogramin B, pleurom: pleuromutilins, quin: quinolones, nal: nalidixic acid, novo: novobiocin, sulfon: sulfonamides, trim: trimethoprim, mu: mupirocin, chloram: chloramphenicol, fosfo: fosfomycin, rifam: rifamycins, nitro: nitroimidazoles, pen: penicillins, ceph: cephalosporins, mono: monobactams, carbp: carbapenems, bet: β -lactams. Adapted from Gan *et al.* *Chem. Soc. Rev.* 2021,50, 7820-7880.

The overall problem intensifies if concerted escaping strategies make antibiotics in non-toxic doses rather useless. Therefore, six highly virulent antibiotic resistant pathogens are summarized in the term: **ESKAPE**, including multidrug-resistant (**MDR**) bacteria of *Enterococcus faecium*, *Staphylococcus aureus*, *Klebsiella pneumoniae*, *Acinetobacter* spp., *Pseudomonas aeruginosa* and

Enterobacter spp. (Tommasi *et al.*, 2015). The relative estimated prevalence of these pathogens is about 16% of hospital acquired infections, may leading to death, because even reserve antibiotics are pointless (Mulani *et al.*, 2019; Dafale *et al.*, 2020). The issue of resistance development is aggravated by e.g. **biofilm formation**, which takes places steadily and can cause adverse effects, when e.g. taking place in the gut (e.g. *Clostridium difficile*) or in wound infections (e.g. *Staphylococcus aureus*). Biofilm formation is supported by **extracellular matrices (ECM)** that consist of an impermeable meshwork including cells, exopolysaccharides, proteins and substantial amounts of extracellular DNA (Gödeke *et al.*, 2011; Binnenkade *et al.*, 2018). Thus, ECM leads to improved biofilm formation, thus a higher tolerance and additionally favors a subpopulation to turn into the metabolic state of persistence (e.g. minimum metabolic activity) (Pendleton *et al.*, 2013; Díaz-Pascual *et al.*, 2019). Hence, susceptibility decreases up to 1000-fold towards antimicrobials, especially targeting protein biosynthesis. A higher AMR transfer rate within biofilms is more likely due to the combination of close cell-to-cell contact, tolerance, and favorability of the persistence state (Bowler *et al.*, 2020).

In summary, resistance, tolerance and persistence mechanisms pose a major issue in respect of antibiotic evasion strategies, which should be addressed to combat the AMR crisis more effectively.

1.4.1. Resistance transmission, tolerance and persistence

How are resistances transmitted? The steadily increasing amount of AMR bacteria is facilitated by particular antibiotic evasion strategies, which can be implications of resistance mechanisms. Resistant bacteria are associated with an higher risk of treatment failures and relapsing infections (Huemer *et al.*, 2020). Resistance towards antimicrobials is defined by their minimum inhibitory concentration (**MIC**) regarding the growth rate of a microorganism. Manifold molecular mechanisms are responsible for the so-called '**resistome**' (Brauner *et al.*, 2016). The resistome includes all genes (efflux pumps, enzymatic activity, mutations in the target, etc.) that are involved in the invulnerability of microorganisms towards certain concentrations of antimicrobials. There are several mechanisms to gain resistance genes – also known as **pathogenicity islands** (Hacker and Kaper, 2000; Frost *et*

al., 2021). The transfer results in new bacterial genotypes, which is gained by **host mutations**, **vertical gene transfer** and **horizontal gene transfer (HGT)**. Resistance is often plasmid-borne among bacterial genera and e.g. transferred via HGT (Sköld, 2000). HTG is being realized via **i) transformation** (the internalization of free DNA by competent cells), **ii) transduction** (the transfer of bacterial DNA shuttled by bacteriophages) and **iii) conjugation** (the active transfer of DNA via pili from the donor to the recipient) (Thomas and Nielsen, 2005).

Moreover, exceeding a critical amount of individuals, planktonic bacteria can form biofilms, facilitating subpopulations therein to fall into a metabolic dormant status, so-called '**persister**' (Lewis, 2007). The term was coined for cells, which reduce the metabolic activity to a minimum, therefore, decrease the susceptibility of antibiotics to a minimum (Høiby *et al.*, 2010). This state of persistence plays a key role during infections, because it defines the way and period of drug administration (Høiby *et al.*, 2011).

The biofilm forming bacterium *E. coli* displays a well-studied example for persister formation, however complete understanding still requires detailed research (Manuse *et al.*, 2021). *E.coli* strains are common inhabitants of human guts, but can evolve to a life-threatening issue. Once at the wrong place it can cause severe implications such as urinary tract infections or lead to kidney failure due to persistent biofilms (Foxman, 2010). Tolerance towards antibiotics is higher in a mature biofilm compared to the early stage of biofilm formation (Brauner *et al.*, 2016). Additionally, gene transfer is enhanced in biofilms due to close cell-cell contact leading to faster exchange of pathogenicity islands. Thus, it is a preferred option to use enzymes, quorum sensing molecules or other compounds to even prevent biofilm formation at its beginning (Orman and Brynildsen, 2016). To this end, high doses of antibiotics are administered in early stages of infections (Høiby *et al.*, 2010). Obviously, this represents a small treatment window, insanely, poses the risk of persister formation occurring frequently by improper doses administered mistimed (Zheng *et al.*, 2020). Often, severe chronic hospital-acquired infections are caused by MDR bacteria, hence, the remaining options are colistin or mitomycin C. Colistin is a pore forming-agent, and Mitomycin C a DNA-crosslinking anti-cancer drug, which both eradicate cells independent of their metabolic status. However, these drugs implicit a range of toxicities in patients,

as signs of nephrotoxicity and leukocytopenia even at low plasma concentrations (Zheng *et al.*, 2020).

In summary, bacteria are more tolerant towards antibiotics in biofilms, may resulting in persister cells, which in turn spread resistances more efficient, ultimately leading to more resistance of the whole population. Hence, it is essential to shine through all stages of persisting bacteria to identify new targets, thus, treatment options.

1.4.2. Toxin-antitoxin-dependent persister in *E. coli*

Species of the genus *E. coli* inhabit a variety of known genes leading to persistence pathways, thus displaying also a model organism towards persister formation. It is known that e.g. *relE*, *smpB*, *glpD*, *umuD*, and *tnaA* are involved in late time points of persister formation after antibiotic treatment. The genes *oxyR*, *dnaK*, *phoU*, *lon*, *recA*, *mqsR* and **tisAB** hypothetically play a role in an early stage. There are several known membrane-associated type I toxins from **toxin-antitoxin systems (TAS)**: *HokB*, **TisB**, *LdrA*, *LdrD*, *IbsC*, *ZorO*, *ShoB*, and *DinQ* (Nonin-Lecomte *et al.*, 2021). The TAS ***tisB/istR-1*** enables persister formation, inhabiting an increased level of tolerance towards DNA-causing agents, due to augmented occurrence of the toxin TisB. Explained briefly, ciprofloxacin targets the type II DNA topoisomerase (DNA gyrase), necessary for replication during cell division. DNA topoisomerases cut double-stranded DNA (dsDNA) due to the hydrolysis of ATP. Upon ciprofloxacin treatment dsDNA breaks occur, thus cells are arrested in a non-dividing stage, ultimately leading to death (Mason *et al.*, 1995). While dsDNA-breaks occur, the **bacterial SOS response** is activated to enhance the DNA repair system (Janion, 2008). If a certain threshold of the SOS response is overleaped, the cell may fall into a persistent state, to prevent death caused by antibiotics for instance. This is facilitated by a tightly regulated cascade, whereas, e.g. production of TisB is triggered in *E.coli* as a result. TisB is a pore-forming toxin, which accumulates in the cell membrane, leading to eradication of the proton motive force (pmf), which in turn leads to **depolarization**.

It is followed by quick ATP-depletion, which in turn causes the cell metabolism to decrease to a minimum (Shan *et al.*, 2017). That opens up an opportunity, in which a subpopulation of a colony is favored to survive the antibiotic treatment (Berghoff *et al.*, 2017). Besides *tisB/ist-R*, there are several known type I toxin-antitoxin modules such as *mqsR*, *lon*, *relE*, *hipA*, *hokB*, *dinQ*, *mazF*, and *dinJ* (Lewis, 2007; Wu *et al.*, 2015; Edelman and Berghoff, 2019). That means, many enzymes, therefore, potential targets for antibiotic treatments are involved in the type I toxin-antitoxin cascades. The evolving knowledge about persister

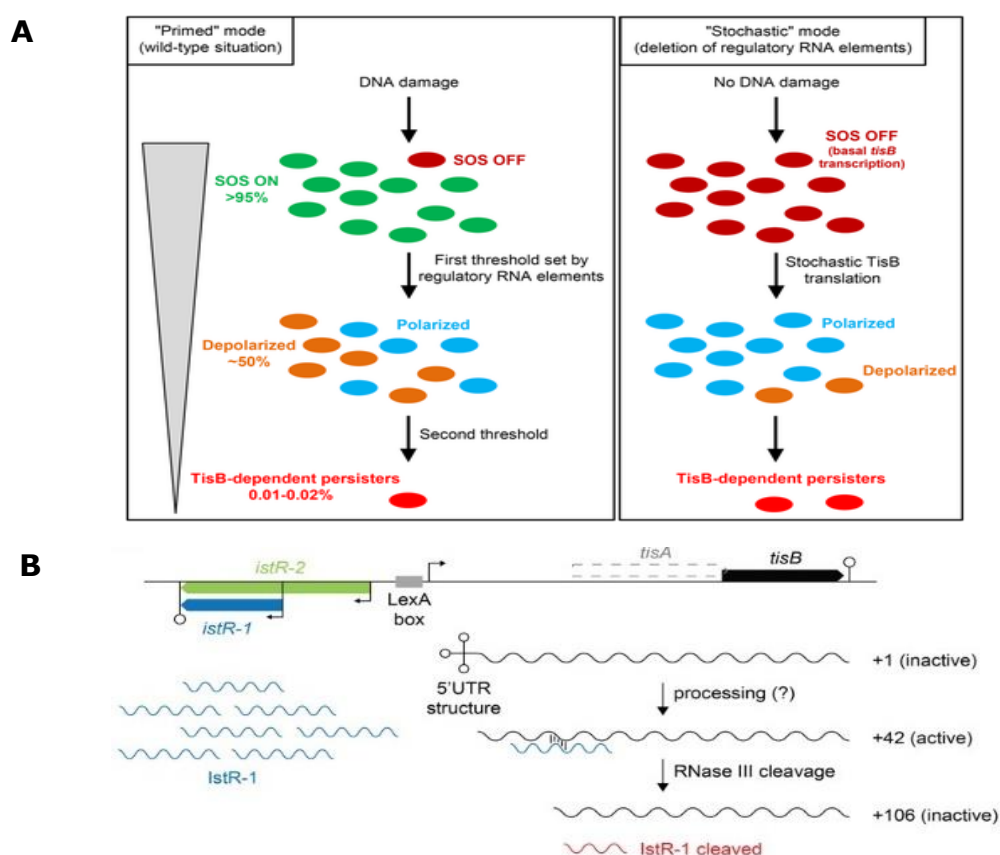


Figure 7: Scheme of toxin TisB-dependent persister formation.

A: While suffering from DNA damage, the ubiquitous SOS response is activated leading to a persistence state in bacteria. The first barrier has been overcome when TisB accumulation leads to pore formation. This results in membrane depolarization by disruption of the proton motive force (pmf), ultimately leading to ATP-depletion, thus low or no metabolic activity. On the one hand the presence of SOS stimulating agents, especially when targeting DNA directly (e.g. Mitomycin C) or indirectly (e.g. Ciprofloxacin) stimulates TisB-dependent persisters. On the other hand this may happen also in absence of strong SOS induction due to stochastic effects, even if the regulatory RNA elements are depleted. Both enhance the survival rate of *E. coli* during antibiotic treatment.

B: The LexA box is repressed by its repressor. TisB translation is regulated by two RNA elements. LexA controls the transcription of *IstR-2* and *tisB*. *IstR-1* gene is expressed constitutively. The primary *tisB* transcript (+1) must be processed into its translationally active +42 form enabling ribosome binding. This transcript leads to expression of TisB toxin, but only if not further inactivated by RNase III cleavage (+106). Adapted from Berghoff *et al. Mol Microbiol.* 2017 Mar;103(6):1020-1033.

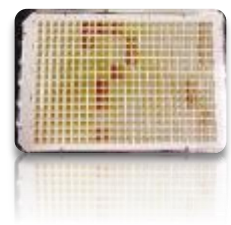
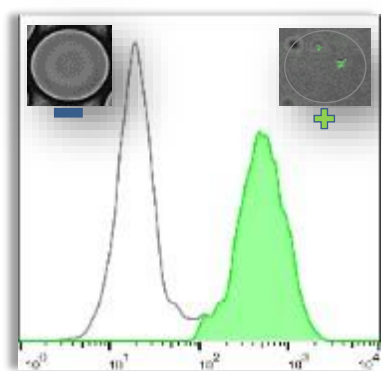
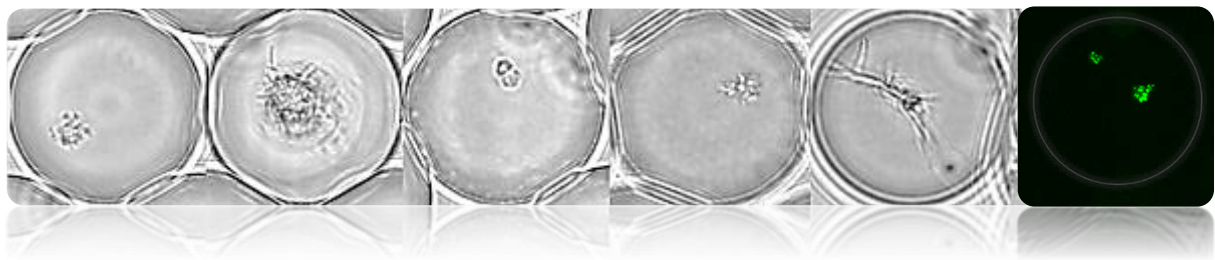
formation, respective mechanisms and especially involved enzymes, may shed light on new targets, functioning as treatment options against hospital-acquired persisting infections (Lewis, 2007, 2020).

The introduction of mechanistic models is a useful tool to understand the cellular cascades leading to persistence. For example, *tisAB*, *lexA* and *recA* knockouts (or a combination thereof) shed light on the mechanistic cascade underlying TisB persister formation (Dörr *et al.*, 2009; Dörr *et al.*, 2010). The rather more subject-oriented double deletion mutant of both regulatory RNA elements $\Delta 1-41$ and $\Delta istR$ ($\Delta\Delta$) (Figure 7) enhanced persister formation by up to 200-fold after antibiotic treatment (Berghoff *et al.*, 2017), therefore giving rise to a **'high persister' (*hip*) phenotype**.

Prospectively, the combination of such models with high-throughput methods that facilitate the analysis of the phenotypes discussed above supports the stochastic evaluation of the proportion of persister cells in the total population. In conclusion, these models promote the investigation and understanding of *E.coli* persister formation, therefore offering a helpful tool for antibiotics research and for the development of new treatment options for relapsing bacterial infections.



CHAPTER 1: IMPLEMENTATION OF HIGH-THROUGHPUT TECHNIQUES TO BIOPROSPECT FOR NATURAL PRODUCTS IN UNDEREXPLORED BIORESOURCES



2. AIMS OF CHAPTER 1

The microbial dark matter offers a rich resource for natural product research, as exemplified by several recent studies (Ling *et al.*, 2015; Lok, 2015; Imai *et al.*, 2019; Quigley *et al.*, 2020; Fiedler, 2021). Different methods have been used to achieve the laboratory cultivation of hitherto uncultivable strains, but high-throughput screening should also be implemented, to leverage the numbers game in natural product discovery. Moreover, chemical novelty should be prospected in new isolates using e.g. metabolomic studies.

- (i) First, a flexible microplate-based high-throughput method should be established to selectively obtain bacterial isolates from underexplored bioresources. This was exemplified by the bacterial phylum Acidobacteria, which has few accessible representatives today (Sikorski *et al.*, 2022). The high-throughput microplate-based approach should be adapted towards their specific needs to obtain more laboratory cultures (Kielak *et al.*, 2016). We observed that a rich source of Acidobacteria is represented by the underexplored nest microbiome of the subterranean termite *C. testaceus* and therefore chose it for this purpose.
- (ii) Second, to increase the success of cultivation of (i) even further, an ultrahigh-throughput microfluidics cultivation approach should be applied before a microplate-based bioactivity-guided screening (Marner *et al.*, 2020), and should be tested on a forest soil microbiome. This should likewise increase the throughput by subsequent arraying into standardized microplate formats for bioactivity screening. Furthermore, in order to reduce the workload associated with the dereplication of bioactivities, suitable computational approaches such as metabolomics studies should be brought in line with the obtained molecular genetic results of the isolated microorganisms.

- (iii & iv) To prospect the expected broad chemical diversity of (i) and (ii), axenic fungal and bacterial strains isolated from the underexplored *Coptotermes* termite nest, which were already deposited in the Fraunhofer strain collection were used. They should be examined to detect bioactivities against bacterial and fungal pathogens, and to isolate novel chemical scaffolds including support of metabolomics-guided approaches.
- (v) Furthermore, a protocol for a flexible integrated screening approach based on the microfluidic setup from (ii) that exchanges the microplate-based screening should be established. To this end, double emulsions should be designed to accelerate the screening for novel natural products in an ultrahigh-throughput manner.

MANUSCRIPT 1: HIGH-THROUGHPUT CULTIVATION FOR THE SELECTIVE ISOLATION OF ACIDOBACTERIA FROM TERMITE NESTS

Status: published on 06/11/2020

Author's contributions: Study design, method validation, contribution to all experiments, data analysis, manuscript writing, figure design.



High-Throughput Cultivation for the Selective Isolation of Acidobacteria From Termite Nests

Markus Oberpaul¹, Celine M. Zumkeller¹, Tanja Culver¹, Marius Spohn¹, Sanja Mihajlovic¹, Benedikt Leis¹, Stefanie P. Glaeser², Rudy Plarre³, Dino P. McMahon^{3,4}, Peter Hammann^{5†}, Till F. Schäberle^{1,6*}, Jens Glaeser^{1*†} and Andreas Vilcinskas^{1,6*}

OPEN ACCESS

Edited by:

George Tsiamis,
University of Patras, Greece

Reviewed by:

Tomislav Cernava,
Graz University of Technology, Austria
Javier Pascual,
Darwin Bioprospecting Excellence,
Spain

*Correspondence:

Till F. Schäberle
Till.F.Schaeberle@agr.uni-
giessen.de
Jens Glaeser
Jens.glaeser@evotec.com
Andreas Vilcinskas
Andreas.Vilcinskas@agr.uni-
giessen.de

† Present address:

Peter Hammann,
Evotec International GmbH,
Göttingen, Germany
Jens Glaeser,
Evotec International GmbH,
Göttingen, Germany

Specialty section:

This article was submitted to
Microbial Symbioses,
a section of the journal
Frontiers in Microbiology

Received: 21 August 2020

Accepted: 19 October 2020

Published: 06 November 2020

Citation:

Oberpaul M, Zumkeller CM,
Culver T, Spohn M, Mihajlovic S,
Leis B, Glaeser SP, Plarre R,
McMahon DP, Hammann P,
Schäberle TF, Glaeser J and
Vilcinskas A (2020) High-Throughput
Cultivation for the Selective Isolation
of Acidobacteria From Termite Nests.
Front. Microbiol. 11:597628.
doi: 10.3389/fmicb.2020.597628

¹ Branch for Bioresources, Fraunhofer Institute for Molecular Biology and Applied Ecology (IME), Giessen, Germany,

² Institute of Applied Microbiology, Justus Liebig University Giessen, Giessen, Germany, ³ Bundesanstalt für
Materialforschung und -prüfung, Berlin, Germany, ⁴ Institute of Biology, Free University of Berlin, Berlin, Germany,

⁵ Sanofi-Aventis Deutschland GmbH, R&D Integrated Drug Discovery, Hoechst Industrial Park, Frankfurt am Main, Germany,

⁶ Institute for Insect Biotechnology, Justus Liebig University Giessen, Giessen, Germany

Microbial communities in the immediate environment of socialized invertebrates can help to suppress pathogens, in part by synthesizing bioactive natural products. Here we characterized the core microbiomes of three termite species (genus *Coptotermes*) and their nest material to gain more insight into the diversity of termite-associated bacteria. Sampling a healthy termite colony over time implicated a consolidated and highly stable microbiome, pointing toward the fact that beneficial bacterial phyla play a major role in termite fitness. In contrast, there was a significant shift in the composition of the core microbiome in one nest during a fungal infection, affecting the abundance of well-characterized *Streptomyces* species (phylum Actinobacteria) as well as less-studied bacterial phyla such as Acidobacteria. High-throughput cultivation in microplates was implemented to isolate and identify these less-studied bacterial phylogenetic group. Amplicon sequencing confirmed that our method maintained the bacterial diversity of the environmental samples, enabling the isolation of novel Acidobacteriaceae and expanding the list of cultivated species to include two strains that may define new species within the genera *Terracidiphilus* and *Acidobacterium*.

Keywords: termites, *Coptotermes*, core microbiome, natural products discovery, Acidobacteria, underexplored phyla, social insects, termite-associated microbes

INTRODUCTION

Subterranean termites play a key role in the decomposition of plant biomass (Scheffrahn et al., 2015; Kuwahara et al., 2017). Their ingestion and degradation of wood can change the composition of soils and remodel entire landscapes (Bonachela et al., 2015). Furthermore, some termites cause damage valued at more than US\$ 22 billion p.a. by attacking wooden structures (Chouvenec et al., 2011; Chouvenec et al., 2016). The genus *Coptotermes* contains the largest number of economically destructive termite species (Scheffrahn et al., 2015), including *C. formosanus* (Su, 2003) and *C. gestroi* (Jenkins et al., 2007; Vargo and Husseneder, 2009), both of which are native to Asia but have spread to other areas as invasive pests. Furthermore, *C. testaceus* is the dominant termite species infesting living trees in the central Amazonian rain forests (Apolinário and Martius, 2004).

Termites are eusocial insects with worker, soldier and reproductive castes. Their social lifestyle includes allogrooming and trophallaxis, which requires frequent direct contact among individuals

and facilitates the spread of microbes (He et al., 2018). Accordingly, termites have evolved behaviors to prevent infections, such as the removal of corpses from the nest (Davis et al., 2018). Furthermore, more than 150 million years of coevolution has established a beneficial relationship between termites and their surrounding microbial community (Bourguignon et al., 2015; Legendre et al., 2015). These microbes not only facilitate the digestion of wood (Long et al., 2010; Poulsen et al., 2014; Wang et al., 2016), but also suppress the growth of entomopathogenic bacteria and fungi (Traniello et al., 2002; Chouvenc et al., 2013; Mevers et al., 2017).

Social insects—especially termites—are protected by parts of the symbiotic and stable microbiota, particularly natural products (NPs) producing organisms, therefore they are discussed as a fruitful source for NPs discovery (Klassen et al., 2019). Such specialized microbial communities are essential for the lifestyle of social insects (Audisio et al., 2005; Kaltenpoth, 2009; Chouvenc et al., 2018). For example, several actinomycete mutualists associated with leaf-cutting ants produce antifungal natural products such as dentigerumycin or antimycotic polyenes (Haeder et al., 2009; Devine et al., 2017). Similar mechanisms have been reported for higher and lower termites (Stroeymeyt et al., 2014; Benndorf et al., 2018). Termite soldiers not only prevent invasion by predators (Husseneder and Simms, 2014), but they also possess a broad range of chemical defense mechanisms including the production of antibacterial agents (Sobotnik et al., 2010; Terrapon et al., 2014; He et al., 2018). Bacteria that synthesize antimicrobial compounds have been isolated from the nest material of *C. formosanus* (Mevers et al., 2017; Chouvenc et al., 2018). Bacterial genera known to form symbiotic interactions with social insects include *Streptomyces* and *Pseudonocardia*, both of which are actinomycetes known to synthesize natural products (Chouvenc et al., 2013). However, termites are also associated with *Burkholderia* species, representing the well-characterized phylum Proteobacteria (Santos et al., 2004), as well as less-studied phyla with the potential to synthesize as yet unexplored natural products (Makonde et al., 2015; Su et al., 2016). A balanced consortium of beneficial microbes in the environment is therefore necessary to maintain the health of the colony (Chouvenc et al., 2011; Rosengaus et al., 2011; Peterson and Scharf, 2016).

Here we carried out a systematic analysis of the microbial core community at different levels in the nest of three *Coptotermes* species, revealing the stability of the core microbiome and its impact on colony fitness. Selected bacterial strains were enriched and cultivated in a high-throughput microplate-based format to gain insight into the roles of less-studied bacterial phyla that are generally underrepresented in culture, such as the Acidobacteria.

MATERIALS AND METHODS

Termite Ancestry, Rearing, and Sampling

Captive colonies of *C. testaceus* (\pm facing fungal burden), *C. formosanus* and *C. gestroi* were reared for more than 15 years at the Federal Institute for Materials Research and Testing in Berlin (BAM) in separate metal tanks with a volume of $\sim 2 \text{ m}^3$ (Supplementary Figure 1). *C. gestroi* was reared at

$26 \pm 2^\circ\text{C}$, $87 \pm 5\%$ relative humidity (RH), and was fed on birch wood, which was refreshed every 3 months. *C. testaceus* and *C. formosanus* were reared at $29 \pm 2^\circ\text{C}$, $75 \pm 5\%$ RH, and were fed on pine wood as above. All three species were identified based on their morphological characters (Scheffrahn et al., 2015).

Samples from the carton nest material of *C. testaceus* were collected at four different time points over 2 years. Sterile plastic spatulas were used to transfer 200–300 g of nest material into sterilized glass Petri dishes. At first, surface material was collected (surface), then wood pieces from feeding events from below the nest surface were placed aside and biofilms were sampled from the fresh eroded base of the wood pieces (wood) (Supplementary Figure 2). Autoclaved steel double spatulas were used to excavate sample material from the carton nest (carton nest). For all termite samples, first, filter carton paper traps were placed in the nests to separate the termite soldiers from the nest material. Using soft tweezers, the termite specimens were collected in 50 mL tubes and directly frozen (termites). All samples were frozen and stored at -50°C for processing and at 4°C for cultivation purposes.

Sample Processing and Environmental DNA Extraction From Nest Material and Termites

Nucleic acids were extracted using the NucleoSpin soil DNA purification kit (Macherey Nagel, Düren, Germany) to combine a gentle mechanical and chemical disruption of samples. To increase the yield, 200–500 mg of nest material or 12–28 termites as a whole were weighed into the NucleoSpin bead tubes before adding 700 μL of lysis buffer SL2. The tubes were vortexed horizontally for 15 min at 40 Hz using a Top Mix 11118 (Fisher Scientific, Schwerte, Germany) and then centrifuged at $12,000 \times g$ for 2 min. Thereby, the samples were mechanically broken and lysed. Subsequent extraction steps were carried out according to the manufacturer's recommendations. Finally, the yield and purity of the received DNA from the termites and from nest material was checked using a NanoDrop ND-1000 UV/Vis spectrophotometer (Thermo Fisher Scientific, Waltham, MA, United States). In the following, we will use the term environmental DNA (eDNA) for these DNA samples and differentiate between the origin (e.g., termites and nest material).

16S rRNA Gene Amplicon Sequencing and Data Processing

PCR amplification and Illumina 300 bp paired-end read sequencing of the eluted eDNA extracts were carried out by LGC Genomics (Berlin, Germany) using an Illumina (San Diego, CA, United States) MiSeq V3 system. The variable V3-V4 region was amplified using forward primer U341F (5'-CCT AYG GGR BGC ASC AG-3') and reverse primer U806R (5'-GGA CTA CNN GGG TAT CTA AT-3') (Klindworth et al., 2013). Data pre-processing, including the demultiplexing of all libraries, was carried out using Illumina bcl2fastq v1.8.4. Reads were sorted by amplicon inline barcodes unique to each sample, allowing one mismatch per barcode and discarding those with missing or one-sided barcodes or conflicting barcode pairs. Reads with a final length < 100 bases were discarded during the clipping of the

sequencing adapter from all reads. During primer detection and clipping, three mismatches were allowed per primer, and pairs of primers had to be present in each sequence fragment. If primer-dimers were detected, the outer primer copies were clipped from the sequence. The sequence fragments were converted to forward-reverse primer orientations after removing the primer sequences. The forward and reverse reads were combined using BBMerge v34.48¹.

Each read was aligned using the SILVA Incremental Aligner (SINA v1.2.10 for ARB SVN revision 21008) (Pruesse et al., 2012) against the SILVA SSU rRNA SEED and quality controlled (Quast et al., 2013). Reads < 300 aligned nucleotides and reads with >2% of ambiguities, or 2% of homopolymers, respectively, were excluded from further analysis. All reads containing a low alignment quality (50 alignment identity, 40 alignment score reported by SINA), were identified and excluded from downstream processing. After this quality control, identical reads were dereplicated, the unique reads were clustered (OTUs), on a per sample basis, and the reference read of each OTU was classified. Dereplication and clustering was done using cd-hit-est (version 3.1.2)² (Li and Godzik, 2006) running in accurate mode, ignoring overhangs, and applying identity criteria of 1.00 and 0.98, respectively.

Classification was achieved by running a local nucleotide BLAST search against the non-redundant version of the SILVA SSU Ref dataset release 132³ using blastn v2.2.30+⁴ with standard settings (Camacho et al., 2009).

The classification of each OTU reference read was mapped onto all reads that were assigned to the respective OTU. This yields quantitative information (number of individual reads per taxonomic path), within the limitations of PCR and sequencing technique biases, as well as, multiple rRNA operons. Reads without any BLAST hits or reads with weak BLAST hits, where the function “(% sequence identity + % alignment coverage)/2” did not exceed the value of 93, remained unclassified. These reads were assigned to the meta group “No Relative” in the SILVAngs fingerprint and Krona Charts (Ondov et al., 2011)⁵. Data were corrected by excluding all reads affiliated to Archaea (5.7%), chloroplasts (0.003%), mitochondria (0.003%), Eukaryota (3.4%), or *No Relative* (0.25%) from further analysis (9.35% excluded in total). Reads affiliated to the domain Bacteria were set to 100%.

Statistical Analysis

Statistical evaluation was carried out using PAST v3.18⁶ (Hammer et al., 2001) including non-metric multidimensional scaling (nMDS) (Taguchi and Oono, 2005) and one-way analysis of similarities (ANOSIM) via 9999 permutations with a statistical significance test (Clarke, 1993) at genus-level resolution for operational taxonomic units (OTUs) assigned to phylogenetic groups, representing clusters of uncultivated

bacteria or genera. ANOSIM and nMDS scores were computed using the Bray-Curtis similarity index. The calculations were used to illustrate the ratio between within-group and between-group dissimilarities of microbial communities associated with nest materials, termite samples, different sampling time points, before and after a 5 µm filtration step during Nycodenz density gradient centrifugation. A ternary plot and heat map charting the relative abundance of phylogenetic groups were used to find overlapping bacterial genera among the three *Coptotermes* species and to address which nest level represents the best source of underexplored bacterial phyla. We calculated diversity indices such as Chao 1, Shannon, dominance, and evenness, considering the number of phylogenetic groups and the number of individual reads per phylogenetic group to show similarities within the non-infected nest material and differences among all samples (Harper, 1999).

Retrieval of Living Cells From Nest Material Using Nycodenz Density Centrifugation

Living cells were retrieved from the *C. testaceus* carton nest material by density gradient centrifugation using a 60% (w/v) Nycodenz solution (Axis Shield, Dundee, United Kingdom) as previously described (Hevia et al., 2015). We transferred 1.0–2.0 g of nest material aseptically into four 50-mL tubes, and added 20 mL of autoclaved Milli-Q ultrapure water to each tube. The samples were homogenized three times at 225 Hz for 5 s using an S25 KD 18 G dispersal tool connected to an Ultra-Thurrax T25 basic (both provided by IKA Werke, Staufen im Breisgau, Germany) to a fineness of 10–50 µm. We added another 10 mL of Milli-Q ultrapure water to each tube and centrifuged briefly at 450 × g at 4°C using an A4-81 swing-out rotor (Eppendorf, Hamburg, Germany). We then transferred 25 mL of the debris-free supernatant to a fresh 50-mL tube. The homogenate was carefully underlain with the autoclaved 60% Nycodenz solution. The tubes were then centrifuged at 3,050 × g for 60 min at 4°C in a swing-out rotor without acceleration and deceleration to form the desired layer of bacteria (Berry et al., 2003). The layer containing the bacteria was passed through a 5-µm cellulose acetate Minisart syringe filter (Sartorius, Göttingen, Germany) and collected in a 5-mL reaction tube.

Cultivation Media

For the cultivation of Acidobacteria from the *C. testaceus* carton nest material, we used VL55 medium (de Castro et al., 2013) (DSMZ no. 1266) supplemented with 0.05% (w/v) xylan instead of glucose (Sait et al., 2002) and used FeCl₃·6 H₂O instead of FeCl₂·4 H₂O for trace element solution SL-10 (Tschech and Pfennig, 1984).

Microplate-Based Cultivation

To estimate the total number of cells per well, the Nycodenz cell phase was diluted 1,000-fold in phosphate buffered saline (PBS) and analyzed by flow cytometry on a FACSCalibur (BD Bioscience, San Jose, CA, United States) following the protocol of the Bacteria Counting Kit (B7277, Thermo Fisher Scientific)

¹<http://bbmap.sourceforge.net>

²<http://www.bioinformatics.org/cd-hit>

³<http://www.arb-silva.de>

⁴<http://blast.ncbi.nlm.nih.gov/Blast.cgi>

⁵<https://github.com/marbl/Krona/wiki>

⁶<https://folk.uio.no/ohammer/past/>

and visualized using FlowJo v10.4.2 (FlowJo, Ashland, OR, United States). Based on a combination of cell enumeration and the live/dead ratio, calculated using the LIVE/DEAD BacLight Bacterial Viability Kit (L34856, Thermo Fisher Scientific), 40 μ L of cell suspension containing an average of 40 cells was distributed using a Matrix WellMate (Thermo Fisher Scientific) into 64 \times 384-well microplates (Greiner Bio-One, Kremsmünster, Austria) minus the media controls on each plate (24,384 wells in total). Following incubation for up to 14 days at 28°C, 70 \pm 5% RH, growth was verified by measuring the optical density at 600 nm (OD₆₀₀) in a Wallac 1420 Victor2 Microplate Reader (Perkin Elmer, Waltham, MA, United States). The threshold was set by averaging the media controls on each plate to establish the media background. All cultures with verified growth were automatically transferred into 96-deepwell microplates (Corning, New York, NY, United States) pre-filled with 1.5 mL medium using a Precision XS liquid-handling system (BioTek Instruments, Bad Friedrichshall, Germany). Then, plates were incubated at 28°C using a Duetz System holder (Adolf Kühner, Birsfelden, Switzerland), shaking at 220 rpm with 2.5 cm deflection for 7 days.

Rapid Identification of Cultures by 16S rRNA Gene Sequencing

Culture broth from the above mentioned cultivation step was divided into aliquots for OD₆₀₀ measurements, DNA extraction, and cryo-conservation using the VIAFLO 384 system (Integra Biosciences, Zizers, Switzerland). Glycerol stocks were prepared by first pre-filling tubes with 300 μ L 80% glycerol using the Matrix Wellmate and then adding 200 μ L of culture broth. For DNA extraction, 200 μ L of broth was transferred to microtubes (Qiagen, Hilden, Germany) containing 2.3-mm zirconia beads (Carl Roth, Karlsruhe, Germany) and the cells were disrupted by 2 \times 1 min pulses at 30 Hz using a TissueLyser II (Qiagen). The tubes were centrifuged for 2 min at 4,000 \times g, incubated at 70°C for 45 min and centrifuged again as above. The supernatant was used for 16S rRNA gene amplification with primer pair E8F (5'-GAG TTT GAT CCT GGC TCA G-3') and 1492R (5'-ACG GYT ACC TTG TTA CGA CTT-3') (Lane, 1991).

Phylogenetic Classification of Isolated Acidobacteria

Liquid cultures affiliated to Acidobacteria via 16S rRNA sequencing (only using the reverse primer), were prioritized to obtain pure cultures. Thus, the liquid cultures were streaked onto solid VL55 medium containing 1.5% (w/v) agar no. 1 (Oxoid Deutschland, Wesel, Germany) and in parallel onto Reasoner's 2A medium (R2A) prepared from DSMZ no. 830 by reducing the pH to 5.5 using 1.95 g/L 2-(N-morpholino)ethanesulfonic acid (MES) (Sigma-Aldrich, St. Louis, MO, United States). The 16S rRNA gene sequence of FhG110202 was used to detect the 40 most similar sequences from the NCBI 16S ribosomal RNA sequences database using BLAST⁷. Multiple sequences were aligned using ClustalW with default parameters, including nearly

full-length 16S rRNA gene sequences of FhG110206, FhG110214 and representatives of different subgroups of Acidobacteria. The phylogenetic tree was calculated using MEGA v7.0.26⁸, by applying the maximum-likelihood method using the Tamura-Nei model (Kumar et al., 2016) with 1,000 bootstrap replications. We used iTOL v4.4.2⁹ for graphical modifications and annotations (Letunic and Bork, 2019).

RESULTS AND DISCUSSION

Experimental Rationale and Strategy

Termite nests maintained for decades at the BAM, offer a unique opportunity to assess a community of microbes, unaffected by abiotic factors. We were inspired by the hypothesis that a stable microbial composition confers protection on a colony and is an indicator of fitness among eusocial insects (Koch and Schmid-Hempel, 2011; Lanan et al., 2016). We compared the microbiomes of three *Coptotermes* species in order to (i) identify the bacterial core microbiome, (ii) analyze the stability of the bacterial community over time, (iii) observe any shifts in the composition when the termite colony was infected by fungi, and (iv) achieve the selective cultivation of underexplored bacterial phyla like Acidobacteria. Our main goal was to screen this resource for underexplored bacterial phyla like Acidobacteria, making them more accessible and thus facilitating the future analysis of their natural products. To this end, we applied a standardized, high-throughput cultivation approach and adapted the conditions to favor the recovery of underexplored and hard-to-cultivate phyla, focusing on the Acidobacteria (Crits-Christoph et al., 2018).

Bacterial Core Microbiome of Three Domesticated *Coptotermes* spp.

To characterize the core microbiomes of three *Coptotermes* species [*C. testaceus* (Ct), *C. formosanus* (Cf) and *C. gestroi* (Cg)] and their nest material, eDNA was isolated from the termites and from different levels of their nests [surface (S), wood (W), and carton nest (C)]. Three samples were taken from each nest level and from corresponding termites. Illumina amplicon sequencing of isolated eDNA yielded 4,724,006 sequences in total, 0.25% of which could not be classified and were defined as *No Relative*. Rarefaction analysis confirmed adequate coverage for statistical calculations (Supplementary Figure 3). Although the rearing temperature and type of wood provided as food differed between Cg and the other species, the termite and nest materials were highly comparable among all three species, with the different nest levels and termites (Figure 1 and Supplementary Figure 4).

Illumina amplicon sequencing revealed that sample *C. testaceus* surface (CtS) featured the greatest number of phylogenetic groups at the genus level (605) and sample *C. gestroi* termite (CgT) featured the least (242) (Table 1). To calculate the ratio between within-group and between-group dissimilarities a one-way ANOSIM was performed including all non-infected

⁷<https://www.ncbi.nlm.nih.gov/>

⁸<https://www.megasoftware.net>

⁹<https://itol.embl.de/>

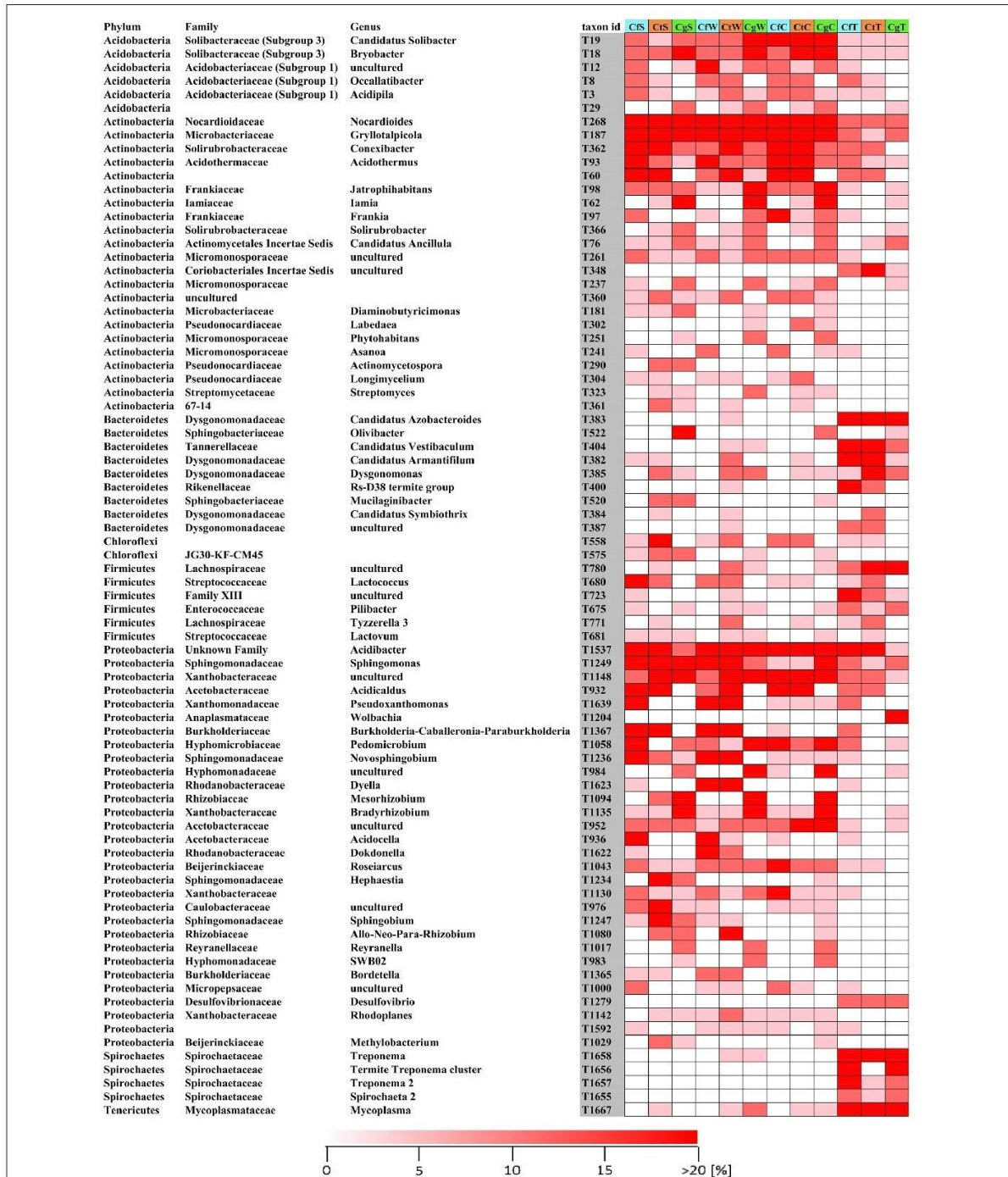


FIGURE 2 | Relative abundances of the 80 most abundant phylogenetic groups. Samples of nest material were collected from the surface, wood and carton nest ($n = 3$), and corresponding termites ($n \geq 12-23$) of three species (*C. formosanus*, *C. gestroi*, and *C. testaceus*). If the assignment of phylogenetic groups to the genus level was not possible it was left blank. Replicates were combined for visualization. Abundances indicate microbial communities shared among all nest levels or associated with termites. Ct, *C. testaceus*; Cg, *C. gestroi*; Cf, *C. formosanus*; C, carton nest material; W, wood material; S, surface; T, termite.

TABLE 1 | Richness and diversity indices based on amplicon sequencing data from termite and termite nest samples.

Termite species	Level	Number of sequences ^a	Number of phylogenetic groups ^b	Simpson ^c	Shannon ^d	Evenness ^e	Chao 1 ^f
<i>C. gestroi</i>	CgS	322,114	549	0.92	3.7	0.05	245
	CgW	318,647	549	0.93	3.6	0.06	221
	CgC	309,675	392	0.93	3.5	0.06	187
	CgT	210,185	242	0.78	2.3	0.03	128
<i>C. testaceus</i>	CtS	896,649	605	0.92	3.0	0.03	232
	CtW	218,641	432	0.95	3.6	0.06	146
	CtC	450,553	404	0.89	2.9	0.04	222
	CtT	306,701	260	0.68	2.3	0.03	125
<i>C. formosanus</i>	CfS	257,399	444	0.91	3.3	0.04	220
	CfW	231,098	392	0.91	3.2	0.05	212
	CfC	217,688	279	0.90	3.0	0.05	136
	CfT	174,613	277	0.75	2.6	0.04	150
Nycodenz	aT	139,879	241	0.85	2.3	0.06	169
	aF	245,690	438	0.90	3.0	0.05	110
Sampling time points	TP1	105,574	217	0.85	3.1	0.05	132
	TP2	35,320	204	0.90	2.4	0.05	196
	TP3	95,298	242	0.86	2.8	0.05	232
	TP4	53,558	275	0.89	2.6	0.05	152
<i>C. testaceus</i> nest material facing fungal burden	eS	34,709	442	0.97	4.2	0.20	325
	IS	100,015	483	0.90	3.4	0.12	238

Replicates of nest materials and termites were combined for analysis. Statistical analysis was performed using PAST v3.18.

Sample abbreviations: Ct, *C. testaceus*; Cg, *C. gestroi*; Cf, *C. formosanus*; C, carton nest material; W, wood material; S, surface; T, termite; TP, time point; aT, before 5 μ m filtration; aF, after 5 μ m filtration during Nycodenz density centrifugation; eS, early stage of fungal infection; IS, late stage of fungal infection.

^aTotal number of sequences per sample derived from Illumina sequencing.

^bTotal number of different phylogenetic groups in each sample.

^cSimpson index represents the diversity. If the value is 0, diversity is at zero level, whereas 1 is the highest.

^dShannon describes the diversity of the data and considers the abundance and number of phylogenetic groups.

^eEvenness represents the equal distribution of phylogenetic groups per sample: 0 = equal and 1 = unequal distribution.

^fEstimated species richness of each sample.

soil habitats (Zhang et al., 2019). To exclude the possibility that spore-forming actinomycetes were under-detected due to an experimental bias in eDNA isolation, the eDNA extraction method was evaluated using an actinomycete spore suspension. This confirmed the detection of actinomycete DNA and ruled out the artifactual exclusion of DNA from spore-forming bacteria (data not shown). Furthermore, nMDS analysis revealed overlaps in the composition of the surface, wood and carton nest microbiomes, suggesting that microbes are transferred within the nest. Compared to the other samples, the carton nest showed the least diverse bacterial microbiome, indicating a specialized bacterial composition (Figure 1 and Table 1).

The total proportion of Acidobacteria in all nest materials (mean = 6.4%, SE = 2.3) was higher than in the termites (mean = 1.5%, SE = 1.99). For example, the abundance of Acidobacteria in sample CtC (7.8%, SE = 2.2) was greater than in sample CtT (2.7%, SE = 2.8) (Supplementary Figure 4). The Acidobacteria in the nest material were also more diverse than those in the termites. The major subgroups of Acidobacteria present in CtC were subgroups 1 (35%), 3 (50%), and 4 (11%), whereas 2% of the reads could not be assigned to a specific subgroup (Supplementary Figure 5). Comparison of the termite and nest material samples revealed clearly distinguishable dissimilarities (Figures 1, 4).

Taken together, these experiments showed that all nest materials had similar diversity indices, indicating that the material was exposed to limited external influences and allowed a diverse microbial community to flourish. The taxonomic diversity of Acidobacteria (in terms of different subdivisions) was not greatly enhanced in CtC compared to the other nest materials, however, their nest material was selected for further investigation, because the statistical analysis and the abundance of Acidobacteria (7.8%, compared to a mean of 6.0%) made it a promising source for the isolation and cultivation of strains representing this phylum.

Stability of the *C. testaceus* Carton Nest Microbiome

Abiotic factors such as aeration, temperature and humidity, which are regulated by the architecture of termite nests, play a key role in microbiome stability (Marins et al., 2016). Among the various nest compartments, the carton nest is expected to contain the most adapted microbiota because it consists of salivary secretions and feces (Enagbonma et al., 2020). Furthermore, the carton nest is frequented by termites and protected from external contact except during feeding. We used the carton nest material as an accessible resource that enables routine sampling and the generation of comparative datasets over time. Therefore, we first investigated the temporal stability of the microbial community.

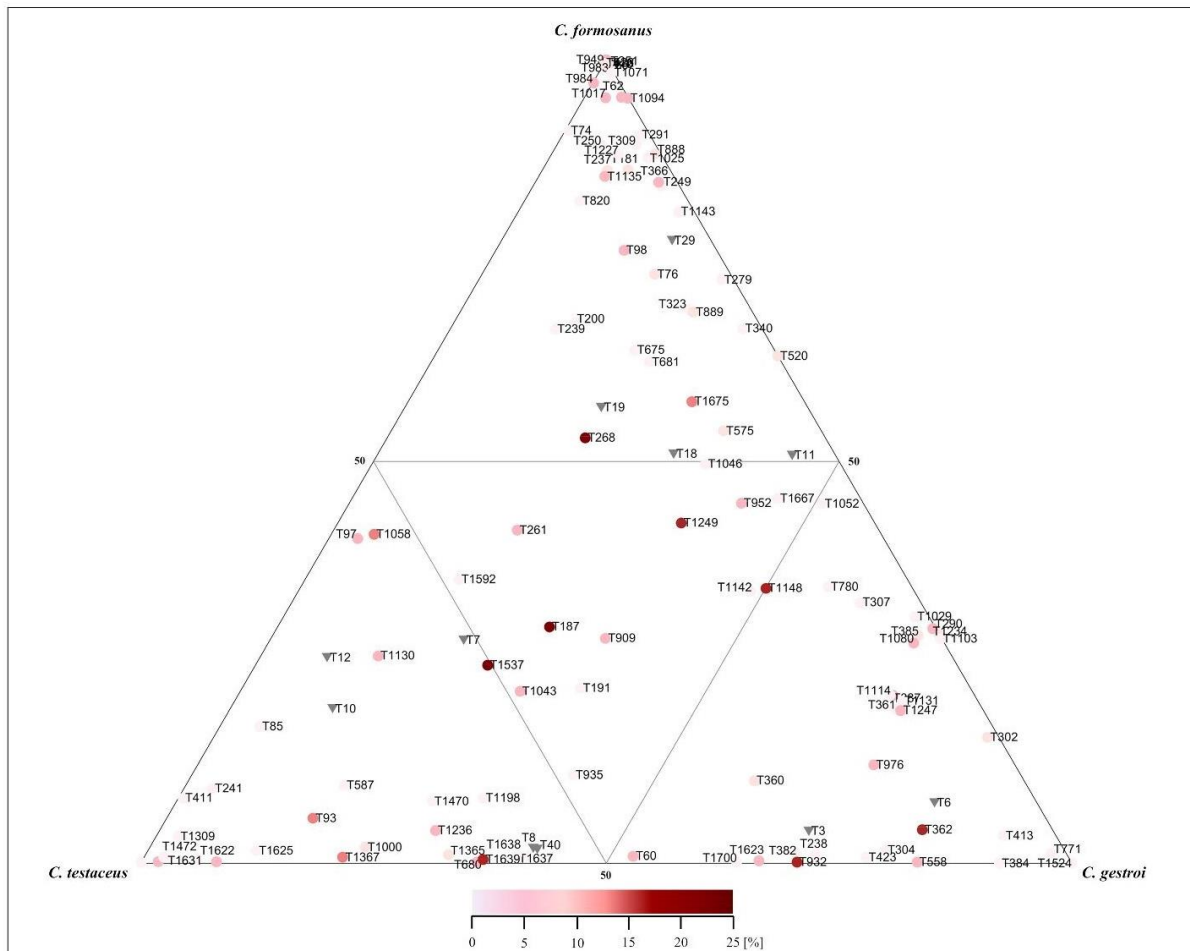


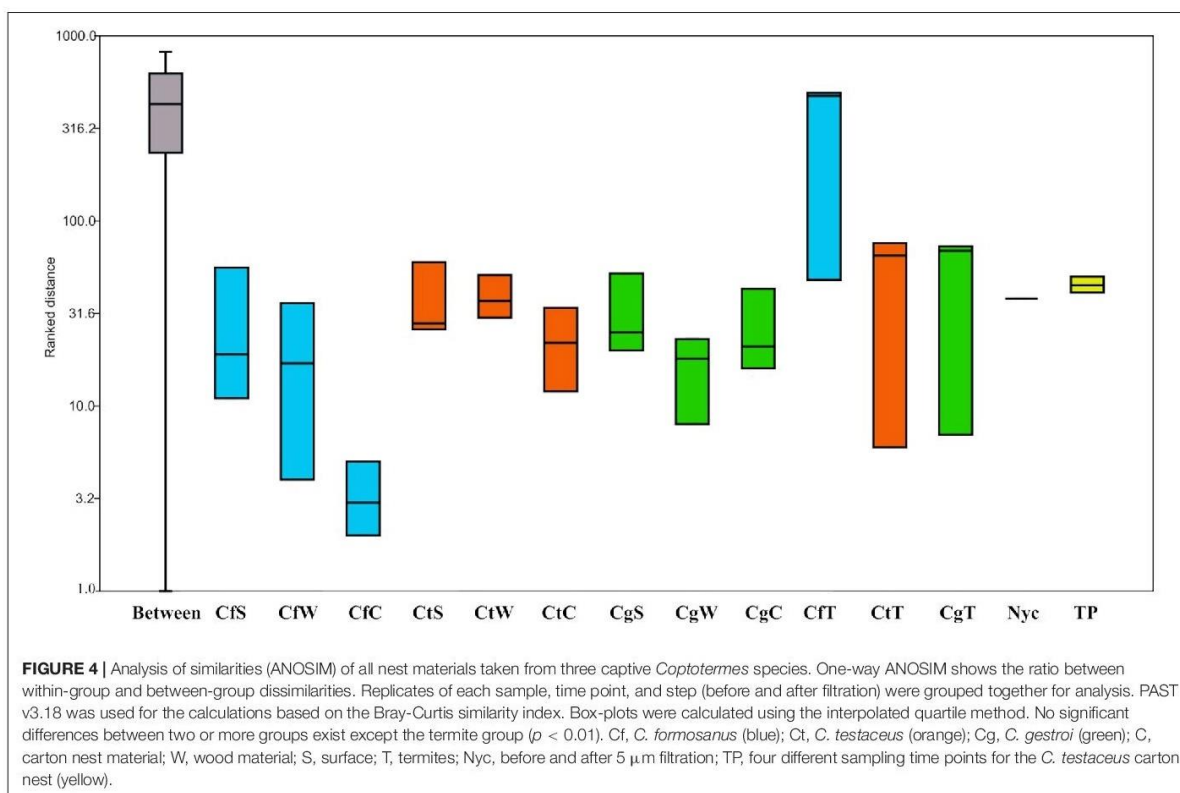
FIGURE 3 | Ternary plot of the relative abundances of shared bacterial phylogenetic groups among all nest materials of three domesticated *Coptotermes* species. Mean values of replicates ($n = 3$) from each nest level were combined. Only phylogenetic groups with a relative abundance $> 0.1\%$ in at least one nest were included in the analysis. Colors indicate the relative abundance per sample of each phylogenetic group as indicated by the scale bar. Shared phylogenetic groups with the same abundance appear in the inner triangle. Phylogenetic groups belonging to the phylum Acidobacteria are marked with inverse triangles. An assignment of each phylogenetic group is provided in **Supplementary Table S1**.

The *C. testaceus* carton nest material was assessed at four time points over a period of 2 years to determine the comparability and statistical robustness of the amplicon sequencing data (Figures 1, 4). Krona pie charts were constructed to compare the composition of the microbiomes over time (Supplementary Figure 6). The most abundant families were ranked as follows: Solirubrobacteraceae, Acetobacteraceae, Xanthobacteraceae, an unknown family of the class Gammaproteobacteria, Solibacteraceae, Acidobacteriaceae, Xipinematobacteraceae, Gemmataceae, Microbacteriaceae, Nocardioideae, IMCC26256 and Acidotermaceae. The stability of this microbial community was confirmed by their mean species evenness of 0.04 ($SE = 0.01$), their Shannon indices (Table 1), their nMDS scores (Figure 1), and the absence of significant changes identified by ANOSIM

($p > 0.05$, $R < 0.35$). The stability of the community is likely to be promoted by the unchanging abiotic and biotic conditions in the carton nest, including the constant temperature, humidity and light, and the consistent diet, which determines the activity of termites and the content of their secretions and excretions. The remarkable stability of the microbiome over time ensured that Acidobacteria were constantly present in the carton nest material.

Relationship Between Microbiome Stability and Termite Fitness

To determine whether the health status of termite populations has an effect on the stability of the microbiome, we studied a second *C. testaceus* nest at this time, which unintentionally suffered from a fungal infection that became progressively more

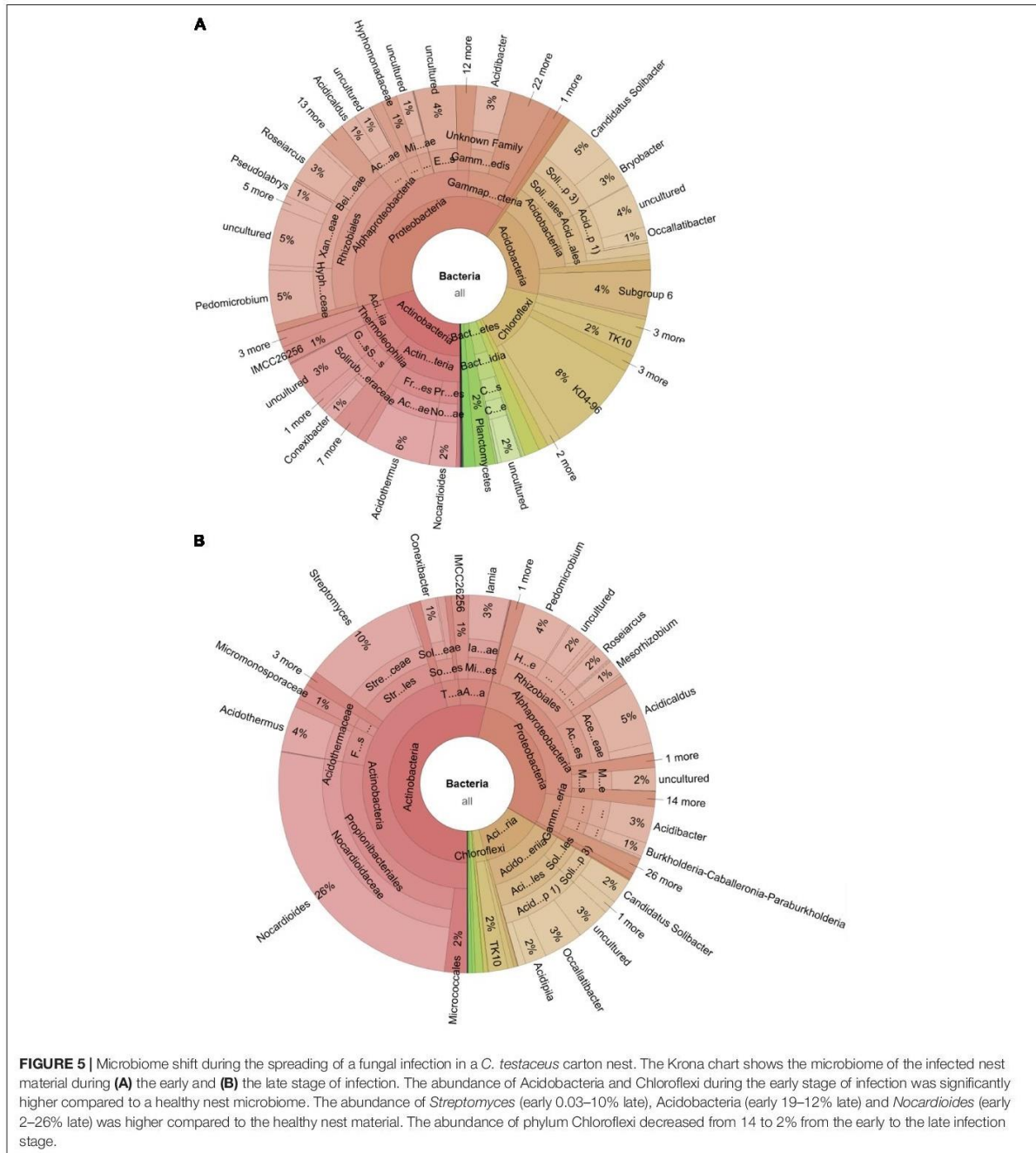


severe between sampling intervals (Supplementary Figure 7). Over time, the number of individual termites in the colony declined, ultimately to zero. No live specimens or even corpses were recovered from the nest material facing a fungal burden at the final sampling point. The microbiome of soldier termites retrieved from non-infected and infected showed little change during the early stages of infection (Supplementary Figure 8). In contrast, there was a remarkable shift in the composition of the nest material microbiome, with particular shifts in the abundance of Chloroflexi, Acidobacteria and the genus *Streptomyces* (Figure 5) compared to healthy nest material (Supplementary Figure 4). The abundance of *Streptomyces* spp. increased by more than 30-fold between the early and late stages of infection, which has been reported before in *C. formosanus* nests due to opportunistic mutualism between the termites and *Streptomyces* spp. with antifungal activity (Chouvenec et al., 2013, 2018). We also found that, during the early stage of infection, Acidobacteria were twice as abundant compared to uninfected nests (Figure 5 and Supplementary Figure 4). Accordingly, we surveyed Acidobacteria in the different *C. testaceus* nest compartments. The carton nest showed generally broad taxonomic diversity and was enriched for Acidobacteria and other underexplored phyla, such as members of the PVC superphylum (Wagner and Horn, 2006), which accounted for more than 10% of the bacterial consortium (Supplementary Figure 4). Genome and metagenome analysis

have shown that underexplored phyla such as Acidobacteria also carry biosynthetic gene clusters for the synthesis of specialized metabolites such as modified ribosomal peptides (Skinnider et al., 2016; Eichorst et al., 2018), polyketides, and non-ribosomal peptides (Crits-Christoph et al., 2018).

The comparative analysis of these gene clusters has shown a remarkable degree of genetic diversity compared to well-characterized gene clusters in other bacteria (Crits-Christoph et al., 2018). The genetic divergence among these clusters is often correlated with structural diversity of the corresponding secondary metabolites, providing confidence that such bacteria may lead to the discovery of new chemical entities (Medema et al., 2014). The opportunity to find gene clusters for secondary metabolism increases in bacteria with genome sizes exceeding 8 Mb (Baltz, 2017). The largest genome reported for a cultivated member of the phylum Acidobacteria is 9.9 Mb (Ward et al., 2009), whereas the mean size of the 23 published type strains of Acidobacteria¹⁰ genomes is ~5.2 Mb. Furthermore, horizontal gene transfer has been reported among the Acidobacteria, which indicates a potential to acquire functions with a defensive or regulatory advantage in their environment (Challacombe et al., 2011). For example, chitinolytic and cellulolytic activities are widespread among the Acidobacteria, which would be useful for the exploitation of

¹⁰<https://www.ezbiocloud.net/search?tn=acidobacteria>



nutritional niches in termite nests (Kielak et al., 2016; Belova et al., 2018). This may also benefit termites facing infections, as already reported for *Streptomyces* spp. associated with termite nest material (Carr et al., 2012; Chouvenec et al., 2018; Klassen et al., 2019). Although, Acidobacteria is the most abundant phylum in some habitats (Chan et al., 2006;

Weijers et al., 2009), fewer than 60 Acidobacteria strains have been cultivated thus far (Kielak et al., 2016), whereas four classes have been proposed with validly published names¹¹. Most of the isolates belong to subgroup 1, but still the

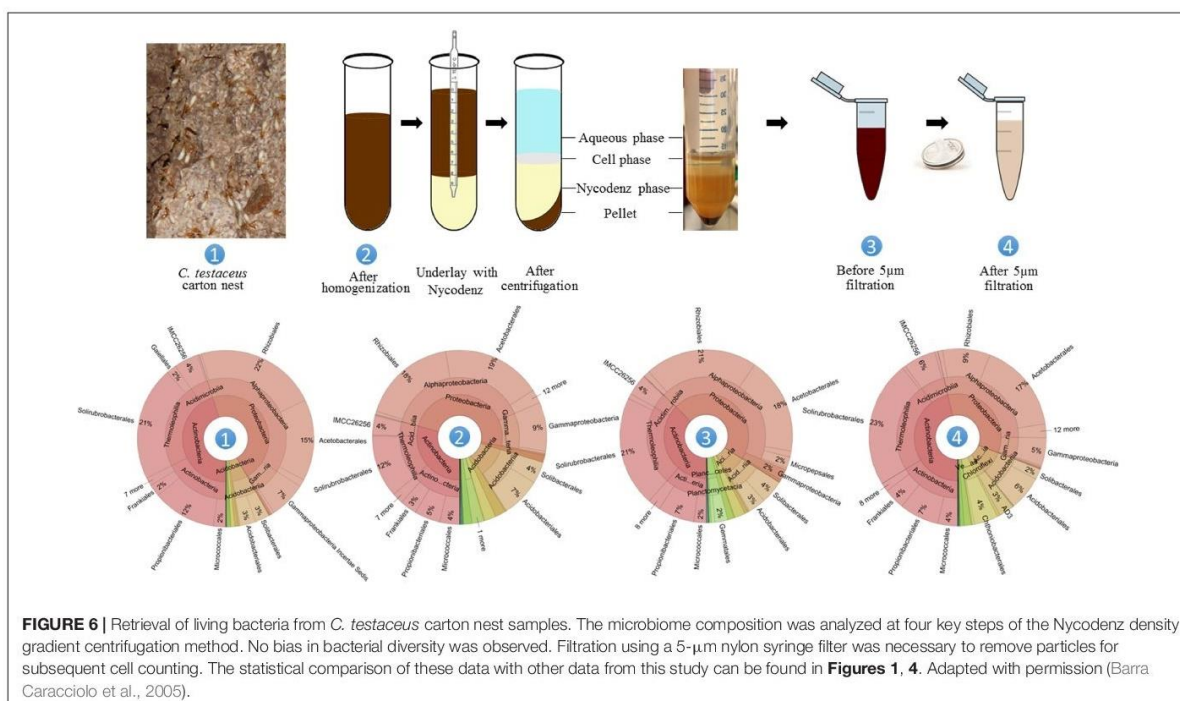
¹¹<https://psn.dsmz.de/phylum/acidobacteria>

number of available strains is only ~ 20 (Damste et al., 2017). A larger number of Acidobacteria strains with broader diversity must be made available in order to exploit their genetic and metabolic repertoire for natural product discovery. Given that the abundance of Acidobacteria doubled to 19% during the early stages of the fungal infection and that they remained more abundant (12%) than *Streptomyces* spp. (10%) even at the later stage (Figure 5), we sought to increase their general accessibility by a combination of targeted and high-throughput cultivation.

Targeted Cultivation and Phylogenetic Classification of Enriched Acidobacteria

The core bacterial community of the healthy *C. testaceus* carton nest material remained stable for 2 years. It showed broad taxonomic diversity but was enriched for Acidobacteria, and this phylum was further enriched by fungal infection. We chose the healthy *C. testaceus* carton nest material as the source for our targeted cultivation process to circumvent the fungal bias. To enable high-throughput cultivation, we used a small-scale microplate format. Thus, cells were retrieved based on Nycodenz density centrifugation used to enrich cells from complex environmental matrices, therefore, to enable subsequent cell enumeration via flow cytometry. Previous reports have indicated that using Nycodenz density centrifugation for soil samples can introduce bias (Holmsgaard et al., 2011). However, this may reflect the sample origin, given that the same method did not affect cell viability, or the distribution and proportion of the microbial community, during the analysis of fecal samples

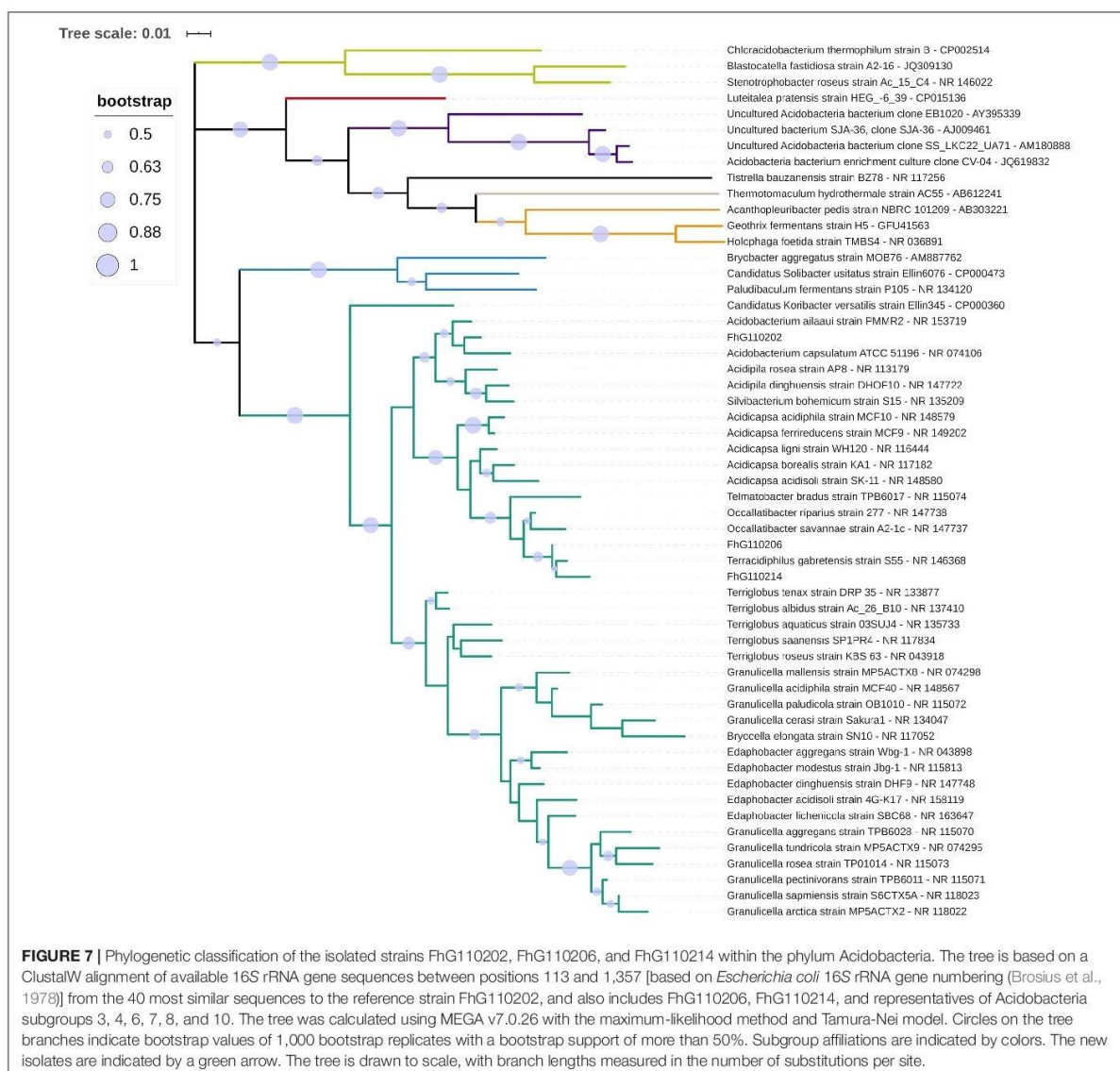
(Hevia et al., 2015). Accordingly, we first evaluated our adapted method to determine whether the retrieval of living cells from termite nest matrices influenced the composition of the bacterial community. We compared crude nest material with a homogenate and with cell layers before and after filtration (Figure 6). Statistical analysis using ANOSIM of the amplicon data revealed no significant shift in the bacterial community ($p > 0.1$), which was supported by bacterial composition analysis (Figure 6). Furthermore, nMDS analysis confirmed that the pivotal steps before and after filtration in the Nycodenz gradient centrifugation protocol are similar compared to the *C. testaceus* carton nest samples (Figure 1). The material was passed through a 5- μm syringe filter to separate cells from residual matrix particles. This is necessary for accurate cell counting by FACS, otherwise particles of the nest matrix can produce background noise. Following this treatment, the composition of the bacterial community (Supplementary Figure 4), the Shannon index (Table 1), and the ANOSIM and nMDS clustering profiles, indicated no remarkable changes (Figure 1). Indeed, the cell suspension derived from the Nycodenz and filtration steps were similar to the untreated nest material samples of *C. testaceus* (aF and aT, Figure 1). This confirms that the procedure we used was able to extract living cells from termite nest material with negligible experimental bias, and our target phylum was reliably extracted from the matrix (Figure 6). In the next step, cells were counted by staining with SYTO9 followed by analysis using flow cytometry, which indicated a total cell concentration (living and dead) of $\sim 8 \times 10^8$ cells/mL (Supplementary Figure 9).



Based on earlier studies concerning the success of cultivating bacteria from environmental samples (Epstein, 2013; Ling et al., 2015), and taking the live/dead ratio (~70:30) into account, we estimated that ~40 cells should be distributed into each well of a 384-well plate containing 40 μ L of medium per well. This was based on the assumption that only a small fraction would be able to grow in the synthetic VL55 medium (pH 5.5) supplemented with xylan as the only carbon source, a medium already shown to be suitable for the cultivation of Acidobacteria (Campanharo et al., 2016). This medium suppresses the growth of bacteria that cannot grow on complex carbon sources at low pH, and therefore favors the growth of the majority of Acidobacteria (Belova et al., 2018; de Chaves et al., 2019). Furthermore, Acidobacteria appear

to thrive when presented with a lower concentration of trace elements than normally found in complex media (de Chaves et al., 2019). An additional advantage of the process described here is its ability to propagate the cultures quickly in order to reduce the risk of competition from faster-growing bacteria that take longer to become established due to the chosen medium, such as certain Proteobacteria (George et al., 2011; Campanharo et al., 2016).

Following the pipeline, 4,291 wells in total were re-inoculated from 384- to 96-deepwell microplates. After seven days of incubation, 4,028 wells were determined as grown via turbidimetry (93.9%). In total, 3,456 individual cultures (85.8%) were successfully sequenced via 16S rRNA gene sequencing (Sanger method, using the reverse primer only).



Among these, 235 wells (6.8%) were affiliated with the target phylum Acidobacteria. After reduction for redundancy—based on 16S rRNA sequencing (Sanger method, using forward and reverse primer)—the unique wells were propagated onto agar plates. Finally, four unique strains were isolated. However, only three could be propagated furthermore and were therefore integrated into our strain collection with the IDs FhG110202, FhG110206, and FhG110214.

The phylogenetic classification of the three strains within the phylum Acidobacteria based on nearly full-length 16S rRNA gene sequences revealed their assignment to three different genera within subgroup 1 (Figure 7). FhG110202 was most closely related to the type strain of *Acidobacterium ailaui* (97.7%), a bacterium that was isolated from a geothermally active microbial mat on Hawaii (Myers and King, 2016). FhG110214 was most closely related to *Terracidiphilus gabretensis* (97.1%), which was isolated from a boreal forest in a Czech national park (Garcia-Fraile et al., 2016). FhG110206 was most closely related to *T. gabretensis* (98.9%), *Occalibacter riparius* (98.4%), and FhG110214 (97.9%). A sequence identity threshold of 98.65% indicates species differentiation (Kim et al., 2014). The sequence identity between the 16S rRNA genes of FhG110214 and strain of *T. gabretensis* S55^T (97.1%), and FhG110202 and strain of *A. ailaui* PMMR2T^T (97.7% identity), suggests that further experiments should be carried out to determine whether those strains represent new species.

Further investigations should also be carried out to determine the beneficial role of Acidobacteria for xylophagous *Coptotermes* spp. in terms of their potential to produce natural products cohering with their enrichment during the early and late stages of a fungal infection such as *Streptomyces*. Our work therefore adds to the number of strains from the interesting phylum of Acidobacteria that are available for further analysis.

CONCLUSION

In this study, we evaluated the use of laboratory-bred termite colonies (*Coptotermes* spp.) and their nest materials as bioresources for the isolation of underexplored Acidobacteria, which are currently difficult to access or cultivate with sufficient diversity for bioprospecting. This is a key requirement because the likelihood of discovering new chemical entities is thought to be higher in underexplored phyla compared to classical phylogenetic groups that are already known to synthesize natural products. Our in-depth analysis at the genus level of microbial communities associated with three different termite species revealed the carton nest as the best source of Acidobacteria, with a 10-fold enrichment compared to the termites themselves. The microbial community showed high temporal stability in the healthy colony but underwent a profound shift during the late stage of a fungal infection favoring the proliferation of *Streptomyces* spp. and Acidobacteria. In summary, we applied a high-throughput cultivation process adapted to the metabolic repertoire of Acidobacteria. This led to the successful isolation of three novel strains of Acidobacteria, which may shed light on their biological relationship with

xylophagous lower termites due to their accessibility for natural product discovery.

DATA AVAILABILITY STATEMENT

The datasets generated for this study can be found in the following online repositories. The data can be accessed under the BioProject PRJNA657759 and the 16S rRNA sequences can be accessed under following numbers: MT895693, MT898545, and MT895791 (<https://www.ncbi.nlm.nih.gov/genbank/>).

AUTHOR CONTRIBUTIONS

MO, MS, and JG conceived and designed the experiments. JG initiated the isolation of Acidobacteria. MO, CZ, TC, MS, BL, and SM contributed to the cultivation and isolation experiments. MO, CZ, TS, JG, and SG analyzed the data. BL and MO implemented the liquid handling processes. MO drafted the first manuscript. RP and DM were responsible for the rearing, supply of termites, and revised the manuscript. MO, TC, JG, and RP performed sampling campaigns. TS, PH, and AV organized the manuscript writing. JG and TS supervised the research, helped to draft the manuscript, and revised it. AV acquired funding from the state of Hesse. AV and PH initiated the public-private partnership between Fraunhofer and Sanofi. All authors contributed to the article and approved the submitted version.

FUNDING

This work was financially supported by the Hessen State Ministry of Higher Education, Research and the Arts (HMWK) via the state initiative for the development of scientific and economic excellence for the LOEWE Center for Insect Biotechnology and Bioresources. Sanofi-Aventis Deutschland GmbH and Evotec International funded this work in the framework of the Sanofi-Fraunhofer Natural Products Center and its follow up, the Fraunhofer-Evotec Natural Products Center of Excellence.

ACKNOWLEDGMENTS

We thank Richard M. Twyman for proofreading the manuscript and Ivonne de Laval (BAM) for her contribution to rearing the termites. Special thanks to Luigi Toti for helpful discussions regarding cultivation techniques and thanks to Mareike Rothenheber and Jennifer Kuhn for their technical support in our laboratory.

SUPPLEMENTARY MATERIAL

The Supplementary Material for this article can be found online at: <https://www.frontiersin.org/articles/10.3389/fmicb.2020.597628/full#supplementary-material>

Supplementary Table 1 | Taxonomic classification and the respective calculated relative abundance using Illumina amplicon sequencing data and additionally the SILVAngs v1.3 analysis pipeline.

REFERENCES

- Apolinário, F. E., and Martius, C. (2004). Ecological role of termites (*Insecta, Isoptera*) in tree trunks in central Amazonian rain forests. *For. Ecol. Manag.* 194, 23–28. doi: 10.1016/j.foreco.2004.01.052
- Audisio, M. C., Terzolo, H. R., and Apella, M. C. (2005). Bacteriocin from honeybee beebread *Enterococcus avium*, active against *Listeria monocytogenes*. *Appl. Environ. Microbiol.* 71, 3373–3375. doi: 10.1128/AEM.71.6.3373-3375.2005
- Baltz, R. H. (2017). Gifted microbes for genome mining and natural product discovery. *J. Ind. Microbiol. Biotechnol.* 44, 573–588. doi: 10.1007/s10295-016-1815-x
- Barra Caracciolo, A., Grenni, P., Cupo, C., and Rossetti, S. (2005). In situ analysis of native microbial communities in complex samples with high particulate loads. *FEMS Microbiol. Lett.* 253, 55–58. doi: 10.1016/j.femsle.2005.09.018
- Belova, S. E., Ravin, N. V., Pankratov, T. A., Rakitin, A. L., Ivanova, A. A., Beletsky, A. V., et al. (2018). Hydrolytic capabilities as a key to environmental success: chitinolytic and cellulolytic *Acidobacteria* from acidic sub-arctic soils and boreal peatlands. *Front. Microbiol.* 9:2775. doi: 10.3389/fmicb.2018.02775
- Bennndorf, R., Guo, H., Sommerwerk, E., Weigel, C., Garcia-Altare, M., Martin, K., et al. (2018). Natural products from actinobacteria associated with fungus-growing termites. *Antibiotics* 7:83. doi: 10.3390/antibiotics7030083
- Berry, A. E., Chiochini, C., Selby, T., Sosio, M., and Wellington, E. M. H. (2003). Isolation of high molecular weight DNA from soil for cloning into BAC vectors. *FEMS Microbiol. Lett.* 223, 15–20. doi: 10.1016/s0378-1097(03)00248-9
- Bonachela, J. A., Pringle, R. M., Sheffer, E. T., Coverdale, C., Guyton, J. A., Caylor, K. K., et al. (2015). Termite mounds can increase the robustness of dryland ecosystems to climatic change. *Science* 347, 651–655. doi: 10.1126/science.1261487
- Bourguignon, T., Lo, N., Cameron, S. L., Sobotnik, J., Hayashi, Y., Shigenobu, S., et al. (2015). The evolutionary history of termites as inferred from 66 mitochondrial genomes. *Mol. Biol. Evol.* 32, 406–421. doi: 10.1093/molbev/msu308
- Brosius, J., Palmer, M. L., Kennedy, P. J., and Noller, H. F. (1978). Complete nucleotide sequence of a 16S ribosomal RNA gene from *Escherichia coli*. *Proc. Natl. Acad. Sci. U.S.A.* 75, 4801–4805. doi: 10.1073/pnas.75.10.4801
- Brune, A., and Dietrich, C. (2015). The gut microbiota of termites: digesting the diversity in the light of ecology and evolution. *Annu. Rev. Microbiol.* 69, 145–166. doi: 10.1146/annurev-micro-092412-155715
- Camacho, C., Coulouris, G., Avagyan, V., Ma, N., Papadopoulos, J., Bealer, K., et al. (2009). BLAST+: architecture and applications. *BMC Bioinformatics* 10:421. doi: 10.1186/1471-2105-10-421
- Campanharo, J. C., Kielak, A. M., Castellane, T. C., Kuramae, E. E., and Lemos, E. G. (2016). Optimized medium culture for *Acidobacteria* subdivision 1 strains. *FEMS Microbiol. Lett.* 363:fnw245. doi: 10.1093/femsle/fnw245
- Carr, G., Poulsen, M., Klassen, J. L., Hou, Y., Wyche, T. P., Bugni, T. S., et al. (2012). Microtermolides A and B from termite-associated *Streptomyces* sp. and structural revision of vinylamycin. *Org. Lett.* 14, 2822–2825. doi: 10.1021/ol301043p
- Challacombe, J. F., Eichorst, S. A., Hauser, L., Land, M., Xie, G., and Kuske, C. R. (2011). Biological consequences of ancient gene acquisition and duplication in the large genome of *Candidatus Solibacter usitatus* Ellin6076. *PLoS One* 6:e24882. doi: 10.1371/journal.pone.0024882
- Chan, O. C., Yang, X., Fu, Y., Feng, Z., Sha, L., Casper, P., et al. (2006). 16S rRNA gene analyses of bacterial community structures in the soils of evergreen broad-leaved forests in south-west China. *FEMS Microbiol. Ecol.* 58, 247–259. doi: 10.1111/j.1574-6941.2006.00156.x
- Chouvenc, T., Efstathiou, C. A., Elliott, M. L., and Su, N. Y. (2013). Extended disease resistance emerging from the faecal nest of a subterranean termite. *Proc. Biol. Sci.* 280:20131885. doi: 10.1098/rspb.2013.1885
- Chouvenc, T., Elliott, M. L., Sobotnik, J., Efstathiou, C. A., and Su, N. Y. (2018). The termite fecal nest: a framework for the opportunistic acquisition of beneficial soil *Streptomyces* (*Actinomycetales: Streptomycetaceae*). *Environ. Entomol.* 47, 1431–1439. doi: 10.1093/ee/nvy152
- Chouvenc, T., Li, H.-F., Austin, J., Bordereau, C., Bourguignon, T., Cameron, S. L., et al. (2016). Revisiting *Coptotermes* (*Isoptera: Rhinotermitidae*): a global taxonomic road map for species validity and distribution of an economically important subterranean termite genus. *Syst. Entomol.* 41, 299–306. doi: 10.1111/syen.12157
- Chouvenc, T., Su, N.-Y., and Kenneth Grace, J. (2011). Fifty years of attempted biological control of termites – Analysis of a failure. *Biol. Control* 59, 69–82. doi: 10.1016/j.biocontrol.2011.06.015
- Clarke, K. R. (1993). Non-parametric multivariate analysis of changes in community structure. *Austral. J. Ecol.* 18, 117–143. doi: 10.1111/j.1442-9993.1993.tb00438.x
- Crits-Christoph, A., Diamond, S., Butterfield, C. N., Thomas, B. C., and Banfield, J. F. (2018). Novel soil bacteria possess diverse genes for secondary metabolite biosynthesis. *Nature* 558, 440–444. doi: 10.1038/s41586-018-0207-y
- Damste, J. S. S., Rijpstra, W. I. C., Dedysh, S. N., Foesel, B. U., and Villanueva, L. (2017). Pheno- and genotyping of hopanoid production in *Acidobacteria*. *Front. Microbiol.* 8:968. doi: 10.3389/fmicb.2017.00968
- Davis, H. E., Meconcelli, S., Radek, R., and McMahon, D. P. (2018). Termites shape their collective behavioural response based on stage of infection. *Sci. Rep.* 8:14433. doi: 10.1038/s41598-018-32721-7
- de Castro, V. H. L., Schroeder, L. F., Quirino, B. F., Kruger, R. H., and Barreto, C. C. (2013). *Acidobacteria* from oligotrophic soil from the Cerrado can grow in a wide range of carbon source concentrations. *Can. J. Microbiol.* 59, 746–753. doi: 10.1139/cjm-2013-0331
- de Chaves, M. G., Silva, G. G. Z., Rossetto, R., Edwards, R. A., Tsai, S. M., and Navarrete, A. A. (2019). *Acidobacteria* subgroups and their metabolic potential for carbon degradation in sugarcane soil amended with vinasse and nitrogen fertilizers. *Front. Microbiol.* 10:1680. doi: 10.3389/fmicb.2019.01680
- Devine, R., Hutchings, M. I., and Holmes, N. A. (2017). Future directions for the discovery of antibiotics from actinomycete bacteria. *Emerg. Top. Life Sci.* 1, 1–12. doi: 10.1042/etls20160014
- Dietrich, C., Köhler, T., and Brune, A. (2014). The cockroach origin of the termite gut microbiota: patterns in bacterial community structure Reflect major evolutionary events. *Appl. Environ. Microbiol.* 80, 2261–2269. doi: 10.1128/aem.04206-13
- Do, T. H., Nguyen, T. T., Nguyen, T. N., Le, Q. G., Nguyen, C., Kimura, K., et al. (2014). Mining biomass-degrading genes through Illumina-based de novo sequencing and metagenomic analysis of free-living bacteria in the gut of the lower termite *Coptotermes gestroi* harvested in Vietnam. *J. Biosci. Bioeng.* 118, 665–671. doi: 10.1016/j.jbiosc.2014.05.010
- Eichorst, S. A., Trojan, D., Roux, S., Herbold, C., Rattei, T., and Wobken, D. (2018). Genomic insights into the *Acidobacteria* reveal strategies for their success in terrestrial environments. *Environ. Microbiol.* 20, 1041–1063. doi: 10.1111/1462-2920.14043
- Enagonnola, B. J., Ajillogba, C. F., and Babalola, O. O. (2020). Metagenomic profiling of bacterial diversity and community structure in termite mounds and surrounding soils. *Arch. Microbiol.* 202, 2697–2709. doi: 10.1007/s00203-020-01994-w
- Epstein, S. S. (2013). The phenomenon of microbial uncultivability. *Curr. Opin. Microbiol.* 16, 636–642. doi: 10.1016/j.mib.2013.08.003
- García-Fraile, P., Benada, O., Cajthaml, T., Baldrian, P., and Llado, S. (2016). *Terracidiphilus gabretensis* gen. nov., sp. nov., an abundant and active forest soil acidobacterium important in organic matter transformation. *Appl. Environ. Microbiol.* 82, 560–569. doi: 10.1128/AEM.03353-15
- George, I. F., Hartmann, M., Liles, M. R., and Agathos, S. N. (2011). Recovery of as-yet-uncultured soil *Acidobacteria* on dilute solid media. *Appl. Environ. Microbiol.* 77, 8184–8188. doi: 10.1128/AEM.05956-11
- Haeder, S., Wirth, R., Herz, H., and Spittler, D. (2009). Candicidin-producing *Streptomyces* support leaf-cutting ants to protect their fungus garden against the pathogenic fungus *Escovopsis*. *Proc. Natl. Acad. Sci. U.S.A.* 106, 4742–4746. doi: 10.1073/pnas.0812082106
- Hammer, Ø, Harper, D. A. T., and Ryan, P. D. (2001). PAST: paleontological statistics software package for education and data analysis. *Palaeontol. Electron.* 4, 1–9.
- Harper, D. A. T. (ed.). (1999). *Numerical Palaeobiology*. New York: John Wiley & Sons.
- He, S., Johnston, P. R., Kurokawa, B., Lokatis, S., Weise, C., Plarre, R., et al. (2018). Termite soldiers contribute to social immunity by synthesizing potent oral secretions. *Insect Mol. Biol.* 27, 564–576. doi: 10.1111/imb.12499
- Hevia, A., Delgado, S., Margolles, A., and Sanchez, B. (2015). Application of density gradient for the isolation of the fecal microbial stool component and the potential use thereof. *Sci. Rep.* 5:16807. doi: 10.1038/srep16807

- Holmsgaard, P. N., Norman, A., Hede, S. C., Poulsen, P. H. B., Al-Soud, W. A., Hansen, L. H., et al. (2011). Bias in bacterial diversity as a result of Nycodenz extraction from bulk soil. *Soil Biol. Biochem.* 43, 2152–2159. doi: 10.1016/j.soilbio.2011.06.019
- Hongoh, Y., Sharma, V. K., Prakash, T., Noda, S., Toh, H., Taylor, T. D., et al. (2008). Genome of an endosymbiont coupling N₂ fixation to cellulolysis within protist cells in termite gut. *Science* 322, 1108–1109. doi: 10.1126/science.1165578
- Husseneder, C., and Simms, D. M. (2014). Effects of caste on the expression of genes associated with septic injury and xenobiotic exposure in the Formosan subterranean termite. *PLoS One* 9:e105582. doi: 10.1371/journal.pone.0105582
- Jenkins, T. M., Jones, S. C., Lee, C. Y., Forschler, B. T., Chen, Z., Lopez-Martinez, G., et al. (2007). Phylogeography illuminates maternal origins of exotic *Coptotermes gestroi* (Isoptera: Rhinotermitidae). *Mol. Phylogenet. Evol.* 42, 612–621. doi: 10.1016/j.ympev.2006.11.024
- Kaltenpoth, M. (2009). Actinobacteria as mutualists: general healthcare for insects? *Trends Microbiol.* 17, 529–535. doi: 10.1016/j.tim.2009.09.006
- Kielak, A. M., Barreto, C. C., Kowalchuk, G. A., van Veen, J. A., and Kuramae, E. E. (2016). The ecology of *Acidobacteria*: moving beyond genes and genomes. *Front. Microbiol.* 7:744. doi: 10.3389/fmicb.2016.00744
- Kim, M., Oh, H. S., Park, S. C., and Chun, J. (2014). Towards a taxonomic coherence between average nucleotide identity and 16S rRNA gene sequence similarity for species demarcation of prokaryotes. *Int. J. Syst. Evol. Microbiol.* 64(Pt 2), 346–351. doi: 10.1099/ijs.0.059774-0
- King, J. H., Mahadi, N. M., Bong, C. F., Ong, K. H., and Hassan, O. (2014). Bacterial microbiome of *Coptotermes curvignathus* (Isoptera: Rhinotermitidae) reflects the coevolution of species and dietary pattern. *Insect Sci.* 21, 584–596. doi: 10.1111/1744-7917.12061
- Klassen, J. L., Lee, S. R., Poulsen, M., Beemelmans, C., and Kim, K. H. (2019). Efomycins K and L From a termite-associated *Streptomyces* sp. m56 and their putative biosynthetic Origin. *Front. Microbiol.* 10:1739. doi: 10.3389/fmicb.2019.01739
- Klindworth, A., Pruesse, E., Schweer, T., Peplies, J., Quast, C., Horn, M., et al. (2013). Evaluation of general 16S ribosomal RNA gene PCR primers for classical and next-generation sequencing-based diversity studies. *Nucleic Acids Res.* 41:e1. doi: 10.1093/nar/gks808
- Koch, H., and Schmid-Hempel, P. (2011). Socially transmitted gut microbiota protect bumble bees against an intestinal parasite. *Proc. Natl. Acad. Sci. U.S.A.* 108, 19288–19292. doi: 10.1073/pnas.1110474108
- Kumar, S., Stecher, G., and Tamura, K. (2016). MEGA7: molecular evolutionary genetics analysis version 7.0 for bigger datasets. *Mol. Biol. Evol.* 33, 1870–1874. doi: 10.1093/molbev/msw054
- Kuwahara, H., Yuki, M., Izawa, K., Ohkuma, M., and Hongoh, Y. (2017). Genome of 'Ca. Desulfobivrio trichonymphae', an H₂-oxidizing bacterium in a tripartite symbiotic system within a protist cell in the termite gut. *ISME J.* 11, 766–776. doi: 10.1038/ismej.2016.143
- Lanan, M. C., Rodrigues, P. A., Agellon, A., Jansma, P., and Wheeler, D. E. (2016). A bacterial filter protects and structures the gut microbiome of an insect. *ISME J.* 10, 1866–1876. doi: 10.1038/ismej.2015.264
- Lane, D. J. (1991). "16S/23S rRNA sequencing," in *Nucleic Acid Techniques in Bacterial Systematics*, eds E. Stackebrandt and M. Goodfellow (New York, NY: Wiley), 115–175.
- Legendre, F., Nel, A., Svenson, G. J., Robillard, T., Pellens, R., and Grandcolas, P. (2015). Phylogeny of dictyoptera: dating the origin of cockroaches, praying mantises and termites with molecular data and controlled fossil evidence. *PLoS One* 10:e0130127. doi: 10.1371/journal.pone.0130127
- Letunic, I., and Bork, P. (2019). Interactive Tree Of Life (iTOL) v4: recent updates and new developments. *Nucleic Acids Res.* 47, W256–W259. doi: 10.1093/nar/gkz239
- Li, W., and Godzik, A. (2006). Cd-hit: a fast program for clustering and comparing large sets of protein or nucleotide sequences. *Bioinformatics* 22, 1658–1659. doi: 10.1093/bioinformatics/btl158
- Ling, L. L., Schneider, T., Peoples, A. J., Spoering, A. L., Engels, L., Conlon, B. P., et al. (2015). A new antibiotic kills pathogens without detectable resistance. *Nature* 517, 455–459. doi: 10.1038/nature14098
- Long, Y.-H., Xie, K., Liu, N., Yan, X., Li, M.-H., Fan, M.-Z., et al. (2010). Comparison of gut-associated and nest-associated microbial communities of a fungus-growing termite (*Odontotermes yunnanensis*). *Insect Sci.* 17, 265–276. doi: 10.1111/j.1744-7917.2010.01327.x
- Makonde, H. M., Mwirichia, R., Osiemo, Z., Boga, H. I., and Klenk, H. P. (2015). 454 Pyrosequencing-based assessment of bacterial diversity and community structure in termite guts, mounds and surrounding soils. *Springerplus* 4:471. doi: 10.1186/s40064-015-1262-6
- Marins, A., Costa, D., Russo, L., Campbell, C., Desouza, O. G., Björnstad, O. N., et al. (2016). Termite cohabitation: the relative effect of biotic and abiotic factors on mound biodiversity. *Ecol. Entomol.* 41, 532–541. doi: 10.1111/een.12323
- Medema, M. H., Cimermancic, P., Sali, A., Takano, E., and Fischbach, M. A. (2014). A systematic computational analysis of biosynthetic gene cluster evolution: lessons for engineering biosynthesis. *PLoS Comput. Biol.* 10:e1004016. doi: 10.1371/journal.pcbi.1004016
- Mevers, E., Chouvenec, T., Su, N. Y., and Clardy, J. (2017). Chemical interaction among termite-associated microbes. *J. Chem. Ecol.* 43, 1078–1085. doi: 10.1007/s10886-017-0900-6
- Myers, M. R., and King, G. M. (2016). Isolation and characterization of *Acidobacterium ailaui* sp. nov., a novel member of *Acidobacteria* subdivision 1, from a geothermally heated Hawaiian microbial mat. *Int. J. Syst. Evol. Microbiol.* 66, 5328–5335. doi: 10.1099/ijsem.0.001516
- Ondov, B. D., Bergman, N. H., and Phillippy, A. M. (2011). Interactive metagenomic visualization in a Web browser. *BMC Bioinformatics* 12:385. doi: 10.1186/1471-2105-12-385
- Peterson, B. F., and Scharf, M. E. (2016). Lower termite associations with microbes: synergy, protection, and interplay. *Front. Microbiol.* 7:422. doi: 10.3389/fmicb.2016.00422
- Poulsen, M., Hu, H., Li, C., Chen, Z., Xu, L., Otani, S., et al. (2014). Complementary symbiont contributions to plant decomposition in a fungus-farming termite. *Proc. Natl. Acad. Sci. U.S.A.* 111, 14500–14505. doi: 10.5524/100055
- Pruesse, E., Peplies, J., and Glockner, F. O. (2012). SINA: accurate high-throughput multiple sequence alignment of ribosomal RNA genes. *Bioinformatics* 28, 1823–1829. doi: 10.1093/bioinformatics/bts252
- Quast, C., Pruesse, E., Yilmaz, P., Gerken, J., Schweer, T., Yarza, P., et al. (2013). The SILVA ribosomal RNA gene database project: improved data processing and web-based tools. *Nucleic Acids Res.* 41, D590–D596. doi: 10.1093/nar/gks1219
- Rosengaus, R. B., Zecher, C. N., Schultheis, K. F., Brucker, R. M., and Bordenstein, S. R. (2011). Disruption of the termite gut microbiota and its prolonged consequences for fitness. *Appl. Environ. Microbiol.* 77, 4303–4312. doi: 10.1128/AEM.01886-10
- Sait, M., Hugenholtz, P., and Janssen, P. H. (2002). Cultivation of globally distributed soil bacteria from phylogenetic lineages previously only detected in cultivation-independent surveys. *Environ. Microbiol.* 4, 654–666. doi: 10.1046/j.1462-2920.2002.00352.x
- Santos, A. V., Dillon, R. J., Dillon, V. M., Reynolds, S. E., and Samuels, R. I. (2004). Occurrence of the antibiotic producing bacterium *Burkholderia* sp. in colonies of the leaf-cutting ant *Atta sexdens rubropilosa*. *FEMS Microbiol. Lett.* 239, 319–323. doi: 10.1016/j.femsle.2004.09.005
- Scheffrahn, R. H., Carrijo, T. F., Křeček, J., Su, N.-Y., Szalanski, A. L., Austin, J. W., et al. (2015). A single endemic and three exotic species of the termite genus *Coptotermes* (Isoptera: Rhinotermitidae) in the New World. *Arthropod Syst. Phylo* 73, 333–348.
- Skinninger, M. A., Johnston, C. W., Edgar, R. E., Dejong, C. A., Merwin, N. J., Rees, P. N., et al. (2016). Genomic charting of ribosomally synthesized natural product chemical space facilitates targeted mining. *Proc. Natl. Acad. Sci. U.S.A.* 113, E6343–E6351. doi: 10.1073/pnas.1609014113
- Sobotnik, J., Jirosova, A., and Hanus, R. (2010). Chemical warfare in termites. *J. Insect Physiol.* 56, 1012–1021. doi: 10.1016/j.jinsphys.2010.02.012
- Stingl, U., Maass, A., Radek, R., and Brune, A. (2004). Symbionts of the gut flagellate *Staurojoenia* sp. from *Neotermes cubanus* represent a novel, termite-associated lineage of Bacteroidales: description of 'Candidatus Vestibaculum illigatum'. *Microbiology* 150(Pt 7), 2229–2235. doi: 10.1099/mic.0.27135-0
- Stroeymeyt, N., Casillas-Pérez, B., and Cremer, S. (2014). Organisational immunity in social insects. *Curr. Opin. Insect Sci.* 5, 1–15. doi: 10.1016/j.cois.2014.09.001
- Su, L., Yang, L., Huang, S., Su, X., Li, Y., Wang, F., et al. (2016). Comparative Gut microbiomes of four species representing the higher and the lower termites. *J. Insect Sci.* 16, 97. doi: 10.1093/jisesa/iew081
- Su, N.-Y. (2003). Overview of the global distribution and control of the Formosan subterranean termite. *Sociobiology* 41, 7–16.
- Sun, X., Yang, Y., Zhang, N., Shen, Y., and Ni, J. (2015). Draft genome sequence of *Dysgonomonas macrotermis* Strain JCM 19375T, Isolated from

- the Gut of a Termite. *Genome Announc* 3:e00963-15. doi: 10.1128/genomeA.00963-15
- Taguchi, Y.-H., and Oono, Y. (2005). Relational patterns of gene expression via non-metric multidimensional scaling analysis. *Bioinformatics* 21, 730–740. doi: 10.1093/bioinformatics/bti067
- Terrapon, N., Li, C., Robertson, H. M., Ji, L., Meng, X., Booth, W., et al. (2014). Molecular traces of alternative social organization in a termite genome. *Nat. Commun.* 5:3636. doi: 10.1038/ncomms4636
- Traniello, J. F., Rosengaus, R. B., and Savoie, K. (2002). The development of immunity in a social insect: evidence for the group facilitation of disease resistance. *Proc. Natl. Acad. Sci. U.S.A.* 99, 6838–6842. doi: 10.1073/pnas.102176599
- Tschech, A., and Pfennig, N. (1984). Growth yield increase linked to caffeate reduction in *Acetobacterium woodii*. *Arch. Microbiol.* 137, 163–167. doi: 10.1007/BF00414460
- Vargo, E. L., and Husseneder, C. (2009). Biology of subterranean termites: insights from molecular studies of *Reticulitermes* and *Coptotermes*. *Annu. Rev. Entomol.* 54, 379–403. doi: 10.1146/annurev.ento.54.110807.090443
- Wagner, M., and Horn, M. (2006). The *Planctomycetes*, *Verrucomicrobia*, *Chlamydiae* and sister phyla comprise a superphylum with biotechnological and medical relevance. *Curr. Opin. Biotechnol.* 17, 241–249. doi: 10.1016/j.copbio.2006.05.005
- Wang, Y., Su, L., Huang, S., Bo, C., Yang, S., Li, Y., et al. (2016). Diversity and resilience of the wood-feeding higher termite *Mironasutitermes shangchengensis* gut microbiota in response to temporal and diet variations. *Ecol. Evol.* 6, 8235–8242. doi: 10.1002/ece3.2497
- Ward, N. L., Challacombe, J. F., Janssen, P. H., Henrissat, B., Coutinho, P. M., Wu, M., et al. (2009). Three genomes from the phylum *Acidobacteria* provide insight into the lifestyles of these microorganisms in soils. *Appl. Environ. Microbiol.* 75, 2046–2056. doi: 10.1128/AEM.02294-08
- Weijers, J. W. H., Panoto, E., van Bleijswijk, J., Schouten, S., Rijpstra, W. I. C., Balk, M., et al. (2009). Constraints on the biological source(s) of the orphan branched tetraether membrane lipids. *Geomicrobiol. J.* 26, 402–414. doi: 10.1080/01490450902937293
- Zhang, B., Wu, X., Tai, X., Sun, L., Wu, M., Zhang, W., et al. (2019). Variation in actinobacterial community composition and potential function in different soil ecosystems belonging to the arid heihe river basin of Northwest China. *Front. Microbiol.* 10:2209. doi: 10.3389/fmicb.2019.02209

Conflict of Interest: The authors declare that the research was conducted in the absence of any commercial or financial relationships that could be construed as a potential conflict of interest.

Copyright © 2020 Oberpaul, Zumkeller, Culver, Spohn, Mihajlovic, Leis, Glaeser, Plarre, McMahon, Hammann, Schäberle, Glaeser and Vilcinskas. This is an open-access article distributed under the terms of the Creative Commons Attribution License (CC BY). The use, distribution or reproduction in other forums is permitted, provided the original author(s) and the copyright owner(s) are credited and that the original publication in this journal is cited, in accordance with accepted academic practice. No use, distribution or reproduction is permitted which does not comply with these terms.

**MANUSCRIPT 2: COMBINATION OF HIGH-THROUGHPUT
MICROFLUIDICS AND FACS
TECHNOLOGIES TO LEVERAGE THE
NUMBERS GAME IN NP DISCOVERY**

Status: published online ahead of print 24/06/2021

Author's contributions: Study design, method validation of Microfluidics, Flow cytometry and genetic fingerprinting, contribution to all experiments, data analysis: Illumina sequencing data, Flow cytometry measurements, elucidation of microbial diversity, manuscript writing, figure design (Figure 1, 3 and 4).

Combination of high-throughput microfluidics and FACS technologies to leverage the numbers game in natural product discovery

Markus Oberpaul,^{1,†}  Stephan Brinkmann,^{1,†} 
Michael Marner,¹  Sanja Mihajlovic,¹ 
Benedikt Leis,¹ Maria A. Patras,¹ 
Christoph Hartwig,¹  Andreas Vilcinskas,^{1,2} 
Peter E. Hammann,³ Till F. Schäberle^{1,2,4,*} 
Marius Spohn^{1,**}  and Jens Glaeser^{3,***}

¹Fraunhofer Institute for Molecular Biology and Applied Ecology (IME), Branch for Bioresources, Giessen, 35392, Germany.

²Institute for Insect Biotechnology, Justus-Liebig-University-Giessen, Giessen, 35392, Germany.

³Evotec International GmbH, Göttingen, 37079, Germany.

⁴German Center for Infection Research (DZIF), Partner Site Giessen-Marburg-Langen, Giessen, 35392, Germany.

Summary

High-throughput platforms facilitating screening campaigns of environmental samples are needed to discover new products of natural origin counteracting the spreading of antimicrobial resistances constantly threatening human and agricultural health. We applied a combination of droplet microfluidics and fluorescence-activated cell sorting (FACS)-based technologies to access and assess a microbial environmental sample. The cultivation performance of our microfluidics workflow was evaluated in respect

to the utilized cultivation media by Illumina amplicon sequencing of a pool of millions of droplets, respectively. This enabled the rational selection of a growth medium supporting the isolation of microbial diversity from soil (five phyla affiliated to 57 genera) including a member of the acidobacterial subgroup 1 (genus *Edaphobacter*). In a second phase, the entire diversity covered by 1071 cultures was used for an arrayed bioprospecting campaign, resulting in > 6000 extracts tested against human pathogens and agricultural pests. After redundancy curation by using a combinatorial chemical and genomic fingerprinting approach, we assigned the causative agents present in the extracts. Utilizing UHPLC-QTOF-MS/MS-guided fractionation and microplate-based screening assays in combination with molecular networking the production of bioactive ionophorous macrotetrolides, phospholipids, the cyclic lipopeptides massetolides E, F, H and serratamolide A and many derivatives thereof was shown.

Introduction

Continuously increasing levels of drug resistance and the consequent loss of existing drug and control agents for the treatment of infections poses an enormous threat to human health care systems and plant disease management strategies (Lewis, 2013; Lakemeyer *et al.*, 2018). This crisis has to be counteracted by continued innovation in discovery campaigns to increase the probability of finding new anti-infective lead structures (Schäberle and Hack, 2014; Tacconelli *et al.*, 2018; Theuretzbacher *et al.*, 2020).

A rich source for new chemical entities are microbial-derived natural products (NPs), which always has been a major inspiration for development of drugs and control agents (Newman and Cragg, 2020). NP evolution brought forth a vast diversity of unique molecules that are optimized for interactions with their respective molecular targets; the latter a plethora of biological macromolecules themselves (Firm and Jones, 2003; Bon and Waldmann, 2010; Hong, 2011). Fortunately, the predicted potential for chemical variety encoded within the microbial diversity is yet only scarcely exploited. This is

Received 2 May, 2021; revised 17 May, 2021; accepted 6 June, 2021.

For correspondence. *E-mail Till.F.Schaeberle@agrar.uni-giessen.de; Tel. +49 641 972-19140; Fax +49 641 972-19499. **E-mail marius.spohn@ime.fraunhofer.de; Tel. +49 641 972-19189; Fax +49 641 972-19499. ***E-mail Jens.Glaeser@evotec.com; Tel. +49 (0)151 25565835; Fax +49 641 972-19499.

[†]These authors contributed equally to this work.

Microbial Biotechnology (2021) 0(0), 1–16

doi:10.1111/1751-7915.13872

Funding information

This work was financially supported by the Hessen State Ministry of Higher Education, Research and the Arts (HMWK) via the state initiative for the development of scientific and economic excellence for the LOEWE Center for Insect Biotechnology and Bioresources. Sanofi-Aventis Deutschland GmbH and Evotec International GmbH funded this work in the framework of the Sanofi-Fraunhofer Natural Products Center and its follow-up, the Fraunhofer-Evotec Natural Products Center of Excellence.

© 2021 The Authors. *Microbial Biotechnology* published by Society for Applied Microbiology and John Wiley & Sons Ltd.

This is an open access article under the terms of the Creative Commons Attribution License, which permits use, distribution and reproduction in any medium, provided the original work is properly cited.

mainly due to the fact that major NP discovery efforts of past decades had been focusing on rather easily cultivable microorganisms and consequently on a limited phylogenetic diversity (Monciardini *et al.*, 2014). Along with the likely also not yet-exhausted potential of classical NP producers, for example *Streptomyces* spp. (Adamek *et al.*, 2019; Belknap *et al.*, 2020), additional phylogenetic branches of the bacterial kingdom represent a promising source for discovery of novelty (Gross and Loper, 2009; Panthee *et al.*, 2016; Tracanna *et al.*, 2017). Thus, driven by the dogma that phylogenetic and genomic divergence translates directly into chemical diversity (Medema *et al.*, 2014; Monciardini *et al.*, 2014), greater effort is demanded to bring a broader diversity of genera and families in culture (Hoffmann *et al.*, 2018; Nicault *et al.*, 2020) while directly exploiting their metabolic capabilities. The still valid functionality of the methodology to valorize bacterial derived NPs was recently shown by the development and market introduction of fenpicoxamid, derived from the antifungal compound UK-2A produced by *Streptomyces* sp. 517-02. This NP provides a new target site for the control of *Zymoseptoria tritici* (SEPTTR), the causative agent of Septoria tritici Blotch (STB) (Butler and Paterson, 2020) by inhibiting the mitochondrial complex III at a target site distinguished from the one attacked by the strobilurin class (Owen *et al.*, 2017). The trend towards the valorization and application of naturally derived fungicides continues to rise, predicted to obtain further attention in the next decades (Umetsu and Shirai, 2020). In antibacterial research, success in discovery of novel NPs with unique modes of action was recently mainly achieved with the isolation of novel anti-infective lead structures from rare Proteobacteria, particularly darobactin (from *Photobacterium* sp.), a heptapeptide antibiotic targeting the gram-negative outer membrane protein *BamA* (Imai *et al.*, 2019) and teixobactin (from *Eleutheria* sp.), which was made accessible by a novel cultivation technique (Ling *et al.*, 2015).

The basis for all such findings is the fundamental accessibility to a broad, thus diverse phylogenetic space of the bacterial kingdom. The challenging task to bring an additional layer of today's microbial dark matter into culture is mainly a numbers game that has to be approached by the development and implementation of new and efficient methods (Lok, 2015). Microbial cultivation strategies, with their common theme in mimicking environmental conditions in laboratory settings (Kaeberlein, 2002), require massive miniaturization and brute force cultivation techniques while still considering the microorganisms' metabolic needs (Keller and Zengler, 2004). Advanced miniaturization approaches are microfluidics-based strategies, posing a rapidly emerging technology for cultivation of microbial diversity that were

also already utilized in the field of NP discovery (Zinchenko *et al.*, 2014; Mahler *et al.*, 2015; Terekhov *et al.*, 2017). Droplet microfluidics is based on converging aqueous and oil phases in a laminar flow with the addition of surfactants as stabilizing agents. Pressurized in microchannels with a diameter ranging from 30 to 500 μm , this ultimately results in aqueous droplets in nl to pl scale (Leman *et al.*, 2015). The production of millions of droplets per hour was improved over years, and simplified systems are nowadays on the market (Nge *et al.*, 2013; Volpatti and Yetisen, 2014). Their combination with further technologies, such as fluorescence-activated cell sorting (FACS), enables the direct identification of desired events and their arrayed sorting (Zinchenko *et al.*, 2014). An advantageous value of these technologies is the downscaling and compartmentalization which allows single cells to be physically separated into distinct vessels while maintaining the overall microbial complexity (Zengler *et al.*, 2002; Theberge *et al.*, 2010). This separation is mandatory to avoid growth competition between different species while also allowing single cells to utilize and shape their microenvironment according to their specific needs and at their own pace (Keller and Zengler, 2004; Boitard *et al.*, 2015). The pico-litre scaled droplets display an environmental mimicry themselves, since the extremely small scale enables even single cells to adapt their environment by, for example accumulating self-mediating growth factors eventually breaking microbial dormancy (Boedicker *et al.*, 2009; Ishii *et al.*, 2010; Stewart, 2012). In principal, high-throughput microfluidic-based platforms increase the microbial cultures in amount but also diversity and consequently the probability to cultivate and identify also underexplored microorganisms (Akselband *et al.*, 2006; Baret *et al.*, 2009).

In this study, we succeeded in isolating an extended taxonomic diversity and accessing microorganisms considered as under- or even unexploited for NP discovery. We implemented a biphasic workflow consisting of (i) an efficient cultivation of microbial diversity using microfluidics and FACS-based technologies, followed by (ii) a miniaturized bioactivity-guided NP discovery process on the obtained isolates focused on the two devastating pathogens, that is *Mycobacterium tuberculosis* (MTB) and SEPTTR. Our here described cultivation platform is based on long-term stable agarose-solidified microdroplets ($\sim 40 \mu\text{m}$ in size, volume of $\sim 33 \text{ pl}$). Droplets were generated up to rates of $\sim 1.3 \text{ kHz}$; thereby, exceeding the dimensions for an application to be affiliated as ultra-high throughput (Payne *et al.*, 2020). At a cell distribution of $\lambda 0.1$, this set up allowed the parallel encapsulation of $\sim 500\,000 \text{ cells h}^{-1}$ with a statistical probability below 0.5% to obtain co-cultures. In total, we brought 1071 microorganisms into culture, from which

~ 74% could be identified by 16S rRNA gene sequencing. The isolated bacteria belong to five different phyla affiliated to 57 different genera. Besides classical NP producing taxa a representative of fastidious Acidobacteria and certain proteobacterial genera which are under-represented in public strain libraries (e.g. *Luteibacter* and *Variovorax*) were brought into culture. The entire obtained microbial diversity was eventually integrated into a bioactivity-guided NP discovery process. After redundancy curation of initially active extracts, the organic extracts of *Erwinia*, *Pseudomonas* and *Streptomyces* which most strongly inhibited the growth of MTB and/or SEPTTR were followed up by bioassay- and UHPLC-QTOF-MS/MS-guided fractionation. Complemented by extensive metabolomic analysis via molecular networking, this led to the identification of serratomolides, massetolides, phospholipids and macrotetro- lides as the bioactivity causing agents.

Results and discussion

Cultivation of microbial diversity using microfluidics and FACS

In this study (platform scheme see Fig. S2), we aimed to bring microbial diversity into culture to expand our strain collection (Fox, 2014) and to exploit the bacterial proportion in a bioactivity-guided NP discovery programme. Known for their highly diverse bacterial communities (Delgado-Baquerizo *et al.*, 2016), we selected a combined soil sample as starting material for our study.

Upfront the main droplet cultivation and screening campaign, we examined the general cultivation success

using our microfluidics platform and explicitly the specific impact of the chosen growth media on the bacterial community. Specifically adapted towards soil and previously shown to be suitable to transfer a high diversity of soil microorganisms into culture, we selected ISEM (Nguyen *et al.*, 2018) as benchmark medium for this study. Considering the importance of using buffered media as well as mimicking neutral and acidic soils for the cultivation success (Overmann *et al.*, 2017), we buffered the media to pH 7.2 and pH 5.5 (Tovar *et al.*, 2020). In order to identify an additional media suitable to access a broad microbial diversity of the bioresource used in this study, we encapsulated the retrieved microorganisms ($\lambda 0.1$) in eight different media (VL55-xyl, VL55-cello, 1:20 CY, 1:20 NB, M13b, 1:20 TSB, 1:10 R2A and M9). Then, we comparatively determined the cultivation success by Illumina amplicon sequencing of the sorted droplet populations among themselves and towards the starting material. The sequencing was conducted on DNA directly isolated from the eight different droplet populations. Illumina amplicon sequencing of isolated DNA yielded in total 1 947 118 classified sequences, of which 0.04% could not be classified and were defined as *No Relative*. The data revealed that cultivation in VL55-xyl resulted in the overall highest diversity on genus level resolution (Shannon index [SI]: 4.1), followed by M9 (SI: 3.5) and 1:20 CY (SI: 3.5) (Fig. 1). Compared to the starting material, the microbial diversity covered by VL55-xyl was not significantly reduced ($P > 0.5$). In contrast, the exchange of the sole C-source xylan by cellobiose led to a significant reduction in diversity ($P < 0.01$) and a lower SI (SI: 2.3). While showing an

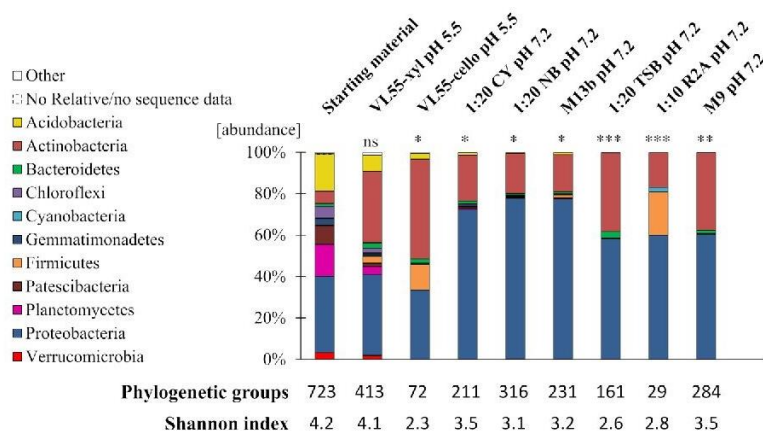


Fig. 1. Microbial diversity grown in agarose-solidified droplets by Illumina amplicon sequencing proves VL55-xyl as best cultivation media to obtain highest diversity. Isolated environmental cells (starting material) were encapsulated in droplets ($\lambda 0.1$) and incubated at 28°C for seven days before total DNA was directly extracted from the droplet populations and sequenced with Illumina 300-bp paired-end 16S V3-V4 amplicon next-generation sequencing, respectively. VL55-xyl outperformed with the highest number of phylogenetic groups (491) and Shannon index on genus level of 4.1. A significant difference between media sample medians was observed on phylum level ($P > 0.005$). Dunn's post hoc test was performed on all samples on phylum level compared to the starting material ($***P < 0.001$; $**P < 0.01$; $*P < 0.1$; ns: not significant).

overall lower diversity, the media (1:20 CY, 1:20 NB, M13b, 1:20 TSB and 1:10 R2A), which contained complex components such as yeast or peptone showed an increased proportion of Proteobacteria (up to 77.7%) in comparison with the VL55-based media (up to 39.2%) and the starting material (36.7%). A similar diversity and an increased proportion of Proteobacteria were observed by using M9. While 1:10 R2A appears to be suitable to enrich Firmicutes (20.8% vs 0.06% in starting material), all other media buffered at pH 7.2 do not show a remarkable difference within their cultivated microbial community ($P > 0.7$; Fig. 1).

Overall, VL55-xyl with its complex C-source and its pH favourable for acidophilic and acid-tolerant bacteria was shown to be the most suitable medium for our soil material and selected it to be included in all subsequent experiments. Considering the observed effects of the Illumina analysis, particularly the impact of the provided C-source and the altered pH profile, we supplemented ISEM with a variation of six complex C-sources including xylan (mISEM¹) and buffered it to pH 5.5 and pH 7.2.

In this study, we applied a micron-scaled cultivation platform to receive axenic cultures from a complex biore-source, adapted for the purpose to also cultivate slow-growing microorganisms. This necessitates the analysis of droplets in high-throughput fashioned manner and the reliable discrimination between droplets harbouring grown microorganisms with manifold morphologies and the

empty droplet background. Therefore, we used a FACS approach utilizing the carbocyanine dye DiOC₂(3) to stain microorganisms with a membrane potential grown inside the agarose-solidified droplets. DiOC₂(3) is a potentiometric probe that exhibited green fluorescence in all bacterial cells; however, the fluorescence shifts towards red emission as the dye molecules self-associate at the higher cytosolic concentrations caused by larger membrane potentials (Shapiro, 2000; Biener *et al.*, 2017). To show the feasibility of using DiOC₂(3) for this process step, a mixed droplet population containing 50% droplets harbouring grown microcolonies of *E. coli* (λ .10) incubated for 4 h at 37°C and 50% empty droplets was stained and subsequently measured using FACS while analysing the ratio of green (FL1-H) and red (FL3-H) fluorescence. The FL1-H to FL3-H scatter exposed 49.7% of all analysed events in the defined gate, congruent with the adjusted 50.0% of the droplet population containing grown *E. coli* microcolonies (Fig. 2A). This verified the applicability of DiOC₂(3) as a fluorescent dye for staining microorganisms grown in agarose-solidified droplets. Based on these distinguishable populations, the FACS settings (e.g. sorting gates for events of interest) were defined and later on applied for the cultivation campaign.

The cell suspension from the used soil sample retrieved using nycodenz gradient centrifugation had an estimated living cell count of $\sim 4.2 \times 10^6$ cells ml⁻¹ determined via FACS [considering live/dead ratio ($\sim 70:30$; Fig. S3)].

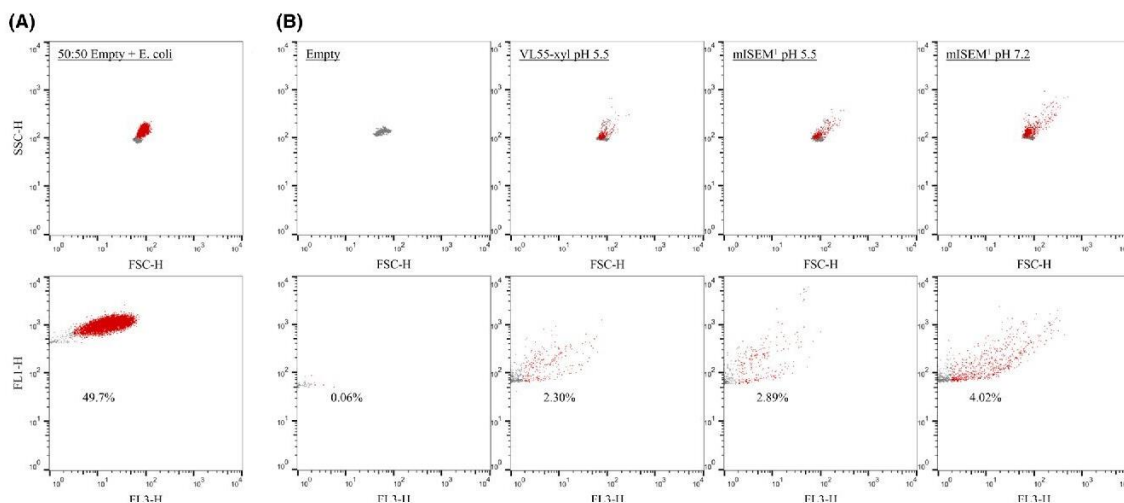


Fig. 2. Sorting of microcolonies grown in agarose-solidified droplets stained using DiOC₂(3).

A. Differentiation of a 50:50 mixture of empty droplets and those containing grown microcolonies of *E. coli* ATCC 25922 (λ .10). 15 000 events were analysed by FACS considering granularity (SSC-H) to size (FSC-H) and green (FL1-H) to red fluorescence (FL3-H) after staining. B. Sorting of droplets containing grown microcolonies of environmental soil microorganisms (λ .0.1) in VL55-xyl pH 5.5, mISEM¹ pH 5.5 and mISEM¹ pH 7.2 (10 000 events displayed). The background noise was 0.06% (empty = control without cells encapsulated). After seven days of incubation at 28°C, grown microcolonies as determined by membrane potential dye were sorted and recovered. Red dots = droplets containing fluorescently labelled cells; grey dots = empty droplets.

This was taken into consideration, while cells were encapsulated in different media (λ 0.1 each) and subsequently incubated at 28°C, respectively. The microbial growth within droplets was frequently monitored over time by microscopy, exemplarily showing the processing of microorganisms with various morphologies (Fig. 3A). After seven days of incubation, the samples were sorted by using DiOC₂(3) staining. We could affiliate 2.30% (VL55-xy1 pH 5.5), 2.89% (mISEM² pH 5.5) and 4.02% (mISEM² pH 7.2) of all evaluated events to droplets containing grown microcolonies (Fig. 2B). These events were sorted and distributed into 384-well MTPs, and microbial growth was again monitored by turbidimetry and microscopy, respectively (Fig. 3B). After automatic transfer of grown cultures into 96-deep well MTPs and further incubation for up to 14 days, this up-scaling procedure provided 1071 cultures in total. Sample aliquots of each culture were taken to generate cryo-conserved cultures and cell lysates for taxonomic identification by 16S rRNA gene sequencing (partial sequencing using primer 1492R). This revealed the processing of 57 different genera affiliated to five different phyla (Fig. 3C and Table S1). Comparing the cultivation,

success of mISEM² at pH 5.5 and pH 7.2 clearly shows the worth of modulating this parameter to increase the cultivated diversity. Together, 55 genera were isolated using mISEM², while only 15 of them could be found under both pH conditions. Medium mISEM² pH 7.2 led to the successful cultivation and affiliation of 46 genera (462 strains, SI: 2.4) while 31 genera were unique to this condition. In contrast, at pH 5.5 a total of 24 genera (108 strains, SI: 2.7) and 9 unique ones were identified. While use of acidified media led to an overall decreased amount of genera, this condition showed a higher diversity and expanded the cultivation success towards a fifth phyla (Acidobacteria) not present at the neutral pH set-up. Within both media comprising pH 5.5, we found eight representatives of the Acidobacteria, all belonging to the genus *Edaphobacter*. A representative thereof was recovered on plate and incorporated into our strain collection. As judged on nearly full-length 16S rRNA sequence comparison, this particular strain, namely FHG110552, is phylogenetically affiliated to the subgroup 1 of Acidobacteria and most closely related to *Edaphobacter modestus* Jbg-1T (~ 98.8% similarity) isolated from alpine and forest soils (Koch *et al.*, 2008;

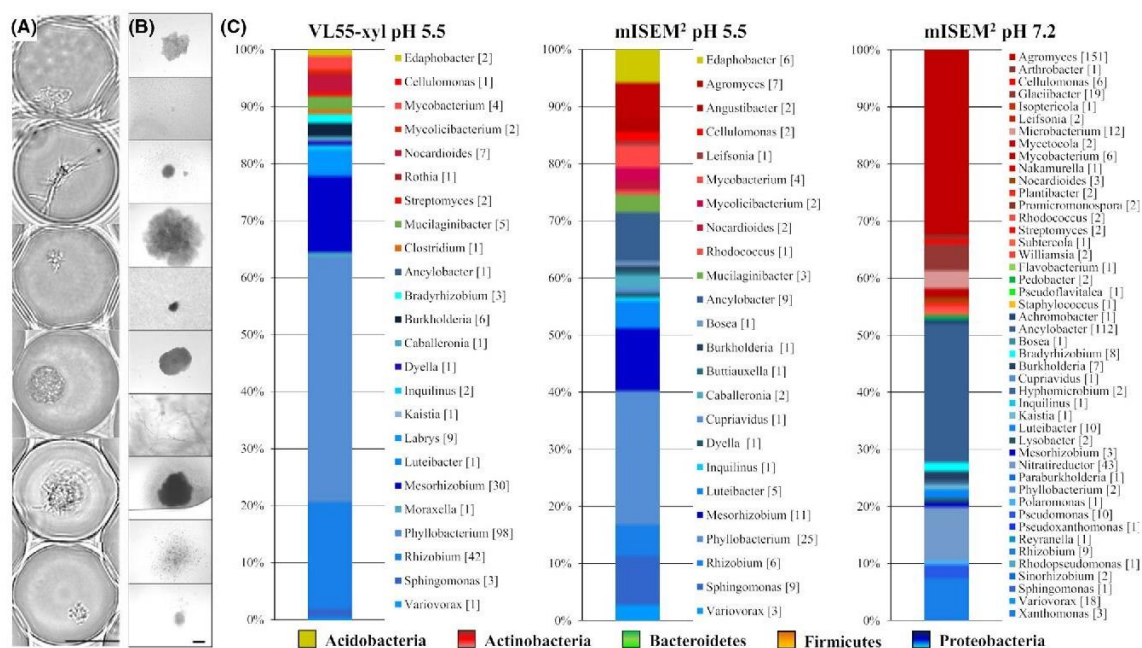


Fig. 3. Successful cultivation of microbial diversity after incubation of solidified-agarose droplets verified by 16S rRNA gene sequencing (1492R primer) and microscopy.

A. Examples of grown microcolonies in agarose-solidified droplets were microscopically examined. Scale bar: 20 μ m.

B. Inverse microscopy of exemplary 384-well MTPs containing arrayed droplets and liquid medium. Different morphologies from microcolonies, which grew out of droplets are indicated, representing a section of the final retrieved and conserved bacterial diversity. Scale bar: 40 μ m.

C. In total, 1071 MOs affiliated to 5 phyla were brought into culture, whereas ~ 74% were initially identified by 16S rRNA gene sequencing (partial sequence using primer 1492R, mISEM² pH 7.2: 462, mISEM² pH 5.5: 106, VL55-xy1 pH 5.5: 225). Numbers in square brackets indicate the amount of 16S rRNA gene sequencing affiliations. For further information and data used for the figure caption, see Table S1.

Fig. S4). The phylum Acidobacteria is postulated to be a promising bioresource for the field of NP discovery based on its predicted biosynthetic potential encoded in their genomes (Kielak *et al.*, 2016; Crits-Christoph *et al.*, 2018). Though, the description of Acidobacteria NPs is yet limited to hopanoids (Damsté *et al.*, 2017).

On phylum level, a major difference between the neutral and acidified media is the ratio between Actinobacteria and Proteobacteria, which is at pH 7.2 shifted towards the Actinobacteria, while towards Proteobacteria at pH 5.5. The same is seen in VL55-xyl covering in total 23 genera (223 strains, SI: 1.9) including *Edaphobacter* but also unique genera such as *Labrys* and *Rothia*, not covered by mISEM². In total, 17 Actinobacteria genera were brought into culture using mISEM² pH 7.2, whereas 8 genera in mISEM² pH 5.5 and 6 genera in VL55-xyl. This is particularly biased by the genus *Agromyces*, which was strongly enriched in mISEM² pH 7.2 (151 strains) while present in low abundance at pH 5.5 (7 strains).

Within the Proteobacteria, such an opposite pH-dependent shift occurs within the class of Alphaproteobacteria. At pH 7.2, the genus *Ancylobacter* represents almost half of all Proteobacteria (112 strains) while being significantly less abundant at pH 5.5. In contrast, the genus *Phyllobacterium* represents > 30% of the Proteobacteria at acidic condition while < 1% at neutral pH. In total, the isolated Proteobacteria proportion comprises member of 33 different genera belonging to the classes of Alpha-, Beta- and Gammaproteobacteria and include also representatives of nine scarcely cultured genera according to our definition (namely *Ancylobacter*, *Buttiauxella*, *Inquilinus*, *Kaistia*, *Labrys*, *Luteibacter*, *Polaromonas*, *Reyranella* and *Variovorax*).

Bioactivity-guided bioprospecting process

To prospect the here cultured microbial diversity for NPs with desired bioactivity, we integrated all arrayed microbes in a downscaled bioactivity-guided NP discovery process. Each culture was grown in its respective isolation medium and in addition in ISP2 and BSM for four and seven days. This process aimed to more sophisticatedly provoke expression of the microbial secondary metabolite production potential. Using 96-deep well Duetz systems and 1 ml culture volumes, 6426 organic extracts were generated and used for bioactivity screenings and metabolome analysis.

In first line, the extracts were screened for their antimicrobial activity against *M. smegmatis*, the opportunistic microbial pathogen *S. aureus* and for their antifungal activity against *Z. tritici*, *C. albicans* and *A. flavus*. Extracts that showed growth inhibitory properties underwent a subsequent diversity assessment by cosine similarity comparison of features detected within each corresponding

UHPLC-UHR-MS chromatogram. This quality control step was included to rule out extensive analysis of redundant samples, unavoidably appearing in every microbial isolation project. After screening the methanolic extracts, 64 cultures were assigned to bioactivity by either inhibiting the growth of *M. smegmatis* and/or the fungal indicator strains. The cosine similarity of their associated UHPLC-UHR-MS chromatograms were determined. After excluding samples with less than 50 features, the remaining 60 samples clustered into eight distinct groups applying the cosine similarity threshold 0.9 (Fig. 4A, Table S2). From the most dominant group, we recovered *Penicillium* sp. (FHG110518). With no focus on fungal metabolites in this project, we decided to discontinue the work on this abundant strain causing the major fractions of observed bioactivities (~70%). In order to now identify the bacterial strains in this dataset, we complemented the redundancy curation process by genotyping the cultures using BOX-PCR (Fig. 4B). By superimposing the patterns of both grouping technologies, we identified and subsequently recovered strains of the genera *Pseudomonas* [FHG110502, FHG110523 and FHG110524 (each unique)], *Xanthomonas* (FHG110521), *Rhizobium* (FHG110501), *Sphingomonas* (FHG110503), *Phyllobacterium* (FHG110504), *Ancylobacter* [FHG110512, FHG110513, FHG110514 (equal)], *Agromyces* [FHG110505, FHG110506, FHG110507 (equal)], *Erwinia* (FHG110488) and *Streptomyces* (FHG110508).

In order to identify the causative NP beyond the observed crude extract activities, the cultivation of the unique strains was scaled-up to 50 ml volumes. The resulting culture broths were extracted by methanol and reconstituted in DMSO for bioactivity screenings. The extracts from the three strains *Pseudomonas* sp. (FHG110502), *Erwinia* sp. (FHG110488) and *Streptomyces* sp. (FHG110508) exhibited the severest growth inhibitory potency and were selected for further analysis. Their crude extract complexity was strongly reduced by their separation into 159 fractions. After rescreening all fractions, the compounds present in the active fractions were identified by their exact masses, characteristic UV absorption spectra and fragmentation signature.

Erwinia sp. FHG110488. Based on the primary activity of the crude extract against *M. smegmatis* and *Z. tritici*, the corresponding extract was fractionated and rescreened. Compound **1** with a *m/z* of 515.3329 [M + H]⁺, corresponding to the molecular formula C₂₆H₄₆N₂O₈, was dereplicated within an active fraction (Fig. S5). On the basis of the molecular formula and the observed MS/MS fragmentation pattern, the bioactive compound was dereplicated as the known serratamolide A (Wasserman *et al.*, 1961; Dwivedi *et al.*, 2008). Using MS/MS networking, six additional derivatives were

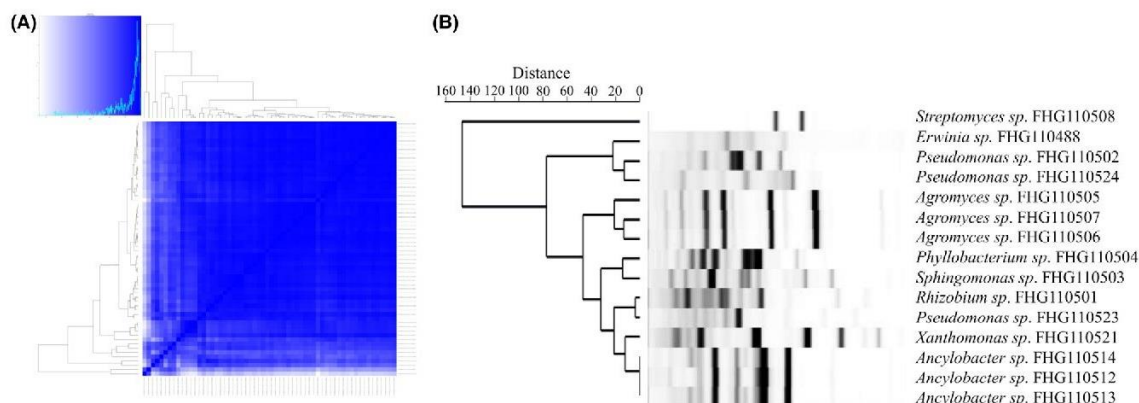


Fig. 4. Metabolic grouping of extracts based on the cosine similarity of their associated UHPLC-UHR-MS chromatograms and the respective genetic fingerprinting by BOX-PCR applied to reduce the redundancy of active strains. (A) Metabolic clustering of extracts of all bioactive strains was analysed via LC-MS. The cosine similarities between samples were calculated. Cosine similarity values for strain-condition pairs were extracted. Samples were sorted according to clustering results, and pairwise similarities were used to define metabolic groups. If the pairwise similarity between two subsequent clustered samples was at the threshold 0.9 or higher, they were assigned to one metabolic group. Figure caption can be found in Table S2. (B) Repetitive genome sequences of all strains initially found to be bioactive were targeted by BOX-PCR to identify unique strains. [Correction added on 01 July 2021, after first online publication: Figure 4 legend has been amended for clarity in this version]

identified (measured **2** m/z 541.3480 $[M + H]^+$, $C_{28}H_{48}N_2O_8$, theoretical m/z 541.3483; **3** m/z 543.3635 $[M + H]^+$, $C_{28}H_{50}N_2O_8$, theoretical m/z 543.3639; **4** m/z 533.3430 $[M + H]^+$, $C_{26}H_{48}N_2O_9$, theoretical m/z 533.3432; **5** m/z 547.3588 $[M + H]^+$, $C_{27}H_{50}N_2O_9$, theoretical m/z 547.3589; **6** m/z 575.3896 $[M + H]^+$, $C_{29}H_{54}N_2O_9$, theoretical m/z 575.3902; **7** m/z 573.3745 $[M + H]^+$, $C_{29}H_{52}N_2O_9$, theoretical m/z 573.3745 (Fig. S6). Serratamolide A is a biosurfactant with plant protecting properties (Thies *et al.*, 2014), additionally alleviating uptake of substances due to its amphiphilic wetting effect, lowering surface and interfacial tensions (Mulligan, 2005). It is known to show antioomycetous activity with particular efficacy against *Pythium ultimum* and *Phytophthora parasitica* (Strobel *et al.*, 2005), a further devastating pest with lack in effective control measures under investigation (Pöppel *et al.*, 2014).

Pseudomonas sp. FHG110502. The antimycobacterial activity caused by *Pseudomonas* strain FHG110502 was associated to three cyclo-lipo-nonapeptide **8–10** (**8** m/z 1112.6811 $[M + H]^+$, $C_{53}H_{93}N_9O_{16}$, theoretical m/z 1112.6813; **9** m/z 1126.6966 $[M + H]^+$, $C_{54}H_{95}N_9O_{16}$, theoretical m/z 1126.6969; and **10** m/z 1154.7288 $[M + H]^+$, $C_{56}H_{99}N_9O_{16}$, theoretical m/z 1154.7282) perfectly matching the MS/MS fragmentation signature of massetolide E, F and H, respectively. Massetolide E and F differ in AA9 by incorporation of valine and leucine, respectively. Massetolide H differs in the fatty acid chain. The hydroxydecanoic acid residue of E and F is replaced by a hydroxyauric acid residue (Fig. S7). At

position AA9, the known antimycobacterial massetolide family is known to be prone to natural variations, with indications in a general correlation between greater lipophilicity and increased potency (Gerard *et al.*, 1997).

Furthermore, three phospholipids dereplicated as lysopalmitoyl-phosphoethanolamine (**11**), palmitoleoyl-palmitoyl-phosphoethanolamine (**12**) and palmitoleoyl-oleoyl-phosphoethanolamine (**13**) (measured **11** m/z 454.2931 $[M + H]^+$, $C_{21}H_{44}N_1O_7P_1$, theoretical m/z 454.2928; **12** m/z 690.5073 $[M + H]^+$, $C_{37}H_{72}N_1O_8P_1$, theoretical m/z 690.5068; and **13** m/z 716.5237 $[M + H]^+$, $C_{39}H_{74}N_1O_8P_1$, theoretical m/z 716.5224), respectively, were assigned the other active fractions (Fig. S8). The bioactivity of phospholipids against several indicator strains has been reported, for example bacillosin as an antifungal active phospholipid isolated from *Bacillus subtilis* (Tamehiro *et al.*, 2002).

Streptomyces sp. FHG110508. A classical NP producer organism that was isolated during our process is *Streptomyces* FHG110508. Its organic extracts showed pronounced activity against *S. aureus* and the fungal indicator strains. Dereplication of active fractions revealed the presence of the macrotetrolides nonactin, monactin, dinactin and macrotetrolide G (Fig. S9, **14–17**) (Phillies, 1975; Řezanka *et al.*, 2010). Additionally, the presence of macrotetrolide D (**18**) was shown by molecular networking (Fig. S10). Ionophore antibiotics of the macrotetrolide family are beyond the most commonly observed bioactive metabolites from actinomycetes passing in various screening disciplines having antibacterial, antifungal,

antiprotozoan, antiparasitic, insecticidal and acaricidal activity (Zizika, 1998).

Conclusive remarks. Our study represents a combination of applied microfluidics and FACS technologies for the cultivation of microorganisms in agarose-solidified droplets. The combination of streamlined high-throughput technologies facilitated the generation and analysis of thousands of droplets within seconds. This paved the way to a fast isolation and characterization of diverse axenic cultures, followed by downstream identification of bioactive natural products. There are no limits on a particular bioresource, organism types or cultivation conditions (media, nutrient limitation, temperature, incubation method, \pm oxygen supply, etc.), since especially all parameters towards cultivation in solidified droplets are highly customizable. Microfluidic platforms are already today a core element to access and assess microbial diversity from environmental samples. Their efficient application on a diversity of bioresources will be of steadily increasing importance for various research disciplines, with particular (but not exclusive) regard to the field of environmental microbiology.

Experimental procedures

Sampling procedure of forest soil

Forrest soil samples (*soil*) were taken from the 'Nature Conservation Area' Bergwerkswald at 50.564032 N 8.672555 E (Hasenkoeppel, Giessen, Germany). Five samples within a radius of ten metres (max. 10 cm in depth) including rhizosphere, lichen, humus soil and sandy loam were pooled. Samples were taken in December 2018 (Illumina approach) and January 2019 (cultivation campaign). Microorganisms were retrieved by Nycodenz density gradient centrifugation (Barra Caracciolo *et al.*, 2005; Oberpaul *et al.*, 2020). All samples were directly chilled and stored at 4°C until processing for the cultivation or at -50°C for Illumina amplicon sequencing.

Encapsulation of microorganisms using microfluidic devices

The cell concentration of retrieved microorganisms was determined using the Bacteria Counting Kit (B7277, Invitrogen, Carlsbad, CA, USA) on a FACSCalibur (BD Bioscience, San Jose, CA, USA) according to the manufacturer's protocol. The live/dead ratio was estimated using the LIVE/DEAD BacLight Bacterial Viability and Counting Kit (L7007, Invitrogen).

The commercially available μ Encapsulator microfluidics set-up, described in detail elsewhere (Caballero-Aguilara *et al.*, 2021), consisting of three pulse-free pressure pumps (Mitos P-Pump), a temperature control unit (TCU-100),

diverse microfluidic chips, polytetrafluoroethylene (PTFE) tubing (1/16" OD, 0.25 mm ID and 0.5 mm ID) and connectors were purchased from Dolomite Microfluidics, a brand of Blacktrace Holdings Ltd (Royston, UK). A high-speed CMOS camera PL-D721CU (Navitar, Rochester, NY, USA) on a stereomicroscope Stemi SV 11 (Carl Zeiss, Oberkochen, Germany) equipped with a halogen light source KL 2500 LCD (Schott AG, Mainz, Germany) was used to image microfluidic operations. Samples for encapsulation were loaded onto the μ Encapsulator Sample Reservoir Chip. Droplet generation was realized on a fluorophilic 50 μ m μ Encapsulator 2 Reagent Droplet Chip with an applied water to water to oil ratio of 1:1:20 at 30°C for ~ 30 min (Video S1). Pico-Surf 1 (2% (w/w) in FC-40) (Sphere Fluidics, Cambridge, UK) was used as the continuous oil phase. Both aqueous phases consisted of cultivation media with adjusted environmental or *E.coli* cell concentrations to obtain target cell distributions following Poisson (Fig. S1; Collins *et al.*, 2015). All liquids except cell suspensions were filtered through a 0.2 μ m CA syringe filter (Corning, Corning, NY, USA) to prevent blocking of the chip. Prior chip loading, media were mixed 50:50 with liquid, pre-warmed 3% (w/v) SeaPlaque agarose (Lonza, Basel, Switzerland) in water. The droplets were collected in 1.5 ml reaction tubes and cooled at 4°C for 10 min to facilitate gelling of the agarose. Thereafter, droplets were incubated at 28°C in a humidity chamber for seven days for the Illumina amplicon sequencing and for the cultivation experiments. Neubauer chambers (0.1 mm depth, Paul Marienfeld GmbH KG, Lauda-Königshofen, Germany) were used for imaging of stationary droplets on a fluorescence microscope DM2000 LED equipped with a DFC450 C camera and LAS V4.7 software (Leica Microsystems, Wetzlar, Germany) for picture analysis.

Cell staining and droplet sorting via FACS

Analysis and sorting of droplets were performed using a FACSCalibur. Surrounding oil was de-emulsified upfront fluorescence staining and FACS analysis using Pico-Break 1 (Dolomite Microfluidics) added in a ratio of 1:200 to a sample diluted with 1 \times PBS to adjust towards an analysis of 2000 events s⁻¹. Fluorescence labelling of microorganisms was achieved by adding 30 μ M DiOC₂(3) (B34950, Invitrogen) to the samples and an incubation time of 5 min. Sorting via FACS (laser ex: 488 nm, em: 530 \pm 30 nm [FL1-H] and 670 \pm 30 nm [FL3-H]) was carried out using the single-cell mode and 1 \times PBS as sheath fluid.

Cultivation media

Media used for the growth of microorganisms in droplets, and the subsequent Illumina 16S V3-V4 gene amplicon

sequencing were as follows: VL55 supplemented with 0.05% (w/v) xylan (VL55-xyl) or 0.05% (w/v) cellobiose (VL55-cello), including selenite–tungstate solution and trace elements SL-10 (Oberpaul *et al.*, 2020) and buffered to pH 5.5. In addition, 1:10 diluted Reasoner's 2A medium (1:10 R2A, DMSZ medium 830), Minimal medium M9 (DMSZ medium 382), 1:20 diluted Casitone-Yeast medium (1:20 CY, DMSZ medium 67), 1:20 diluted Nutrient Broth (1:20 NB, DMSZ medium 1), M13 with 200 mg l⁻¹ ampicillin (M13b; (Wiegand *et al.*, 2019)) and 1:20 diluted Tryptic Soy Broth medium (1:20 TSB, Sigma-Aldrich, St. Louis, MO, USA) were used.

For the cultivation campaign of microbial diversity using microfluidics and FACS, either VL55-xyl or modified intensive soil extract medium (ISEM) (Nguyen *et al.*, 2018) were used. ISEM was modified by addition of 1% (w/v) C-source solution consisting of arabinogalactan, D-(+)-cellobiose, D-(+)-melezitose, xylan, galacto-D-mannan from *Ceratonia siliqua* and N-acetylglucosamine (25 mg l⁻¹ of each in deionized water) (mISEM¹). For the cultivation of sorted and arrayed events in 384-well microplates (MTPs), we exchanged the soil extract with 0.1 g l⁻¹ yeast extract (Oxoid) and 0.1 g l⁻¹ casamino acids (Difco), 0.1 g l⁻¹ proteose peptone (Roth, Karlsruhe, Germany) (mISEM²). Trace elements SL-10 and selenite-tungstate solution (each 2 ml l⁻¹) were added to all media used for the cultivation experiments.

For the bioprospecting campaign, cultures were fermented in small-scaled 96-well Duetz system (Duetz *et al.*, 2000) (Adolf Kühner AG, Birsfelden, Switzerland) using VL55-xyl, ISP2 (DSMZ medium 987), basal salt medium (BSM) supplemented with glycerol (Mamer *et al.*, 2020) and mISEM², adjusted to pH 5.5 and 7.2.

Illumina amplicon sequencing and statistical analysis

In order to evaluate the relative cultivation success, we encapsulated the retrieved environmental microorganisms ($\lambda 0.1$) considering the live/dead ratio in eight different media and incubated the droplets for seven days at 28°C. Environmental DNA was extracted using the NucleoSpin[®] Soil DNA purification kit (Macherey Nagel, Düren, Germany) according to manufacturer's protocol. The bacterial community composition of samples was assessed by Illumina 300-bp paired-end 16S V3-V4 amplicon next-generation sequencing using the degenerate primer pair 341F (3'-CCTACGGGNGGC WGCAG-5') and 785R (3'-GACTACHVGGGTATCTAA KCC-5'). Sequencing was performed by LGC Genomics GmbH (Berlin, Germany) on a MiSeq (Illumina, San Diego, CA, USA), and data evaluation was supported by the SILVAngs pipeline (SILVA SSU Ref dataset; release 132; <http://www.arb-silva.de>; SILVA

Incremental Aligner (SINA SINA v1.2.10 for ARB SVN [revision 21008] Riboccon GmbH, Bremen, Germany)) and BLASTN v2.2.30+ as previously described (Oberpaul *et al.*, 2020). Phylogenetic groups with a relative abundance < 0.001% of total were excluded. Statistical calculations were done by using PAST v4.03 (Hammer *et al.*, 2001)) including the several-sample one-way ANOVA test on ranks (Daniel, 1990) followed by a Dunn's post hoc test (Dunn, 1964) to judge on significances among samples.

Microbial cultivation and extract preparation

Sorted droplets were concentrated using a 0.5 μ m CA membrane filter (Whatman plc, Little Chalfont, UK) and a laboratory vacuum filtration system (Sartorius AG, Göttingen, Germany). Concentrated droplets were recovered in the respective growth medium (VL55-xyl, mISEM² pH 5.5 or pH 7.2) and arrayed into 384-well MTPs with a distribution probability of approx. 0.25 droplets per well using a Matrix Wellmate microplate dispenser (Thermo Fisher Scientific, Waltham, MA, USA). After incubation as static cultures at 28°C in a humidity chamber for up to seven days, growth detection was assessed via turbidimetry (OD) at 600 nm using a Wallac 1420 Victor2 Microplate Reader (Perkin Elmer, Waltham, MA, USA) and by microscopy using a Zeiss Axiovert 200M (Carl Zeiss Microscopy GmbH, Jena, Germany) equipped with an SPOT RT Monochrome 2.1.1 camera (Diagnostic Instruments, Sterling Heights, MI, USA). All cultures exceeding our defined turbidity threshold (determined based on media control blanks present on each processed microplate) were automatically transferred into 96-deep well MTPs pre-filled with media (Corning, New York, NY, USA) using a Precision XS liquid handling system (BioTek Instruments GmbH, Bad Friedrichshall, Germany). These plates were incubated using the Duetz system at 28°C for seven days, shaking at 220 rpm, and 2.5 cm deflection. Sample aliquots were taken for DNA preparation (for 16S rRNA gene sequencing) and to generate a cryo-conserved culture for long-term conservation at -80°C.

For preparation of cryo-conserved samples, 70% (v/v) glycerol and 5% (v/v) DMSO were filled into 96-deep well MTPs and mixed with grown culture broths (ratio 2:3) using a VIAFLO 384 (Integra Biosciences, Biebertal, Germany).

Cryo-conserved strains were recovered by agar plating and integrated into our strain collection. Bioprospecting campaigns were conducted either in 1 ml culture volume using 96-well Duetz systems or in 50 ml culture volume using 300 ml Erlenmeyer flasks, respectively. Incubation of Erlenmeyer flasks occurred at 28°C using an RC-406 orbital shaker (Infors, Bottmingen, Switzerland) with

5 cm deflection at 180 rpm for four and seven days. Fermentations were stopped by cooling microbial cultures and medium controls to -50°C . Frozen samples were lyophilized using a delta 2-24 LSCplus (Martin Christ Gefriertrocknungsanlagen GmbH, Osterode am Harz, Germany), and an equal volume of methanol (related to the culture volume) was added. Extracts were further concentrated *in vacuo* (50-fold in relation to the culture volume) for UHPLC-QTOF-MS/MS analysis. For screening purposes, extract aliquots were reconstituted in DMSO (100-fold in relation to the culture broth).

Phylogenetic classification and genotyping of isolated strains

DNA extraction was carried out by transferring 200 μl of each grown culture supernatant into Collection Microtubes (Qiagen, Hilden, Germany) containing three zirconia beads (2.3 mm, Carl Roth, Karlsruhe, Germany). Cells were disrupted (twice, 30 Hz for 1 min) by using a TissueLyser II (Qiagen). Plates were centrifuged at $4000 \times g$ for 5 min, incubated at 70°C for 45 min and again centrifuged. The supernatants were transferred into fresh 96-V-bottom plates and used as template for 16S rRNA gene amplification following the PCR protocol described by (Kämpfer *et al.*, 2014) using the primer pair E8F (5'-GAGTTTGATCCTGGCTCAG-3') and 1492R (5'-AGAGTTTGATCCTGGCTCAG-3') and for 18S rRNA gene amplification using the primer pair NS1 (5'-GTAGTCATATGCTTGCTC-3') and FR1 (5'-AICCATTC AATCGGTAIT-3') following the protocol described by (Panzer *et al.*, 2015). Genera belonging to Proteobacteria were defined as rarely cultured if less than ten representatives are recorded in the List of Prokaryotic names with Standing in Nomenclature (Parte, 2018, 2018; <https://psn.dsmz.de/> access date: 01/2021).

All cultures affiliated to Acidobacteria were propagated on buffered R2A pH 5.5 agar to receive higher culture densities. All recovered nearly full-length 16S and rRNA sequences were affiliated to the most similar sequences of type strains using BLASTN (version: BLAST+ 2.11.0; <http://blast.ncbi.nlm.nih.gov/Blast.cgi>) with the NCBI Reference Sequence Database (version: RefSeq Release 202; <https://www.ncbi.nlm.nih.gov/refseq/>). All recovered nearly full-length 18S rRNA sequences were affiliated to the most similar sequences of type strains using the pairwise alignment tool from MycoBank (https://www.mycobank.org/page/Pairwise_alignment). Representatives of different subgroups of Acidobacteria were included to visualize the phylogenetic relationship towards isolated Acidobacteria of this study. Therefore, multiple sequence alignment was done by CLUSTALW. Using the maximum-likelihood method, a phylogenetic tree was calculated in

MEGA v7.0.26 (<https://www.megasoftware.net>) under the Tamura–Nei model (Kumar *et al.*, 2016) performing 1000 bootstrap replications. Graphical modifications and annotations were made with iTOL v5.6.3 (<https://itol.embl.de/>; Letunic and Bork, 2019).

BOX-A1R-based repetitive extragenic palindromic sequence PCR (5'-CTACGGCAAGGCGACGCTGACG-3') was used to amplify repetitive elements to perform molecular genotyping (Koeuth *et al.*, 1995). Genomic fingerprinting patterns (BOX-pattern) were analysed by LabChip GX Touch HT using DNA 5K Assay (Cat. No. CLS760675, PerkinElmer, Waltham, MA, USA) and GEL-COMPAR II software version 6.5 (Applied Maths, Sint-Martens-Latem, Belgium) for data interpretation. A hierarchical cluster of the obtained data was calculated based on Dice similarity matrix data by applying Ward's method (Ward, 1963) to discriminate genotypic redundancies within pure cultures.

Bioassays

Crude extract screening was done by microplate broth dilution assays in final assay conc. 0.25-fold, 0.5-fold and onefold (in relation to the culture volume) against pathogenic bacteria and fungi (*Staphylococcus aureus* ATCC25923, *Mycobacterium smegmatis* ATCC 607, *Aspergillus flavus* ATCC 9170, *Zygomoseptoria* campaign *ici* Roberge in Desmazières MUCL 45407 and *Candida albicans* FH 2173).

To evaluate the growth inhibitory effect of microbial extracts, a seeding cell suspension of the indicator strains was prepared from pre-cultures or previously prepared spore solutions: for *S. aureus*, an overnight culture (37°C , 18 h, 180 rpm) was diluted to 2×10^4 cells ml^{-1} in cation adjusted Mueller Hinton II medium (MHII). *M. smegmatis* was cultured in brain-heart infusion medium (BD) supplemented with 1% (w/v) Tween-80 (Sigma) for 48 h, before the assay cell concentration was adjusted (1×10^5 cells ml^{-1}). The pre-culture of *C. albicans* was incubated for 48 h at 28°C before a 1×10^5 cells ml^{-1} suspension was prepared in MHII. Spore solutions of *A. flavus* and *Z. tritici* were diluted to 1×10^5 spores ml^{-1} . A dilution series of gentamycin, isoniazid or nystatin was used as positive control and cell suspensions without extract or antibiotic as negative control. Test plates were incubated in the dark (37°C , 180 rpm, 85% rH) for 18 h (*A. flavus*, *S. aureus*), 48 h (*C. albicans*, *M. smegmatis*) and 72 h at 25°C (*Z. tritici*). End-point detection towards optical density was determined using a LUMIstar® Omega (BMG Labtech GmbH, Ortenberg, Germany) by measuring the turbidity at 600 nm or by ATP quantification using BacTiter-Glo™ according to manufacturer's protocol (Promega Corporation, Fitchburg, WI, USA).

Mass spectrometry

All mass spectrometry experiments were performed on a 1290 UHPLC system (Agilent, Santa Clara, CA, USA) equipped with DAD, ELSD and maXis II™ (Bruker, Billerica, MA, USA) ESI-QTOF-UHRMS with the gradient: 0 min: 95% A; 0.30 min: 95% A; 18.00 min: 4.75% A; 18.10 min: 0% A; 22.50 min: 0% A; 22.60 min: 95% A; 25.00 min: 95% A (A: H₂O, 0.1% formic acid (FA); B: acetonitrile, 0.1% FA; flow: 600 µl min⁻¹). Column oven temperature: 45°C. Column: Acquity UPLC BEH C18 1.7 µm (2.1 × 100 mm) with Acquity UPLC BEH C18 1.7 µm VanGuard Pre-Column (2.1 × 5 mm). Injection volume was either 1 or 2 µl.

Cosine similarity calculations

Data processing was performed with Data Analysis 4.4 (Bruker, Billerica, MA, USA) using recalibration with sodium formate. *RecalculateLinespectra* with threshold 10 000 and subsequent *FindMolecularFeatures* (0.5–25 min, S/N = 0, correlation coefficient threshold = 0.7, minimum compound length = 8 spectra, smoothing width = 2) was performed. Bucketing was performed using *ProfileAnalysis* 2.3 (Bruker, Billerica, MA, USA) (30–1080 s, 100–1600 m/z, Advanced Bucketing with 12 s, 5 ppm, no transformation, Bucketing basis = H⁺). Samples with less than 50 features were excluded from further analysis. The generated bucket table was subsequently used as input for analysis via R (version 3.6.0) (R Core Team, 2020) with libraries readr (<https://CRAN.R-project.org/package=readr>), coop (<https://cran.r-project.org/package=coop>), gplots (<https://CRAN.R-project.org/package=gplots>), data.table (<https://CRAN.R-project.org/package=data.table>), and parallelDist (<https://CRAN.R-project.org/package=parallelDist>). The cosine similarities (dot product of vectors) between samples were calculated. Samples were sorted according to clustering results, and pairwise similarities were extracted and subsequently used to define metabolic groups. The script used in this publication was deposited in a GitHub repository (Hartwig, 2020). If the pairwise similarity between two subsequent clustered samples is at the threshold 0.9 or higher, they were assigned to one metabolic group.

Dereplication of bioactive extracts using UHPLC-UHR MS/MS

Crude extracts showing at least 70% growth inhibition were considered as bioactive and were subjected to microfractionation. Five or ten microliter of concentrated methanolic extracts (50-fold relative to the culture volume) were partitioned into 159 fractions (~ 7 s each) in a 384-well MTP. UHPLC-UHR-MS analysis was performed

(settings see Section Mass spectrometry). For microfractionation, 90% of the flow was collected with a custom made fraction collector (Zinsser–Analytic, Eschborn, Germany) while the rest was analysed in MS/MS mode in maXis II™. Collision induced dissociation was performed at 28.0–35.05 eV using argon at 10⁻² mbar. Additionally to the chromatographically separated 159 fractions, crude extract was applied as fraction 160 in the same amount as the injection volume serving as positive control. All extracts were evaporated in a GeneVac HT-12 (SP Industries Warrminster, PA, USA) and were rescreened against the same test strain. Correlation between bioactive fractions and the corresponding MS data of analytes detected in those fractions was performed. Dereplication was facilitated by comparison of mass to charge ratios, retention time and fragmentation signatures with our in-house reference database containing ~ 1700 structurally characterized microbial metabolites at the time of data processing. Molecular formula assignment was done manually for all compounds present in the active fractions, allowing a mass accuracy tolerance of ± 2 ppm. Annotation of the MS/MS spectra was performed manually for all the compounds present in active fractions, whenever no hits were found in the in-house compound database. Molecular formula searches were performed on AntiBase 2017 (Laatsch, 2017) and Dictionary of Natural Products (<http://dnp.chemnetbase.com/faces/chemical/ChemicalSearch.xhtml>; accessed on Nov 16, 2020).

Molecular networking

Based on published protocols, molecular networking with a cosine similarity cut-off of > 0.7 was performed (Yang *et al.*, 2013; Allard *et al.*, 2016). The tool MSConvert (ProteoWizard package32) was used to convert the raw data (*.d files) into plain text files (*.mgf), wherein all detected fragment ions are expressed as a list of mass/intensity value pairs sorted according to their parent ions (peak picking: vendor MS level = 1–2; threshold type = absolute intensity, value = 1000, orientation = most-intense). Sharing at least six fragments (tolerance Δppm 0.05) with at least one partner ion those ions were included in the final network (Riyanti *et al.*, 2020). Known NPs were highlighted by including deposited compounds from the *in silico* fragmented (Allen *et al.*, 2015) commercial database AntiBase 2017 (Laatsch, 2017) and our *in-house* reference compound MS/MS database. The data were visualized with CYTOSCAPE v3.6.0 (Shannon, 2003) as described elsewhere (Mamer *et al.*, 2020).

Acknowledgements

The authors would like to thank Dr. Michael Mourez, Dr. Luigi Toti, Dr. Jochen Fracowiak and Mai Ngyuen for

helpful discussions. We thank Mareike Rothenheber, Christine Wehr, Jennifer Kuhn, Nadine Zucchetto, Sina Abdo, Regina Zweigert, Veronika Eckert, and Kirsten-Susann Bommersheim for their technical support during the experiments.

Authors contributions

MO, SB, JG, and MS conceived and designed the experiments. MO, SB, MS, SM, BL, MM, CH, MP performed the experiments. MO, SB, MS, SM, MM, CH and MP analysed the data. MO, SB, MS and TFS drafted the first manuscript. TFS, JG and MS revised the manuscript. AV and PH initiated the public-private partnership between Fraunhofer and Sanofi (later Evotec). All authors accepted the final version of the manuscript.

Conflict of interest

The authors declare no conflict of interest. The authors declare no competing financial interest.

Data availability statement

The Illumina amplicon sequencing data supporting the findings of this study are openly available under the BioProject PRJNA699730 (<https://www.ncbi.nlm.nih.gov/bioproject/PRJNA699730>).

References

- Adamek, M., Alanjary, M., and Ziemert, N. (2019) Applied evolution: phylogeny-based approaches in natural products research. *Nat Prod Rep* **36**: 1295–1312.
- Akselband, Y., Cabral, C., Castor, T.P., Chikarmane, H.M., and McGrath, P. (2006) Enrichment of slow-growing marine microorganisms from mixed cultures using gel microdrop (GMD) growth assay and fluorescence-activated cell sorting. *J Exp Mar Biol Ecol* **329**: 196–205.
- Allard, P.-M., Péresse, T., Bisson, J., Gindro, K., Marcourt, L., van Pham, C., *et al.* (2016) Integration of molecular networking and in-silico MS/MS fragmentation for natural products dereplication. *Anal Chem* **88**: 3317–3323.
- Allen, F., Greiner, R., and Wishart, D. (2015) Competitive fragmentation modeling of ESI-MS/MS spectra for putative metabolite identification. *Metabolomics* **11**: 98–110.
- Baret, J.-C., Miller, O.J., Taly, V., Ryckelynck, M., El-Harrak, A., Frenz, L., *et al.* (2009) Fluorescence-activated droplet sorting (FADS): efficient microfluidic cell sorting based on enzymatic activity. *Lab Chip* **9**: 1850.
- Barra Caracciolo, A., Grenni, P., Cupo, C., and Rossetti, S. (2005) In situ analysis of native microbial communities in complex samples with high particulate loads. *FEMS Microbiol Lett* **253**: 55–58.
- Belknap, K.C., Park, C.J., Barth, B.M., and Andam, C.P. (2020) Genome mining of biosynthetic and chemotherapeutic gene clusters in *Streptomyces* bacteria. *Sci Rep* **10**: 1–9.
- Biener, G., Masson-Meyers, D.S., Bumah, V.V., Hussey, G., Stoneman, M.R., Enwemeka, C.S., and Raicu, V. (2017) Blue/violet laser inactivates methicillin-resistant *Staphylococcus aureus* by altering its transmembrane potential. *J Photochem Photobiol B Biol* **170**: 118–124.
- Boedicker, J.Q., Vincent, M.E., and Ismagilov, R.F. (2009) Microfluidic confinement of single cells of bacteria in small volumes initiates high-density behavior of quorum sensing and growth and reveals its variability. *Angew Chem Int Ed Engl* **48**: 5908–5911.
- Boitard, L., Cottinet, D., Bremond, N., Baudry, J., and Bibette, J. (2015) Growing microbes in millifluidic droplets. *Eng Life Sci* **15**: 318–326.
- Bon, R.S., and Waldmann, H. (2010) Bioactivity-guided navigation of chemical space. *Acc Chem Res* **43**: 1103–1114.
- Butler, M.S., and Paterson, D.L. (2020) Antibiotics in the clinical pipeline in October 2019. *J Antibiot* **73**: 329–364.
- Caballero-Aguilar, L.M., Duchib, S., Quigley, A., Onofriolo, C., Di Bellab, C., and Moultona, S.E. (2021) Microencapsulation of growth factors by microfluidic system. *MethodsX* **8**: 101324.
- Collins, D.J., Neild, A., deMello, A., Liu, A.Q., and Ai, Y. (2015) The Poisson distribution and beyond: methods for microfluidic droplet production and single cell encapsulation. *Lab Chip* **15**: 3439–3459.
- Crits-Christoph, A., Diamond, S., Butterfield, C.N., Thomas, B.C., and Banfield, J.F. (2018) Novel soil bacteria possess diverse genes for secondary metabolite biosynthesis. *Nature* **558**: 440–444.
- Damsté, J.S.S., Rijpstra, W.I.C., Dedysh, S.N., Foesel, B.U., and Villanueva, L. (2017) Pheno- and Genotyping of Hopanoid Production in Acidobacteria. *Front Microbiol* **8**: 968.
- Daniel, W.W. (1990) *Applied nonparametric statistics*. PWS-KENT Pub. University of Michigan. URL <https://books.google.de/books?id=0hPvAAAAMAAJ>.
- Delgado-Baquerizo, M., Maestre, F.T., Reich, P.B., Jeffries, T.C., Gaitan, J.J., Encinar, D., *et al.* (2016) Microbial diversity drives multifunctionality in terrestrial ecosystems. *Nat Commun* **7**: 10541.
- Duetz, W.A., Rüedi, L., Hermann, R., O'Connor, K., Büchs, J., and Witholt, B. (2000) Methods for intense aeration, growth, storage, and replication of bacterial strains in microtiter plates. *Appl Environ Microbiol* **66**: 2641–2646.
- Dunn, O.J. (1964) Multiple comparisons using rank sums. *Technometrics* **6**: 241–252.
- Dwivedi, D., Jansen, R., Molinari, G., Nimtz, M., Johri, B.N., and Wray, V. (2008) Antimycobacterial serratomolides and diacyl peptoglycosamine derivatives from *Serratia* sp. *J Nat Prod* **71**: 637–641.
- Firn, R.D., and Jones, C.G. (2003) Natural products - a simple model to explain chemical diversity. *Nat Prod Rep* **20**: 382–391.
- Fox, J.L. (2014) Fraunhofer to mine Sanofi microbial collection. *Nat Biotechnol* **32**: 305.
- Gerard, J., Lloyd, R., Barsby, T., Haden, P., Kelly, M.T., and Andersen, R.J. (1997) Massetolides A-H, antimycobacterial cyclic depsipeptides produced by two *Pseudomonas* isolated from marine habitats. *J Nat Prod* **60**: 223–229.

- Gross, H., and Loper, J.E. (2009) Genomics of secondary metabolite production by *Pseudomonas* spp. *Nat Prod Rep* **26**: 1408.
- Hammer, Ø., Harper, D.A.T., and Ryan, P.D. (2001) PAST: Paleontological statistics software package for education and data analysis. *Palaeontol Electron* **4**: 1–9.
- Hartwig, C. (2020) christoph-hartwig-ime-br/cosine-V2: cosine-v2. *Zenodo*.
- Hoffmann, T., Krug, D., Bozkurt, N., Duddela, S., Jansen, R., Garcia, R., *et al.* (2018) Correlating chemical diversity with taxonomic distance for discovery of natural products in myxobacteria. *Nat Commun* **9**: 803.
- Hong, J. (2011) Role of natural product diversity in chemical biology. *Curr Opin Chem Biol* **15**: 350–354.
- Imai, Y.u., Meyer, K.J., Iinishi, A., Favre-Godal, Q., Green, R., Manuse, S., *et al.* (2019) A new antibiotic selectively kills Gram-negative pathogens. *Nature* **576**: 459–464.
- Ishii, S., Tago, K., and Senoo, K. (2010) Single-cell analysis and isolation for microbiology and biotechnology: methods and applications. *Appl Microbiol Biotechnol* **86**: 1281–1292.
- Kaeberlein, T. (2002) Isolating “Uncultivable” microorganisms in pure culture in a simulated natural environment. *Science* **296**: 1127–1129.
- Kämpfer, P., Dott, W., Martin, K., and Glaeser, S.P. (2014) *Rhodococcus defluvi* sp. nov., isolated from wastewater of a bioreactor and formal proposal to reclassify [*Corynebacterium hoagii*] and *Rhodococcus equi* as *Rhodococcus hoagii* comb. nov. *Int J Syst Evol Microbiol* **64**(Pt 3): 755–761.
- Keller, M., and Zengler, K. (2004) Tapping into microbial diversity. *Nat Rev Microbiol* **2**: 141–150.
- Kielak, A.M., Barreto, C.C., Kowalchuk, G.A., van Veen, J.A., and Kuramae, E.E. (2016) The ecology of Acidobacteria: moving beyond genes and genomes. *Front Microbiol* **7**: 744.
- Koch, I.H., Gich, F., Dunfield, P.F., and Overmann, J. (2008) *Edaphobacter modestus* gen. nov., sp. nov., and *Edaphobacter aggregans* sp. nov., acidobacteria isolated from alpine and forest soils. *Int J Syst Evol Microbiol* **58**: 1114–1122.
- Koeth, T., Versalovic, J., and Lupski, J.R. (1995) Differential subsequence conservation of interspersed repetitive *Streptococcus pneumoniae* BOX elements in diverse bacteria. *Genome Res* **5**: 408–418.
- Kumar, S., Stecher, G., and Tamura, K. (2016) MEGA7: Molecular Evolutionary Genetics Analysis Version 7.0 for Bigger Datasets. *Mol Biol Evol* **33**: 1870–1874.
- Laatsch, H. (2017) *AntiBase: The Natural Compound Identifier*. Weinheim, Germany: Wiley-VCH.
- Lakemeyer, M., Zhao, W., Mandl, F.A., Hammann, P., and Sieber, S.A. (2018) Über bisherige Denkweisen hinaus - neue Wirkstoffe zur Überwindung der Antibiotika-Krise. *Angew Chem* **130**: 14642–14682.
- Leman, M., Abouakil, F., Griffiths, A.D., and Tabeling, P. (2015) Droplet-based microfluidics at the femtolitre scale. *Lab Chip* **15**: 753–765.
- Letunic, I., and Bork, P. (2019) Interactive Tree Of Life (iTOL) v4: recent updates and new developments. *Nucleic Acids Res* **47**: W256–W259.
- Lewis, K. (2013) Platforms for antibiotic discovery. *Nat Rev Drug Discov* **12**: 371–387.
- Ling, L.L., Schneider, T., Peoples, A.J., Sporing, A.L., Engels, I., Conlon, B.P., *et al.* (2015) A new antibiotic kills pathogens without detectable resistance. *Nature* **517**: 455–459.
- Lok, C. (2015) Mining the microbial dark matter. *Nature* **522**: 270–273.
- Mahler, L., Tovar, M., Weber, T., Brandes, S., Rudolph, M.M., Ehgartner, J., *et al.* (2015) Enhanced and homogeneous oxygen availability during incubation of microfluidic droplets. *RSC Adv* **5**: 101871–101878.
- Mamer, M., Patras, M.A., Kurz, M., Zubeil, F., Förster, F., Schuler, S., *et al.* (2020) Molecular networking-guided discovery and characterization of stechlinsins, a group of cyclic lipopeptides from a *Pseudomonas* sp. *J Nat Prod* **83**: 2607–2617.
- Medema, M.H., Cimermancic, P., Sali, A., Takano, E., and Fischbach, M.A. (2014) A systematic computational analysis of biosynthetic gene cluster evolution: lessons for engineering biosynthesis. *PLoS Comput Biol* **10**: e1004016.
- Monciardini, P., Iorio, M., Maffioli, S., Sosio, M., and Donadio, S. (2014) Discovering new bioactive molecules from microbial sources. *Microb Biotechnol* **7**: 209–220.
- Mulligan, C.N. (2005) Environmental applications for biosurfactants. *Environ Pollut* **133**: 183–198.
- Newman, D.J., and Cragg, G.M. (2020) Natural products as sources of new drugs over the nearly four decades from 01/1981 to 09/2019. *J Nat Prod* **83**: 770–803.
- Nge, P.N., Rogers, C.I., and Woolley, A.T. (2013) Advances in microfluidic materials, functions, integration, and applications. *Chem Rev* **113**: 2550–2583.
- Nguyen, T.M., Seo, C., Ji, M., Paik, M.-J., Myung, S.-W., and Kim, J. (2018) Effective soil extraction method for cultivating previously uncultured soil bacteria. *Appl Environ Microbiol* **84**: e01145-18.
- Nicault, M., Tidjani, A.-R., Gauthier, A., Dumarcay, S., Gelhaye, E., Bontemps, C., and Leblond, P. (2020) Mining the biosynthetic potential for specialized metabolism of a *Streptomyces* soil community. *Antibiotics* **9**: 271.
- Oberpaul, M., Zumkeller, C.M., Culver, T., Spohn, M., Mihajlovic, S., Leis, B., *et al.* (2020) High-throughput cultivation for the selective isolation of Acidobacteria from termite nests. *Front Microbiol* **11**: 597628.
- Overmann, J., Abt, B., and Sikorski, J. (2017) Present and future of culturing bacteria. *Annu Rev Microbiol* **71**: 711–730.
- Owen, W.J., Yao, C., Myung, K., Kemmitt, G., Leader, A., Meyer, K.G., *et al.* (2017) Biological characterization of fenpicoxamid, a new fungicide with utility in cereals and other crops. *Pest Manag Sci* **73**: 2005–2016.
- Panthee, S., Hamamoto, H., Paudel, A., and Sekimizu, K. (2016) *Lysobacter* species: a potential source of novel antibiotics. *Arch Microbiol* **198**: 839–845.
- Panzer, K., Yilmaz, P., Weiß, M., Reich, L., Richter, M., Wiese, J., *et al.* (2015) Identification of habitat-specific biomes of aquatic fungal communities using a comprehensive nearly full-length 18S rRNA dataset enriched with contextual data. *PLoS One* **10**: e0134377.

- Parte, A.C. (2018) LPSN - List of Prokaryotic names with Standing in Nomenclature (bacterio.net), 20 years on. *Int J Syst Evol Microbiol* **68**: 1825–1829.
- Payne, E.M., Holland-Moritz, D.A., Sun, S., and Kennedy, R.T. (2020) High-throughput screening by droplet microfluidics: perspective into key challenges and future prospects. *Lab Chip* **20**: 2247–2262.
- Phillies, G. (1975) Nonactin, monactin, dinactin, trinactin, and tetranactin. A Raman Spectroscopic Study. *Biopolymers* **14**: 2311–2327.
- Pöppel, A.-K., Koch, A., Kogel, K.-H., Vogel, H., Kollwe, C., Wiesner, J., and Vilcinskas, A. (2014) Lucimycin, an antifungal peptide from the therapeutic maggot of the common green bottle fly *Lucilia sericata*. *Biol Chem* **395**: 649–656.
- R Core Team (2020) *R: A Language and Environment for Statistical Computing*. Vienna, Austria: R Foundation for Statistical Computing.
- Rezanka, T., Prell, A., Spížek, J., and Sigler, K. (2010) Pilot-plant cultivation of *Streptomyces griseus* producing homologues of nonactin by precursor-directed biosynthesis and their identification by LC/MS-ESI. *J Antibiot* **63**: 524–529.
- Riyanti, Marner, M., Hartwig, C., Patras, M., Wodi, S., Rieuwpassa, F., *et al.* (2020) Sustainable low-volume analysis of environmental samples by Semi-Automated Prioritization of Extracts for Natural Product Research (SeaPEPR). *Mar Drugs* **18**: 649.
- Schäberle, T.F., and Hack, I.M. (2014) Overcoming the current deadlock in antibiotic research. *Trends Microbiol* **22**: 165–167.
- Shannon, P. (2003) Cytoscape: A software environment for integrated models of biomolecular interaction networks. *Genome Res* **13**: 2498–2504.
- Shapiro, H.M. (2000) Membrane potential estimation by flow cytometry. *Methods* **21**: 271–279.
- Stewart, E.J. (2012) Growing unculturable bacteria. *J Bacteriol* **194**: 4151–4160.
- Strobel, G.A., Morrison, S.L., and Cassella, M. (2005) Protecting plants from oomycete pathogens by treatment with compositions containing serratomolide and oocydin a from *Serratia marcescens*. Patent No.: US6926892B2.
- Tacconelli, E., Carrara, E., Savoldi, A., Harbarth, S., Mendelson, M., Monnet, D.L., *et al.* (2018) Discovery, research, and development of new antibiotics: the WHO priority list of antibiotic-resistant bacteria and tuberculosis. *Lancet Infect Dis* **18**: 318–327.
- Tamehiro, N., Okamoto-Hosoya, Y., Okamoto, S., Ubukata, M., Hamada, M., Naganawa, H., and Ochi, K. (2002) Bacilysocin, a Novel phospholipid antibiotic produced by *Bacillus subtilis* 168. *Antimicrob Agents Chemother* **46**: 315–320.
- Terekhov, S.S., Smirnov, I.V., Stepanova, A.V., Bobik, T.V., Mokrushina, Y.A., Ponomarenko, N.A., *et al.* (2017) Microfluidic droplet platform for ultrahigh-throughput single-cell screening of biodiversity. *Proc Natl Acad Sci USA* **114**: 2550–2555.
- Theberge, A.B., Courtois, F., Schaerli, Y., Fischlechner, M., Abell, C., Hollfelder, F., and Huck, W.T. (2010) Microdroplets in microfluidics: an evolving platform for discoveries in chemistry and biology. *Angew Chem Int Ed Engl* **49**: 5846–5868.
- Theuretzbacher, U., Outtersson, K., Engel, A., and Karlén, A. (2020) The global preclinical antibacterial pipeline. *Nat Rev Microbiol* **18**: 275–285.
- Thies, S., Santiago-Schübel, B., Kovačić, F., Rosenau, F., Hausmann, R., and Jaeger, K.-E. (2014) Heterologous production of the lipopeptide biosurfactant serrawettin W1 in *Escherichia coli*. *J Biotechnol* **181**: 27–30.
- Tovar, M., Mahler, L., Buchheim, S., Roth, M., and Rosenbaum, M.A. (2020) Monitoring and external control of pH in microfluidic droplets during microbial culturing. *Microb Cell Fact* **19**: 16.
- Tracanna, V., de Jong, A., Medema, M.H., and Kuipers, O.P. (2017) Mining prokaryotes for antimicrobial compounds: from diversity to function. *FEMS Microbiol Rev* **41**: 417–429.
- Umetsu, N., and Shirai, Y. (2020) Development of novel pesticides in the 21st century. *J Pestic Sci* **45**: 54–74.
- Volpatti, L.R., and Yetisen, A.K. (2014) Commercialization of microfluidic devices. *Trends Biotechnol* **32**: 347–350.
- Ward, J.H. (1963) Hierarchical grouping to optimize an objective function. *J Am Stat Assoc* **58**: 236–244.
- Wasseman, H.H., Keggi, J.J., and McKeon, J.E. (1961) Serratamolide, a metabolic product of *Serratia*. *J Am Chem Soc* **83**: 4107–4108.
- Wiegand, S., Jogler, M., Boedecker, C., Pinto, D., Vollmers, J., Rivas-Marín, E., *et al.* (2019) Cultivation and functional characterization of 79 planctomycetes uncovers their unique biology. *Nat Microbiol* **5**: 126–140.
- Yang, J.Y., Sanchez, L.M., Rath, C.M., Liu, X., Boudreau, P.D., Bruns, N., *et al.* (2013) Molecular networking as a dereplication strategy. *J Nat Prod* **76**: 1686–1699.
- Zengler, K., Toledo, G., Rappe, M., Elkins, J., Mathur, E.J., Short, J.M., and Keller, M. (2002) Cultivating the uncultured. *Proc Natl Acad Sci USA* **99**: 15681–15686.
- Zinchenko, A., Devenish, S.R., Kintsjes, B., Colin, P.Y., Fischlechner, M., and Hollfelder, F. (2014) One in a million: flow cytometric sorting of single cell-lysate assays in monodisperse picolitre double emulsion droplets for directed evolution. *Anal Chem* **86**: 2526–2533.
- Zizika, Z. (1998) Biological effects of macrotetrolide antibiotics and nonactin acids. *Folia Microbiol* **43**: 7–14.

Supporting information

Additional supporting information may be found online in the Supporting Information section at the end of the article.

Fig. S1. Poisson distribution of $\lambda 0.1$ and $\lambda 10$ showing the probability of the amount of cells encapsulated per droplet.

Fig. S2. Work scheme of this study showing the microfluidics workflow, the subsequent cultivation, screening and dereplication

Fig. S3. Live/dead staining using the LIVE/DEAD BacLight Bacterial Viability and Counting Kit (L7007, Invitrogen). Manufacturer's protocol was applied on the cells retrieved by nycodenz density gradient centrifugation (A: SYTO 9, B: propidium iodide, C: merged) directly after bacterial isolation. Exemplary pictures are shown, ten independent stains were done and considered for the calculation. Live:dead ratio was estimated resulting in $\sim 70:30 \pm 6.7\%$.

Fig. S4. Phylogenetic classification of FHG110511 within the phylum Acidobacteria clustering into subgroup 1. The tree is based on a ClustalW alignment of available 16S rRNA gene sequences from the ref_seq database between positions 113 and 1357 [based on Escherichia coli 16S rRNA gene numbering (Brosius et al., 1978)] from the most similar sequences to the isolated strains, and also includes representatives of Acidobacteria subgroups 1, 3, 4, 6, 7, 8, and 10. The tree was calculated using MEGA v7.0.26 with the maximum-likelihood method and GTR-Gamma model. Circles on the tree branches indicate values of 1000 bootstrap replicates with a bootstrap support of more than 50%. Subgroup affiliations are indicated by colors. The new isolate is indicated by a black arrow. The tree is drawn to scale, with branch lengths measured in the number of substitutions per site.

Fig. S5. (A) Assay read-out of μ -fractionation plates of strain FHG110488 against *M. smegmatis* ATCC 607. Fractions are numbered and those causing at least 70% rel. growth inhibition were considered "active" and marked red. Column 1: medium control; Column 2+3: antibiotic standard (isoniazid); Column 4: growth control. Area AH05-AH24 top: 5 μ l injection volume; Area AH05-AH24 bottom: 10 μ l injection; Crude: crude extract as a control. (B) Overlaid Base peak Chromatogram (grey), fraction collector analog signal (light blue bars) and extracted ion chromatogram of m/z 515.3329 \pm 0.005 [M+H]⁺ (1, red) of the 50 fold concentrated extract (in MeOH) with 5 μ l injection volume. (C) UV and MS spectrum of fractions 84-87. (D) MS/MS fragmentation of the precursor ion at m/z 515.3330 [M+H]⁺ (dereplicated as Serratamolide A, displayed in red) with manual annotation of the neutral losses.

Fig. S6. (A) MS2-network of "active" extract of FHG110488 against *Septoria tritici* MUCL45407 focusing on the cluster representing all seven detected serratamolide derivatives and their literature known structures (dots of parent ions found as hits in our internal database or AntiBase are marked in gold). (B) Overlaid Base peak Chromatogram (grey) and extracted ion chromatograms of serratamolides 1-7 (1 m/z 515.3327 [M+H]⁺, C₂₆H₄₇N₂O₈⁺ (red); 2 m/z 541.3483 [M+H]⁺, C₂₈H₄₉N₂O₈⁺ (blue); 3 m/z 543.3640 [M+H]⁺, C₂₈H₅₁N₂O₈⁺ (black); 4 m/z 533.3433 [M+H]⁺, C₂₆H₄₉N₂O₉⁺ (cyan); 5 m/z 547.3598 [M+H]⁺, C₂₇H₅₁N₂O₉⁺ (yellow); 6 m/z 575.3902 [M+H]⁺, C₂₉H₅₅N₂O₉⁺ (light green); 7 m/z 573.3746 [M+H]⁺, C₂₉H₅₃N₂O₉⁺ (dark green)) of the 50 fold concentrated extract (in MeOH) with 5 μ l injection volume. (C) MS/MS fragmentation of the precursor ions 1-7.

Fig. S7. (A) Assay read-out of μ -fractionation plate of strain FHG110502 against *Mycobacterium smegmatis* ATCC 607. Fractions are numbered and those causing at least 70% rel. growth inhibition were considered "active" and marked red. Column 1: medium control; Column 2+3: antibiotic standard (isoniazid); Column 4: growth control. Area AH05-AH24: 2 μ l injection volume; Area IP05-IP24: 5 μ l injection; Crude: crude extract as a control. (B) Overlaid Base peak Chromatograms (grey), Fraction collector analog signals (light blue bars) and extracted ion chromatograms of m/z 1112.6814 \pm 0.005 [M+H]⁺ (8, red) with corresponding m/z 556.8446 \pm 0.005 [M+2H]²⁺ (green), m/z 1126.6973 \pm 0.005 [M+H]⁺ (9, yellow) with corresponding m/z 563.8524 \pm 0.005 [M+2H]²⁺ (blue), and m/z 1154.7288 \pm 0.005 [M+H]⁺ (10,

purple) with corresponding m/z 577.8680 \pm 0.005 [M+2H]²⁺ (magenta) of the 50 fold concentrated extract (in MeOH) with 5 μ l injection volume. (C) UV and MS spectrum of fractions 105-106 (left), 108-118 (middle) and 116 (right). (D) MS/MS fragmentation of the precursor ion at m/z 1112.6814 [M+H]⁺, m/z 1126.6973 [M+H]⁺, and m/z 1154.7288 [M+H]⁺ (dereplicated as massetolide E, massetolide F and massetolide H, respectively), manual annotation of the neutral losses and proposed structures of the fragment ions at m/z 284.2229 and m/z 312.2533. (E) Structures of all three dereplicated compounds 8-10.

Fig. S8. (A) Assay read-out of μ -fractionation plate of strain FHG110502 against *Mycobacterium smegmatis* ATCC 607. Fractions are numbered and those causing at least 70% rel. growth inhibition were considered "active" and marked red. Column 1: medium control; Column 2+3: antibiotic standard (isoniazid); Column 4: growth control. Area AH05-AH24: 2 μ l injection volume; Area IP05-IP24: 5 μ l injection; Crude: crude extract as a control. (B) Overlaid Base peak Chromatograms (grey), Fraction collector analog signals (light blue bars) and extracted ion chromatograms of m/z 454.2931 \pm 0.005 [M+H]⁺ (11, red), m/z 690.5073 \pm 0.005 [M+H]⁺ (12, blue) and m/z 716.5237 \pm 0.005 [M+H]⁺ (13, green) of the 50 fold concentrated extract (in MeOH) with 5 μ l injection volume. (C) UV and MS spectrum of fractions 93-94 (left) and 130-136 (right). (D) MS/MS fragmentation of the precursor ion at m/z 454.2931 [M+H]⁺, m/z 690.5073 [M+H]⁺, and m/z 716.5237 [M+H]⁺ (dereplicated as lyso-palmitoyl-phosphoethanolamine, palmitoleoyl-palmitoyl-phosphoethanolamine and palmitoleoyl-oleoyl-phosphoethanolamine, respectively), manual annotation of the neutral losses and proposed structures of the fragment ions. (E) Putative structures of all three dereplicated compounds 11-13.

Fig. S9. (A) Assay read-out of μ -fractionation plate of strain FHG110508 against *Staphylococcus aureus* ATCC 25923. Fractions are numbered and those causing at least 70% rel. growth inhibition were considered "active" and marked red. Column 1: medium control; Column 2+3: antibiotic standard (gentamycin); Column 4: growth control. Area AH05-AH24: 2 μ l injection volume; Area IP05-IP24: 5 μ l injection; Crude: crude extract as a control. (B) Overlaid Base peak Chromatograms (grey), Fraction collector analog signals (light blue bars) and extracted ion chromatograms of m/z 737.4475 \pm 0.005 [M+H]⁺ (14, red), m/z 751.4636 \pm 0.005 [M+H]⁺ (15, green), m/z 765.4794 \pm 0.005 [M+H]⁺ (16, blue), and m/z 779.4956 \pm 0.005 [M+H]⁺ (17, yellow) of the 50 fold concentrated extract (in MeOH) with 5 μ l injection volume. (C) UV and MS spectrum of fractions 120, 124, 128 and 131-132 (from left to right). (D) MS/MS fragmentation of the precursor ion at m/z 737.4462 [M+H]⁺, m/z 751.4618 [M+H]⁺, m/z 765.4779 [M+H]⁺, and m/z 779.4933 [M+H]⁺ (dereplicated as nonactin, monactin, dinactin and macrotretolide G, respectively) with manual annotation of the neutral loss and proposed structure of the fragment ion at m/z 213.1482 of parent ion at m/z 779.4933 indicating the presence of macrotretolide G instead of trinactin. (E) Structures of all four dereplicated macrotretolides. Me: methyl; Et: ethyl; iPr: isopropyl.

Fig. S10. (A) MS2-network of "active" extract of FHG110508 against *Staphylococcus aureus* ATCC 25923 with focus on the cluster representing all five detected macrotretolide derivatives and their adduct ions (dots of parent ions found as hits in our internal database or AntiBase

Supplementary material

Combination of high-throughput Microfluidics- and FACS technologies to leverage the numbers game in natural product discovery

Markus Oberpaul^{1,λ}, Stephan Brinkmann^{1,λ}, Michael Marner¹, Sanja Mihajlovic¹, Benedikt Leis¹, Maria A. Patras¹, Christoph Hartwig¹, Andreas Vilcinskas^{1,2}, Peter E. Hammann³, Till F. Schäberle^{1,2,4*}, Marius Spohn^{1,**} and Jens Glaeser^{3,***}

¹ Fraunhofer Institute for Molecular Biology and Applied Ecology (IME), Branch for Bioresources, 35392 Giessen, Germany

² Institute for Insect Biotechnology, Justus-Liebig-University-Giessen, 35392 Giessen, Germany

³ Evotec International GmbH, 37079 Göttingen, Germany

⁴ German Center for Infection Research (DZIF), partner site Giessen-Marburg-Langen, 35392 Giessen, Germany

Correspondence: *Till F. Schäberle Till.F.Schaeberle@agrar.uni-giessen.de; **Marius Spohn marius.spohn@ime.fraunhofer.de; ***Jens Glaeser Jens.Glaeser@evotec.com;

^λ Authors contributed equally

Running title: Microfluidics-FACS bioprospecting platform

Keywords: Microfluidics, FACS, high-throughput cultivation, underexplored bacterial phyla, natural product discovery, antimycobacterial, crop disease management, Acidobacteria

Supplementary Fig. S1. Poisson distribution of $\lambda 0.1$ and $\lambda 10$ showing the probability of the amount of cells encapsulated per droplet.

Supplementary Fig. S2. Work scheme of this study showing the microfluidics workflow, the subsequent cultivation, screening and dereplication

Supplementary Fig. S3. Live/dead staining using the LIVE/DEAD BacLight Bacterial Viability and Counting Kit (L7007, Invitrogen).

Supplementary Tab. S1. Overview of the cultured genera separated by sample and media.

Supplementary Fig. S4. Phylogenetic classification of FHG110511 within the phylum Acidobacteria.

Supplementary Tab. S2. Cosine similarity table – Data for Fig. affiliation

Supplementary Fig. S5. Assay read-out of μ -fractionation plates of strain FHG110488 against *M. smegmatis* ATCC 607.

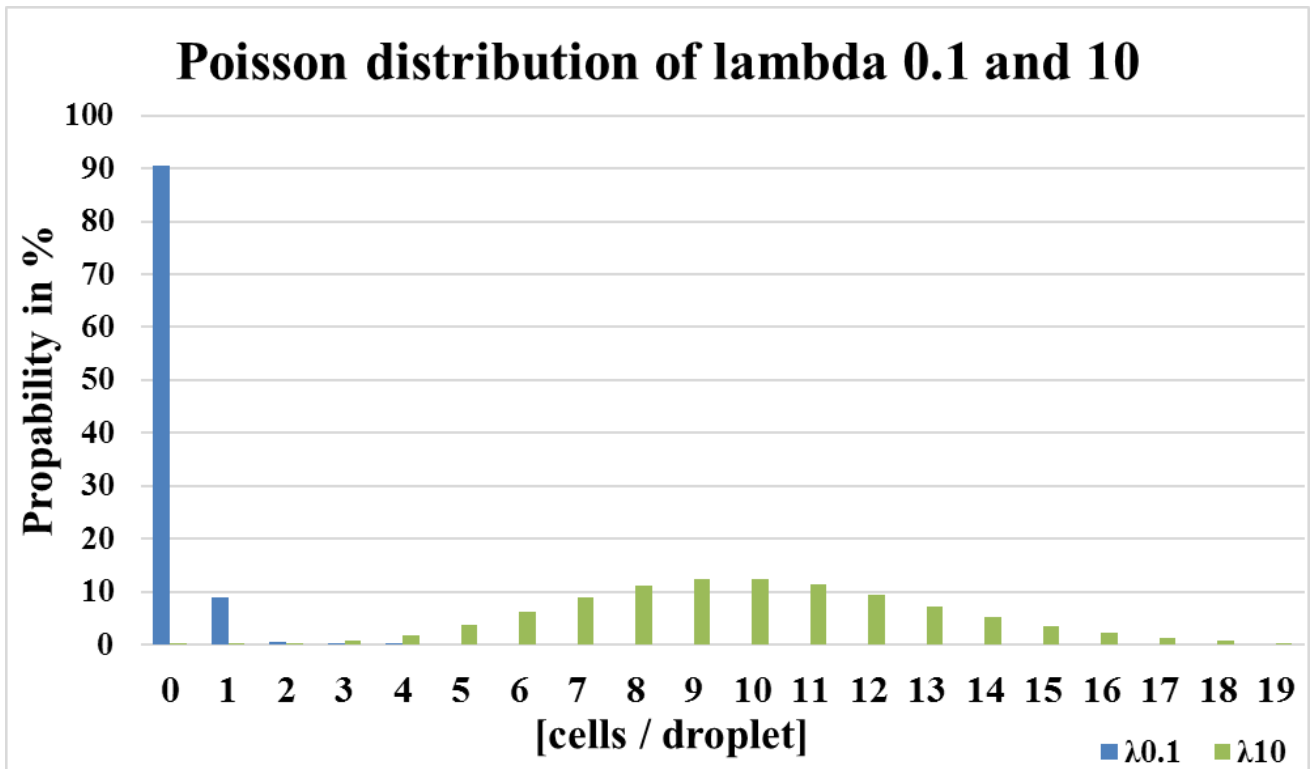
Supplementary Fig. S6. MS2-network of “active” extract of FHG110488 against *Septoria tritici* MUCL45407 focusing on the cluster representing all seven detected serratamolide derivatives and their literature known structures.

Supplementary Fig. S7. Assay read-out of fractions 104+105, 107-113 and 116 of μ -fractionation plate of strain FHG110502 against *Mycobacterium smegmatis* ATCC 607.

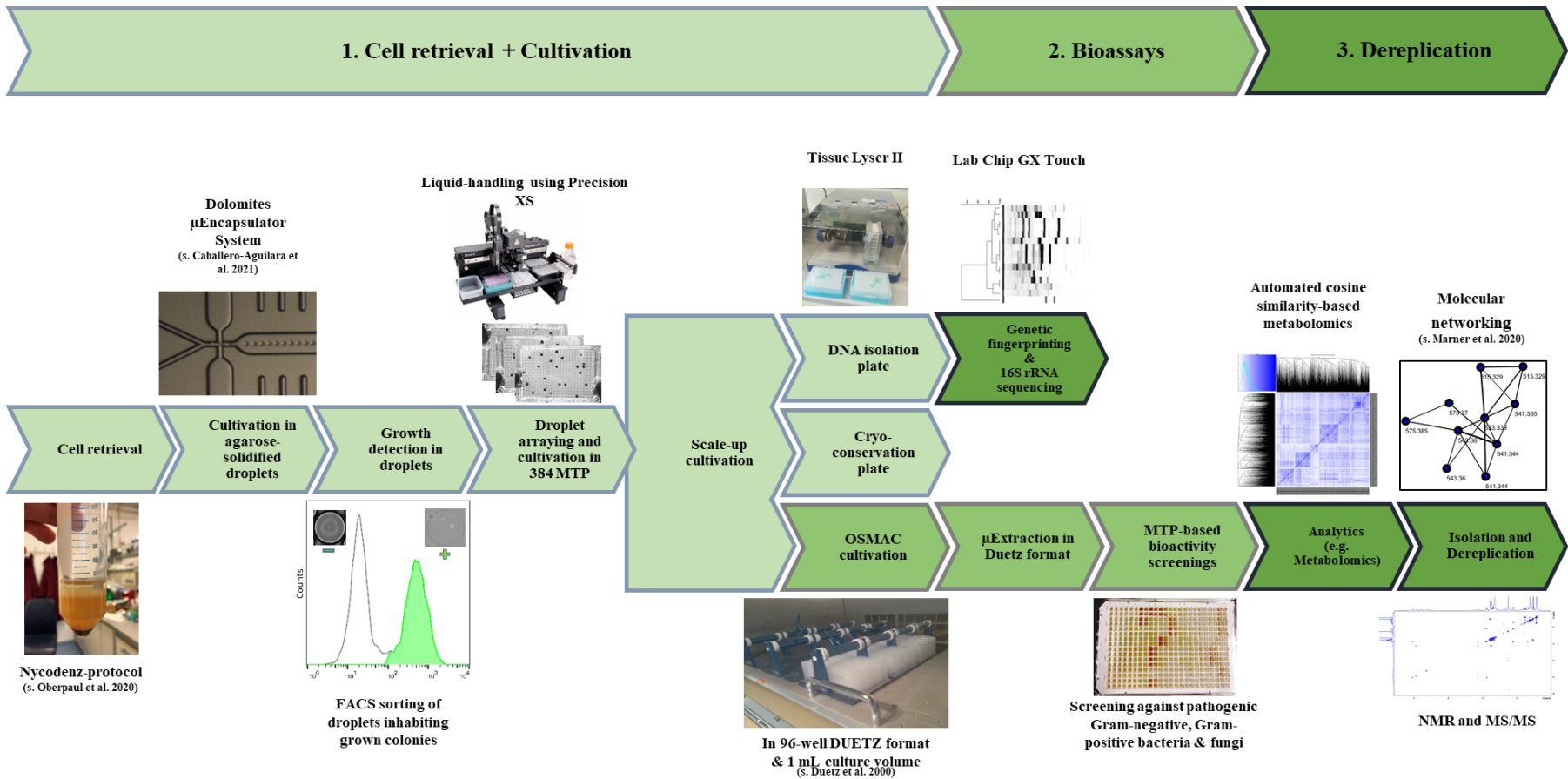
Supplementary Fig. S8. Assay read-out of fractions 92+93 and 130-135 of μ -fractionation plate of strain FHG110502 against *Mycobacterium smegmatis* ATCC 607.

Supplementary Fig. S9. Assay read-out of μ -fractionation plate of strain FHG110508 against *Staphylococcus aureus* ATCC 25923.

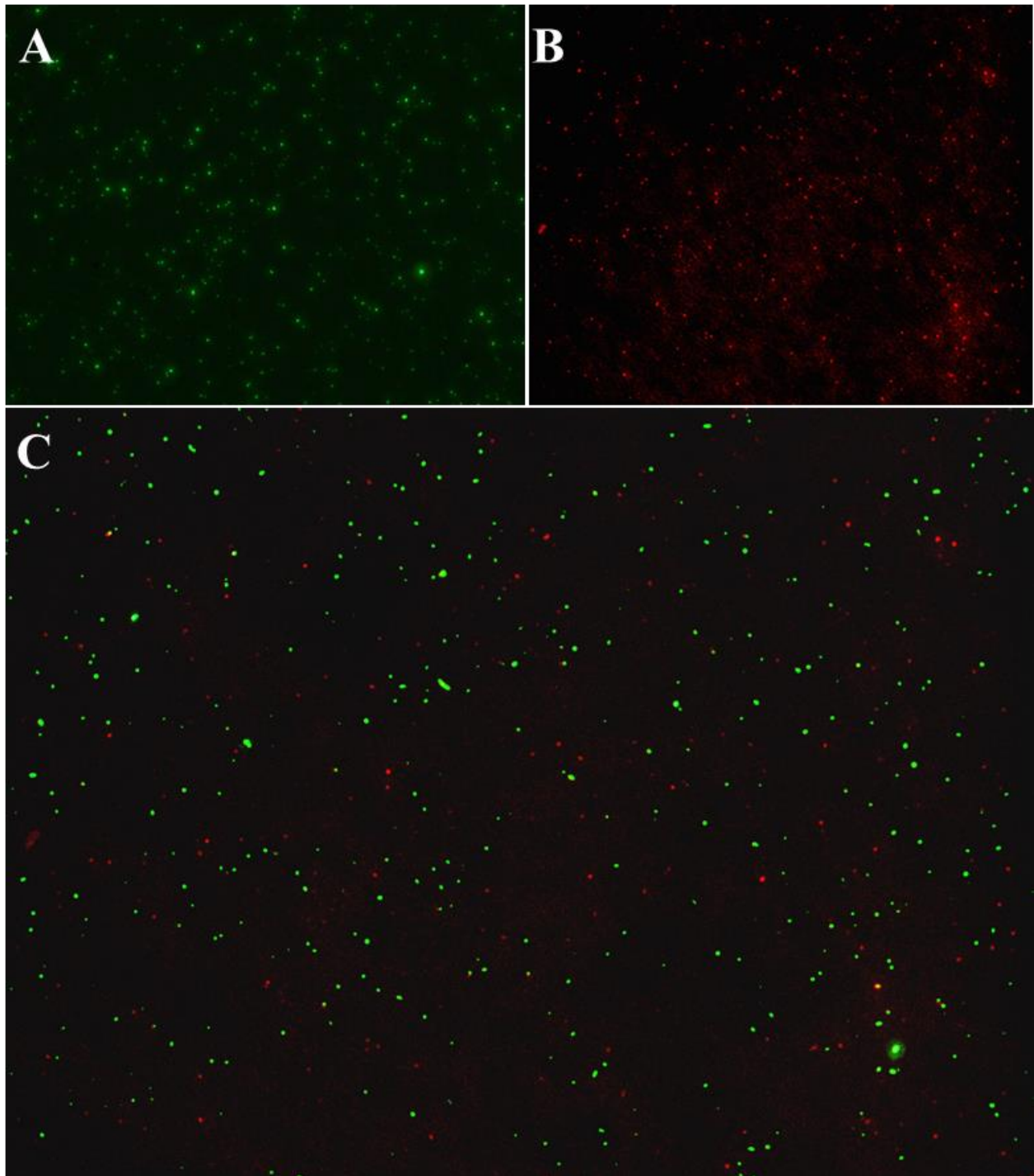
Supplementary Fig. S10. MS2-network of “active” extract of FHG110508 against *Staphylococcus aureus* ATCC 25923 with focus on the cluster representing all five detected macrotetrolide derivatives and their adduct ions.



Supplementary Fig. S1. Poisson distribution of $\lambda=0.1$ and $\lambda=10$ showing the probability of the amount of cells encapsulated per droplet.



Supplementary Fig. S2. Work scheme of this study showing the microfluidics workflow, the subsequent cultivation, screening and dereplication.



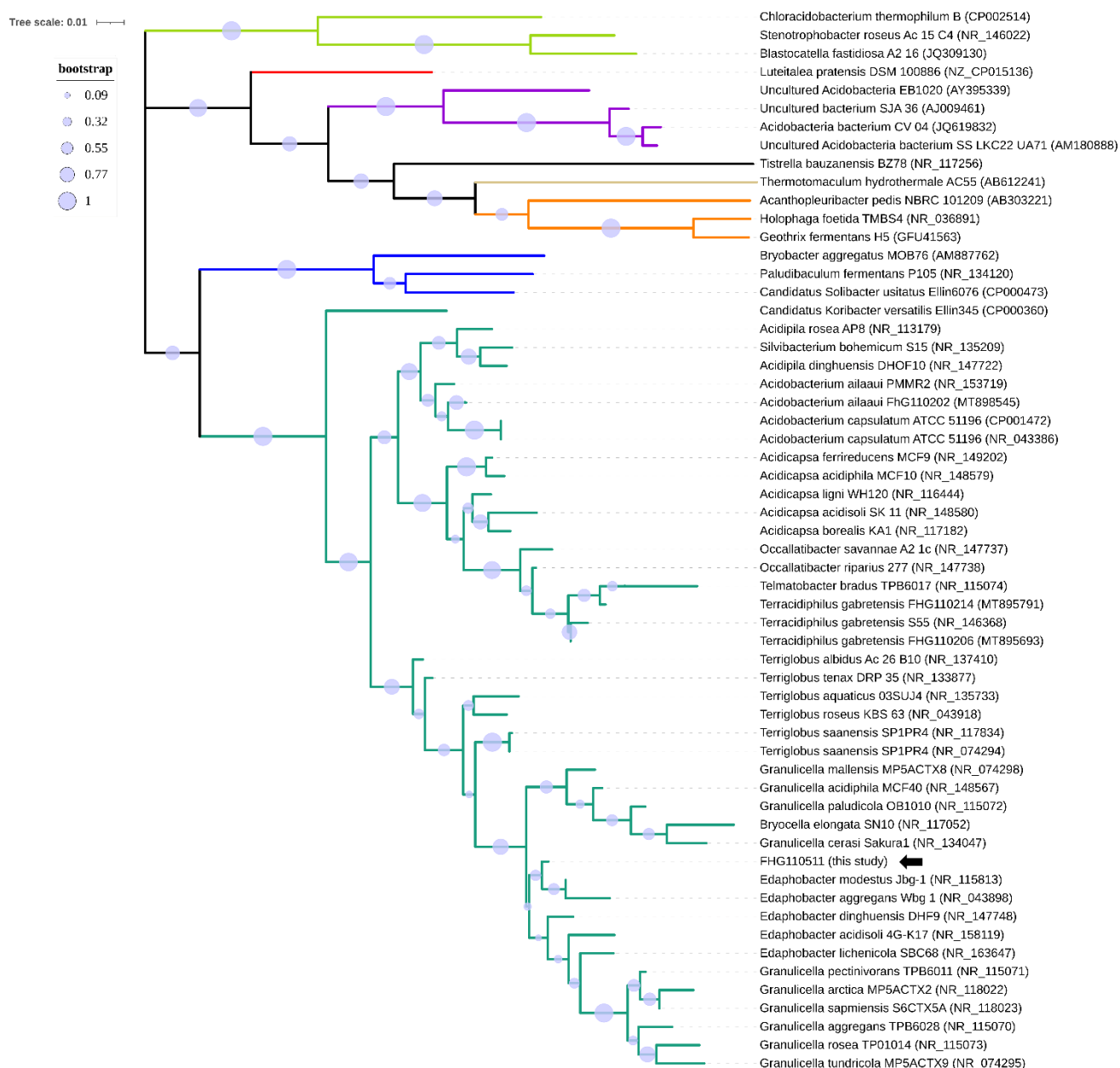
Supplementary Fig. S3. Live/dead staining using the LIVE/DEAD BacLight Bacterial Viability and Counting Kit (L7007, Invitrogen). Manufacturer's protocol was applied on the cells retrieved by nycodenz density gradient centrifugation (**A**: SYTO 9, **B**: propidium iodide, **C**: merged) directly after bacterial isolation. Exemplary pictures are shown, ten independent stains were done and considered for the calculation. Live:dead ratio was estimated resulting in $\sim 70:30 \pm 6.7\%$.

Tab. S1. Overview of the cultured genera in mISEM² pH 7.2, pH 5.5 and VL55-xyl pH 5.5. 16S rRNA gene sequencing was applied using the primer 1492R on mechanically disrupted culture broth grown for 7 days

Phylum	Class	Genus	No. of identified sequences	Collection date	Sampling site	Sampling coordinates	Local environment	Isolation medium
Acidobacteria	Acidobacteriia	<i>Edaphobacter</i>	2	29.01.2019	Bergwerkswald Gießen, Germany	50.564032 N, 8.672555 E	forrest soil	VL55-Xylan
Actinobacteria	Actinobacteria	<i>Mycobacterium</i>	4	29.01.2019	Bergwerkswald Gießen, Germany	50.564032 N, 8.672555 E	forrest soil	VL55-Xylan
Actinobacteria	Actinobacteria	<i>Cellulomonas</i>	1	29.01.2019	Bergwerkswald Gießen, Germany	50.564032 N, 8.672555 E	forrest soil	VL55-Xylan
Actinobacteria	Actinobacteria	<i>Nocardioides</i>	7	29.01.2019	Bergwerkswald Gießen, Germany	50.564032 N, 8.672555 E	forrest soil	VL55-Xylan
Actinobacteria	Actinobacteria	<i>Rothia</i>	1	29.01.2019	Bergwerkswald Gießen, Germany	50.564032 N, 8.672555 E	forrest soil	VL55-Xylan
Actinobacteria	Actinobacteria	<i>Streptomyces</i>	2	29.01.2019	Bergwerkswald Gießen, Germany	50.564032 N, 8.672555 E	forrest soil	VL55-Xylan
Actinobacteria	Actinobacteria	<i>Mycolicibacterium</i>	2	29.01.2019	Bergwerkswald Gießen, Germany	50.564032 N, 8.672555 E	forrest soil	VL55-Xylan
Bacteroidetes	Sphingobacteriia	<i>Mucilaginibacter</i>	5	29.01.2019	Bergwerkswald Gießen, Germany	50.564032 N, 8.672555 E	forrest soil	VL55-Xylan
Firmicutes	Clostridia	<i>Clostridium</i>	1	29.01.2019	Bergwerkswald Gießen, Germany	50.564032 N, 8.672555 E	forrest soil	VL55-Xylan
Proteobacteria	Alphaproteobacteria	<i>Ancylobacter</i>	1	29.01.2019	Bergwerkswald Gießen, Germany	50.564032 N, 8.672555 E	forrest soil	VL55-Xylan
Proteobacteria	Alphaproteobacteria	<i>Bradyrhizobium</i>	3	29.01.2019	Bergwerkswald Gießen, Germany	50.564032 N, 8.672555 E	forrest soil	VL55-Xylan
Proteobacteria	Alphaproteobacteria	<i>Inquilinus</i>	2	29.01.2019	Bergwerkswald Gießen, Germany	50.564032 N, 8.672555 E	forrest soil	VL55-Xylan
Proteobacteria	Alphaproteobacteria	<i>Kaistia</i>	1	29.01.2019	Bergwerkswald Gießen, Germany	50.564032 N, 8.672555 E	forrest soil	VL55-Xylan
Proteobacteria	Alphaproteobacteria	<i>Labrys</i>	9	29.01.2019	Bergwerkswald Gießen, Germany	50.564032 N, 8.672555 E	forrest soil	VL55-Xylan
Proteobacteria	Alphaproteobacteria	<i>Mesorhizobium</i>	30	29.01.2019	Bergwerkswald Gießen, Germany	50.564032 N, 8.672555 E	forrest soil	VL55-Xylan
Proteobacteria	Alphaproteobacteria	<i>Phyllobacterium</i>	98	29.01.2019	Bergwerkswald Gießen, Germany	50.564032 N, 8.672555 E	forrest soil	VL55-Xylan
Proteobacteria	Alphaproteobacteria	<i>Rhizobium</i>	42	29.01.2019	Bergwerkswald Gießen, Germany	50.564032 N, 8.672555 E	forrest soil	VL55-Xylan
Proteobacteria	Alphaproteobacteria	<i>Sphingomonas</i>	3	29.01.2019	Bergwerkswald Gießen, Germany	50.564032 N, 8.672555 E	forrest soil	VL55-Xylan
Proteobacteria	Betaproteobacteria	<i>Burkholderia</i>	6	29.01.2019	Bergwerkswald Gießen, Germany	50.564032 N, 8.672555 E	forrest soil	VL55-Xylan
Proteobacteria	Betaproteobacteria	<i>Variovorax</i>	1	29.01.2019	Bergwerkswald Gießen, Germany	50.564032 N, 8.672555 E	forrest soil	VL55-Xylan
Proteobacteria	Betaproteobacteria	<i>Caballeronia</i>	1	29.01.2019	Bergwerkswald Gießen, Germany	50.564032 N, 8.672555 E	forrest soil	VL55-Xylan
Proteobacteria	Gammaproteobacteria	<i>Moraxella</i>	1	29.01.2019	Bergwerkswald Gießen, Germany	50.564032 N, 8.672555 E	forrest soil	VL55-Xylan
Proteobacteria	Gammaproteobacteria	<i>Luteibacter</i>	1	29.01.2019	Bergwerkswald Gießen, Germany	50.564032 N, 8.672555 E	forrest soil	VL55-Xylan
Proteobacteria	Gammaproteobacteria	<i>Dyella</i>	1	29.01.2019	Bergwerkswald Gießen, Germany	50.564032 N, 8.672555 E	forrest soil	VL55-Xylan
		No Relative /no sequence data	117	29.01.2019	Bergwerkswald Gießen, Germany	50.564032 N, 8.672555 E	forrest soil	VL55-Xylan
Acidobacteria	Acidobacteriia	<i>Edaphobacter</i>	6	29.01.2019	Bergwerkswald Gießen, Germany	50.564032 N, 8.672555 E	forrest soil	mISEM ² pH 5.5
Actinobacteria	Actinobacteria	<i>Agromyces</i>	7	29.01.2019	Bergwerkswald Gießen, Germany	50.564032 N, 8.672555 E	forrest soil	mISEM ² pH 5.5
Actinobacteria	Actinobacteria	<i>Angustibacter</i>	2	29.01.2019	Bergwerkswald Gießen, Germany	50.564032 N, 8.672555 E	forrest soil	mISEM ² pH 5.5
Actinobacteria	Actinobacteria	<i>Cellulomonas</i>	2	29.01.2019	Bergwerkswald Gießen, Germany	50.564032 N, 8.672555 E	forrest soil	mISEM ² pH 5.5
Actinobacteria	Actinobacteria	<i>Leifsonia</i>	1	29.01.2019	Bergwerkswald Gießen, Germany	50.564032 N, 8.672555 E	forrest soil	mISEM ² pH 5.5
Actinobacteria	Actinobacteria	<i>Mycobacterium</i>	4	29.01.2019	Bergwerkswald Gießen, Germany	50.564032 N, 8.672555 E	forrest soil	mISEM ² pH 5.5
Actinobacteria	Actinobacteria	<i>Mycolicibacterium</i>	2	29.01.2019	Bergwerkswald Gießen, Germany	50.564032 N, 8.672555 E	forrest soil	mISEM ² pH 5.5
Actinobacteria	Actinobacteria	<i>Nocardioides</i>	2	29.01.2019	Bergwerkswald Gießen, Germany	50.564032 N, 8.672555 E	forrest soil	mISEM ² pH 5.5
Actinobacteria	Actinobacteria	<i>Rhodococcus</i>	1	29.01.2019	Bergwerkswald Gießen, Germany	50.564032 N, 8.672555 E	forrest soil	mISEM ² pH 5.5
Bacteroidetes	Sphingobacteriia	<i>Mucilaginibacter</i>	3	29.01.2019	Bergwerkswald Gießen, Germany	50.564032 N, 8.672555 E	forrest soil	mISEM ² pH 5.5
Proteobacteria	Alphaproteobacteria	<i>Ancylobacter</i>	9	29.01.2019	Bergwerkswald Gießen, Germany	50.564032 N, 8.672555 E	forrest soil	mISEM ² pH 5.5
Proteobacteria	Alphaproteobacteria	<i>Bosea</i>	1	29.01.2019	Bergwerkswald Gießen, Germany	50.564032 N, 8.672555 E	forrest soil	mISEM ² pH 5.5

Proteobacteria	Betaproteobacteria	<i>Burkholderia</i>	1	29.01.2019	Bergwerkswald Gießen, Germany	50.564032 N, 8.672555 E	forrest soil	mISEM ² pH 5.5
Proteobacteria	Gammaproteobacteria	<i>Buttiauxella</i>	1	29.01.2019	Bergwerkswald Gießen, Germany	50.564032 N, 8.672555 E	forrest soil	mISEM ² pH 5.5
Proteobacteria	Betaproteobacteria	<i>Caballeronia</i>	2	29.01.2019	Bergwerkswald Gießen, Germany	50.564032 N, 8.672555 E	forrest soil	mISEM ² pH 5.5
Proteobacteria	Betaproteobacteria	<i>Cupriavidus</i>	1	29.01.2019	Bergwerkswald Gießen, Germany	50.564032 N, 8.672555 E	forrest soil	mISEM ² pH 5.5
Proteobacteria	Gammaproteobacteria	<i>Dyella</i>	1	29.01.2019	Bergwerkswald Gießen, Germany	50.564032 N, 8.672555 E	forrest soil	mISEM ² pH 5.5
Proteobacteria	Alphaproteobacteria	<i>Inquilinus</i>	1	29.01.2019	Bergwerkswald Gießen, Germany	50.564032 N, 8.672555 E	forrest soil	mISEM ² pH 5.5
Proteobacteria	Gammaproteobacteria	<i>Luteibacter</i>	5	29.01.2019	Bergwerkswald Gießen, Germany	50.564032 N, 8.672555 E	forrest soil	mISEM ² pH 5.5
Proteobacteria	Alphaproteobacteria	<i>Mesorhizobium</i>	11	29.01.2019	Bergwerkswald Gießen, Germany	50.564032 N, 8.672555 E	forrest soil	mISEM ² pH 5.5
Proteobacteria	Alphaproteobacteria	<i>Phyllobacterium</i>	25	29.01.2019	Bergwerkswald Gießen, Germany	50.564032 N, 8.672555 E	forrest soil	mISEM ² pH 5.5
Proteobacteria	Alphaproteobacteria	<i>Rhizobium</i>	6	29.01.2019	Bergwerkswald Gießen, Germany	50.564032 N, 8.672555 E	forrest soil	mISEM ² pH 5.5
Proteobacteria	Alphaproteobacteria	<i>Sphingomonas</i>	9	29.01.2019	Bergwerkswald Gießen, Germany	50.564032 N, 8.672555 E	forrest soil	mISEM ² pH 5.5
Proteobacteria	Betaproteobacteria	<i>Variovorax</i>	3	29.01.2019	Bergwerkswald Gießen, Germany	50.564032 N, 8.672555 E	forrest soil	mISEM ² pH 5.5
		No Relative /no sequence data	20	29.01.2019	Bergwerkswald Gießen, Germany	50.564032 N, 8.672555 E	forrest soil	mISEM ² pH 5.5
Proteobacteria	Betaproteobacteria	<i>Achromobacter</i>	1	29.01.2019	Bergwerkswald Gießen, Germany	50.564032 N, 8.672555 E	forrest soil	mISEM ² pH 7.2
Actinobacteria	Actinobacteria	<i>Agromyces</i>	151	29.01.2019	Bergwerkswald Gießen, Germany	50.564032 N, 8.672555 E	forrest soil	mISEM ² pH 7.2
Actinobacteria	Actinobacteria	<i>Arthrobacter</i>	1	29.01.2019	Bergwerkswald Gießen, Germany	50.564032 N, 8.672555 E	forrest soil	mISEM ² pH 7.2
Actinobacteria	Actinobacteria	<i>Cellulomonas</i>	6	29.01.2019	Bergwerkswald Gießen, Germany	50.564032 N, 8.672555 E	forrest soil	mISEM ² pH 7.2
Actinobacteria	Actinobacteria	<i>Glaciibacter</i>	19	29.01.2019	Bergwerkswald Gießen, Germany	50.564032 N, 8.672555 E	forrest soil	mISEM ² pH 7.2
Actinobacteria	Actinobacteria	<i>Isoptericola</i>	1	29.01.2019	Bergwerkswald Gießen, Germany	50.564032 N, 8.672555 E	forrest soil	mISEM ² pH 7.2
Actinobacteria	Actinobacteria	<i>Leifsonia</i>	2	29.01.2019	Bergwerkswald Gießen, Germany	50.564032 N, 8.672555 E	forrest soil	mISEM ² pH 7.2
Actinobacteria	Actinobacteria	<i>Microbacterium</i>	12	29.01.2019	Bergwerkswald Gießen, Germany	50.564032 N, 8.672555 E	forrest soil	mISEM ² pH 7.2
Actinobacteria	Actinobacteria	<i>Mycetocola</i>	2	29.01.2019	Bergwerkswald Gießen, Germany	50.564032 N, 8.672555 E	forrest soil	mISEM ² pH 7.2
Actinobacteria	Actinobacteria	<i>Mycobacterium</i>	6	29.01.2019	Bergwerkswald Gießen, Germany	50.564032 N, 8.672555 E	forrest soil	mISEM ² pH 7.2
Actinobacteria	Actinobacteria	<i>Nakamurella</i>	1	29.01.2019	Bergwerkswald Gießen, Germany	50.564032 N, 8.672555 E	forrest soil	mISEM ² pH 7.2
Actinobacteria	Actinobacteria	<i>Nocardioides</i>	3	29.01.2019	Bergwerkswald Gießen, Germany	50.564032 N, 8.672555 E	forrest soil	mISEM ² pH 7.2
Actinobacteria	Actinobacteria	<i>Plantibacter</i>	2	29.01.2019	Bergwerkswald Gießen, Germany	50.564032 N, 8.672555 E	forrest soil	mISEM ² pH 7.2
Actinobacteria	Actinobacteria	<i>Promicromonospora</i>	2	29.01.2019	Bergwerkswald Gießen, Germany	50.564032 N, 8.672555 E	forrest soil	mISEM ² pH 7.2
Actinobacteria	Actinobacteria	<i>Rhodococcus</i>	2	29.01.2019	Bergwerkswald Gießen, Germany	50.564032 N, 8.672555 E	forrest soil	mISEM ² pH 7.2
Actinobacteria	Actinobacteria	<i>Streptomyces</i>	2	29.01.2019	Bergwerkswald Gießen, Germany	50.564032 N, 8.672555 E	forrest soil	mISEM ² pH 7.2
Actinobacteria	Actinobacteria	<i>Subtercola</i>	1	29.01.2019	Bergwerkswald Gießen, Germany	50.564032 N, 8.672555 E	forrest soil	mISEM ² pH 7.2
Actinobacteria	Actinobacteria	<i>Williamsia</i>	2	29.01.2019	Bergwerkswald Gießen, Germany	50.564032 N, 8.672555 E	forrest soil	mISEM ² pH 7.2
Bacteroidetes	Flavobacterium	<i>Flavobacterium</i>	1	29.01.2019	Bergwerkswald Gießen, Germany	50.564032 N, 8.672555 E	forrest soil	mISEM ² pH 7.2
Bacteroidetes	Sphingobacteria	<i>Pedobacter</i>	2	29.01.2019	Bergwerkswald Gießen, Germany	50.564032 N, 8.672555 E	forrest soil	mISEM ² pH 7.2
Bacteroidetes	Chitinophaga	<i>Pseudoflavitalea</i>	1	29.01.2019	Bergwerkswald Gießen, Germany	50.564032 N, 8.672555 E	forrest soil	mISEM ² pH 7.2
Firmicutes	Bacilli	<i>Staphylococcus</i>	1	29.01.2019	Bergwerkswald Gießen, Germany	50.564032 N, 8.672555 E	forrest soil	mISEM ² pH 7.2
Proteobacteria	Alphaproteobacteria	<i>Ancylobacter</i>	112	29.01.2019	Bergwerkswald Gießen, Germany	50.564032 N, 8.672555 E	forrest soil	mISEM ² pH 7.2
Proteobacteria	Alphaproteobacteria	<i>Nitratireductor</i>	43	29.01.2019	Bergwerkswald Gießen, Germany	50.564032 N, 8.672555 E	forrest soil	mISEM ² pH 7.2
Proteobacteria	Alphaproteobacteria	<i>Bosea</i>	1	29.01.2019	Bergwerkswald Gießen, Germany	50.564032 N, 8.672555 E	forrest soil	mISEM ² pH 7.2
Proteobacteria	Alphaproteobacteria	<i>Bradyrhizobium</i>	8	29.01.2019	Bergwerkswald Gießen, Germany	50.564032 N, 8.672555 E	forrest soil	mISEM ² pH 7.2
Proteobacteria	Betaproteobacteria	<i>Burkholderia</i>	7	29.01.2019	Bergwerkswald Gießen, Germany	50.564032 N, 8.672555 E	forrest soil	mISEM ² pH 7.2
Proteobacteria	Betaproteobacteria	<i>Cupriavidus</i>	1	29.01.2019	Bergwerkswald Gießen, Germany	50.564032 N, 8.672555 E	forrest soil	mISEM ² pH 7.2
Proteobacteria	Alphaproteobacteria	<i>Hyphomicrobium</i>	2	29.01.2019	Bergwerkswald Gießen, Germany	50.564032 N, 8.672555 E	forrest soil	mISEM ² pH 7.2
Proteobacteria	Alphaproteobacteria	<i>Inquilinus</i>	1	29.01.2019	Bergwerkswald Gießen, Germany	50.564032 N, 8.672555 E	forrest soil	mISEM ² pH 7.2

Proteobacteria	Alphaproteobacteria	<i>Kaistia</i>	1	29.01.2019	Bergwerkswald Gießen, Germany	50.564032 N, 8.672555 E	forrest soil	mISEM ² pH 7.2
Proteobacteria	Gammaproteobacteria	<i>Luteibacter</i>	10	29.01.2019	Bergwerkswald Gießen, Germany	50.564032 N, 8.672555 E	forrest soil	mISEM ² pH 7.2
Proteobacteria	Gammaproteobacteria	<i>Lysobacter</i>	2	29.01.2019	Bergwerkswald Gießen, Germany	50.564032 N, 8.672555 E	forrest soil	mISEM ² pH 7.2
Proteobacteria	Alphaproteobacteria	<i>Mesorhizobium</i>	3	29.01.2019	Bergwerkswald Gießen, Germany	50.564032 N, 8.672555 E	forrest soil	mISEM ² pH 7.2
Proteobacteria	Betaproteobacteria	<i>Paraburkholderia</i>	1	29.01.2019	Bergwerkswald Gießen, Germany	50.564032 N, 8.672555 E	forrest soil	mISEM ² pH 7.2
Proteobacteria	Alphaproteobacteria	<i>Phyllobacterium</i>	2	29.01.2019	Bergwerkswald Gießen, Germany	50.564032 N, 8.672555 E	forrest soil	mISEM ² pH 7.2
Proteobacteria	Betaproteobacteria	<i>Polaromonas</i>	1	29.01.2019	Bergwerkswald Gießen, Germany	50.564032 N, 8.672555 E	forrest soil	mISEM ² pH 7.2
Proteobacteria	Gammaproteobacteria	<i>Pseudomonas</i>	10	29.01.2019	Bergwerkswald Gießen, Germany	50.564032 N, 8.672555 E	forrest soil	mISEM ² pH 7.2
Proteobacteria	Gammaproteobacteria	<i>Pseudoxanthomonas</i>	1	29.01.2019	Bergwerkswald Gießen, Germany	50.564032 N, 8.672555 E	forrest soil	mISEM ² pH 7.2
Proteobacteria	Alphaproteobacteria	<i>Reyranela</i>	1	29.01.2019	Bergwerkswald Gießen, Germany	50.564032 N, 8.672555 E	forrest soil	mISEM ² pH 7.2
Proteobacteria	Alphaproteobacteria	<i>Rhizobium</i>	9	29.01.2019	Bergwerkswald Gießen, Germany	50.564032 N, 8.672555 E	forrest soil	mISEM ² pH 7.2
Proteobacteria	Alphaproteobacteria	<i>Rhodopseudomonas</i>	1	29.01.2019	Bergwerkswald Gießen, Germany	50.564032 N, 8.672555 E	forrest soil	mISEM ² pH 7.2
Proteobacteria	Alphaproteobacteria	<i>Sinorhizobium/Ensifer</i>	2	29.01.2019	Bergwerkswald Gießen, Germany	50.564032 N, 8.672555 E	forrest soil	mISEM ² pH 7.2
Proteobacteria	Alphaproteobacteria	<i>Sphingomonas</i>	1	29.01.2019	Bergwerkswald Gießen, Germany	50.564032 N, 8.672555 E	forrest soil	mISEM ² pH 7.2
Proteobacteria	Betaproteobacteria	<i>Variovorax</i>	18	29.01.2019	Bergwerkswald Gießen, Germany	50.564032 N, 8.672555 E	forrest soil	mISEM ² pH 7.2
Proteobacteria	Gammaproteobacteria	<i>Xanthomonas</i>	3	29.01.2019	Bergwerkswald Gießen, Germany	50.564032 N, 8.672555 E	forrest soil	mISEM ² pH 7.2
		No Relative/no sequence data total	141	29.01.2019	Bergwerkswald Gießen, Germany	50.564032 N, 8.672555 E	forrest soil	mISEM ² pH 7.2
		No Relative /no sequence data total	278					



Supplementary Fig. S4. Phylogenetic classification of FHG110511 within the phylum Acidobacteria clustering into subgroup 1. The tree is based on a ClustalW alignment of available 16S rRNA gene sequences from the ref_seq database between positions 113 and 1,357 [based on Escherichia coli 16S rRNA gene numbering (Brosius et al., 1978)] from the most similar sequences to the isolated strains, and also includes representatives of Acidobacteria subgroups 1, 3, 4, 6, 7, 8, and 10. The tree was calculated using MEGA v7.0.26 with the maximum-likelihood method and GTR-Gamma model. Circles on the tree branches indicate values of 1,000 bootstrap replicates with a bootstrap support of more than 50%. Subgroup affiliations are indicated by colors. The new isolate is indicated by a black arrow. The tree is drawn to scale, with branch lengths measured in the number of substitutions per site.

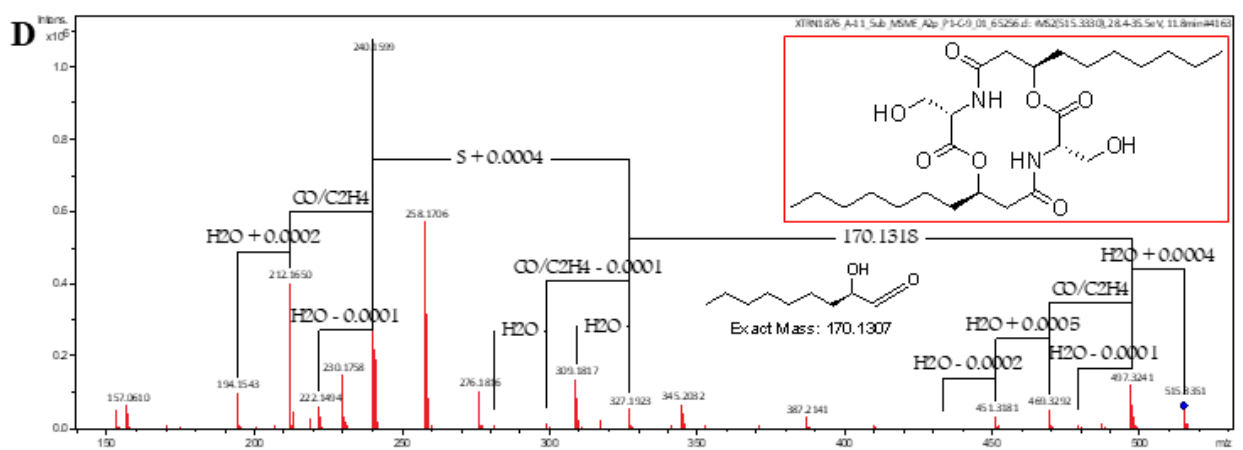
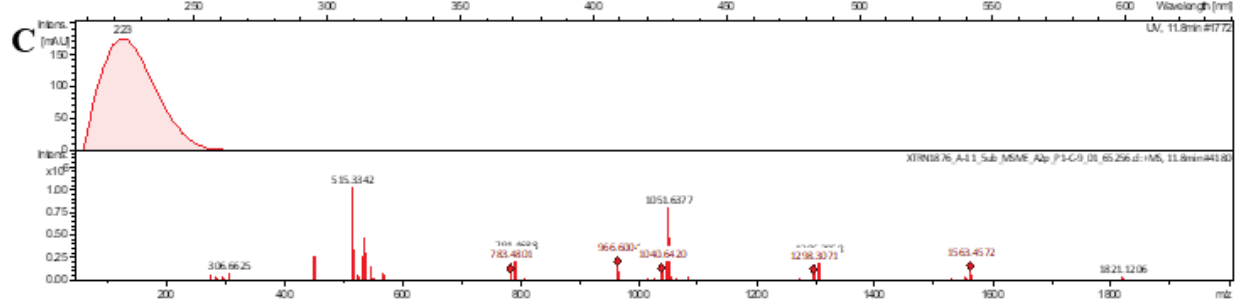
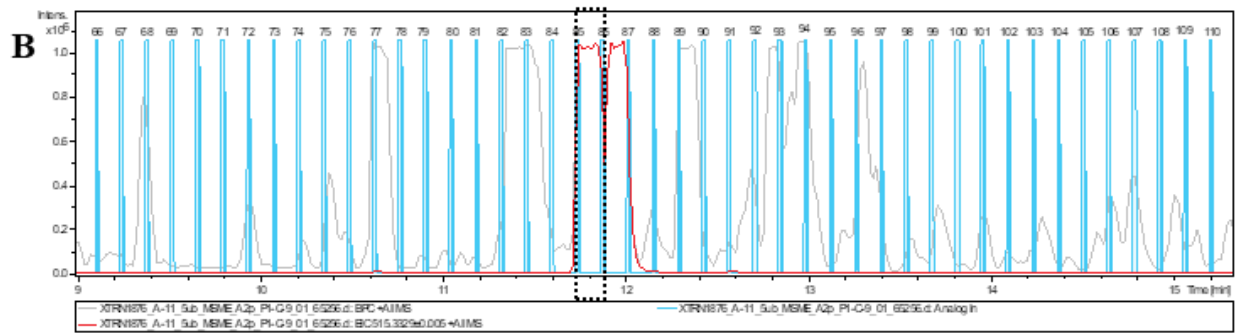
Supplementary Tab. S2. Cosine Similarity table – Data for Fig. affiliation.

Data point	Pairwise cosine similarity	Metabolic group affiliation
COD00090 E-07 Alp P1-E-7 01 49346.d	0	1
COD00090 E-10 Alp P1-E-10 01 49349.d	0,996525855	1
COD00090 D-04 Alp P1-D-4 01 49332.d	0,994506405	1
COD00090 D-05 Alp P1-D-5 01 49333.d	0,996323071	1
COD00090 E-03 Alp P1-E-3 01 49342.d	0,989886248	1
COD00090 E-06 Alp P1-E-6 01 49345.d	0,995331905	1
COD00090 E-09 Alp P1-E-9 01 49348.d	0,99494112	1
COD00090 D-03 Alp P1-D-3 01 49331.d	0,988141974	1
COD00090 B-04 Alp P1-B-4 01 49175.d	0,992537824	1
COD00090 B-09 Alp P1-B-9 01 49187.d	0,981227556	1
COD00090 E-04 Alp P1-E-4 01 49343.d	0,983954903	1
COD00090 D-07 Alp P1-D-7 01 49335.d	0,992699045	1
COD00090 D-11 Alp P1-D-11 01 49339.d	0,989752564	1
COD00090 E-08 Alp P1-E-8 01 49347.d	0,989333574	1
COD00090 D-08 Alp P1-D-8 01 49336.d	0,978173932	1
COD00090 C-08 Alp P1-C-8 01 49310.d	0,995030321	1
COD00090 C-06 Alp P1-C-6 01 49308.d	0,990078579	1
COD00090 B-06 Alp P1-B-6 01 49177.d	0,984810504	1
COD00090 C-09 Alp P1-C-9 01 49327.d	0,960325517	1
COD00090 A-06 Alp P1-A-6 01 49165.d	0,956355956	1
COD00090 A-07 Alp P1-A-7 01 49166.d	0,996660716	1
COD00090 A-11 Alp P1-A-11 01 49170.d	0,994957861	1
COD00090 A-04 Alp P1-A-4 01 49126.d	0,98914863	1
COD00090 A-09 Alp P1-A-9 01 49168.d	0,988868587	1
COD00090 A-10 Alp P1-A-10 01 49169.d	0,993676537	1
COD00090 B-03 Alp P1-B-3 01 49173.d	0,98513016	1
COD00090 C-03 Alp P1-C-3 01 49305.d	0,981021653	1
COD00090 A-08 Alp P1-A-8 01 49167.d	0,991637074	1
COD00090 C-12 Alp P1-C-12 01 49330.d	0,991598453	1
COD00090 F-11 Alp P2-F-11 01 49568.d	0,985669881	1
COD00090 E-12 Alp P1-E-12 01 49351.d	0,971662968	1
COD00090 C-11 Alp P1-C-11 01 49329.d	0,973623794	1
COD00090 C-10 Alp P1-C-10 01 49328.d	0,992987138	1
COD00090 B-08 Alp P1-B-8 01 49186.d	0,989997964	1
COD00090 D-06 Alp P1-D-6 01 49334.d	0,986453388	1
COD00090 E-05 Alp P1-E-5 01 49344.d	0,992392656	1
COD00090 F-10 Alp P2-F-10 01 49567.d	0,971880085	1
COD00090 F-09 Alp P2-F-9 01 49566.d	0,995962731	1
COD00090 F-08 Alp P2-F-8 01 49565.d	0,993330272	1
COD00090 C-04 Alp P1-C-4 01 49306.d	0,979506743	1
COD00090 A-05 Alp P1-A-5 01 49127.d	0,972899421	1

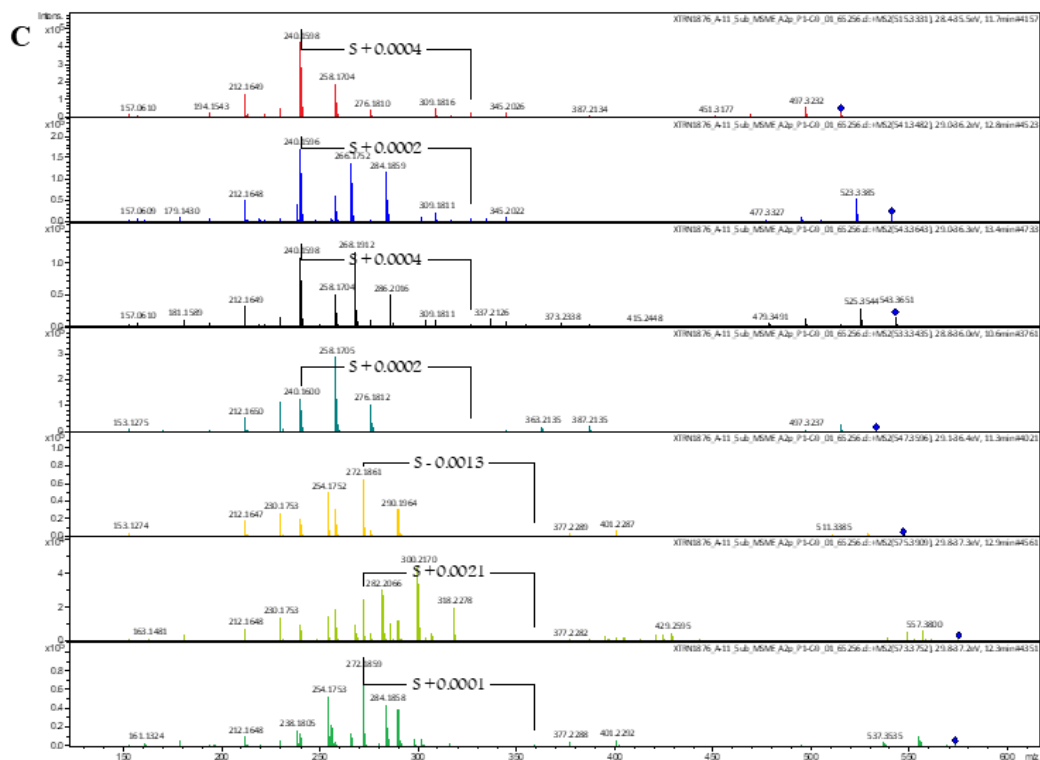
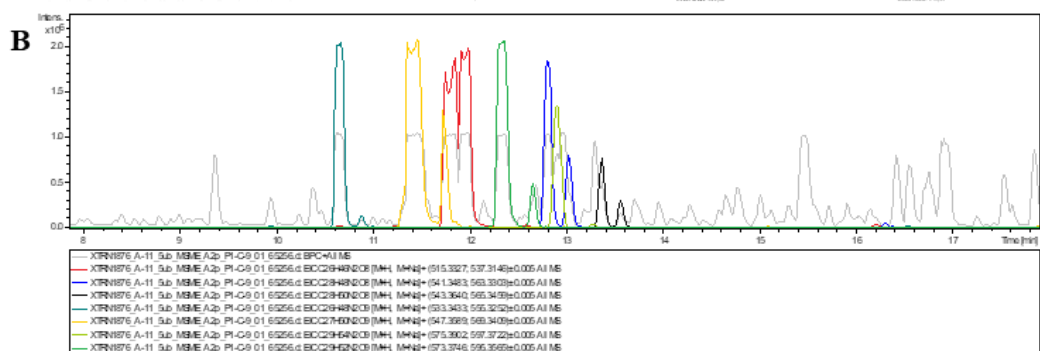
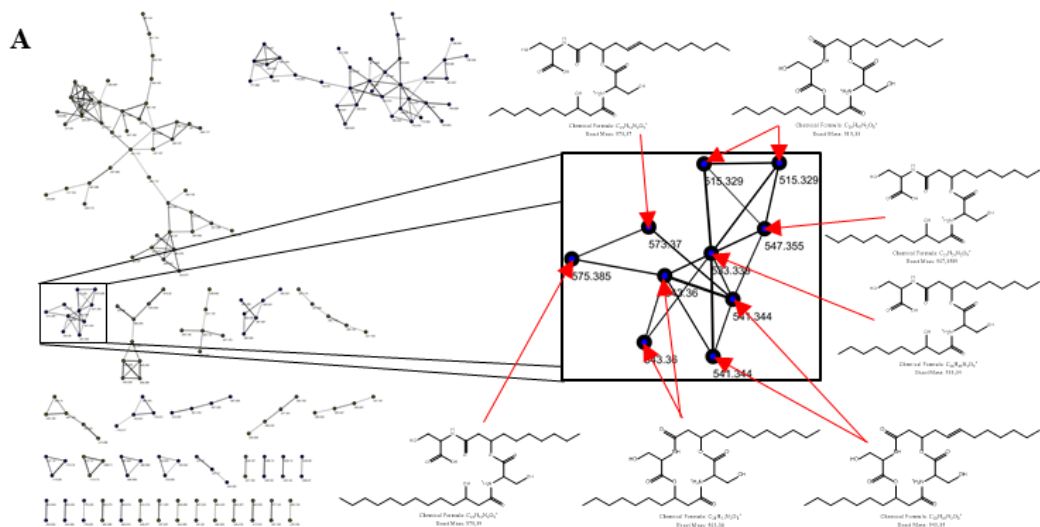
COD00090 B-10 Alp P1-B-10 01 49188.d	0,965508761	1
COD00090 B-11 Alp P1-B-11 01 49189.d	0,98021242	1
COD00090 D-10 Alp P1-D-10 01 49338.d	0,970851409	1
COD00090 B-12 Alp P1-B-12 01 49190.d	0,979346376	1
COD00090 F-04 Alp P1-F-4 01 49353.d	0,933395646	1
COD00090 E-11 Alp P1-E-11 01 49350.d	0,970731424	1
COD00090 D-12 Alp P2-D-12 01 64190.d	0,922166996	1
COD00090 D-11 Alp P2-D-11 01 64189.d	0,995436642	1
COD00090 E-03 Alp P2-E-3 01 64191.d	0,987316104	1
COD00090 F-05 Alp P2-F-5 01 49562.d	0,946636407	1
COD00090 F-06 Alp P2-F-6 01 49563.d	0,930737067	1
COD00090 F-03 Alp P1-F-3 01 49352.d	0,828152621	2
COD00090 C-05 Alp P1-C-5 01 49307.d	0,93614162	2
COD00090 D-09 Alp P1-D-9 01 49337.d	0,859523476	3
COD00090 F-12 Alp P2-F-12 01 49569.d	0,846525324	4
COD00090 D-12 Alp P1-D-12 01 49340.d	0,881502833	5
COD00090 G-03 Alp P2-G-3 01 49571.d	0,893182206	6
COD00090 F-07 Alp P2-F-7 01 49564.d	0,661510307	7
COD00090 A-12 Alp P1-A-12 01 49172.d	0,822655257	8

A

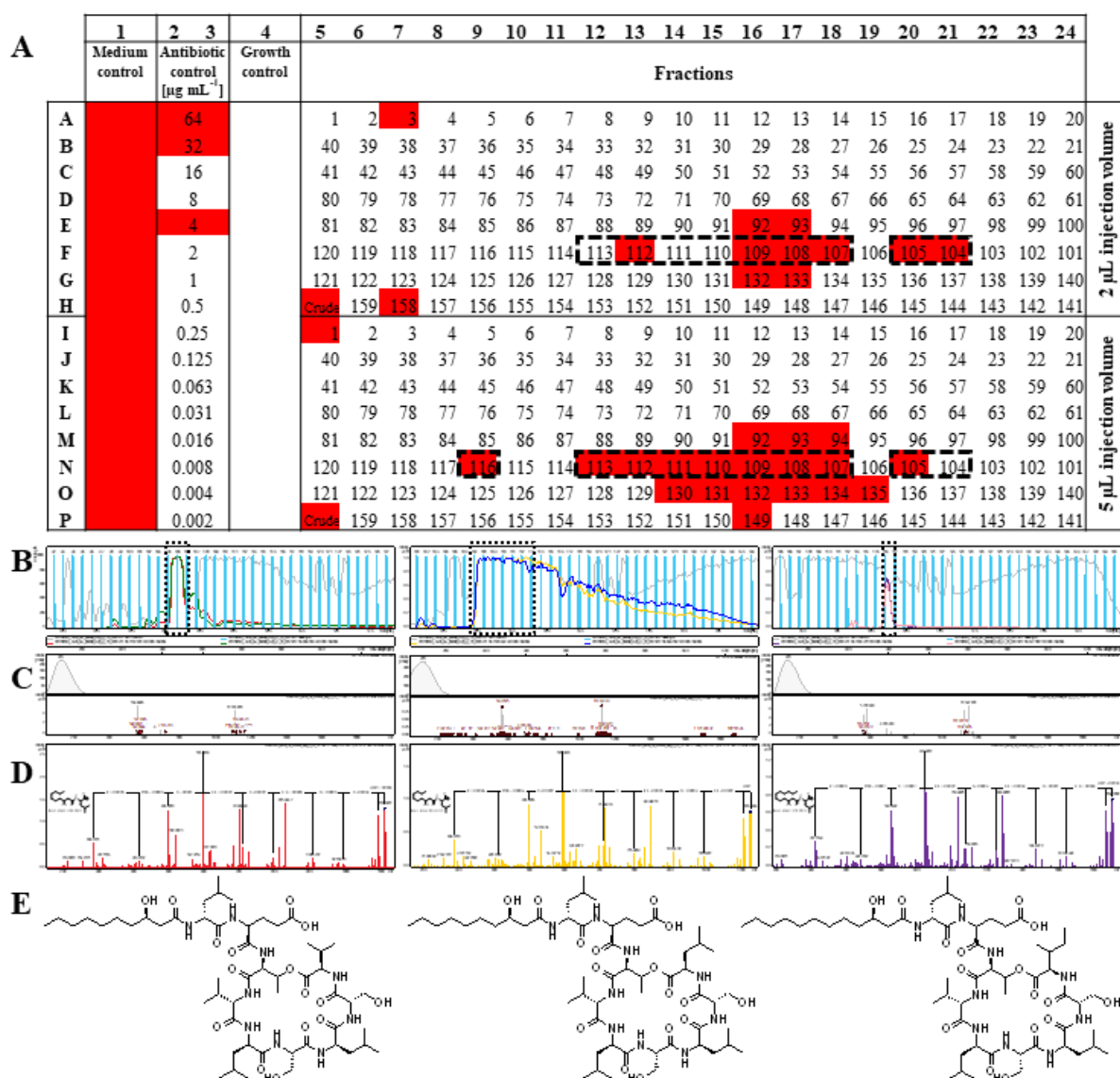
	1	2	3	4	5	6	7	8	9	10	11	12	13	14	15	16	17	18	19	20	21	22	23	24	
	Medium control	Antibiotic control [µg mL ⁻¹]		Growth control	Fractions																				
A			64		1	2	3	4	5	6	7	8	9	10	11	12	13	14	15	16	17	18	19	20	
B					40	39	38	37	36	35	34	33	32	31	30	29	28	27	26	25	24	23	22	21	
C					41	42	43	44	45	46	47	48	49	50	51	52	53	54	55	56	57	58	59	60	
D					80	79	78	77	76	75	74	73	72	71	70	69	68	67	66	65	64	63	62	61	
E					81	82	83	84	85	86	87	88	89	90	91	92	93	94	95	96	97	98	99	100	
F					120	119	118	117	116	115	114	113	112	111	110	109	108	107	106	105	104	103	102	101	
G					121	122	123	124	125	126	127	128	129	130	131	132	133	134	135	136	137	138	139	140	
H					Crude	159	158	157	156	155	154	153	152	151	150	149	148	147	146	145	144	143	142	141	
I					0.25	1	2	3	4	5	6	7	8	9	10	11	12	13	14	15	16	17	18	19	20
J					0.125	40	39	38	37	36	35	34	33	32	31	30	29	28	27	26	25	24	23	22	21
K					0.063	41	42	43	44	45	46	47	48	49	50	51	52	53	54	55	56	57	58	59	60
L					0.031	80	79	78	77	76	75	74	73	72	71	70	69	68	67	66	65	64	63	62	61
M					0.016	81	82	83	84	85	86	87	88	89	90	91	92	93	94	95	96	97	98	99	100
N					0.008	120	119	118	117	116	115	114	113	112	111	110	109	108	107	106	105	104	103	102	101
O					0.004	121	122	123	124	125	126	127	128	129	130	131	132	133	134	135	136	137	138	139	140
P					0.002	Crude	159	158	157	156	155	154	153	152	151	150	149	148	147	146	145	144	143	142	141



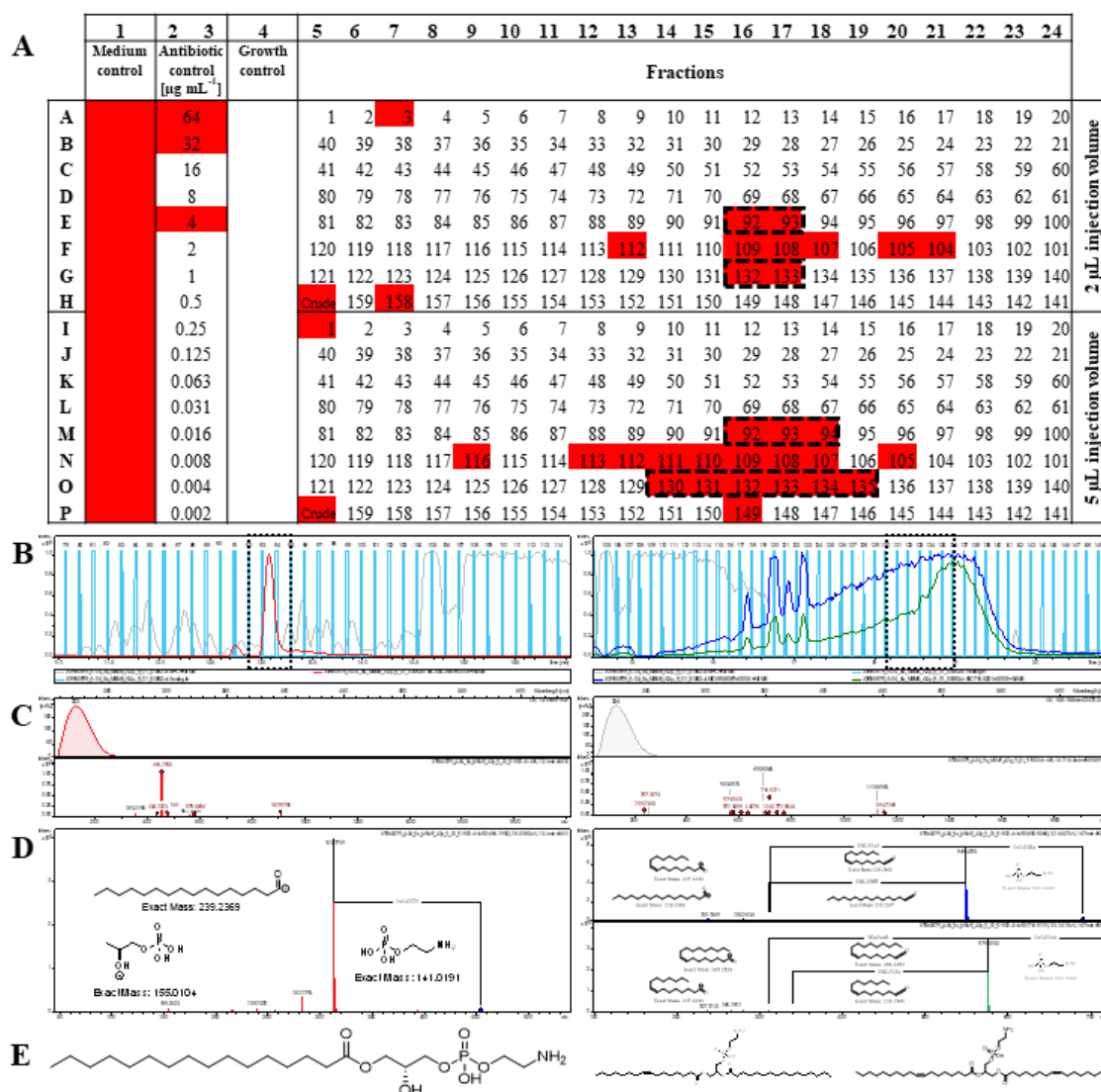
Supplementary Fig. S5. (A) Assay read-out of μ -fractionation plates of strain FHG110488 against *M. smegmatis* ATCC 607. Fractions are numbered and those causing at least 70% rel. growth inhibition were considered “active” and marked red. Column 1: medium control; Column 2+3: antibiotic standard (isoniazid); Column 4: growth control. Area AH05-AH24 top: 5 μ L injection volume; Area AH05-AH24 bottom: 10 μ L injection; Crude: crude extract as a control. (B) Overlaid Base peak Chromatogram (grey), fraction collector analog signal (light blue bars) and extracted ion chromatogram of m/z 515.3329 \pm 0.005 [M+H]⁺ (**1**, red) of the 50 fold concentrated extract (in MeOH) with 5 μ L injection volume. (C) UV and MS spectrum of fractions 84-87. (D) MS/MS fragmentation of the precursor ion at m/z 515.3330 [M+H]⁺ (dereplicated as Serratamolide A, displayed in red) with manual annotation of the neutral losses.



Supplementary Fig. S6. (A) MS²-network of “active” extract of FHG110488 against *Septoria tritici* MUCL45407 focusing on the cluster representing all seven detected serratamolide derivatives and their literature known structures (dots of parent ions found as hits in our internal database or AntiBase are marked in gold). (B) Overlaid Base peak Chromatogram (grey) and extracted ion chromatograms of serratamolides **1-7** (**1** m/z 515.3327 [M+H]⁺, C₂₆H₄₇N₂O₈⁺ (red); **2** m/z 541.3483 [M+H]⁺, C₂₈H₄₉N₂O₈⁺ (blue); **3** m/z 543.3640 [M+H]⁺, C₂₈H₅₁N₂O₈⁺ (black); **4** m/z 533.3433 [M+H]⁺, C₂₆H₄₉N₂O₉⁺ (cyan); **5** m/z 547.3598 [M+H]⁺, C₂₇H₅₁N₂O₉⁺ (yellow); **6** m/z 575.3902 [M+H]⁺, C₂₉H₅₅N₂O₉⁺ (light green); **7** m/z 573.3746 [M+H]⁺, C₂₉H₅₃N₂O₉⁺ (dark green)) of the 50 fold concentrated extract (in MeOH) with 5 μL injection volume. (C) MS/MS fragmentation of the precursor ions **1-7**.



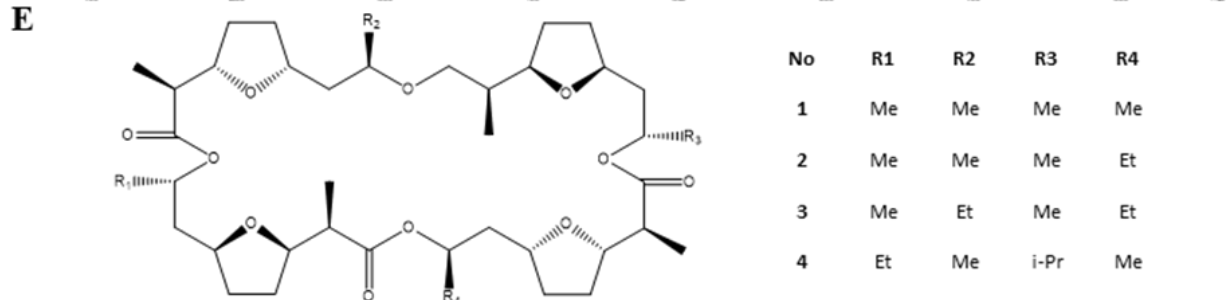
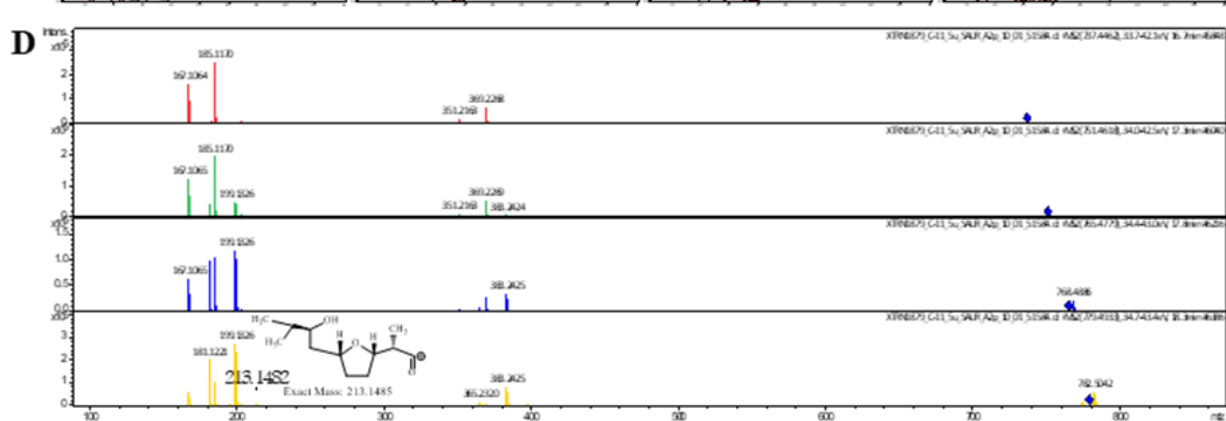
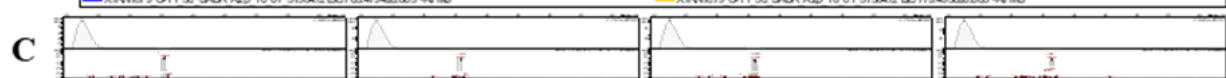
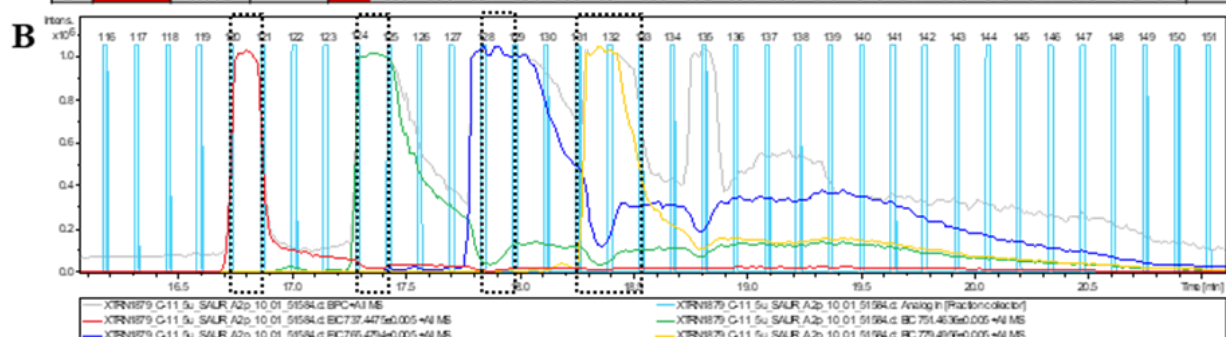
Supplementary Fig. S7. (A) Assay read-out of μ -fractionation plate of strain FHG110502 against *Mycobacterium smegmatis* ATCC 607. Fractions are numbered and those causing at least 70% rel. growth inhibition were considered “active” and marked red. Column 1: medium control; Column 2+3: antibiotic standard (isoniazid); Column 4: growth control. Area AH05-AH24: 2 μ L injection volume; Area IP05-IP24: 5 μ L injection; Crude: crude extract as a control. (B) Overlaid Base peak Chromatograms (grey), Fraction collector analog signals (light blue bars) and extracted ion chromatograms of m/z 1112.6814 \pm 0.005 [M+H]⁺ (**8**, red) with corresponding m/z 556.8446 \pm 0.005 [M+2H]²⁺ (green), m/z 1126.6973 \pm 0.005 [M+H]⁺ (**9**, yellow) with corresponding m/z 563.8524 \pm 0.005 [M+2H]²⁺ (blue), and m/z 1154.7288 \pm 0.005 [M+H]⁺ (**10**, purple) with corresponding m/z 577.8680 \pm 0.005 [M+2H]²⁺ (magenta) of the 50 fold concentrated extract (in MeOH) with 5 μ L injection volume. (C) UV and MS spectrum of fractions 105-106 (left), 108-118 (middle) and 116 (right). (D) MS/MS fragmentation of the precursor ion at m/z 1112.6814 [M+H]⁺, m/z 1126.6973 [M+H]⁺, and m/z 1154.7288 [M+H]⁺ (dereplicated as massetolide E, massetolide F and massetolide H, respectively), manual annotation of the neutral losses and proposed structures of the fragment ions at m/z 284.2229 and m/z 312.2533. (E) Structures of all three dereplicated compounds **8-10**.



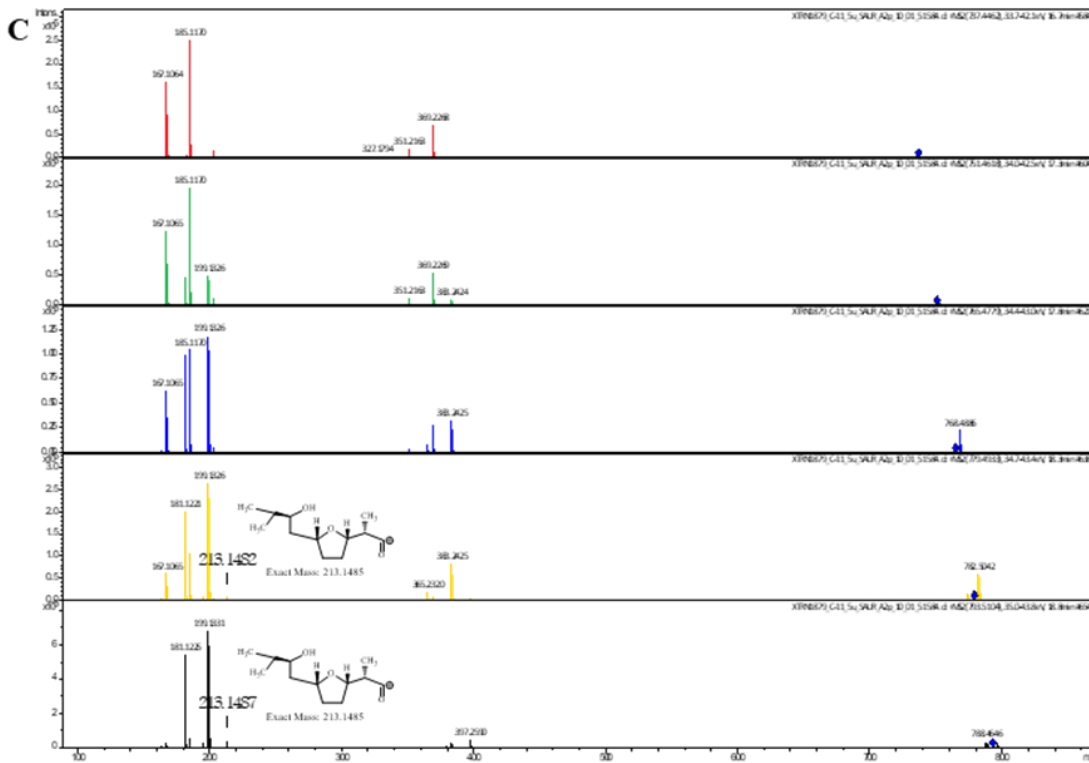
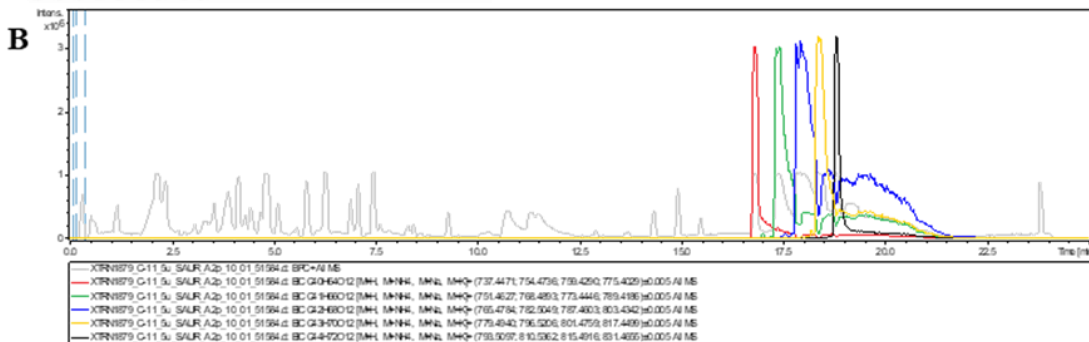
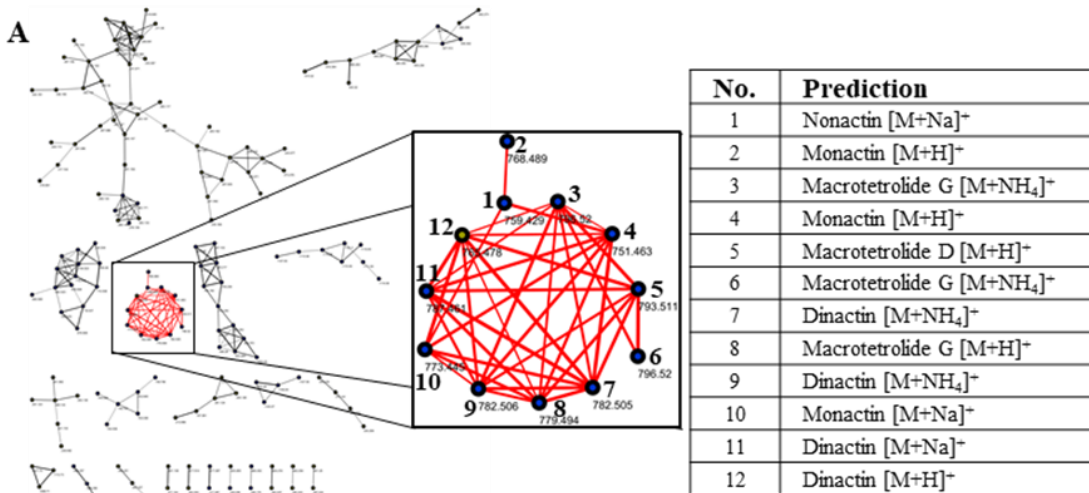
Supplementary Fig. S8. (A) Assay read-out of μ -fractionation plate of strain FHG110502 against *Mycobacterium smegmatis* ATCC 607. Fractions are numbered and those causing at least 70% rel. growth inhibition were considered “active” and marked red. Column 1: medium control; Column 2+3: antibiotic standard (isoniazid); Column 4: growth control. Area AH05-AH24: 2 μ L injection volume; Area IP05-IP24: 5 μ L injection; Crude: crude extract as a control. (B) Overlaid Base peak Chromatograms (grey), Fraction collector analog signals (light blue bars) and extracted ion chromatograms of m/z 454.2931 \pm 0.005 [M+H]⁺ (**11**, red), m/z 690.5073 \pm 0.005 [M+H]⁺ (**12**, blue) and m/z 716.5237 \pm 0.005 [M+H]⁺ (**13**, green) of the 50 fold concentrated extract (in MeOH) with 5 μ L injection volume. (C) UV and MS spectrum of fractions 93-94 (left) and 130-136 (right). (D) MS/MS fragmentation of the precursor ion at m/z 454.2931 [M+H]⁺, m/z 690.5073 [M+H]⁺, and m/z 716.5237 [M+H]⁺ (dereplicated as lyso-palmitoyl-phosphoethanolamine, palmitoleoyl-palmitoyl-phosphoethanolamine and palmitoleoyl-oleoyl-phosphoethanolamine, respectively), manual annotation of the neutral losses and proposed structures of the fragment ions. (E) Putative structures of all three dereplicated compounds **11-13**.

A

	1	2	3	4	5	6	7	8	9	10	11	12	13	14	15	16	17	18	19	20	21	22	23	24
	Medium control	Antibiotic control [μg mL ⁻¹]		Growth control	Fractions																			
A		64			1	2	3	4	5	6	7	8	9	10	11	12	13	14	15	16	17	18	19	20
B		32			40	39	38	37	36	35	34	33	32	31	30	29	28	27	26	25	24	23	22	21
C		16			41	42	43	44	45	46	47	48	49	50	51	52	53	54	55	56	57	58	59	60
D		8			80	79	78	77	76	75	74	73	72	71	70	69	68	67	66	65	64	63	62	61
E		4			81	82	83	84	85	86	87	88	89	90	91	92	93	94	95	96	97	98	99	100
F		2			120	119	118	117	116	115	114	113	112	111	110	109	108	107	106	105	104	103	102	101
G		1			121	122	123	124	125	126	127	128	129	130	131	132	133	134	135	136	137	138	139	140
H		0.5		Crud.	159	158	157	156	155	154	153	152	151	150	149	148	147	146	145	144	143	142	141	
I		0.25			1	2	3	4	5	6	7	8	9	10	11	12	13	14	15	16	17	18	19	20
J		0.125			40	39	38	37	36	35	34	33	32	31	30	29	28	27	26	25	24	23	22	21
K		0.063			41	42	43	44	45	46	47	48	49	50	51	52	53	54	55	56	57	58	59	60
L		0.031			80	79	78	77	76	75	74	73	72	71	70	69	68	67	66	65	64	63	62	61
M		0.016			81	82	83	84	85	86	87	88	89	90	91	92	93	94	95	96	97	98	99	100
N		0.008		Crud.	120	119	118	117	116	115	114	113	112	111	110	109	108	107	106	105	104	103	102	101
O		0.004			121	122	123	124	125	126	127	128	129	130	131	132	133	134	135	136	137	138	139	140
P		0.002		Crud.	159	158	157	156	155	154	153	152	151	150	149	148	147	146	145	144	143	142	141	



Supplementary Fig. S9. (A) Assay read-out of μ -fractionation plate of strain FHG110508 against *Staphylococcus aureus* ATCC 25923. Fractions are numbered and those causing at least 70% rel. growth inhibition were considered “active” and marked red. Column 1: medium control; Column 2+3: antibiotic standard (gentamycin); Column 4: growth control. Area AH05-AH24: 2 μ L injection volume; Area IP05-IP24: 5 μ L injection; Crude: crude extract as a control. (B) Overlaid Base peak Chromatograms (grey), Fraction collector analog signals (light blue bars) and extracted ion chromatograms of m/z 737.4475 \pm 0.005 [M+H]⁺ (**14**, red), m/z 751.4636 \pm 0.005 [M+H]⁺ (**15**, green), m/z 765.4794 \pm 0.005 [M+H]⁺ (**16**, blue), and m/z 779.4956 \pm 0.005 [M+H]⁺ (**17**, yellow) of the 50 fold concentrated extract (in MeOH) with 5 μ L injection volume. (C) UV and MS spectrum of fractions 120, 124, 128 and 131-132 (from left to right). (D) MS/MS fragmentation of the precursor ion at m/z 737.4462 [M+H]⁺, m/z 751.4618 [M+H]⁺, m/z 765.4779 [M+H]⁺, and m/z 779.4933 [M+H]⁺ (dereplicated as nonactin, monactin, dinactin and macrotetrolide G, respectively) with manual annotation of the neutral loss and proposed structure of the fragment ion at m/z 213.1482 of parent ion at m/z 779.4933 indicating the presents of macrotetrolide G instead of trinactin. (E) Structures of all four dereplicated macrotetrolides. Me: methyl; Et: ethyl; iPr: isopropyl.



Supplementary Fig. S10. (A) MS²-network of “active” extract of FHG110508 against *Staphylococcus aureus* ATCC 25923 with focus on the cluster representing all five detected macrotetrolide derivatives and their adduct ions (dots of parent ions found as hits in our internal database or AntiBase are marked in gold). (B) Overlaid Base peak Chromatogram (grey) and extracted ion chromatograms of macrotetrolide **14-18** (**14** m/z 737.4462 [M+H]⁺, C₄₀H₆₅O₁₂⁺ (red); **15** m/z 751.4618 [M+H]⁺, C₄₁H₆₇O₁₂⁺ (green); **16** m/z 765.4779 [M+H]⁺, C₄₂H₆₉O₁₂⁺ (blue); **17** m/z 779.4933 [M+H]⁺, C₄₃H₇₁O₁₂⁺ (yellow); **18** m/z 793.5104 [M+H]⁺, C₄₄H₇₃O₁₂⁺ (black)) of the 50 fold concentrated extract (in MeOH) with 5 μ L injection volume. (C) MS/MS fragmentation of the precursor ions **14-18** dereplicated as nonactin, monactin, dinactin, macrotetrolide G, and macrotetrolide D, respectively, with manual annotation of the neutral loss and proposed structure of the fragment ion at m/z 213.1482 of parent ion at m/z 779.4933 indicating the presents of macrotetrolide G instead of trinactin and fragment ion at m/z 213.1487 of parent ion at m/z 793.5104 indicating the presents of macrotetrolide D instead of tetranactin.

References

- Caballero-Aguilara, L.M., Duchib, S., Quigleyd, A., Onofrillo, C., Di Bellab, C., and Moultona, S.E. (2021) Microencapsulation of Growth Factors by microfluidic system. *MethodsX*, doi: 10.1016/j.mex.2021.101324.
- Duetz, W.A., Rüedi, L., Hermann, R., O'Connor, K., Büchs, J., and Witholt, B. (2000) Methods for Intense Aeration, Growth, Storage, and Replication of Bacterial Strains in Microtiter Plates. *Applied and Environmental Microbiology*, doi: 10.1128/AEM.66.6.2641-2646.2000.
- Marnier, M., Patras, M.A., Kurz, M., Zubeil, F., Förster, F., Schuler, S., *et al.* (2020) Molecular Networking-Guided Discovery and Characterization of Stechlisins, a Group of Cyclic Lipopeptides from a Pseudomonas sp. *Journal of Natural Products*, doi: 10.1021/acs.jnatprod.0c00263.
- Oberpaul, M., Zumkeller, C.M., Culver, T., Spohn, M., Mihajlovic, S., Leis, B., *et al.* (2020) High-Throughput Cultivation for the Selective Isolation of Acidobacteria From Termite Nests. *Frontiers in Microbiology*, doi: 10.3389/fmicb.2020.597628.

**MANUSCRIPT 3: NOVEL GLYCEROPHOSPHOLIPID, LIPO-
AND N-ACYL AMINO ACIDS FROM
BACTEROIDETES: ISOLATION,
STRUCTURE ELUCIDATION AND
BIOACTIVITY**

Status: published on 27/09/2021

Author's contributions: isolation and characterization of the Bacteroidetes species *Olivibacter* sp. FHG000416 used in this study, methods writing, and manuscript revision.

Article

Novel Glycerophospholipid, Lipo- and N-acyl Amino Acids from Bacteroidetes: Isolation, Structure Elucidation and Bioactivity

Mona-Katharina Bill ^{1,†}, Stephan Brinkmann ^{1,†}, Markus Oberpaul ¹, Maria A. Patras ¹, Benedikt Leis ¹, Michael Marner ¹, Marc-Philippe Maitre ², Peter E. Hammann ^{3,4}, Andreas Vilcinskas ^{1,5}, Sören M. M. Schuler ^{4,*} and Till F. Schäberle ^{1,5,*}

- ¹ Fraunhofer Institute for Molecular Biology and Applied Ecology (IME), Branch for Bioresources, 35392 Giessen, Germany; mona.bill@ime.fraunhofer.de (M.-K.B.); stephan.brinkmann@ime.fraunhofer.de (S.B.); markus.oberpaul@ime.fraunhofer.de (M.O.); maria.patras@ime.fraunhofer.de (M.A.P.); benedikt.leis@gmx.net (B.L.); michael.marner@ime.fraunhofer.de (M.M.); andreas.vilcinskas@ime.fraunhofer.de (A.V.)
² Sanofi Pasteur, R&D, 69280 Marcy L'Etoile, France; MarcPhilippe.Maitre@sanofi.com
³ Sanofi-Aventis Deutschland GmbH, R&D, 65926 Frankfurt am Main, Germany; peter.hammann@npconsult.me
⁴ Evotec International GmbH, 37079 Göttingen, Germany
⁵ Institute for Insect Biotechnology, Justus-Liebig-University of Giessen, 35392 Giessen, Germany
 * Correspondence: soeren.schuler@evotec.com (S.M.M.S.); till.f.schaerberle@agr.uni-giessen.de (T.F.S.)
 † These authors contributed equally to this work.



Citation: Bill, M.-K.; Brinkmann, S.; Oberpaul, M.; Patras, M.A.; Leis, B.; Marner, M.; Maitre, M.-P.; Hammann, P.E.; Vilcinskas, A.; Schuler, S.M.M.; et al. Novel Glycerophospholipid, Lipo- and N-acyl Amino Acids from Bacteroidetes: Isolation, Structure Elucidation and Bioactivity. *Molecules* **2021**, *26*, 5195. <https://doi.org/10.3390/molecules26175195>

Academic Editor: Natalizia Miceli

Received: 31 July 2021

Accepted: 25 August 2021

Published: 27 August 2021

Publisher's Note: MDPI stays neutral with regard to jurisdictional claims in published maps and institutional affiliations.



Copyright: © 2021 by the authors. Licensee MDPI, Basel, Switzerland. This article is an open access article distributed under the terms and conditions of the Creative Commons Attribution (CC BY) license (<https://creativecommons.org/licenses/by/4.0/>).

Abstract: The 'core' metabolome of the Bacteroidetes genus *Chitinophaga* was recently discovered to consist of only seven metabolites. A structural relationship in terms of shared lipid moieties among four of them was postulated. Here, structure elucidation and characterization via ultra-high resolution mass spectrometry (UHR-MS) and nuclear magnetic resonance (NMR) spectroscopy of those four lipids (two lipoamino acids (LAAs), two lysophosphatidylethanolamines (LPEs)), as well as several other undescribed LAAs and N-acyl amino acids (NAAAs), identified during isolation were carried out. The LAAs represent closely related analogs of the literature-known LAAs, such as the glycine-serine dipeptide lipids 430 (**2**) and 654. Most of the here characterized LAAs (**1**, **5–11**) are members of a so far undescribed glycine-serine-ornithine tripeptide lipid family. Moreover, this study reports three novel NAAAs (N-(5-methyl)hexanoyl tyrosine (**14**) and N-(7-methyl)octanoyl tyrosine (**15**) or phenylalanine (**16**)) from *Olivibacter* sp. FHG000416, another Bacteroidetes strain initially selected as best in-house producer for isolation of lipid 430. Antimicrobial profiling revealed most isolated LAAs (**1–3**) and the two LPE 'core' metabolites (**12**, **13**) active against the Gram-negative pathogen *M. catarrhalis* ATCC 25238 and the Gram-positive bacterium *M. luteus* DSM 20030. For LAA **1**, additional growth inhibition activity against *B. subtilis* DSM 10 was observed.

Keywords: linear lipoamino acid; lipid 430; lipid 654; N-acyl amino acid; lysophosphatidylethanolamine; bacteroidetes; *Chitinophaga*; *Olivibacter*; LC-MS/MS; antimicrobial lipids

1. Introduction

Lipids are a diverse group of natural biomolecules. Thousands of distinct lipids, such as glycerolipids, sterol lipids, sphingolipids, lipoamino acids (LAAs), and phospholipids, are ubiquitous in all organisms. Each of them is chemically unique, and they exhibit different biological functions. Given the diversity in both the chemical and physical properties of lipids and the fact that each lipid type is involved at various stages of cellular processes, the definition of lipid function besides their primary biological role, i.e., the formation of cell membrane matrixes, is challenging. Described functions in cellular signaling, energy storage, or an implication as substrate for metabolite or protein lipidation are only examples [1].

Bacterial membrane composition differs among bacterial species and depends on the exposed environmental conditions [2]. In most cases and conditions studied, amphiphilic lipids such as glycerophospholipids are composed of two fatty acids, a glycerol moiety, a phosphate group, and variable head groups. Common examples are phosphatidylethanolamine (PE), phosphatidylglycerol (PG), cardiolipin (CL), lysyl-phosphatidylglycerol (LPG), phosphatidylinositol (PI), phosphatidic acid (PA), and phosphatidylserine (PS). Additionally, a small fraction of the bacterial membrane consists of lysophospholipids (LPLs). They are metabolic intermediates of bacterial phospholipid synthesis or they derive from membrane degradation. The most abundant member of this class is lysophosphatidylethanolamine (LPE). LPLs result from partial hydrolysis of phospholipids mediated by phospholipase A [3]. Other phosphorus-free lipids, such as sulfolipids, LAAs [2,4–14], or the growing lipid class of the *N*-acyl amino acids (NAAAs), are also reported [15]. The latter are found in all biological systems, but their functions remain unclear. It is hypothesized that these lipids are putative signaling molecules with a wide range of biological activities [16–23].

In general, a variety of physicochemical properties and bioactivities have been associated with all kinds of bacterial lipids, including hemagglutination [9], macrophage activation [10], bacterial virulence factors [24], involvement in the development of multiple sclerosis [25], and antimicrobial activities [26,27]. Moreover, simple representatives of the LAAs such as the glycine-serine dipeptide lipid 654 (also referred to as flavolipin [28], topostin D654 [29], and WB-3559 D [6,7]) and glycine-serine dipeptide lipid 430 were isolated from pathogenic Bacteroidetes strains associated with chronic periodontitis [30]. They account for osteoclast formation from RAW cells [31] and TLR2-dependent inhibition of osteoblast differentiation and function [32], and they are implicated in dendritic cell release of IL-6 mediated through engagement of TLR2 [33,34]. Furthermore, antimicrobial activity was reported for lipid 430 [35], the de-esterified enzymatic hydrolysis product of lipid 654 hydrolyzed by phospholipase A2 (PLA2) [36].

For enabling doubtless structure elucidation, various analytical methods such as MS and NMR are well established and intensively used in the field of natural product research in general. For lipids as one important sub-class, first, gas or liquid chromatography coupled to diverse mass spectrometry methods represent two key analytical techniques [37–39]. Second, NMR spectroscopy is not only widely utilized for structure elucidations of single lipids, successful applications regarding qualitative and quantitative analysis of lipids in complex mixtures are also reported in this context [40–45].

In a previous study, we identified the ‘core’ metabolome of the Bacteroidetes genus *Chitinophaga*, consisting of only seven metabolites [46]. We postulated a structural relationship among four of them based on their MS/MS fragmentation pattern, which suggested them to be unknown LAAs and LPEs. Here, we report the identification in total of 16 diverse lipids (11 LAAs, 2 LPEs, 3 NAAAs) produced by *Chitinophaga* spp. and *Olivibacter* sp. FHG000416, the ‘core’ ones included. Isolation and structure elucidation of nine of those lipids isolated from *Chitinophaga eiseniae* DSM 22224 [47] and FHG000416 was successfully achieved. Based on the four *Chitinophaga* core lipids, the known lipid 430, several novel LAA analogs thereof, and three undescribed NAAAs were characterized. In this context, we identified a novel glycine-serine-ornithine LAA family that is closely related to the previously described glycine and glycine-serine LAA families that lipid 430 and 654 belong to. Investigating them for their antimicrobial activity revealed a common growth inhibition effect against the Gram-negative pathogen *M. catarrhalis* ATCC 25238 and the Gram-positive bacterium *M. luteus* DSM 20030, with LAA 1 as the most potent one, also showing growth-inhibiting activity against *B. subtilis* DSM 10.

2. Results

2.1. Lipoamino Acids

A previous study revealed a small core metabolome of the Bacteroidetes genus *Chitinophaga*, identified as a genus of underexplored talented producers of natural products. The analyzed 25 strains commonly share only 7 of the 2736 identified metabolite buckets. Four of those seven 'core' metabolites correspond to the UHR-ESI-MS ion peaks at m/z 545.3908 $[M + H]^+$, 452.2769 $[M + H]^+$, 440.2767 $[M + H]^+$, and 767.5896 $[M + H]^+$, with retention times (RTs) of 11.2, 11.7, 12.1, and 17.4 min, respectively (Table S1). Based on their MS/MS fragmentation pattern, similar lipid moieties were postulated, suggesting a structural relationship [46].

For the first core metabolite, the molecular formula $C_{27}H_{52}N_4O_7$ (**1**) was assigned according to the UHR-ESI-MS ion peak at m/z 545.3908 $[M + H]^+$. The MS/MS fragmentation of **1** revealed neutral losses of H_2O , followed by the three amino acids ornithine, serine, and glycine, resulting in the fragment ion of m/z 251.2366 $[M + H]^+$. The corresponding ion formula of $C_{17}H_{31}O^+$ indicated a fatty acyl group based on the molecular composition and apparent carbon-to-hydrogen ratio (Figure 1A). A missing hit in a database search indicated the potential novelty of LAA **1**, containing a glycine-serine-ornithine tripeptide. However, very close relatives, such as lipid 430 (**2**) and lipid 654, belong to the glycine-serine dipeptide LAA family, known to be biosynthesized by several bacteria, including representatives of the phylum Bacteroidetes [14,30,34]. Therefore, the metabolomics data generated in our previous study was examined for the presence of both dipeptide lipids. A corresponding ion peak for lipid 430 (**2**) at m/z 431.3114 $[M + H]^+$ with a RT of 13.0 min was identified in 23 of the analyzed 25 *Chitinophaga* metabolomes (Table S1). Similar serial neutral losses of H_2O , serine, and glycine, together with the same remaining fragment ion of m/z 251.2367 $[M + H]^+$, strongly suggested **1** being a close derivative of **2**, expanded by an additional ornithine residue (Figure 1B). To provide a sufficient amount of the compounds for structure confirmation via NMR, our in-house Bacteroidetes-based extract library was examined for enhanced production of **1** and **2**. Lipid 430 (**2**) was enriched in extracts of strain FHG000416, which was assigned by 16S rRNA sequence analysis to the Bacteroidetes genus *Olivibacter* due to a sequence identity of ~94.5% towards *Olivibacter domesticus* DSM 18733 [48,49]. Extracts from both strains, *C. eiseniae* DSM 22224 and FHG000416, were considered as starting points for compound isolation. NMR analysis confirmed compound **2** to be lipid 430 since the data were in good agreement with the literature (Table 1) [35]. Compared thereto, 1H and 2D spectra of **1** were highly similar. Accordingly, the fatty acyl motif linked to glycine and serine was identified as *iso*-heptadecanoic acid (*iso*- $C_{17:0}$). An additional amide proton $2'''-NH$ (δ_H 7.66–7.59 ppm) was observed showing COSY correlation to methine proton $H-2'''$ (δ_H 3.82–3.75 ppm, δ_C 53.6 ppm). Further correlations to methylene protons $H-3'''$, $H-4'''$, and $H-5'''$ confirmed the presence of a C-terminal ornithine residue, as postulated based on the MS/MS fragmentation, identifying lipid **1** as 5-amino-2-(3-hydroxy-2-(2-(3-hydroxy-15-methylhexadecanamido)acetamido)propanamido)pentanoic acid (Figure 2; Table 1).

The stereochemistry of the chiral amino acids incorporated in LAA **1** and lipid 430 (**2**) was determined by advanced Marfey's analysis, using N_{α} -(2,4-dinitro-5-fluorophenyl)-L-valinamide (L-FDVA) as Marfey's reagent [50]. D- and L-enantiomers of serine and ornithine served as RT references. In agreement with published data, the serine residue of lipid 430 (**2**) was identified as L-serine (Figure S1) [34]. This was also true for lipid **1**, which furthermore contains L-ornithine (Figure S1; Figure S2).

During processing, the extracts of FHG000416, two further derivatives of **1** and **2**, were recognized and identified based on their similar MS/MS fragmentation patterns. The two ions of m/z 344.2802 $[M + H]^+$ and m/z 376.2696 $[M + H]^+$ were assigned to putative lipids with molecular formulae $C_{19}H_{37}NO_4$ (**3**) and $C_{19}H_{37}NO_6$ (**4**). Compared with **1** and **2**, the MS/MS fragmentation of **3** showed the identical resulting fragment ion at m/z 251.2370 $[M + H]^+$ after neutral losses of two water and one glycine molecule (Figure 1C).

Therefore, we assumed that **1**, **2**, and **3** share the same acyl chain and glycine residue. In contrast, the MS/MS fragmentation pattern of **4** also showed admittedly the neutral loss of a glycine but also the loss of several water molecules. The resulting fragment ion at m/z 265.2162 $[M + H]^+$ corresponded to the formula of $C_{17}H_{29}O_2^+$, indicating modifications in the acyl residue (Figure 1D). Finally, 1D and 2D-NMR spectra confirmed an *iso*- $C_{17:0}$ aliphatic acyl group linked to glycine via a peptide bond (Table 1). In the case of lipid **3**, the α -methylene protons of the acyl group H-2 (δ_H 2.19 ppm) showed COSY correlation with the single methine proton H-3 (δ_H 3.79–3.74 ppm), suggesting substitution. The chemical shift of the HSQC-correlating carbon atom C-3 (δ_C 67.4 ppm) furthermore supported the hypothesis of a hydroxyl group being attached in β -position (Table 1). Thus, **3** was identified as (3-hydroxy-15-methylhexadecanoyl)glycine (Figure 2). For derivative **4**, NMR spectra undergirded the expected similarities, except for the methine proton H-3 (δ_H 3.44 ppm, δ_C 74.5 ppm) showing COSY correlations with methine instead of methylene protons in α - (H-2, δ_H 4.19 ppm) and γ -position (H-4, δ_H 3.40–3.35 ppm) of the acyl chain. In agreement with the chemical shift of the HSQC-correlating carbon atoms C-2 and C-4 (δ_{C-2} 70.9 ppm, δ_{C-4} 69.5 ppm), hydroxylation was determined at both sites, thereby identifying **4** as (2,3,4-trihydroxy-15-methylhexadecanoyl)glycine (Figure 2; Table S2).

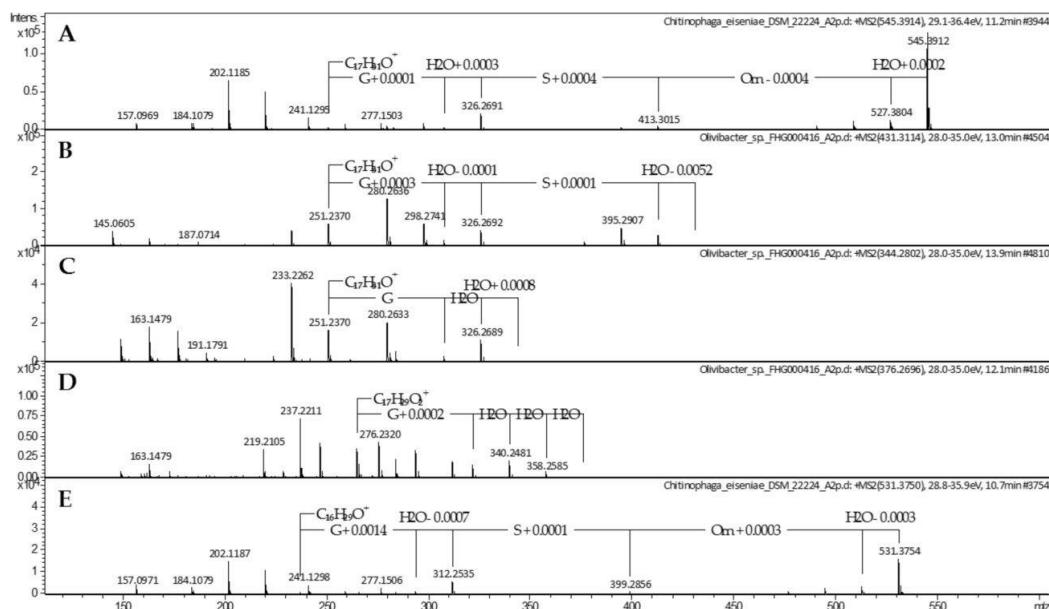


Figure 1. MS/MS spectra of lipoamino acids **1–4** (A–D) and **7** (E) produced by *Chitinophaga eiseniae* DSM 22224 (**1**, **7**) and *Olivibacter* sp. FHG000416 (**2–4**).

In contrast with its de-esterified hydrolysis product lipid 430 (**2**) [36], lipid 654 (m/z 655.525 $[M + H]^+$) carrying an additional ester-linked *iso*-pentadecenoic acid (*iso*- $C_{15:0}$) was not observed in our previously generated *Chitinophaga* extracts (Table S1) [46]. Nevertheless, we searched for corresponding lipid 654 analogs because LAA **1** represents a close derivative of lipid 430 (**2**) containing an additional ornithine amino acid attached to the glycine-serine dipeptide. In 8 of 25 *Chitinophaga* metabolomes, the corresponding parent ion at m/z 769.6051 $[M + H]^+$ with molecular formula $C_{42}H_{80}N_4O_8$ (**5**) was found (Table S1). Neutral losses of ornithine-serine-glycine and the resulting fragment ion at m/z 251.2372 $[M + H]^+$ were identical to the MS spectrum of compound **1** (Figure 3A). Moreover, the MS/MS fragmentation pattern containing the characteristic fragment ion at m/z 527.3814 $[M + H]^+$ (loss of 242.2251 Da ($C_{15}H_{30}O_2$)) proved the

presence of the expected ester-linked fatty acyl moiety (*iso*-C_{15:0}) at C-3. Therefore, compound **5** (2-(3-aminopropyl)-5-(hydroxymethyl)-26-methyl-12-(12-methyltridecyl)-4,7,10,14-tetraoxo-13-oxa-3,6,9-triazaheptacosanoic acid) was clearly identified as the ornithine analog of the literature-known lipid 654 [34] (Figure 4).

Table 1. ¹H and ¹³C data of compounds **1–3** (**1**: 500 MHz/126 MHz, DMSO-*d*₆; **2**: 400 MHz/101 MHz, MeOD-*d*₄; **3**: 600 MHz/101 MHz, DMSO-*d*₆).

Position	1		2		3	
	δ_{H} , (J in Hz)	δ_{C} , Type ^a	δ_{H} , (J in Hz)	δ_{C} , Type	δ_{H} , (J in Hz)	δ_{C} , Type
1		171.1, C		175.0, C		171.1, C
2	2.20, d (6.1)	43.3, CH ₂	2.41, dd (14.0, 4.3), 2.34, dd (14.0, 8.6)	44.8, CH ₂	2.19, d (6.4)	43.6, CH ₂
3	3.82–3.75, m	67.2, CH	4.02–3.94, m	70.0, CH	3.79–3.74, m	67.4, CH
4	1.39–1.31, m	36.7, CH ₂	1.53–1.46, m	38.4, CH ₂	1.40–1.34, m, 1.33–1.27, m	36.8, CH ₂
5	1.39–1.31, m ^b , 1.31–1.26, m ^b	24.8, CH ₂	1.50–1.43, m, 1.38–1.32, m	26.7, CH ₂	1.40–1.35, m, 1.31–1.25, m	25.1, CH ₂
6	1.26–1.22, m ^b	28.0–28.9 ^c , CH ₂	1.36–1.25, m ^e	30.7–31.0 ^f , CH ₂	1.26–1.21, m ^g	29.0–29.3 ^h , CH ₂
7	1.26–1.22, m ^b	28.0–28.9 ^c , CH ₂	1.36–1.25, m ^e	30.7–31.0 ^f , CH ₂	1.26–1.21, m ^g	29.0–29.3 ^h , CH ₂
8	1.26–1.22, m ^b	28.0–28.9 ^c , CH ₂	1.36–1.25, m ^e	30.7–31.0 ^f , CH ₂	1.26–1.21, m ^g	29.0–29.3 ^h , CH ₂
9	1.26–1.22, m ^b	28.0–28.9 ^c , CH ₂	1.36–1.25, m ^e	30.7–31.0 ^f , CH ₂	1.26–1.21, m ^g	29.0–29.3 ^h , CH ₂
10	1.26–1.22, m ^b	28.0–28.9 ^c , CH ₂	1.36–1.25, m ^e	30.7–31.0 ^f , CH ₂	1.26–1.21, m ^g	29.0–29.3 ^h , CH ₂
11	1.26–1.22, m ^b	28.0–28.9 ^c , CH ₂	1.36–1.25, m ^e	30.7–31.0 ^f , CH ₂	1.26–1.21, m ^g	29.0–29.3 ^h , CH ₂
12	1.26–1.22, m ^b	28.0–28.9 ^c , CH ₂	1.36–1.25, m ^e	30.7–31.0 ^f , CH ₂	1.26–1.21, m ^g	29.0–29.3 ^h , CH ₂
13	1.26–1.22, m ^b	26.4, CH ₂	1.36–1.25, m ^e	28.5, CH ₂	1.26–1.21, m ^g	26.8, CH ₂
14	1.16–1.11, m	38.1, CH ₂	1.17, q (6.7)	40.2, CH ₂	1.15–1.11, m	38.5, CH ₂
15	1.50, non (6.6)	27.0, CH	1.50, sept (6.6)	29.2, CH	1.49, non (6.6)	27.4, CH
16	0.85, d (6.6)	22.2, CH ₃	0.88, d (6.7)	23.0, CH ₃	0.84, d (6.6)	22.5, CH ₃
1'		168.6, C		171.6, C		n.o. ^d
2'	3.73, d (4.6)	41.5, CH ₂	3.98, d (16.8), 3.90, d (16.7)	43.5, CH ₂	3.70, dd (17.4, 5.7), 3.65, dd (17.4, 5.7)	41.0, CH ₂
2-NH	8.10–8.04, m		8.30, t (5.6)		8.01, t (5.7)	
1'''		n.o. ^d		173.4, C		
2''	4.25, dd (12.6, 6.2)	54.7, CH	4.50, t (4.3)	56.2, CH		
2''-NH	7.91–7.83, m		8.04, d (7.7)			
3''	3.56, m, 3.46, m	62.0, CH ₂	3.91, dd (11.5, 4.5), 3.83, dd (11.3, 3.8)	63.0, CH ₂		
1'''		n.o. ^d				
2'''	3.82–3.75, m	53.6, CH				
2'''-NH	7.66–7.59, m					
3'''	1.80–1.71, m, 1.69–1.61, m	n.o. ^d				
4'''	1.66–1.56, m	24.0, CH ₂				
5'''	2.80–2.73, m	38.4, CH ₂				

^a Extracted from HSQC spectra; ^{b,c,e-h} Signals are overlapping; ^d Not observed due to extreme line broadening.

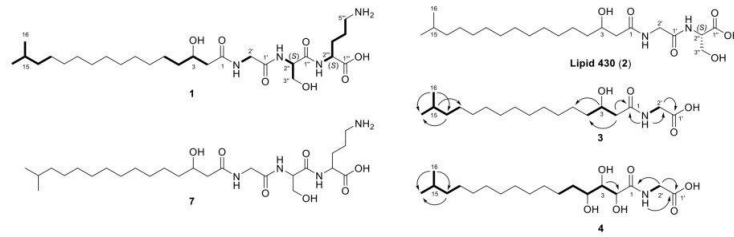


Figure 2. Chemical structures of liposaminic acids **1–4** and **7** produced by *C. eiseniae* DSM 22224 (**1, 7**) and *Olivibacter* sp. FHG000416 (**2–4**). The COSY (in bold) and key H→C HMBC (arrows) correlations observed for lipids **1, 3**, and **4** are indicated.

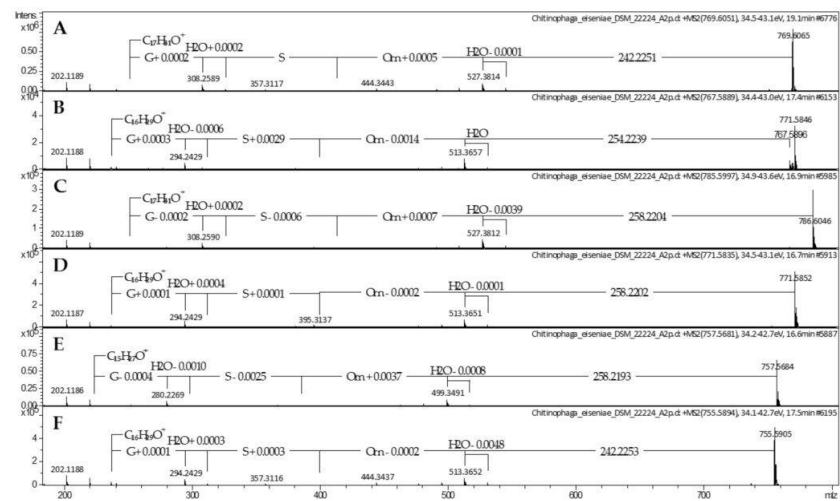


Figure 3. MS/MS spectra of liposaminic acids **5** (A), **6** (B), and **8–11** (C–F) produced by *Chitinophaga eiseniae* DSM 22224.

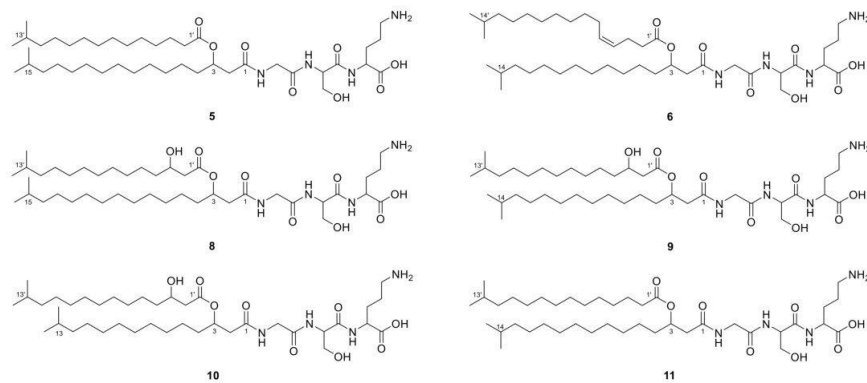


Figure 4. Postulated chemical structures based on UHR-ESI-MS/MS spectra of liposaminic acids **5, 6**, and **8–11**, produced by *Chitinophaga eiseniae* DSM 22224.

Based on this finding, the second *Chitinophaga* core metabolite with a UHR-ESI-MS ion peak at m/z 767.5896 $[M + H]^+$ was assigned the molecular formula $C_{42}H_{78}N_4O_8$ (**6**). Compared with compound **5**, a difference of 2.0155 Da indicated a double bond in one of the fatty acid residues. The MS/MS fragmentation pattern revealed the amino acid sequence ornithine-serine-glycine. Furthermore, compared with lipid **5**, a fragment ion at m/z 513.3657 $[M + H]^+$ resulted from the loss of an ester-linked fatty acid residue (254.2239 Da) with additional 11.9988 Da ($1 \times C$) at C-3. Together with the remaining fragment ion at m/z 237.2212 $[M + H]^+$, $C_{16}H_{29}O^+$, 14.0160 Da less compared with **1–3** and **5**), we postulate lipid **6** to carry two *iso*-palmitic acid (*iso*- C_{16}) residues, a saturated amide-linked *iso*- $C_{16:0}$, and an ester-linked mono-unsaturated *iso*- $C_{16:1}$ (Figure 3B). In line with reported glycine and glyceryl-serine analogs [13], we assume the double bond to be in Δ^4 position and with Z configuration for lipid **6**, identifying it as (Z)-2-(3-aminopropyl)-5-(hydroxymethyl)-27-methyl-12-(11-methyldodecyl)-4,7,10,14-tetraoxo-13-oxa-3,6,9-triazaoctacos-17-enoic acid (Figure 4). However, structural confirmation by NMR was not possible due to a low production titer in large-scale fermentation of *C. eiseniae* DSM 22224.

With lipid **6** carrying a different amide-linked fatty acid residue than **5**, we assumed to find a correlating close derivative of lipids **1–3** that carried an amide-linked *iso*- $C_{16:0}$ fatty acid residue instead of an *iso*- $C_{17:0}$. In total, 18 *Chitinophaga* strain data sets contained the matching positive parent ion at m/z 531.3754 according to molecular formula $C_{26}H_{50}N_4O_7$ (**7**) (Table S1). A missing ester-linked fatty acid residue and an otherwise identical UHR-ESI-MS/MS spectrum of compound **7** compared with lipid **6** confirmed the presence of an *iso*- $C_{16:0}$ fatty acid residue amide linked to a glycine-serine-ornithine amino acid motif (Figure 1E). Therefore, lipid **7** was identified as 5-amino-2-(3-hydroxy-2-(2-(3-hydroxy-14-methylpentadecanamido)acetamido)propanamido)pentanoic acid (Figure 2).

In addition to lipids **5** and **6**, we observed four closely related metabolites with similar masses and RTs: **8** (m/z 785.6016 $[M + H]^+$, $C_{42}H_{80}N_4O_9$, 16.9 min), **9** (m/z 771.5852 $[M + H]^+$, $C_{40}H_{78}N_4O_9$, 16.7 min), **10** (m/z 757.5681 $[M + H]^+$, $C_{40}H_{76}N_4O_9$, 16.6 min), and **11** (m/z 755.5894 $[M + H]^+$, $C_{41}H_{78}N_4O_8$, 17.5 min) in the extract of *C. eiseniae* DSM 22224. Sharing the same tripeptide moiety of glycine-serine-ornithine, these lipid **654** analogs vary in the length and hydroxylation of their acyl chains. The analysis of the UHR-ESI-MS/MS spectra of LAAs **8–10** revealed a neutral loss of 258.2204 Da ($C_{15}H_{28}O_3$). Compared with the neutral loss of 242.2251 Da ($C_{15}H_{28}O_2$) of LAA **5**, the additional 15.9953 Da depicted the presence of an additional oxygen atom in the ester-linked *iso*- $C_{15:0}$ fatty acid residue (Figure 3C–E). In accordance with the isolated LAAs **2** and **3**, the corresponding hydroxyl group was assigned to C-3' position. With all other fragment ions identical to LAA **5**, the structure of LAA **8** was postulated as 2-(3-aminopropyl)-16-hydroxy-5-(hydroxymethyl)-26-methyl-12-(12-methyltridecyl)-4,7,10,14-tetraoxo-13-oxa-3,6,9-triazaheptacosanoic acid (Figure 4). LAA **9** shared the characteristic fragment ion at m/z 237.2213 $[M + H]^+$, identified as an unsaturated amide-linked *iso*- $C_{16:0}$ fatty acid residue with LAA **6** (Figure 3D). Therefore, **9** was identified as 2-(3-aminopropyl)-16-hydroxy-5-(hydroxymethyl)-26-methyl-12-(11-methyldodecyl)-4,7,10,14-tetraoxo-13-oxa-3,6,9-triazaheptacosanoic acid (Figure 4). For LAA **10**, a characteristic fragment ion was detected at m/z 223.2059 ($[M + H]^+$, $C_{15}H_{27}O^+$) with 14.0154 Da less compared with the one of **9** (Figure 3E). This indicated lipid **10** to be a LAA with an ornithine-serine-glycine tripeptide amide linked to an *iso*- $C_{15:0}$ fatty acid residue that carries another C-3 ester-linked hydroxylated *iso*- $C_{15:0}$ fatty acid residue. The chemical structure of the new compound **10** is 2-(3-aminopropyl)-16-hydroxy-5-(hydroxymethyl)-26-methyl-12-(10-methylundecyl)-4,7,10,14-tetraoxo-13-oxa-3,6,9-triazaheptacosanoic acid (Figure 4). The analysis of the UHR-ESI-MS/MS spectrum of the last derivative of this lipid family revealed the ester-linked fatty acid to have an *iso*- $C_{15:0}$ and the amide-linked one an *iso*- $C_{16:0}$ moiety without further modifications (Figure 3F). Thus, the new LAA **11** was identified as 2-(3-aminopropyl)-5-(hydroxymethyl)-26-methyl-12-(11-methyldodecyl)-4,7,10,14-tetraoxo-13-oxa-3,6,9-triazaheptacosanoic acid (Figure 4).

2.2. Phospholipids

In addition to the aforementioned LAAs, dereplication of the last two *Chitinophaga* core buckets with m/z 452.2769 $[M + H]^+$ and 440.2767 $[M + H]^+$ suggested the closely related molecular formulae $C_{21}H_{42}NO_7P$ (**12**) and $C_{20}H_{42}NO_7P$ (**13**), respectively. A database query for **12** provided LPE 451 as a structural hypothesis, based on similar MS and MS/MS spectra in accordance with the literature [51]. Neutral losses of the phosphatidylethanolamine group (141.018 Da) followed by the CH_2OH group (30.994 Da) or the glycerol moiety (74.037 Da), which are reported for phospholipids such as the identified LPE [52,53], resulted in a key fragment ion at m/z 237.2210 $[M + H]^+$ ($C_{16}H_{29}O^+$, DBE = 3). Highly similar MS/MS fragmentation of **13** led to the fragment ion at m/z 225.2212 $[M + H]^+$ ($C_{15}H_{29}O^+$, DBE = 2), indicating the structural variance to be located in the acyl motif. For NMR analysis, the isolation of these compounds was again carried out from extracts of *Olivibacter* sp. FHG000416, as higher production titers were observed compared with *C. eiseniae* DSM 22224. For **12**, NMR data confirmed the occurrence of lysophosphatidylethanolamine ($C_{16:1}$), as postulated by dereplication. According to published data for LPE 451, the double bond ($\delta_{H-15/16}$ 5.24–5.12 ppm) of the mono-unsaturated palmitoyl motif was assigned to Δ^9 position with Z configuration, with the acyl chain being attached to the glycerol moiety at *sn*-1 position (Table S3) [51]. Thus, **12** was identified as 1-(9Z-palmitoyl)-2-hydroxy-*sn*-glycerol-3-phosphoethanol-amine (Figure 5). In comparison, 1D and 2D-NMR data acquired for **13** revealed the double bond of the acyl chain to be missing. Instead, an isopropyl moiety (δ_{H-19} 1.29 ppm, δ_{C-20} 27.7 ppm/ δ_{H-20} 0.63 ppm, δ_{C-20} 22.2 ppm) was observed, identifying the acyl chain as *iso*- $C_{15:0}$ attached to the otherwise identical molecule (Table S3). Therefore, **13** was identified as 1-isopentadecanoyl-2-hydroxy-*sn*-glycerol-3-phosphoethanolamine (Figure 5).

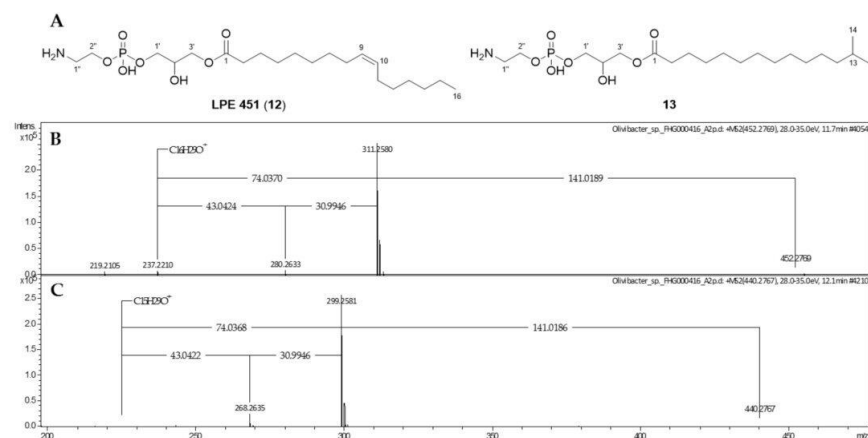


Figure 5. Chemical structures (A) and MS/MS spectra of LPE 451 (**12**, B) and its new derivative (**13**, C), isolated from *Olivibacter* sp. FHG000416.

2.3. N-acyl Amino Acids from *Olivibacter* sp. FHG000416

During processing extracts from *Olivibacter* sp. FHG000416, three additional metabolites with lipid-like properties (e.g., surface activity) were observed. For compound **14**, the molecular formula $C_{16}H_{23}NO_4$ (m/z 294.1696 $[M + H]^+$) was determined by UHR-ESI-MS. The MS/MS fragmentation pattern showed a fragment at m/z 182.0811, matching the protonated form of tyrosine ($[M + H]^+$, $C_9H_{12}NO_3^+$). This hypothesis was further supported by neutral losses of NH_3 and H_2O , commonly known for the fragmentation of amino acids (Figure S3A) [15]. Furthermore, the neutral loss of 112.0885 Da ($C_7H_{12}O$) implied the loss of a saturated acyl group. The 1D and 2D NMR experiments confirmed this structural proposal (Table 2), showing an isopropyl group at the end of the *iso*- $C_{7:0}$ acyl

moiety, which was attached to tyrosine via a peptide bond. Therefore, **14** was identified as *N*-(5-methyl)hexanoyl tyrosine (Figure 6).

Table 2. ^1H and ^{13}C data of compounds **14–16** (^1H : 400 MHz, ^{13}C : 101 MHz, MeOD- d_4).

Position	14		15		16	
	δ_{H} (J in Hz)	δ_{C} , Type	δ_{H} (J in Hz)	δ_{C} , Type	δ_{H} (J in Hz)	δ_{C} , Type
1'		157.3, C		157.2, C	7.23–7.17, m	127.8, CH
2'	6.69, dd (6.6, 1.9)	116.1, CH	6.68, dd (6.5, 2.1)	116.1, CH	7.30–7.22, m	129.4, CH
3'	7.04, dd (6.6, 1.9)	131.2, CH	7.03, dd (6.6, 1.5)	131.3, CH	7.26–7.21, m	130.3, CH
4'		129.2, C		129.4, C		138.7, C
5'	3.11, dd (14.0, 4.8), 2.83, dd (14.0, 9.3)	37.7, CH ₂	3.11, dd (14.0, 4.9), 2.84, dd (13.9, 8.9)	37.9, CH ₂	3.22, dd (13.9, 4.8), 2.93, dd (13.9, 9.5)	38.5, CH ₂
6'	4.59, dd (9.3, 4.6)	55.3, CH	4.57, dd (8.9, 4.9)	55.7, CH	4.66, dd (9.4, 4.8)	55.1, CH
7'		175.3, C		175.9, C		175.2, C
1		176.1, C		175.9, C		176.1, C
2	2.13, t (7.5)	37.1, CH ₂	2.15, t (7.4)	37.0, CH ₂	2.14, t (7.4)	36.9, CH ₂
3	1.55–1.47, m	24.8, CH ₂	1.56–1.48, m	27.0, CH ₂	1.55–1.46, m	26.9, CH ₂
4	1.14–1.05, m	39.4, CH ₂	1.32–1.24, m	28.2, CH ₂	1.32–1.23, m	28.2, CH ₂
5	1.52–1.46, m	29.0, CH	1.24–1.18, m	30.4, CH ₂	1.23–1.14, m	30.4, CH ₂
6	0.86, d (6.6)	22.8/22.9, CH ₃	1.20–1.12, m	40.0, CH ₂	1.22–1.10, m	40.0, CH ₂
7			1.57–1.49, m	29.1, CH	1.55–1.49, m	29.1, CH
8			0.88, d (6.6)	23.0, CH ₃	0.87, d (6.6)	23.1/23.0, CH ₃

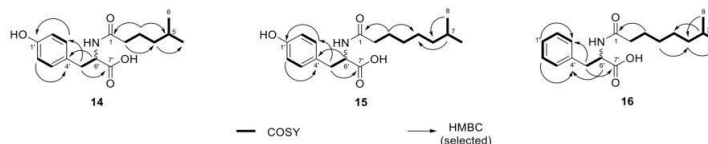


Figure 6. Chemical structures of *N*-acyl amino acids (**14–16**) isolated from *Olivibacter* sp. FHG000416, with observed COSY (in bold) and key H→C HMBC (arrows) correlations.

Based on UHR-ESI-MS analysis, compounds **15** (m/z 322.2013 $[\text{M} + \text{H}]^+$, $\text{C}_{18}\text{H}_{27}\text{NO}_4$) and **16** (m/z 306.2063 $[\text{M} + \text{H}]^+$, $\text{C}_{18}\text{H}_{27}\text{NO}_3$) shared the same saturated acyl group indicated by the neutral loss of 140.1201 Da ($\text{C}_9\text{H}_{16}\text{O}$). The difference of 28.0317 Da compared with **14** is equivalent to two additional methylene groups matching an *iso*- $\text{C}_{9,0}$ acyl group. Identical to NAAA **14**, the acyl group of **15** was attached to tyrosine (Figure S3B). In contrast, the fragment ion of NAAA **16** at m/z 166.0862 ($[\text{M} + \text{H}]^+$, $\text{C}_9\text{H}_{12}\text{NO}_2^+$) corresponded to one oxygen atom less and was thereby assumed to be phenylalanine (Figure S3C). NMR analysis confirmed both structural proposals based on the MS data. NAAA **15** was determined as *N*-(7-methyl)octanoyl tyrosine and **16** as *N*-(7-methyl)octanoyl phenylalanine (Figure 6, Table 2). Finally, advanced Marfey's analysis of NAAAs (**14–16**) revealed that all three compounds had been isolated as an enantiomeric mixture. The D/L-ratio was determined by UV signal integration as 1:16 for **14**, 1:1.7 for **15**, and 1.6:1 for **16** (Figure S4–S6).

2.4. Antimicrobial Activity of Lipids Isolated from Bacteroidetes

The antimicrobial activity of compounds **1–4** and **12–16** isolated either from *C. eiseniae* DSM 22224 or *Olivibacter* sp. FHG000416 was determined by microbroth dilution assay against a panel of 12 indicator strains up to a test concentration of 64 µg/mL. No growth inhibition effect was observed for LAA **4** and the NAAAs **15** and **16**. *N*-(5-methyl)hexanoyl tyrosine (**14**) exhibited very low effect against Gram-negative *M. catarrhalis* ATCC 25238 and Gram-positive *M. luteus* DSM 20030 at the highest concentration of 64 µg/mL. In contrast, LAAs **1–3** and both LPEs (**12** and **13**) showed growth inhibiting activity in a range of 4–16 µg/mL and 16–64 µg/mL against *M. catarrhalis* ATCC 25238 and *M. luteus* DSM 20030, respectively. Moreover, LAA **1** inhibited *B. subtilis* DSM 10 up to 8 µg/mL and *C. albicans* FH2173 as well as *E. coli* ATCC 35218 up to 64 µg/mL—the latter only when tested in bicarbonate-supplemented screening medium (MHC) (Table 3).

Table 3. MIC values (µg/mL) of compounds **1–4** and **12–16**. MHC = cation-adjusted Mueller–Hinton II medium supplemented with 3.7 g/L bicarbonate, n.d. = not determined.

	Compounds									
	1	2	3	4	12	13	14	15	16	
<i>E. coli</i> ATCC 35218 (MH-II)	>64	>64	>64	>64	>64	>64	>64	>64	>64	>64
<i>E. coli</i> ATCC 35218 (MHC)	64	>64	>64	>64	>64	>64	>64	>64	>64	>64
<i>E. coli</i> ATCC 25922 ΔTolC	>64	>64	>64	>64	>64	>64	>64	>64	>64	>64
<i>P. aeruginosa</i> ATCC 27853	>64	>64	>64	>64	>64	>64	>64	>64	>64	>64
<i>K. pneumoniae</i> ATCC 13883	>64	>64	>64	>64	>64	>64	>64	>64	>64	>64
<i>M. catarrhalis</i> ATCC 25238	4–8	16–32	8	>64	4–8	16	64	>64	>64	
<i>A. baumannii</i> ATCC 19606	n.d.	n.d.	>64	>64	n.d.	n.d.	>64	>64	>64	
<i>B. subtilis</i> DSM 10	8	>64	>64	>64	>64	>64	>64	>64	>64	
<i>S. aureus</i> ATCC 25923	>64	>64	>64	>64	>64	>64	>64	>64	>64	
<i>M. luteus</i> DSM 20030	64	32–64	>64	>64	16	16	64	>64	>64	
<i>L. monocytogenes</i> DSM 20600	n.d.	n.d.	>64	>64	>64	n.d.	>64	>64	>64	
<i>M. smegmatis</i> ATCC 607	>64	n.d.	>64	n.d.	>64	n.d.	>64	>64	>64	
<i>C. albicans</i> FH2173	64	>64	>64	>64	>64	>64	>64	>64	>64	

3. Discussion

Bacterial small molecules are of great importance for medicinal, industrial, and agricultural applications [54]. Within this class of compounds, lipids represent a structurally diverse class of metabolites with a variety of biological functions [2,26,30]. Advances in LC-MS emerged the field of lipidomics, allowing high-throughput detection and sophisticated analysis of complex lipid samples. Identification of abundant known lipid classes and structure predictions of lipids new to science are possible. However, compared with NMR techniques, LC-MS measurements that require lower amounts of sample will not provide enough data to deduce the planar structure unambiguously [39].

In the current study, we described the characterization and structure elucidation of the unknown previously determined core lipids of the Bacteroidetes genus *Chitinophaga* [46]. Interestingly, we observed the highest production titers of three of the four lipids in extracts of *Olivibacter* sp. FHG000416, a strain belonging to another Bacteroidetes genus. Therefore, compound isolation was carried out from these two strains: *Olivibacter* sp. FHG000416 and *Chitinophaga eiseniae* DSM 22,224. Two of the four lipids are identified as LPEs, with **13** being an undescribed derivative of the literature-known LPE 451 (**12**). The remaining ones (**1** and **6**), together with several further derivatives thereof, are novel lipids classified as LAAs. The literature frequently described the production of LAAs by various bacteria, with some of them being isolated and chemically fully characterized [5]. These are often mono- or dipeptide lipids containing glycine, serine, ornithine, or glycine-serine as amino acid residues amide-linked to an *iso*-fatty acid ester at C-3 with different degrees of unsaturation [6–12]. Based on MS/MS and NMR experiments, the lipids **3** and **4** were identified as new LAA glycine derivatives. The *Chitinophaga* core lipids **1** and **6**, as well

as lipids 5 and 8–11 form a LAA family with an undescribed tripeptide moiety of glycine-serine-ornithine. This novel tripeptide LAA family is most closely related to the intensively studied glycine-serine dipeptide lipids 654 and 430 (2). Interestingly, with lipid 430 (2), only the de-esterified hydrolysis product of lipid 654 [34] was detected in the methanolic extracts of 23 of 25 *Chitinophaga* strains generated in our previous study [46]. Recent intensive studies of human pathogenic Bacteroidetes such as *P. gingivalis* revealed both dipeptide lipids to engage TLR2 [34]. They are involved in the development of two chronic inflammatory diseases, including periodontitis and atherosclerosis [30]. Furthermore, studies implicated lipid 654 to be involved in the development of multiple sclerosis [25]. Therefore, further studies are necessary to investigate the effects of the here described novel tripeptide LAAs in terms of immune response and whether they might also be part of the cell membrane of pathogens such as *P. gingivalis*.

The same applies to the new *N*-acyl tyrosine and phenylalanine analogs. They belong to a growing family of microbial secondary metabolites isolated from bacteria [22,23], fungi [21], or from environmental DNA expressed in heterologous hosts such as *E. coli* [16–20]. It is hypothesized that these lipids are possible signaling molecules with a wide range of biological activities from anti-cancer therapy targets to antimicrobial lipids [16–23]. With no antimicrobial activity observed, further studies are necessary to elucidate their biological function.

In addition to the structure-associated as well as the target organism-oriented antimicrobial activities of lipids, a membrane destabilization mechanism has been investigated for several decades [26,55]. In this context, a ‘carpet’ mechanism is suggested, which results in a detergent-like membrane permeation and/or disintegration [55,56]. Based on the reported findings, we selected a panel of 12 microorganisms to cover a wide range of possible targets for the herein described NPs. The antimicrobial profiling of the herein tested lipids revealed a frequent growth inhibitory effect towards *M. catarrhalis*, with lipid 1 additionally showing growth inhibiting activity against *B. subtilis*. The more hydrophobic cell surface of *M. catarrhalis*, compared with the surfaces of, e.g., *E. coli* and *P. aeruginosa*, is believed to be the reason for high accessibility of hydrophobic agents to the cell surface [57–59]. Therefore, we assume *M. catarrhalis* to be the most susceptible pathogen towards a suggested membranolytic mode of action mediated by LAAs carrying a hydrophobic lipid moiety and a short hydrophilic amino acid moiety. The mode of action needs to be confirmed in further studies.

4. Materials and Methods

4.1. Isolation of *Olivibacter* sp. FHG000416

Olivibacter sp. FHG000416 is incorporated into the Fraunhofer strain collection. This strain was isolated in 2016 from termite carton nest material of *Coptotermes gestroi* kindly provided by Prof. Dr. Rudy Plarre (Bundesanstalt für Materialforschung und -prüfung, Berlin). In brief, living cells were retrieved using nycodenz density gradient method, as described elsewhere [60]. Diluted cell suspensions (10^{-2} – 10^{-6}) were plated on R2A Agar (DMSZ medium 830) and incubated for seven days at 28 °C. In order to isolate single strains, single colonies were propagated four times, then affiliated by using 16S rRNA gene sequencing with the primer pair E8F (5′-GAGTTTGATCCTGGCTCAG-3′) and 1492R (5′-AGAGTTTGATCCTGGCTCAG-3′) [61]. As judged on nearly full-length 16S rRNA sequence (MZ073637) comparison, FHG000416 is phylogenetically most closely related to *Olivibacter domesticus* DSM 18733 [48,49], with only ~94.5% identity.

4.2. Mass Spectrometric Analysis

For all UHPLC-QTOF-UHR-MS and MS/MS measurements, a quadrupole time-of-flight spectrometer (LC-QTOF maXis II, Bruker Daltonics, Bremen, Germany) equipped with an electrospray ionization source in line with an Agilent 1290 infinity LC system (Agilent Technologies, Santa Clara, CA, USA) was used. C18 RP-UHPLC (ACQUITY UPLC BEH C18 column (130 Å, 1.7 µm, 2.1 × 100 mm)) was performed at 45 °C with the following

linear gradient (A: H₂O, 0.1% HCOOH; B: CH₃CN, 0.1% HCOOH; flow rate: 0.6 mL/min): 0 min: 95% A; 0.30 min: 95% A; 18.00 min: 4.75% A; 18.10 min: 0% A; 22.50 min: 0% A; 22.60 min: 95% A; 25.00 min: 95% A. A 50 to 2000 *m/z* scan range at 1 Hz scan rate was used to acquire mass spectral data. The injection volume was set to 5 μ L. MS/MS experiments were performed at 6 Hz, and the top five most intense ions in each full MS spectrum were targeted for fragmentation by higher-energy collisional dissociation at 25 eV using N₂ at 10⁻² mbar. Precursors were excluded after 2 spectra, released after 0.5 min, and reconsidered if the intensity of an excluded precursor increased by a factor of 1.5 or more. Data were analyzed using the Bruker Data Analysis 4.0 software package.

4.3. Isolation of Lipids

C. eiseniae DSM 22224 and *Olivibacter* sp. FHG000416 were inoculated from plate (R2A) in 300 mL Erlenmeyer flasks filled with 100 mL R2A and incubated at 28 °C with agitation at 180 rpm for 3 d. A 20 L fermentation (separated in 500 mL culture volume per 2 L flasks) of *C. eiseniae* in medium 3018 (1 g/L yeast extract, 5 g/L casitone, pH 7.0) was inoculated with 2% (*v/v*) pre-culture and incubated under the same conditions for 4 d. Using the same conditions, 7 and 20 L fermentations of *Olivibacter* sp. were performed in medium 5065 (15 g/L soluble starch, 10 g/L glucose, 10 g/L soy flour, 1 g/L yeast extract, 0.1 g/L K₂HPO₄, 3 g/L NaCl, pH 7.4) and 5294 (10 g/L soluble starch, 10 g/L glucose, 10 g/L glycerol 99%, 2.5 g/L liquid corn steep, 5 g/L peptone, 2 g/L yeast extract, 1 g/L NaCl, 3 g/L CaCO₃, pH 7.2), respectively. An additional 40 L cultivation of *Olivibacter* sp. in medium 5294 was carried out using the same conditions as before. Cultures were subsequently lyophilized using a delta 2–24 LSCplus (Martin Christ Gefriertrocknungsanlagen GmbH, Osterode am Harz, Germany).

The dried culture of *C. eiseniae* and the 7 L culture of *Olivibacter* sp. were extracted with one-time culture volume MeOH for the isolation of lipid 1, lipid 430 (2), and 3, respectively. The extracts were evaporated to dryness using rotary evaporation under reduced pressure, resuspended in 3 L of 10% MeOH/H₂O, and separately loaded onto a XAD16N column (1 L bed volume). Step-wise elution with 10%, 40%, 60%, 80%, and 100% MeOH (2-times bed volume each) was performed. The 80% and 100% fractions containing the lipids were further fractionated by preparative (Synergi™ Fusion-RP 80 Å, 10 μ m, 250 \times 21.2 mm) and/or semi-preparative HPLC (Nucleodur® C18 Gravity-SB, 3 μ m, 250 \times 10 mm) using gradients of 60–95% and 50–95% CH₃CN (0.1% HCOOH) in water (0.1% HCOOH), respectively. Final purification was achieved by analytical HPLC (Synergi™ Fusion-RP 80 Å, 4 μ m, 250 \times 4.6 mm) or UHPLC fractionation (Acquity UPLC® BEH C18, 1.7 μ m, 100 \times 2.1 mm) using a custom-made fraction collector (Zinsser-Analytik, Eschborn, Germany).

The 20 L fermentation of *Olivibacter* sp. was the starting point for the isolation of lipid 4. Due to the enlarged volume, LLE was performed as an additional purification step after MeOH extraction using ethyl acetate and water. In addition to that, the isolation procedure was highly identical for lipid 3. For semi-preparative HPLC, an adapted gradient of 55–95% CH₃CN in water was used.

Extraction of the dried 40 L culture of *Olivibacter* sp. with MTBE/MeOH [62] was performed to isolate LPE 451 (12), 13, and NAAAs 14–16. Combined organic layers were subsequently fractionated by preparative and semi-preparative HPLC using gradients of 40–95% and 60–95% CH₃CN (0.1% HCOOH) in water (0.1% HCOOH), respectively. Again, final purification was achieved by UHPLC fractionation. After each step, fractions containing compounds of interest were evaporated to dryness using a high performance evaporator (Genevac HT-12).

(2S)-5-Amino-2-((2S)-3-hydroxy-2-(2-(3-hydroxy-15 methylhexadecanamido)acetamido)prop anamido)pentanoic acid (1). Colorless solid; [α]_D^{20.6} +21.1 (*c* 0.19, MeOH); LC-UV (CH₃CN/H₂O) λ _{max} 223 nm; ¹H-NMR (500 MHz, DMSO-*d*₆) data and 2D spectra, see Table 1, Figure S7–S10; UHRMS (ESI-TOF) *m/z* [M + H]⁺ calcd for C₂₇H₅₂N₄O₇⁺ 545.3909, found 545.3914.

Lipid 430 (**2**). Colorless solid; $[\alpha]_D^{25.9} +16.3$ (*c* 0.37, MeOH); LC-UV (CH₃CN/H₂O) λ_{\max} 220 nm; ¹H-NMR (400 MHz, MeOD-*d*₄) and ¹³C-NMR (101 MHz, MeOD-*d*₄) data, see Table 1; UHRMS (ESI-TOF) *m/z* [M + H]⁺ calcd for C₂₂H₄₂N₂O₆⁺ 431.3116, found 431.3115.

(3-Hydroxy-15-methylhexadecanoyl)glycine (**3**). Colorless solid; $[\alpha]_D^{21.7} +66.7$ (*c* 0.02, MeOH); LC-UV (CH₃CN/H₂O) λ_{\max} 224 nm; ¹H (600 MHz, DMSO-*d*₆) and ¹³C-NMR (151 MHz, DMSO-*d*₆) data, see Table 1, Figure S11–S15; UHRMS (ESI-TOF) *m/z* [M + H]⁺ calcd for C₁₉H₃₇NO₄⁺ 344.2795, found 344.2802.

(2,3,4-Trihydroxy-15-methylhexadecanoyl)glycine (**4**). Colorless solid; $[\alpha]_D^{21.7} -76.9$ (*c* 0.03, MeOH); LC-UV (CH₃CN/H₂O) λ_{\max} 224 nm; ¹H (600 MHz, DMSO-*d*₆) and ¹³C-NMR (151 MHz, DMSO-*d*₆) data, see Table S2, Figure S16–S20; UHRMS (ESI-TOF) *m/z* [M + H]⁺ calcd for C₁₉H₃₇NO₆⁺ 376.2694, found 376.2696.

1-(9*Z*-Palmitoyl)-2-hydroxy-*sn*-glycerol-3-phosphoethanol-amine (**12**). Colorless solid; LC-UV (CH₃CN/H₂O) λ_{\max} 223 nm; ¹H (600 MHz, CDCl₃/MeOD-*d*₄ 2:1) and ¹³C-NMR (151 MHz, CDCl₃/MeOD-*d*₄ 2:1) data, see Table S3, Figure S21–S23; UHRMS (ESI-TOF) *m/z* [M + H]⁺ calcd for C₂₁H₄₂NO₇P⁺ 452.2772, found 452.2769.

1-Isopentadecanoyl-2-hydroxy-*sn*-glycerol-3-phosphoethanolamine (**13**). Colorless solid; LC-UV (CH₃CN/H₂O) λ_{\max} 224 nm; ¹H (600 MHz, CDCl₃/MeOD-*d*₄ 2:1) and ¹³C-NMR (151 MHz, CDCl₃/MeOD-*d*₄ 2:1) data, see Table S3, Figure S24–S29; UHRMS (ESI-TOF) *m/z* [M + H]⁺ calcd for C₂₀H₄₂NO₇P⁺ 440.2772, found 440.2767.

N-(5-Methyl)hexanoyl tyrosine (**14**). Yellowish solid; LC-UV (CH₃CN/H₂O) λ_{\max} 224, 277 nm; ¹H and ¹³C-NMR data, see Table 2, Figure S30–S34; UHRMS (ESI-TOF) *m/z* [M + H]⁺ calcd for C₁₆H₂₃NO₄⁺ 294.1700, found 294.1698.

N-(7-Methyl)octanoyl tyrosine (**15**). Yellowish solid; LC-UV (CH₃CN/H₂O) λ_{\max} 225, 277 nm; ¹H and ¹³C-NMR data, see Table 2, Figure S35–S39; UHRMS (ESI-TOF) *m/z* [M + H]⁺ calcd for C₁₈H₂₇NO₄⁺ 322.2013, found 322.2009.

N-(7-Methyl)octanoyl phenylalanine (**16**). Off-white solid; LC-UV (CH₃CN/H₂O) λ_{\max} 217 nm; ¹H and ¹³C-NMR data, see Table 2, Figure S40–S44; UHRMS (ESI-TOF) *m/z* [M + H]⁺ calcd for C₁₈H₂₇NO₃⁺ 306.2064, found 306.2062.

NMR Studies

NMR spectra of LAA **1** were recorded on a Bruker AVANCE III 500 spectrometer (¹H: 500 MHz, ¹³C: 125 MHz) equipped with a 10 mm MNP cryo probe. For all remaining compounds, NMR spectra were acquired on a Bruker AVANCE II/III HD 400 spectrometer (¹H: 400 MHz, ¹³C: 101 MHz) or an AVANCE III HD 600 spectrometer (¹H: 600 MHz, ¹³C: 151 MHz). Chemical shifts (δ) given in parts per million (ppm) are referenced to the residual solvent signals of DMSO-*d*₆ (δ_{H} 2.50 and δ_{C} 39.5), CD₃OD (δ_{H} 3.31 and δ_{C} 49.0), and CDCl₃ (δ_{H} 7.26 and δ_{C} 77.2, in a 2:1 mixture with CD₃OD).

4.4. Optical Rotation

Specific rotation was determined on a digital polarimeter (P3,000, A. Krüss Optronic GmbH). Standard wavelength was the sodium D-line with 589 nm. Temperature, concentration (g/100 mL), and solvents are reported with the determined value.

4.5. Advanced Marfey's Analysis

The absolute configuration of all amino acids was determined by derivatization using Marfey's reagent [50]. Stock solutions of amino acid standards (50 mM in H₂O), NaHCO₃ (1 M in H₂O), and L-FDVA (70 mM in acetone) were prepared. Commercially available standards were derivatized using molar ratios of amino acid to FDVA and NaHCO₃ (1/1.4/8). After stirring at 40 °C for 3 h, 1 M HCl was added to obtain a final concentration of 170 mM to end the reaction. Samples were subsequently evaporated to dryness and dissolved in DMSO (final concentration 50 mM). L- and D-amino acids were analyzed

separately using C18 RP-UHPLC-MS with the standard gradient (for details see Section 4.2) at a flow rate of 0.6 mL/min.

Total hydrolysis of compounds **1**, lipid 430 (**2**), and **14–16** was carried out by dissolving 250 µg of each compound in 6 M deuterio-hydrochloric acid (DCl in D₂O) and stirring for 7 h at 160 °C. The sample was subsequently evaporated to dryness. Samples were dissolved in 100 µL H₂O, derivatized, and analyzed using the same parameters as described before.

4.6. Minimal Inhibitory Concentration (MIC)

Microbroth dilution assays were performed in 96-well plates to determine the minimum inhibitory concentrations (MIC) of purified compounds dissolved in DMSO and were tested in triplicate following EUCAST instructions with minor adaptations [63,64]. A cell concentration of 5×10^5 cells/mL was adjusted for all bacteria from an overnight culture (37 °C, 180 rpm) in cation-adjusted Mueller–Hinton II medium (BD). All tested organisms are summarized in Table 3. Dilution series of rifampicin, tetracycline, and gentamicin were used as control antibiotics (64–0.03 µg/mL) to ensure that concentrations achieved a range of effects from none to complete growth inhibition of the test strain. Negative controls were cell suspensions without test sample or antibiotic control. The turbidity was measured with a microplate spectrophotometer at 600 nm (LUMIstar Omega BMG Labtech) to assess cell growth after overnight incubation (18 h, 37 °C, 180 rpm, 85% rH).

Mycobacterium smegmatis ATCC 607 was grown in brain–heart infusion broth supplemented with Tween 80 (1.0% v/v) at 37 °C and 180 rpm for 48 h before the cell density was adjusted in cation-adjusted Mueller–Hinton II medium. The gentamicin control was replaced with isoniazid. Assay read out was done by cell viability assessment after 48 h (37 °C, 180 rpm, 85% rH) by ATP quantification (BacTiter-Glo, Promega), according to the manufacturer’s instructions.

Candida albicans FH2173 was incubated at 28 °C for 48 h before diluting to 1×10^6 cells/mL in cation-adjusted Mueller–Hinton II medium. Assays were incubated at 37 °C for 48 h with nystatin as positive control and were evaluated by ATP quantification (BacTiter-Glo, Promega).

Pre- and main cultures of *Micrococcus luteus* DSM 20030 and *Listeria monocytogenes* DSM 20600 were incubated for two days, and the assay readout was done by ATP quantification, as described before.

Supplementary Materials: The following are available online, Figure S1: L-FDVA adducts of serine, Figure S2: L-FDVA adducts of ornithine, Figure S3: MS/MS spectra of NAAAs **14–16** (A–C) including postulated MS/MS fragmentation pathway, Figure S4: Double L-FDVA adducts of tyrosine, Figure S5: Integrated UV signals corresponding to double L-FDVA adducts of tyrosine for hydrolyzed NAAA **14** (top) and hydrolyzed NAAA **15** (bottom), Figure S6: L-FDVA adducts of phenylalanine, Figure S7: ¹H-NMR (500 MHz, DMSO-*d*₆) of lipid **1**, Figure S8: ¹H-¹H COSY (500 MHz, DMSO-*d*₆) spectrum of lipid **1**, Figure S9: ¹H-¹³C HSQC (500 MHz, DMSO-*d*₆) spectrum of lipid **1**, Figure S10: ¹H-¹³C HMBC (500 MHz, DMSO-*d*₆) spectrum of lipid **1**, Figure S11: ¹H-NMR (600 MHz, DMSO-*d*₆) of lipid **3**, Figure S12: ¹H-¹H COSY (600 MHz, DMSO-*d*₆) spectrum of lipid **3**, Figure S13: ¹H-¹³C HSQC (600 MHz, DMSO-*d*₆) spectrum of lipid **3**, Figure S14: ¹H-¹³C HMBC (600 MHz, DMSO-*d*₆) spectrum of lipid **3**, Figure S15: ¹³C-NMR (151 MHz, DMSO-*d*₆) of lipid **3**, Figure S16: ¹H-NMR (600 MHz, DMSO-*d*₆) of lipid **4**, Figure S17: ¹H-¹H COSY (600 MHz, DMSO-*d*₆) spectrum of lipid **4**, Figure S18: ¹H-¹³C HSQC (600 MHz, DMSO-*d*₆) spectrum of lipid **4**, Figure S19: ¹H-¹³C HMBC (600 MHz, DMSO-*d*₆) spectrum of lipid **4**, Figure S20: ¹³C-NMR (151 MHz, DMSO-*d*₆) of lipid **4**, Figure S21: ¹H-NMR (600 MHz, CDCl₃/MeOD-*d*₄ 2:1) of LPE 451 (**12**), Figure S22: ¹³C-NMR (151 MHz, CDCl₃/MeOD-*d*₄ 2:1) of LPE 451 (**12**), Figure S23: ³¹P-NMR (243 MHz, CDCl₃/MeOD-*d*₄ 2:1) of LPE 451 (**12**), Figure S24: ¹H-NMR (600 MHz, CDCl₃/MeOD-*d*₄ 2:1) of LPE **13**, Figure S25: ¹H-¹H COSY (600 MHz, CDCl₃/MeOD-*d*₄ 2:1) of LPE **13**, Figure S26: ¹H-¹³C HSQC (600 MHz, CDCl₃/MeOD-*d*₄ 2:1) of LPE **13**, Figure S27: ¹H-¹³C HMBC (600 MHz, CDCl₃/MeOD-*d*₄ 2:1) of LPE **13**, Figure S28: ¹³C-NMR (151 MHz, CDCl₃/MeOD-*d*₄ 2:1) of LPE **13**, Figure S29: ³¹P-NMR (243 MHz, CDCl₃/MeOD-*d*₄ 2:1) of LPE **13**, Figure S30: ¹H-NMR (400 MHz, MeOD-*d*₄) of NAAA **14**, Figure S31: ¹H-¹H COSY (400 MHz, MeOD-*d*₄) of NAAA **14**, Figure S32: ¹H-¹³C HSQC (400 MHz, MeOD-*d*₄) of NAAA **14**, Figure S33: ¹H-¹³C HMBC (400 MHz, MeOD-*d*₄) of NAAA **14**, Figure S34:

¹³C-NMR (101 MHz, MeOD-*d*₄) of NAAA 14, Figure S35: ¹H-NMR (400 MHz, MeOD-*d*₄) of NAAA 15, Figure S36: ¹H-¹H COSY (400 MHz, MeOD-*d*₄) of NAAA 15, Figure S37: ¹H-¹³C HSQC (400 MHz, MeOD-*d*₄) of NAAA 15, Figure S38: ¹H-¹³C HMBC (400 MHz, MeOD-*d*₄) of NAAA 15, Figure S39: ¹³C-NMR (101 MHz, MeOD-*d*₄) of NAAA 15, Figure S40: ¹H-NMR (400 MHz, MeOD-*d*₄) of NAAA 16, Figure S41: ¹H-¹H COSY (400 MHz, MeOD-*d*₄) of NAAA 16, Figure S42: ¹H-¹³C HSQC (400 MHz, MeOD-*d*₄) of NAAA 16, Figure S43: ¹H-¹³C HMBC (400 MHz, MeOD-*d*₄) of NAAA 16, Figure S44: ¹³C-NMR (101 MHz, MeOD-*d*₄) of NAAA 16, Table S1: Overview of all lipids with their molecular formula, predicted and found masses within the metabolomics data of our previous study, and in how many of the investigated 25 *Chitinophaga* metabolomes each lipid is present, Table S2: ¹H and ¹³C data of compound 4 (¹H: 600 MHz, ¹³C: 151 MHz, DMSO-*d*₆), Table S3: ¹H and ¹³C data of compounds 12 and 13 (¹H: 600 MHz, ¹³C: 151 MHz, CDCl₃/MeOD-*d*₄ 2:1).

Author Contributions: Conceptualization, M.-K.B., S.B., P.E.H., S.M.M.S. and T.F.S.; investigation, M.-K.B., S.B., M.O., M.A.P., B.L., M.M. and M.-P.M.; data curation, M.-K.B. and S.B.; writing—original draft preparation, M.-K.B. and S.B.; writing—review and editing, all authors; visualization, M.-K.B. and S.B.; supervision, S.M.M.S. and T.F.S.; project administration, P.E.H.; funding acquisition, P.E.H. and A.V. All authors have read and agreed to the published version of the manuscript.

Funding: This work was financially supported by the Hessen State Ministry of Higher Education, Research and the Arts (HMWK) via the state initiative for the development of scientific and economic excellence for the LOEWE Center for Insect Biotechnology and Bioresources. Sanofi-Aventis Deutschland GmbH and Evotec International GmbH contributed to the framework of the Sanofi-Fraunhofer Natural Products Center of Excellence/Fraunhofer-Evotec Natural Products Center of Excellence.

Institutional Review Board Statement: Not applicable.

Informed Consent Statement: Not applicable.

Data Availability Statement: The 16S rRNA gene sequence of *Olivibacter* sp. FHG000416 is available at reference number MZ073637 (GenBank).

Acknowledgments: The authors thank Luigi Toti, Marius Spohn, Sanja Mihajlovic, Jennifer Kuhn, and Christine Wehr for assistance in fermentation, Mona Abdullahi for assisting the isolation, Christoph Hartwig for technical support, as well as Kirsten-Susann Bommersheim for determination of MICs. We thank Jens Glaeser and Heike Hausmann for valuable discussions and the NMR department of the Justus-Liebig-University Giessen for technical assistance.

Conflicts of Interest: S.M.M.S. and P.E.H. are or have been employed by Evotec International GmbH and Sanofi-Aventis Deutschland GmbH, respectively.

Sample Availability: Samples of the compounds are not available from the authors.

References

- Harayama, T.; Riezman, H. Understanding the diversity of membrane lipid composition. *Nat. Rev. Mol. Cell Biol.* **2018**, *19*, 281–296. [[CrossRef](#)]
- Sohlenkamp, C.; Geiger, O. Bacterial membrane lipids: Diversity in structures and pathways. *FEMS Microbiol. Rev.* **2016**, *40*, 133–159. [[CrossRef](#)]
- Snijder, H.J.; Dijkstra, B.W. Bacterial phospholipase A: Structure and function of an integral membrane phospholipase. *Biochim. Biophys. Acta (BBA) Mol. Cell Biol. Lipids* **2000**, *1488*, 91–101. [[CrossRef](#)]
- Asselineau, J. Bacterial Lipids Containing Amino Acids or Peptides Linked by Amide Bonds. In *Fortschritte der Chemie Organischer Naturstoffe/Progress in the Chemistry of Organic Natural Products*; Asselineau, J., Kagan, J., Eds.; Springer: Vienna, Austria, 1991; pp. 1–85. ISBN 978-3-7091-9084-5.
- Batrakov, S.G.; Nikitin, D.I.; Mosezhnyi, A.E.; Ruzhitsky, A.O. A glycine-containing phosphorus-free lipoaminoacid from the gram-negative marine bacterium *Cyclobacterium marinus* WH. *Chem. Phys. Lipids* **1999**, *99*, 139–143. [[CrossRef](#)]
- Yoshida, K.; Iwami, M.; Umehara, Y.; Nishikawa, M.; Uchida, I.; Kohsaka, M.; Aoki, H.; Imanaka, H. Studies on WB-3559 A, B, C and D, new potent fibrinolytic agents. I. Discovery, identification, isolation and characterization. *J. Antibiot.* **1985**, *38*, 1469–1475. [[CrossRef](#)]
- Uchida, I.; Yoshida, K.; Kawai, Y.; Takase, S.; Itoh, Y.; Tanaka, H.; Kohsaka, M.; Imanaka, H. Studies on WB-3559 A, B, C and D, new potent fibrinolytic agents. II. Structure elucidation and synthesis. *J. Antibiot.* **1985**, *38*, 1476–1486. [[CrossRef](#)]
- Tahara, Y.; Kameda, M.; Yamada, Y.; Kondo, K. A new lipid the ornithine and taurine-containing “Cerilipin”. *Agric. Biol. Chem.* **1976**, *40*, 243–244. [[CrossRef](#)]

9. Kawai, Y.; Yano, I.; Kaneda, K. Various kinds of lipoamino acids including a novel serine-containing lipid in an opportunistic pathogen *Flavobacterium*. Their structures and biological activities on erythrocytes. *Eur. J. Biochem.* **1988**, *171*, 73–80. [[CrossRef](#)] [[PubMed](#)]
10. Kawai, Y.; Akagawa, K. Macrophage activation by an ornithine-containing lipid or a serine-containing lipid. *Infect. Immun.* **1989**, *57*, 2086–2091. [[CrossRef](#)] [[PubMed](#)]
11. Kawazoe, R.; Okuyama, H.; Reichardt, W.; Sasaki, S. Phospholipids and a novel glycine-containing lipoamino acid in *Cytophaga johnsonae* Stanier strain C21. *J. Bacteriol.* **1991**, *173*, 5470–5475. [[CrossRef](#)] [[PubMed](#)]
12. Morishita, T.; Sato, A.; Hisamoto, M.; Oda, T.; Matsuda, K.; Ishii, A.; Kodama, K. N-type calcium channel blockers from a marine bacterium, *Cytophaga* sp. SANK 71996. *J. Antibiot.* **1997**, *50*, 457–468. [[CrossRef](#)]
13. Chianese, G.; Esposito, F.P.; Parrot, D.; Ingham, C.; de Pascale, D.; Tasdemir, D. Linear Aminolipids with Moderate Antimicrobial Activity from the Antarctic Gram-Negative Bacterium *Aequorivita* sp. *Mar. Drugs* **2018**, *16*, 187. [[CrossRef](#)]
14. Gomi, K.; Kawasaki, K.; Kawai, Y.; Shiozaki, M.; Nishijima, M. Toll-like receptor 4-MD-2 complex mediates the signal transduction induced by flavolipin, an amino acid-containing lipid unique to *Flavobacterium meningosepticum*. *J. Immunol.* **2002**, *168*, 2939–2943. [[CrossRef](#)] [[PubMed](#)]
15. Tan, B.; O'Dell, D.K.; Yu, Y.W.; Monn, M.F.; Hughes, H.V.; Burstein, S.; Walker, J.M. Identification of endogenous acyl amino acids based on a targeted lipidomics approach. *J. Lipid Res.* **2010**, *51*, 112–119. [[CrossRef](#)] [[PubMed](#)]
16. Brady, S.F.; Clardy, J. Long-Chain N-Acyl Amino Acid Antibiotics Isolated from Heterologously Expressed Environmental DNA. *J. Am. Chem. Soc.* **2000**, *122*, 12903–12904. [[CrossRef](#)]
17. Brady, S.F.; Chao, C.J.; Clardy, J. New natural product families from an environmental DNA (eDNA) gene cluster. *J. Am. Chem. Soc.* **2002**, *124*, 9968–9969. [[CrossRef](#)] [[PubMed](#)]
18. Brady, S.F.; Clardy, J. Palmitoylputrescine, an antibiotic isolated from the heterologous expression of DNA extracted from bromeliad tank water. *J. Nat. Prod.* **2004**, *67*, 1283–1286. [[CrossRef](#)]
19. Brady, S.F.; Clardy, J. N-acyl derivatives of arginine and tryptophan isolated from environmental DNA expressed in *Escherichia coli*. *Org. Lett.* **2005**, *7*, 3613–3616. [[CrossRef](#)]
20. Clardy, J.; Brady, S.F. Cyclic AMP directly activates NasP, an N-acyl amino acid antibiotic biosynthetic enzyme cloned from an uncultured beta-proteobacterium. *J. Bacteriol.* **2007**, *189*, 6487–6489. [[CrossRef](#)] [[PubMed](#)]
21. Phoon, C.W.; Somanadhan, B.; Heng, S.C.H.; Ngo, A.; Ng, S.B.; Butler, M.S.; Buss, A.D.; Sim, M.M. Isolation and total synthesis of gymnastatin N, a POLO-like kinase 1 active constituent from the fungus *Arachniotus punctatus*. *Tetrahedron* **2004**, *60*, 11619–11628. [[CrossRef](#)]
22. Touré, S.; Desrat, S.; Pellissier, L.; Allard, P.M.; Wolfender, J.L.; Dusfour, I.; Stien, D.; Eparvier, V. Characterization, Diversity, and Structure–Activity Relationship Study of Lipoamino Acids from *Pantoea* sp. and Synthetic Analogues. *Int. J. Mol. Sci.* **2019**, *20*, 1083. [[CrossRef](#)]
23. Vitale, G.A.; Sciarretta, M.; Cassiano, C.; Buonocore, C.; Festa, C.; Mazzella, V.; Núñez Pons, L.; D'Auria, M.V.; de Pascale, D. Molecular Network and Culture Media Variation Reveal a Complex Metabolic Profile in *Pantoea* cf. *eucrina* D2 Associated with an Acidified Marine Sponge. *Int. J. Mol. Sci.* **2020**, *21*, 6307. [[CrossRef](#)] [[PubMed](#)]
24. Teng, O.; Ang, C.K.E.; Guan, X.L. Macrophage-Bacteria Interactions-A Lipid-Centric Relationship. *Front. Immunol.* **2017**, *8*, 1836. [[CrossRef](#)] [[PubMed](#)]
25. Farrokhi, V.; Nemati, R.; Nichols, F.C.; Yao, X.; Anstadt, E.; Fujiwara, M.; Grady, J.; Wakefield, D.; Castro, W.; Donaldson, J.; et al. Bacterial lipopeptide, Lipid 654, is a microbiome-associated biomarker for multiple sclerosis. *Clin. Transl. Immunol.* **2013**, *2*, e8. [[CrossRef](#)]
26. Yoon, B.K.; Jackman, J.A.; Valle-González, E.R.; Cho, N.J. Antibacterial Free Fatty Acids and Monoglycerides: Biological Activities, Experimental Testing, and Therapeutic Applications. *Int. J. Mol. Sci.* **2018**, *19*, 1114. [[CrossRef](#)]
27. Alves, E.; Dias, M.; Lopes, D.; Almeida, A.; Domingues, M.D.R.; Rey, F. Antimicrobial Lipids from Plants and Marine Organisms: An Overview of the Current State-of-the-Art and Future Prospects. *Antibiotics* **2020**, *9*, 441. [[CrossRef](#)]
28. Shiozaki, M.; Deguchi, N.; Mochizuki, T.; Wakabayashi, T.; Ishikawa, T.; Haruyama, H.; Kawai, Y.; Nishijima, M. Revised structure and synthesis of flavolipin. *Tetrahedron* **1998**, *54*, 11861–11876. [[CrossRef](#)]
29. Nemoto, T.; Ojika, M.; Takahata, Y.; Andoh, T.; Sakagami, Y. Structures of topostins, DNA topoisomerase I inhibitors of bacterial origin. *Tetrahedron* **1998**, *54*, 2683–2690. [[CrossRef](#)]
30. Olsen, I.; Nichols, F.C. Are Sphingolipids and Serine Dipeptide Lipids Underestimated Virulence Factors of *Porphyromonas gingivalis*? *Infect. Immun.* **2018**, *86*, e00035–18. [[CrossRef](#)] [[PubMed](#)]
31. Mirucki, C.S.; Abedi, M.; Jiang, J.; Zhu, Q.; Wang, Y.-H.; Safavi, K.E.; Clark, R.B.; Nichols, F.C. Biologic Activity of *Porphyromonas endodontalis* complex lipids. *J. Endod.* **2014**, *40*, 1342–1348. [[CrossRef](#)] [[PubMed](#)]
32. Wang, Y.-H.; Nemati, R.; Anstadt, E.; Liu, Y.; Son, Y.; Zhu, Q.; Yao, X.; Clark, R.B.; Rowe, D.W.; Nichols, F.C. Serine dipeptide lipids of *Porphyromonas gingivalis* inhibit osteoblast differentiation: Relationship to Toll-like receptor 2. *Bone* **2015**, *81*, 654–661. [[CrossRef](#)]
33. Nichols, F.C.; Housley, W.J.; O'Connor, C.A.; Manning, T.; Wu, S.; Clark, R.B. Unique lipids from a common human bacterium represent a new class of Toll-like receptor 2 ligands capable of enhancing autoimmunity. *Am. J. Pathol.* **2009**, *175*, 2430–2438. [[CrossRef](#)] [[PubMed](#)]

34. Clark, R.B.; Cervantes, J.L.; Maciejewski, M.W.; Farrokhi, V.; Nemati, R.; Yao, X.; Anstadt, E.; Fujiwara, M.; Wright, K.T.; Riddle, C.; et al. Serine lipids of *Porphyromonas gingivalis* are human and mouse Toll-like receptor 2 ligands. *Infect. Immun.* **2013**, *81*, 3479–3489. [[CrossRef](#)]
35. Schneider, Y.K.-H.; Hansen, K.Ø.; Isaksson, J.; Ullsten, S.; H Hansen, E.; Hammer Andersen, J. Anti-Bacterial Effect and Cytotoxicity Assessment of Lipid 430 Isolated from *Aligibacter* sp. *Molecules* **2019**, *24*, 3991. [[CrossRef](#)]
36. Nemati, R.; Dietz, C.; Anstadt, E.J.; Cervantes, J.; Liu, Y.; Dewhirst, F.E.; Clark, R.B.; Finegold, S.; Gallagher, J.J.; Smith, M.B.; et al. Deposition and hydrolysis of serine dipeptide lipids of Bacteroidetes bacteria in human arteries: Relationship to atherosclerosis. *J. Lipid Res.* **2017**, *58*, 1999–2007. [[CrossRef](#)]
37. Blanksby, S.J.; Mitchell, T.W. Advances in mass spectrometry for lipidomics. *Annu. Rev. Anal. Chem.* **2010**, *3*, 433–465. [[CrossRef](#)]
38. Hancock, S.E.; Poad, B.L.J.; Batarseh, A.; Abbott, S.K.; Mitchell, T.W. Advances and unresolved challenges in the structural characterization of isomeric lipids. *Anal. Biochem.* **2017**, *524*, 45–55. [[CrossRef](#)] [[PubMed](#)]
39. Cajka, T.; Fiehn, O. Comprehensive analysis of lipids in biological systems by liquid chromatography-mass spectrometry. *Trends Analyt. Chem.* **2014**, *61*, 192–206. [[CrossRef](#)] [[PubMed](#)]
40. Swieżewska, E.; Wójcik, J. NMR of carbohydrates, lipids and membranes. In *Nuclear Magnetic Resonance: A Review of the Literature Published between January 2009 and May 2010*; Kamińska-Trela, K., Aliev, A.E., Eds.; RSC Publications: Cambridge, UK, 2011; pp. 344–390. ISBN 978-1-84973-147-8.
41. Swieżewska, E.; Wójcik, J. NMR of lipids and membranes. In *Nuclear Magnetic Resonance*; Kamińska-Trela, K., Wojcik, J., Eds.; Royal Society of Chemistry: Cambridge, UK, 2012; pp. 320–347; ISBN 978-1-84973-373-1.
42. Pikula, S.; Bandorowicz-Pikula, J.; Groves, P. NMR of lipids. In *Nuclear Magnetic Resonance*; Wójcik, J., Kamińska-Trela, K., Eds.; The Royal Society of Chemistry: Cambridge, UK, 2013; pp. 362–382; ISBN 978-1-84973-577-3.
43. Pikula, S.; Bandorowicz-Pikula, J.; Groves, P. NMR of lipids. In *Nuclear Magnetic Resonance*; Kamińska-Trela, K., Aliev, A.E., Bandorowicz-Pikula, J., Buda, S., D’Errico, G., de Dios, A.C., Eds.; Royal Society of Chemistry: Cambridge, UK, 2015; pp. 385–406; ISBN 978-1-78262-052-5.
44. Pikula, S.; Bandorowicz-Pikula, J.; Groves, P. Recent Advances in NMR Studies of Lipids. In *Annual Reports on NMR Spectroscopy*; Webb, G.A., Ed.; Elsevier Science: Burlington, NJ, USA, 2015; pp. 195–246; ISBN 9780128030905.
45. Alexandri, E.; Ahmed, R.; Siddiqui, H.; Choudhary, M.I.; Tsiafoulis, C.G.; Gerothanassis, I.P. High Resolution NMR Spectroscopy as a Structural and Analytical Tool for Unsaturated Lipids in Solution. *Molecules* **2017**, *22*, 1663. [[CrossRef](#)] [[PubMed](#)]
46. Brinkmann, S.; Kurz, M.; Patras, M.A.; Hartwig, C.; Marner, M.; Leis, B.; Billion, A.; Kleiner, Y.; Bauer, A.; Toti, L.; et al. Genomic and chemical decryption of the Bacteroidetes phylum for its potential to biosynthesize natural products. *BioRxiv* **2021**. [[CrossRef](#)]
47. Yasir, M.; Chung, E.J.; Song, G.C.; Bibi, F.; Jeon, C.O.; Chung, Y.R. *Chitinophaga eiseniae* sp. nov., isolated from vermicompost. *Int. J. Syst. Evol. Microbiol.* **2011**, *61*, 2373–2378. [[CrossRef](#)]
48. Vaz-Moreira, I.; Nobre, M.F.; Nunes, O.C.; Manaia, C.M. *Pseudosphingobacterium domesticum* gen. nov., sp. nov., isolated from home-made compost. *Int. J. Syst. Evol. Microbiol.* **2007**, *57*, 1535–1538. [[CrossRef](#)]
49. Siddiqi, M.Z.; Liu, Q.; Lee, S.Y.; Choi, K.D.; Im, W.-T. *Olivibacter ginsenosidimitans* sp nov., with ginsenoside converting activity isolated from compost, and reclassification of *Pseudosphingobacterium domesticum* as *Olivibacter domesticus* comb. nov. *Int. J. Syst. Evol. Microbiol.* **2018**, *68*, 2509–2514. [[CrossRef](#)] [[PubMed](#)]
50. Bhushan, R.; Brückner, H. Marfey’s reagent for chiral amino acid analysis: A review. *Amino Acids* **2004**, *27*, 231–247. [[CrossRef](#)] [[PubMed](#)]
51. Woznica, A.; Cantley, A.M.; Beemelmans, C.; Freinkman, E.; Clardy, J.; King, N. Bacterial lipids activate, synergize, and inhibit a developmental switch in choanoflagellates. *Proc. Natl. Acad. Sci. USA* **2016**, *113*, 7894–7899. [[CrossRef](#)]
52. Kayganich, K.A.; Murphy, R.C. Fast atom bombardment tandem mass spectrometric identification of diacyl, alkylacyl, and alk-1-enylacyl molecular species of glycerophosphoethanolamine in human polymorphonuclear leukocytes. *Anal. Chem.* **1992**, *64*, 2965–2971. [[CrossRef](#)] [[PubMed](#)]
53. Murphy, R.C.; Harrison, K.A. Fast atom bombardment mass spectrometry of phospholipids. *Mass Spectrom. Rev.* **1994**, *13*, 57–75. [[CrossRef](#)]
54. Bérdy, J. Bioactive microbial metabolites. *J. Antibiot.* **2005**, *58*, 1–26. [[CrossRef](#)]
55. Makovitzki, A.; Avrahami, D.; Shai, Y. Ultrashort antibacterial and antifungal lipopeptides. *Proc. Natl. Acad. Sci. USA* **2006**, *103*, 15997–16002. [[CrossRef](#)]
56. Shai, Y. Mode of action of membrane active antimicrobial peptides. *Biopolymers* **2002**, *66*, 236–248. [[CrossRef](#)]
57. Gotoh, N.; Tanaka, S.; Nishino, T. Supersusceptibility to hydrophobic antimicrobial agents and cell surface hydrophobicity in *Branhamella catarrhalis*. *FEMS Microbiol. Lett.* **1989**, *59*, 211–213. [[CrossRef](#)]
58. Fomsgaard, J.S.; Fomsgaard, A.; Høiby, N.; Bruun, B.; Galanos, C. Comparative immunochemistry of lipopolysaccharides from *Branhamella catarrhalis* strains. *Infect. Immun.* **1991**, *59*, 3346–3349. [[CrossRef](#)] [[PubMed](#)]
59. Tsujimoto, H.; Gotoh, N.; Nishino, T. Diffusion of macrolide antibiotics through the outer membrane of *Moraxella catarrhalis*. *J. Infect. Chemother.* **1999**, *5*, 196–200. [[CrossRef](#)]
60. Oberpaul, M.; Zumkeller, C.M.; Culver, T.; Spohn, M.; Mihajlovic, S.; Leis, B.; Glaeser, S.P.; Plarre, R.; McMahon, D.P.; Hammann, P.; et al. High-Throughput Cultivation for the Selective Isolation of Acidobacteria From Termite Nests. *Front. Microbiol.* **2020**, *11*, 597628. [[CrossRef](#)]

61. Kämpfer, P.; Dott, W.; Martin, K.; Glaeser, S.P. *Rhodococcus defluvii* sp. nov., isolated from wastewater of a bioreactor and formal proposal to reclassify *Corynebacterium hoagii* and *Rhodococcus equi* as *Rhodococcus hoagii* comb. nov. *Int. J. Syst. Evol. Microbiol.* **2014**, *64*, 755–761. [[CrossRef](#)]
62. Matyash, V.; Liebisch, G.; Kurzchalia, T.V.; Shevchenko, A.; Schwudke, D. Lipid extraction by methyl-tert-butyl ether for high-throughput lipidomics. *J. Lipid Res.* **2008**, *49*, 1137–1146. [[CrossRef](#)]
63. Determination of minimum inhibitory concentrations (MICs) of antibacterial agents by broth dilution. *Clin. Microbiol. Infect.* **2003**, *9*, ix. [[CrossRef](#)]
64. Arendrup, M.C.; Guinea, J.; Cuenca-Estrella, M.; Meletiadis, J.; Mouton, J.W.; Lagrou, K.; Howard, S.J.; The Subcommittee on Antifungal Susceptibility Testing (AFST) of the ESCMID European Committee for Antimicrobial Susceptibility Testing (EUCAST). Eucast definitive document EDef 7.1: Method for the determination of broth dilution MICs of antifungal agents for fermentative yeasts. *Clin. Microbiol. Infect.* **2008**, *14*, 398–405. [[CrossRef](#)]

**MANUSCRIPT 4: TRICHODERMA-DERIVED
PENTAPEPTIDES FROM THE INFECTED
NEST MYCOBIOME OF THE
SUBTERRANEAN TERMITE
COPTOTERMES TESTACEUS**

Status: First published on 17/03/2022 (online ahead of print)

Author's contributions: Study design, method validation, contribution to all experiments, data analysis, manuscript writing, figure design.

Trichoderma-Derived Pentapeptides from the Infected Nest Mycobiome of the Subterranean Termite *Coptotermes testaceus*

Markus Oberpaul,^[a] Stephan Brinkmann,^[a] Marius S. Spohn,^[a] Sanja Mihajlovic,^[a] Michael Marner,^[a] Maria A. Patras,^[a] Luigi Toti,^[b] Michael Kurz,^[b] Peter E. Hammann,^[b, d] Andreas Vilcinskas,^[a, c] Jens Glaeser,^{*[a, d]} and Till F. Schäberle^{*[a, c, e]}

Termites live in a dynamic environment where colony health is strongly influenced by surrounding microbes. However, little is known about the mycobiomes of lower termites and their nests, and how these change in response to disease. Here we compared the individual and nest mycobiomes of a healthy subterranean termite colony (*Coptotermes testaceus*) to one infected and ultimately eradicated by a fungal pathogen. We identified *Trichoderma* species in the materials of both nests, but they were also abundant in the infected termites. Meth-

anolic extracts of *Trichoderma* sp. FHG000531, isolated from the infected nest, were screened for secondary metabolites by UHPLC-HR MS/MS-guided molecular networking. We identified many bioactive compounds with potential roles in the eradication of the infected colony, as well as a cluster of six unknown peptides. The novel peptide FE011 was isolated and characterized by NMR spectroscopy. The function of this novel peptide family as well as the role of *Trichoderma* species in dying termite colonies therefore requires further investigation.

Introduction

Termites share a dynamic environment with many species of bacteria and fungi whose roles are not well understood. The mycobiomes of captive and free-living subterranean termites and their nest compartments have therefore been investigated to identify the dominant taxa.^[1–5] The genera *Debaryomyces*, *Candida*, *Exophiala*, GS23 (Umbelopsidomycetes), *Scytalidium*, *Talaromyces*, *Trichoderma* and *Xylaria* were found to be more

abundant in the nest material than the surrounding environment, and have the potential for both mutualistic and parasitic interactions.^[1–3] Mutualistic yeasts are present in the termite gut, where they facilitate the digestion of wood and support detoxification.^[6] Similarly, fungi present in termite nests, such as *Trichoderma* spp., may be mutualistic under most circumstances, but they may also be opportunists that can later become antagonistic, as shown for *Xylariales* spp.^[2,7–9] *Trichoderma* spp. produce a variety of secondary metabolites that may facilitate their interactions with termites.^[10] For example, they produce peptides such as trichodestruxins,^[11] trichovirins,^[12] trichorzins^[13] and peptaibols^[14] with antibiotic, antifungal and/or insecticidal activities.^[12,15–17] *Xylariales* spp. and *Trichoderma* spp. are ubiquitously distributed in natural environments, especially on rotting wood, but their relative abundance in the termite nest material and gut requires careful analysis.^[2]

Termites may recruit certain bacteria that synthesize natural products to maintain the nest biome and thus support colony fitness.^[4] We previously investigated the bacterial biomes of two captive subterranean termite nests (*Coptotermes testaceus*) over a period of 2 years. One nest was healthy, whereas the other was undergoing a microbiome shift caused by a fungal infection.^[18] Accordingly, we have now used this rare opportunity to also compare the mycobiomes of healthy and infected nests, as well as those of individual termites.

We isolated several fungal species from the infected samples including those representing the genera *Apiotrichum*, *Byssoscleromyces*, *Exophiala*, *Galactomyces*, *Geotrichum*, *Penicillium* and *Trichoderma*. We focused on the secondary metabolites produced by *Trichoderma* spp. and analyzed them by UHPLC-HR MS/MS-guided molecular networking. Following automatic clustering of parent ions and subsequent manual data curation, a cluster containing unknown peptides was selected for

[a] M. Oberpaul, S. Brinkmann, Dr. M. S. Spohn, Dr. S. Mihajlovic, Dr. M. Marner, Dr. M. A. Patras, Prof. Dr. A. Vilcinskas, Dr. J. Glaeser, Prof. Dr. T. F. Schäberle
Branch for Bioresources
Fraunhofer Institute for Molecular Biology and Applied Ecology (IME)
Ohlebergsweg 12, 35392 Gießen (Germany)
E-mail: till.f.schaeberle@ime.fraunhofer.de

[b] Dr. L. Toti, Dr. M. Kurz, Prof. Dr. P. E. Hammann
Sanofi-Aventis Deutschland GmbH
Industriepark Höchst, 65926 Frankfurt am Main (Germany)

[c] Prof. Dr. A. Vilcinskas, Prof. Dr. T. F. Schäberle
Institute for Insect Biotechnology
Justus-Liebig-University Giessen
Heinrich-Buff-Ring 26–32, 35392 Giessen (Germany)

[d] Prof. Dr. P. E. Hammann, Dr. J. Glaeser
Evotec International GmbH
Marie-Curie-Straße 7, 37079 Göttingen (Germany)
E-mail: jens.glaeser@evotec.com

[e] Prof. Dr. T. F. Schäberle
Partner Site Giessen-Marburg-Langen
German Center for Infection Research (DZIF)
35392 Giessen (Germany)

Supporting information for this article is available on the WWW under <https://doi.org/10.1002/cbic.202100698>

© 2022 The Authors. ChemBioChem published by Wiley-VCH GmbH. This is an open access article under the terms of the Creative Commons Attribution Non-Commercial License, which permits use, distribution and reproduction in any medium, provided the original work is properly cited and is not used for commercial purposes.

detailed analysis. The most abundant derivative was isolated and structurally elucidated by NMR and MS/MS, and the structure of additional five derivatives was also tentatively proposed on the basis of their MS/MS fragmentation patterns.

Results and Discussion

The mycobiome differs between healthy and infected termite nests

A healthy and functional termite colony may require homeostasis of the bacterial and fungal biomes,^[19] although it is unclear why the nest mycobiome differs from the surrounding environment.^[2] The captive termite nests herein were reared for decades. We observed a fungal infection, which might have been introduced during the feeding routine of the colonies. It was speculated that the nest may have disrupted the microbiome balance. We therefore compared the infected colony to a healthy one to characterize the mycobiome. Hence, we recovered triplicate samples of material from various nest levels as well as termites from the healthy and infected colonies and characterized them by Illumina amplicon sequencing. We obtained 1,013,693 reads representing 446 operational taxonomic units (OTUs) and 146 phylogenetic groups from 27 samples (12 infected, 12 healthy, 3 fungal mat). Some groups were found in samples of both the healthy and infected environments, namely *Apiotrichum*, *Athrocladium*, *Candida*, *Colletotrichum*, GS23, *Hawksworthiomyces*, *Myrothecium*, *Shiraia*, *Vischniacozyma*, *Xylariales* and 'no hit' (Figure 1A). The genera *Debaryomyces*, *Stictis*, *Termitomyces* and *Wallemia* were solely connected to a healthy nest environment (Figure 1B). In contrast, the genera *Colacogloea*, *Exophiala*, *Malbranchea*, *Paecilomyces*, *Sugiyamaella*, *Scytalidium*, *Talaromyces* and *Trichoderma* were predominantly abundant in the infected nest material or termites.

The genera *Apiotrichum*, *Colletotrichum* and GS23 were highly abundant in healthy termite samples but absent in the termites suffering fungal infection (Figure 1B). *Paecilomyces*, *Sugiyamaella*, *Yamadazyma* and *Trichoderma* were prominently abundant in the infected termites and the material overgrown by fungus (Figure 1, S1). Similarity percentages breakdown (SIMPER) analysis was used to calculate the greatest statistical influence in the dataset.^[20] Although, this does not prove the contribution of particular genera towards termite health, it indicates possible influence factors. The analysis revealed a cumulative contribution of >80% by the phylogenetic groups *Apiotrichum* (20%), *Trichoderma* (11%), *Stictis* (8%), *Sugiyamaella* (8%), *Colletotrichum* (6%), *Debaryomyces* (6%), GS23 (6%), *Paecilomyces* (6%), *Candida* (4%), *Exophiala* (2%), *Talaromyces* (2%) and *Xylariales* (2%) (Table S1).

We also observed a spreading mycelial mat in the infected nest at a later stage (Figure S1). The abundance of *Xylariales* was low (3%) compared to all other phylogenetic groups, including *Apiotrichum* (26%), *Sugiyamaella* (26%), *Paecilomyces* (17%), GS23 (8%), *Scytalidium* (6%) and *Hawksworthiomyces* (4%) (Table S1; Figure 1A, Fungal mat), suggesting that *Xylar-*

iales alone is not responsible for the biome shift and eradication of the nest. However, representatives of *Xylariales* are often associated with fungus-growing termites^[21] and may act as specialized mutualists or opportunists given their presence in abandoned termite nests.^[2,22,23] They produce many natural products, including insecticides.^[24]

We also identified the genus *Exophiala* in infected termites and their nest (Figure 1A and B). This genus was reported as part of the microenvironment of leaf-cutting ants^[25] and other social insects.^[26] *Exophiala* spp. were found to produce an insecticidal natural product, causing larval mortality as well as deformities in emerging adults of *Spodoptera litura*.^[27]

Furthermore, *Paecilomyces* spp. were abundant in all samples, but particularly in the infected specimens (Figure 1). The entomopathogenic genus *Isaria* (formerly *Paecilomyces*) was reviewed and patented as a biocontrol agent against plant pathogens, nematodes, and insects,^[28] especially to control Formosan subterranean termites.^[29] *Paecilomyces* spp. produce multiple bioactive substances including insecticides and mycotoxins.^[28,30] *Trichoderma* spp. were the most abundant in the infected termite individuals (Figure 1A). *Trichoderma* spp. are abundant in habitats linked to termites that feed on decayed wood, but it is unclear whether they are beneficial or detrimental.^[2,3,8,31] They are ubiquitous saprophytes and endophytes that produce numerous secondary metabolites,^[32] including bioactive peptaibols, alkaloids, polyketides and non-ribosomal peptides (NRPs)^[16,17] with antibacterial, cytotoxic, antifungal, antiviral and anti-inflammatory properties.^[10,33] *Trichoderma virens* and others have been evaluated as biocontrol agents against subterranean termites.^[34] The phytotoxic fungal steroid viridol and the peptaibol trichokonin VI are produced by several *Trichoderma* species.^[10,16,33] Trichokonin VI, a Ca²⁺ channel antagonist,^[36] suppresses plant cell division and proliferation,^[37] whereas viridol kills plant cells and bacteria.^[38]

In summary, these data suggest that *Exophiala*, *Paecilomyces*, *Trichoderma* and *Xylariales* are involved in the changing health of the termite colony. However, the abundance of individual taxa cannot explain the interactions between biomes and their impact on colony health. Thus, we herein focused on the screening of secondary metabolites produced by *Trichoderma* spp. using a molecular networking approach.

Structural analysis of the novel pentapeptide FE011

We used potato dextrose agar (5367) to culture fungi from the infected samples. Propagation and subsequent partial 18S rRNA gene sequencing (only NS1) indicated the presence of axenic cultures belonging to the genera *Apiotrichum*, *Byssoschlamys*, *Exophiala*, *Galactomyces*, *Geotrichum*, *Penicillium* and *Trichoderma*. The complete 18S rRNA sequence (NS1 and FR1) alignment of strain FHG000531 (Figure S1), which was isolated from infected nest material, was 99.9% identical to *Trichoderma longibrachiatum* H9^T, *T. harzianum* Iy-12^T and *T. reesei* Qm6a^T.^[39] To determine the metabolic profile of the new strain, we grew it in five different media for 4 and 7 days. Subsequently, methanolic extracts were prepared for analysis by mass

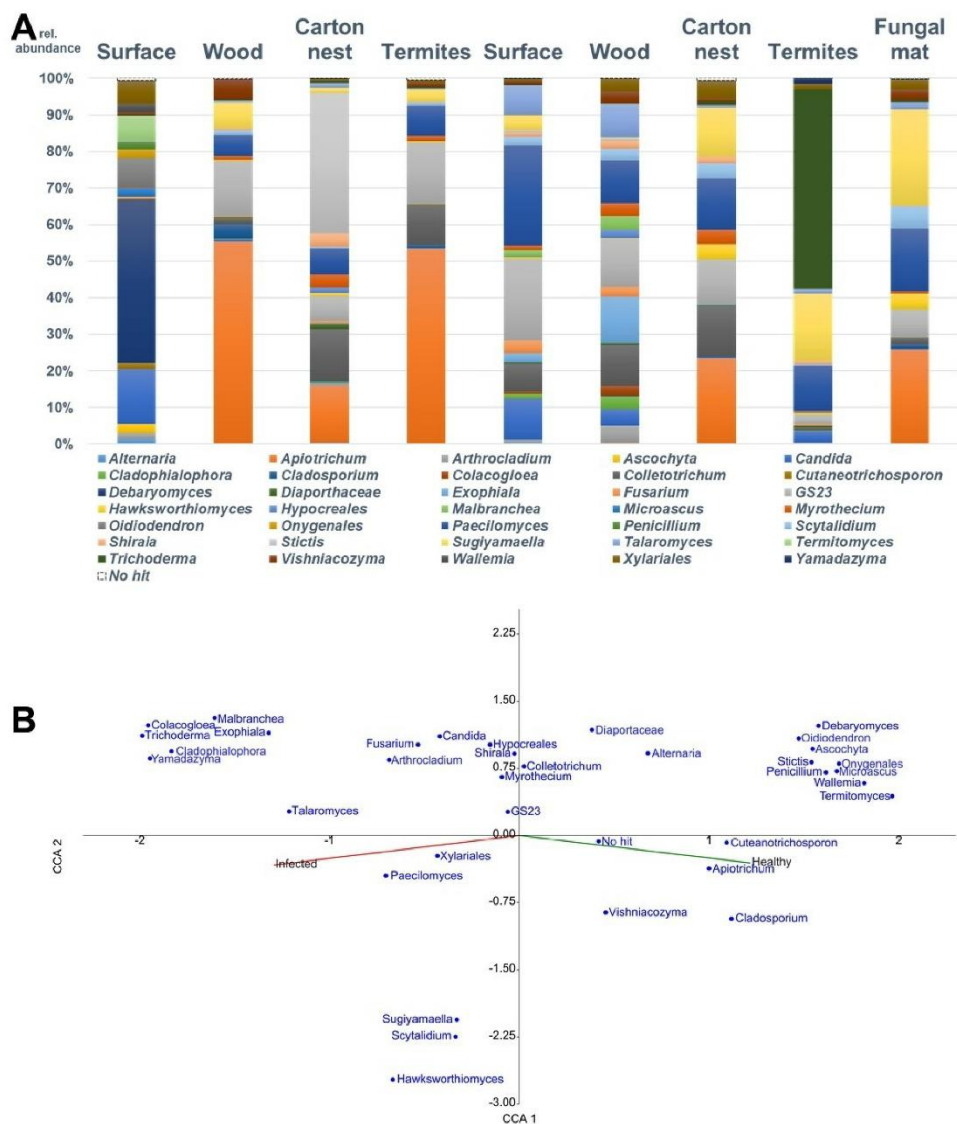


Figure 1. Phylogenetic analysis of *Coptotermes testaceus* termite nests. (A) Comparative abundance of fungal phylogenetic groups at the genus level in healthy and infected captive *C. testaceus* termite nests and specimens, and their correlation with colony health. Three replicates of each sample were used to calculate the mean percentage. (B) Canonical correspondence analysis (CCA) triplot of all Illumina amplicon sequencing data with the greatest influence on the dataset (> 80%). The numbers of the axes (no dimension) represent the distances between the samples. Similar objects are located near to each other and dissimilar objects are farther apart from each other. Inclusion of two environmental factors 'healthy' and 'infected' resulted in a triplot, which displays the relationship of the fungal genera to colony health status.^[20] Three replicates were used to determine the mean abundance of fungal ITS2 gene sequence affiliations. All data (healthy and infected nests and specimens) were used for the calculation, revealing that certain phylogenetic groups associate more with infected nest material or specimens than healthy ones.

spectrometry (MS) including molecular networking. By screening Antibase⁴⁰ and our in-house database (at the time containing ~1700 structurally characterized metabolites), we annotated 24 clusters (≥ 3 nodes) by using *in silico* MS/MS fragmentation comparison (Table S2). This indicated the potential of strain FHG00531 to produce bioactive secondary metabolites. For example, known parent masses were affiliated to destruxin A (m/z 578.354 [M+H]⁺), viridiol (m/z 355.117 [M+H]⁺), trichokonin VI (m/z 647.04 [M+3H]³⁺), and desferri-ferricrocin (m/z 718.337 [M+H]⁺), which are part of our in-house database (Figure 2). Destruxins are hexadepsipeptides with activity against several bacteria, fungi⁴¹ and insects, including *S. litura* larvae.⁴² These compounds open Ca²⁺ channels in insects, causing tetanic contraction and ultimately death.⁴³ Furthermore, we identified an unknown cluster of metabolites containing an abundant ion (m/z 703.485 [M+H]⁺)

with the predicted molecular formula C₃₆H₆₃N₆O₆ and five derivatives thereof (Figure 2 and Figure 3).

MS/MS fragmentation data indicated a set of related peptides (Figures S3–S8). *Trichoderma* spp. produce peptides with properties suitable for biotechnological and agricultural applications.^{10,14} We therefore selected this cluster of metabolites for further analysis.

MS/MS fragmentation analysis of the unknown peptide 1 (FE011) (depicted in Table 1) revealed a C-terminal Arg (aa5), one Leu/Ile (aa3), one Phe (aa2), and a neutral loss unit of 127.0999 Da (aa4) with the predicted molecular formula C₇H₁₂N₁O₁ (suggesting methylated Leu/Ile) and an N-terminal unit with the formula C₈H₁₄N₁O₁ (Figure S3). The target ion (m/z 703.4870 [M+H]⁺) was isolated for analysis by NMR spectroscopy due to its prominence in the methanolic extract of potato dextrose broth (PDB). The structure was determined by

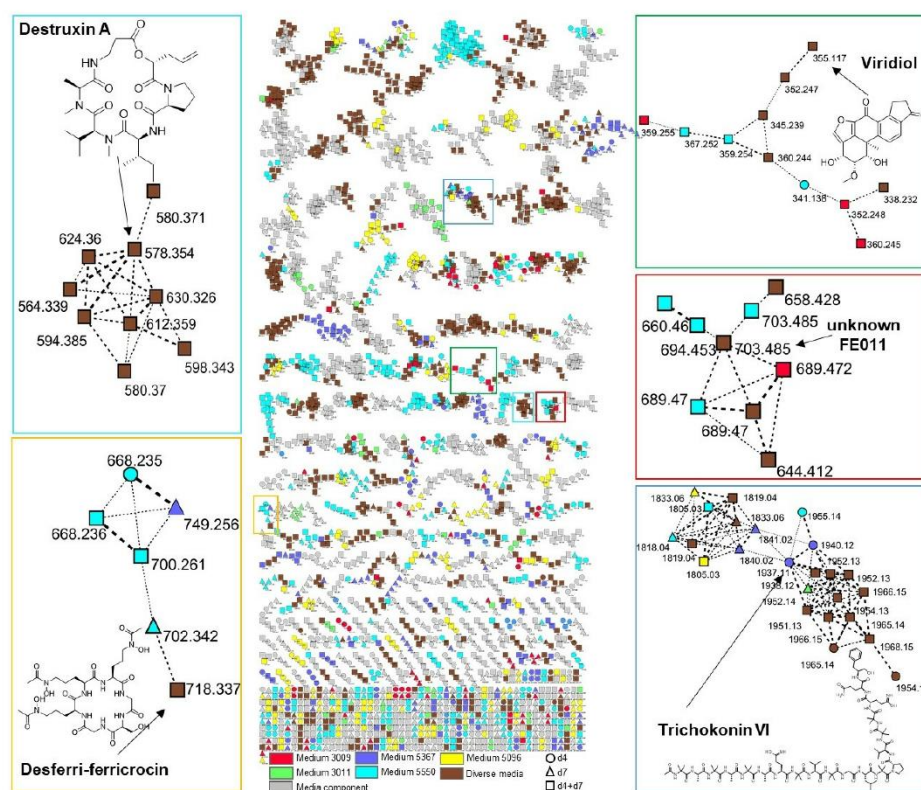


Figure 2. MS/MS molecular networking of all methanolic extracts derived from *Trichoderma* strain FHG00531 grown in five different media. Different known clusters are highlighted in color, focusing on the cluster representing peptide FE011 and its derivatives. Twenty-four clusters were annotated following *in silico* generated fragment spectra (Table S2). Each dot represents a single parent ion. Colors represent the culture medium associated with the parent ion: red = medium 3009, green = medium 3011, yellow = medium 5096, violet = medium 5367, blue = medium 5550, brown = parent ion was detected in more than one media used herein and is not a medium component. If parent ions were also detected in any of the five used media, dots were colored gray. Shapes represent the day of detection: circle = exclusively produced at day 4, triangle = exclusively produced at day 7. If produced on both days 4 and 7, dots were displayed as square. Cytoscape v3.8.2 was used to visualize the data.^{54–56}

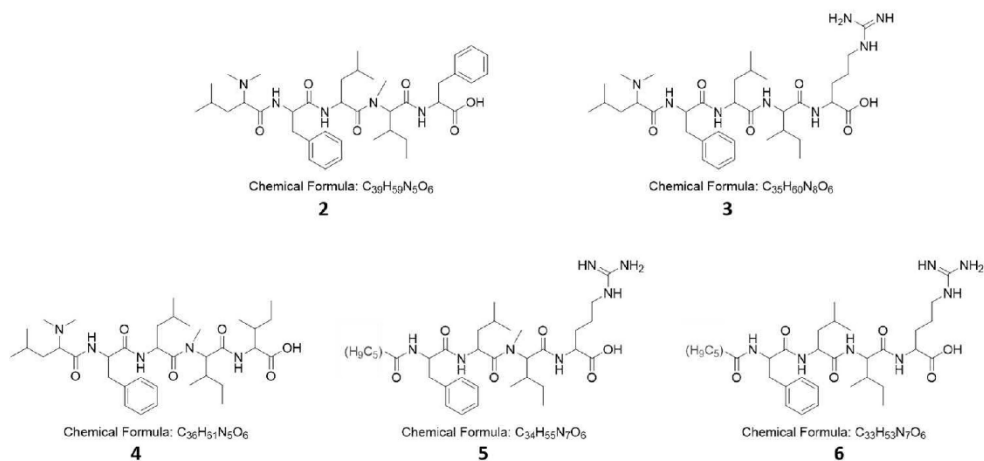


Figure 3. Tentative structures of the FE011 derivatives, inferred from the MS/MS signatures. For all compounds, structures of Leu and Ile were conventionally chosen to depict aa3 and aa4, respectively, by analogy with the elucidated structure of FE011. For compounds 2–4, *N,N*-dimethyl-Leu was conventionally chosen to depict aa1, by analogy with the elucidated structure of FE011. For compounds 5 and 6, identity of the C6:1 fatty acid remains open.

comprehensive NMR analysis, comprising 1H , ^{13}C , ROESY, TOCSY and HSQC spectra (Figures S9–S13). This revealed the presence of the three natural amino acids Phe, Leu and Arg (Figures S9–S13). In addition, we identified spin systems of a second Leu and an Ile side chain that did not include an amide proton. For the Ile residue, the amide proton was replaced with a methyl group, as indicated by correlation between the C_{α} of the Ile and *N*-methyl protons (2.93 parts per million [ppm]) in the HMBC spectrum. Likewise, the C_{α} of the second Leu revealed a coupling to a singlet at 1.91 ppm, corresponding to six protons and thus indicating the structure of an *N,N*-dimethyl-Leu residue. The sequential assignment was based predominantly on correlations in the ROESY spectrum, in particular three $NH_i + 1/H_{\alpha i}$ correlations (Arg-NH/*N*-methyl-Ile- H_{α} , Leu-NH/Phe- H_{α} and Phe-NH/*N,N*-dimethyl-Leu- H_{α}) and a close correlation between the *N*-methyl group of *N*-methyl-Ile and the H_{α} proton of Leu (Figure S13). These correlations led to the sequence *N,N*-dimethyl-Leu-Phe-Leu-*N*-methyl-Ile-Arg (Table 1, Figure S13). The incorporation of *N,N*-dimethyl-Leu introduces an unusual adduct that is poorly described.^[44] The stereochemistry was solely elucidated for the proteinogenic amino acids of **1**, which are L-Phe as aa2, L-Leu as aa3 and L-Arg as aa5 (Figure S14).

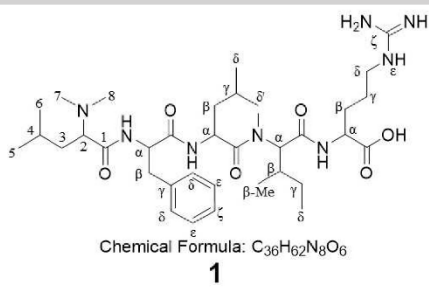
Identification of five additional FE011 derivatives

For the remaining five compounds in the cluster, manual analysis of the MS/MS fragmentation patterns confirmed their structural similarity to FE011 (Figures S3–S8). Ion 689.4717 $[M + H]^+$ was found in at least two isomeric forms, that were only present in medium 3009 and 5550 on both days (Figure 2). Pentapeptide **2** differs from FE011 at the C-terminus, where Arg

is replaced with Phe (Figure 3). Pentapeptide **3** is an *N*-demethylated analog of **1**, lacking the methyl-Ile at position 4. Pentapeptide **4** differs from **3** at the C-terminus, where Arg is replaced with Leu/Ile (MS cannot distinguish between isobaric units, so the C-terminal amino acid remains unclear). Compound **5** is a lipo-tetrapeptide in which the *N,N*-dimethyl-Leu at position 1 in FE011 is replaced with a C(6:1) fatty acid, inferred from the neutral loss of 96.0575 Da. Compound **6** is the *N*-demethylated analog of **5** (Figure 3). Interestingly, the differences between the derivatives were not confined to alternative methylation, but also included the replacement of terminal amino acids. The methylation of amino acids by methyltransferases can take place before or after peptide synthesis.^[45] Backbone *N*-methylation of (cyclic) peptides alters the conformation, can dramatically improve receptor subtype selectivity and synchronize oral bioavailability, and is therefore added to improve pharmacokinetics in medicinal chemistry.^[46,47] *N*-Methylation of exposed amino groups enhances passive permeability,^[48] increases stability and thus confers a longer half-life *in vivo*.^[46]

Given the antimicrobial effects of several *Trichoderma* metabolites,^[38,49] we tested purified compound **1** against *Escherichia coli* ATCC 35218, *Staphylococcus aureus* ATCC 25923, and *Mycobacterium smegmatis* ATCC 607 for antibacterial activity, against *Aspergillus flavus* ATCC 91 for antifungal activity, against *Brassica rapa* subsp. *rapa* for phytotoxic activity, and against *C. elegans* for activity against invertebrates. However, no bioactivity was observed against a microbial and fungal panel ($> 64 \mu\text{g/mL}$), against *B. rapa* subsp. *rapa* at concentrations up to $10 \mu\text{M}$, against *C. elegans* ($> 64 \mu\text{g/mL}$) and MDCK II cells (Table S3, Figure S15). Therefore, the biological role of **1**

Table 1. The ^1H (600 Mz) and ^{13}C (150 MHz) NMR data for FE011 in $\text{DMSO-}d_6$ at 303 K.



Chemical Formula: $\text{C}_{36}\text{H}_{62}\text{N}_8\text{O}_6$

1

	δ ^1H [ppm]	δ ^{13}C [ppm]
N,N-di-Me-Leu		
1	–	170.86, C
2	2.82, t (7.2)	65.52, CH
3	1.26, m	~38.1 (b), CH_2
4	1.35, m	24.42, CH
5	0.81, m	22.32, CH_3
6	0.76, m	22.97, CH_3
7,8	1.91, s	41.37, CH_3
Phe		
NH	7.86, d (8.4)	–
A	4.63, m	~53.0 (b), CH
B	2.97/2.73	~37.4 (b), CH_2
γ	–	137.7 (b), C
δ	7.25, m	129.15, CH
ϵ	7.22, m	127.82, CH
ζ	7.15, m	~126.1 (b), CH
C'	–	171.01, C
Leu		
NH	8.27, d (8.3)	–
A	4.78, m	~46.8 (b), CH
B	1.46/1.38, m	~40.4 (b), CH_2
γ	1.59, m	24.11, CH
δ	0.87, m	23.00, CH_3
δ'	0.86, m	21.67, CH_3
C'	–	172.16, C
NMe-Ile		
Nme	2.93	29.96
α	4.65	~59.8 (b)
β	1.95	~31.0 (b)
β -Me	0.83	15.40
γ	1.27/0.89	23.92
δ	0.78	10.28
C'	–	n.a.
Arg		
NH	7.20, b	–
α	3.85, b	~52.8 (b), CH
β	1.59, m	~28.9 (b), CH_2
γ	1.40, m	~24.8 (b), CH_2
δ	3.04, b	~40.3 (b), CH_2
ϵ	n.a.	–
ζ	–	n.a.
C'	–	~173.8 (b), C

n.a. = not available.

remains unclear and should be investigated in more detailed studies using a wider range of assays.

Conclusion

The novel pentapeptide FE011 (1) was isolated from *Trichoderma* sp. FHG000531, which was enriched in an infected termite nest. Phytotoxic, antibacterial, antifungal, and insecticidal metabolites were dereplicated by molecular networking. However, FE011 showed no bioactivity in our panel of tests, so its function remains unclear, as does the role of *Trichoderma* spp. in wood-feeding subterranean termites.^[2,4,7,14,31] Besides *Trichoderma*, other abundant fungi in the infected nest were isolated including *Exophiala*, *Paecilomyces*, *Trichoderma*, *Penicillium* and *Xylariales*. From these genera the production of insecticidal secondary metabolites is reported, and therefore they might have been involved in the changing health status of the termite colony. Thus, further experiments on the mycobiome of the nest and isolates thereof are required to gain insight into the inter-kingdom relationships and interactions within the termite biomes. This could shed light on the ecology of termites and their related fungi, offering strategies for termite pest control involving the introduction of fungi that affect termite fitness.

Experimental Section

Rearing of captive termites and sampling procedure: The captive colonies of *C. testaceus* (Ct) were identified based on their morphological characters.^[50] They originate from British Honduras and their rearing started in 1972 at the Federal Institute for Materials Research and Testing (BAM) in Berlin, in separate metal tanks with a volume of ~2 m³. Colonies were reared at 29 ± 2 °C and 75 ± 5% relative humidity, and were fed on pine wood every 3 months. We collected three samples from each nest level (*wood* [W], *surface* [S] and *carton nest* [C]) as well as three termite soldiers from a healthy (*h*) nest (Figure S1A) and an infected (*i*) nest (Figure S1B). For all termite samples, filter carton paper traps were placed in the nests to separate the termite soldiers from the nest material (Figure S16) using soft tweezers. The termite specimens were then collected in 50-mL tubes and directly frozen (*termites* [T]). We also collected three replicates of a piece of material overgrown by a fungal mat at a later stage of infection (*fungi* [F]) (Figure S1C,D). All samples were frozen and stored at –50 °C for processing or at 4 °C for cultivation.

Illumina amplicon sequencing: Nucleic acids were extracted from the samples using the NucleoSpin soil DNA purification kit (Macherey Nagel, Düren, Germany). To increase the yield, ~500 mg of nest material or 20 termites were transferred to the NucleoSpin bead tubes before adding 700 μL of lysis buffer SL2. The tubes were vortexed horizontally for 15 min at 40 Hz using a Top Mix 11118 (Thermo Fisher Scientific, Schwerte, Germany) and centrifuged at 12,000 $\times g$ for 2 min. Subsequent extraction steps were carried out according to the manufacturer's recommendations. Finally, the yield and purity of the DNA was checked using a NanoDrop ND-1000 UV/Vis spectrophotometer (Thermo Fisher Scientific) and adjusted to 5 ng/mL. Illumina amplicon sequencing on a Miseq V₂ device (Illumina, San Diego, CA, USA) was carried out by LGC Genomics (Berlin, Germany) using degenerate primer pair ITS7F (5'-GTG ART CAT CGA ATC TTT G –3') and ITS4R (5'-TCC TCC GCT TAT TGA TAT GC-3'). Demultiplexing of libraries for each sequencing lane was achieved using Illumina bcl2fastq v2.17.1.14 (<https://support.illumina.com/downloads/bcl2fastqconversion-software-v2-19.html>). Reads with missing barcodes, one-sided barcodes or conflicting barcode pairs were discarded. The sequence frag-

ments were converted to forward-reverse primer orientation after removing the primer sequences and combined using BBMerge v34.48 (<http://jgi.doe.gov/data-and-tools/bbtools>). To identify OTUs, the resulting file was processed using the PIPITS pipeline.^[51] The automatic classification was manually curated and completed by affiliation to the most similar genus using the pairwise alignment tool from Mycobank.^[52] Non-identifiable sequences (0.2%) were classified as 'no hit' in the database. Three replicates of each sample were combined for further analysis to reduce the influence of outliers. The Illumina amplicon sequencing data supporting the findings of this study are openly available under the BioProject PRJNA788263 (<https://www.ncbi.nlm.nih.gov/bioproject/PRJNA788263>).

Statistical analysis: Statistical analysis was carried out using PAST v4.03.^[53] Canonical correspondence analysis (CCA) was used to compare the mycobionemes of the healthy and infected nests, complemented by an analysis of similarities (ANOSIM) and an analysis of the similarity percentage (SIMPER) to identify data with the greatest statistical effect in the whole data set.^[20]

Media preparation: Difco PDB (VWR, Radnor, PA, USA) was prepared according to the manufacturer's protocol, with an additional 0.20 g/L yeast extract to give medium 5367. Basal salt medium (BSM) was prepared as described before.^[54] This was supplemented with 10 g/L xylan and 10 g/L xylose, and brought to pH 7 with NaOH to prepare medium 3011. BSM was supplemented with 10 g *N*-acetylglucosamine and 10 g chitin instead of xylan and xylose to prepare medium 3009. Rice medium (5550) was prepared by weighing 40 g of rice grains into a 300-mL Erlenmeyer flask and adding 40 mL of fresh medium 3011 before autoclaving. Tomato/cornsteep medium (5158) was prepared by mixing 5 g cornsteep liquid, 40 g tomato paste, and 10 g ground oatmeal with 1 L MilliQ water, then adding 1 mL of trace element solution (1.0 g/L FeSO₄ × 7H₂O, 1.0 g/L MnSO₄ × 1 H₂O, 0.05 g/L CuCl₂ × 2H₂O, 0.1 g/L CaCl₂ × 2H₂O, 0.01 g/L H₃BO₃, 0.02 g/L (NH₄)₆Mo₇O₂₄ × 4 H₂O and 0.2 g/L ZnSO₄ × 7 H₂O) and adjusting the pH to 6.8 before autoclaving.

Cultivation and propagation of isolated fungi: Material from the infected termite nest (500 mg) was weighed into 50-mL tubes and mixed with 10 mL PBS. The slurry was homogenized for 5 s at 225 Hz using an S25 KD 18 G dispersal tool connected to an Ultra-Thurax T25 basic (IKA Werke, Staufen im Breisgau, Germany). The suspension was distributed onto PDB agar (5367) plates in three 10-fold dilutions starting from 10³. The plates were incubated at 25 °C. Growing colonies were transferred daily to fresh 5367 until axenic cultures were obtained. Isolated pure colonies were stored in 80% glycerol (v/v) in liquid nitrogen.

Phylogenetic classification of strains by 18S rRNA gene sequencing: Fungal culture broth (500 µL) was collected in 1.5-mL tubes and the cells were pelleted by centrifugation (12,000 × g, 30 s). We added 700 µL lysis buffer SL2 from the NucleoSpin soil DNA kit, two 3-mm tungsten carbide beads (69997; Qiagen, Hilden, Germany) and two 12.3-mm zirconia beads (N036; Carl Roth, Karlsruhe, Germany), then disrupted the cells in a TissueLyser II (Qiagen) twice at 30 Hz for 30 s. DNA was extracted using the NucleoSpin soil DNA kit, starting with the precipitation step of the manufacturer's protocol. The purified DNA was used as the template for 18S rRNA gene amplification with primer pair NS1 (5'-GTA GTC ATA TGC TTG TCT C-3') and FR1 (5'-AIC CAT TCA ATC GGT AIT-3') as previously described.^[55] Ambiguities were manually curated, the forward and reverse strands were aligned, and the sequences were affiliated to the most similar genus using the pairwise alignment tool from Mycobank.^[52] Data supporting the findings of this study are available under the BioProject PRJNA788263 (<https://www.ncbi.nlm.nih.gov/bioproject/PRJNA788263>).

Fermentation of fungal strains: Glycerol stocks were inoculated into medium 5367 and cultivated as above for 4 days, transferred to 5367 agar plates for 4 days, then inoculated into fresh medium 5367 and cultivated for another 4 days. From this pre-culture, fresh batches of medium 3009, 3011, 5096, 5367 and 5550 were inoculated (5% v/v) in Erlenmeyer flasks and incubated at 25 °C, shaking at 180 rpm with a 5-cm deflection. After 4 or 7 days of fermentation, the broth was freeze-dried and 50-fold methanolic extracts were prepared.

Isolation of the unknown peptide FE011: *Trichoderma* strain FHG000531 was inoculated 10 × from the same agar plate into 30 mL PDB in 100-mL Erlenmeyer flasks at 25 °C, shaking at 180 rpm with 5 cm deflection for 4 days. The culture broth was then combined to inoculate 2-L Erlenmeyer flasks (5% v/v) under the same conditions. After 4 or 7 days, cell pellets were separated from the culture broth, and both components were frozen at -50 °C and subsequently lyophilized. The dried cell pellets were extracted with a 1:40 mixture of water and dichloromethane, and the water phase was evaporated under vacuum. The resulting dry extract was extracted three times with 3 L methanol, and all three organic phases were combined and dried. The dried cell-free supernatant was also extracted four times with 2 L methanol and dried as above. Both extracts were reconstituted in water containing 10% methanol, combined, and sequentially fractionated on an XAD16 N column (~1 L bed volume). Following stepwise elution in ~2 L 20%, 40%, 60% and 80% methanol in water, the fractions were identified by UHPLC-UHR-MS using a maxisil device (Bruker Daltonics, Bremen, Germany). Fractions containing FE011 were combined *in vacuo* and adjusted to 200 mg/mL using methanol for preparative HPLC on a Synergi 4u Fusion-RP column (80 Å, 250 × 21.2 mm) over 16.5 min in a linear gradient of 5–50% acetonitrile containing 0.1% formic acid. Target fractions were dried *in vacuo* and redissolved in methanol to a concentration of 30 mg/mL before elution by semi-preparative HPLC on a Nucleodur C18 Gravity-SB column (3 µm, 150 × 2 mm) over 25 min in a linear gradient of 5–95% acetonitrile. Final purification was achieved by UHPLC on an Acquity UPLC BEH C18 column (130 Å, 1.7 µm, 100 × 2.1 mm) coupled to a custom-made fraction collector (Zinsser Analytics, Eschborn, Germany) over 10 min with a linear gradient of 5–60% acetonitrile.

Mass spectrometry: We used a 1290 UHPLC system (Agilent Technologies, Santa Clara, CA, USA) equipped with DAD, ELSD and maxis II (Bruker Daltonics). Samples were separated in a gradient of solvent A (0.1% formic acid in water) and solvent B (0.1% formic acid in acetonitrile) at a flow rate of 600 µL/min. The following program was used: 0 min, 95% A; 0.30 min, 95% A; 18.00 min, 4.75% A; 18.10 min, 0% A; 22.50 min, 0% A; 22.60 min, 95% A; 25.00 min, 95% A. We used an Acquity UPLC BEH C18 column (1.7 µm, 2.1 × 100 mm) with an Acquity UPLC BEH C18 VanGuard Pre-Column (1.7 µm, 2.1 × 5 mm) at 45 °C, with an injection volume of 2 or 5 µL. All data were analyzed with the Bruker Data Analysis 4.0 software package (Bruker Daltonics).

Molecular networking and automated UHPLC-HR MS/MS-guided dereplication *in silico*: Dereplications of known and unknown metabolites from UHPLC-HR MS/MS data were achieved by comparing chromatograms derived from all extracts using molecular networking (five different media, sampled at d4 and d7 including controls) as described before.^[34] In brief, by using MSConvert (ProteoWizard package^[56]) raw data were converted to plain text files (.mgf), which contained MS/MS peak lists, wherein each parent ion is signified by a list of fragment mass/intensity value pairs (peak picking: vendor MS level = 1–2; threshold: absolute intensity, 1000, most intense). Molecular networking was performed by applying established

protocols using a cosine similarity cutoff of 0.7.^[57] In addition, ions need a minimum of six shared fragments (tolerance 0.05 Da) with at least one partner ion to be depicted in the final molecular networking. *In silico*, the retention time and fragmented compounds^[58] were compared with our in-house reference database containing >1700 characterized metabolites at the time of data evaluation.^[54] We also used the freely accessible AntiBase^[60] (AB) 2017 and the Dictionary of Natural Products (<http://dnp.chemnetbase.com/faces/chemical/ChemicalSearch.xhtml>; accessed Nov 16, 2020) for molecular formula searches as previously described,^[59] which implies different degrees of confidence for the obtained annotations.^[60] Cytoscape v3.8.2 was used to visualize the data as a network comprising nodes and edges, wherein each node represents a parent ion and its color reflects the sample (see caption Figure 2) from which the MS/MS file was obtained.^[54,61]

NMR spectroscopy: NMR spectra were recorded on a Bruker AVANCE III 600 spectrometer operating at a proton frequency of 600.05 MHz and a ¹³C frequency of 150.88 MHz. Chemical shifts (δ) are given in ppm and were referenced to the solvent signals of *d*₆-DMSO (¹H 2.50 and ¹³C 39.5 ppm). Measurements were done in the NMR department of the Justus-Liebig-University Giessen.

Marfey's analysis: Stereochemistry of the proteinogenic amino acids of **1** was determined by derivatization using Marfey's reagent.^[62] The stock solutions of NaHCO₃ (1 M in H₂O), amino acid standards (50 mM in H₂O), and 1-fluoro-2-4-dinitrophenyl-5-L-valine amide (D-FDVA, Sigma-Aldrich, St. Louis, MO, United States) (70 mM in acetone) were prepared. Commercially available standards (all Sigma) were derivatized using molar ratios of amino acid to D-FDVA and NaHCO₃ (1:1.4:8). To end the reaction after stirring at 40 °C for 3 h, 1 M HCl was added to obtain a final concentration of 170 mM. Total hydrolysis of **1** was done by dissolving 250 μ g in 6 M DCL in D₂O and stirring for 8 h at 160 °C. Subsequently, samples were evaporated to dryness and dissolved in DMSO to obtain a final concentration of 50 mM. All D- and L-amino acids were measured separately using C18 UHPLC-MS with the standard gradient described in the isolation section.

Bioassays: FE011 was screened against a panel of pathogenic microbes as previously described.^[59] Briefly,^[59] cell suspensions of the test strains were prepared from pre-cultures and adjusted to a concentration of 1×10^5 cells/mL before the assay. A dilution series of isoniazid or gentamicin was used as the positive control, and untreated cell suspensions were used as negative controls. End optical density readings after 24 h (*E. coli* ATCC 35218, *S. aureus* ATCC 33592 and *B. subtilis* DSM 10) or 48 h (*M. smegmatis* ATCC 607, *A. flavus* ATCC 91 and *C. albicans*) were determined using a LUMIstar Omega (BMG Labtech, Ortenberg, Germany) or ATP was quantified using BacTiter-Glo (Promega, Madison, WI, USA) according to the manufacturers' protocols. Phytotoxicity was evaluated by sterilizing *B. rapa* subsp. *rapa* seeds in 30% bleach solution and placing them in disposable culture tubes (Thermo Fisher Scientific) containing 0.32% Schenk and Hildebrandt Basal Salt Mixture (Sigma-Aldrich), solidified with 0.25% gellan gum (Sigma-Aldrich) and allowing the plants to grow at 20 °C and 40% relative humidity, with a 16-h photoperiod. Test compounds at 10, 5 and 1 μ M were applied to the plants 7 days after seeding. Phytotoxicity was confirmed if >50% of the plant tissue was affected. Viridiol (Cayman Chemicals, Ann Harbor, MI, USA) was used as the positive control. Nematocidal activity was assessed against the model organism *Caenorhabditis elegans* N2. *C. elegans* was kept on NGM Agar plates with *E. coli* OP50 as food source.^[63] After 4 days, worms were collected in M9 buffer. Alkaline hypochlor-

ite solution (5 M NaOH + 5% NaClO 1:2) was used to isolate the worm eggs. After several washing steps (M9-buffer), the eggs were incubated overnight in NGM medium on a rotator. After incubation the tube contained solely hatched L1/L2 larvae. This synchronized worm culture was diluted to 100 worms/mL. Before the assay, the worms were supplemented with 5 μ g/mL cholesterol, 25 μ g/mL carbenicillin and *E. coli* OP50 (0.5% v/v). The solution was distributed into 96-well microtiter plates (100 μ L assay volume). FE011 was tested in an eight point dilution series (64 - 0.5 μ g/mL) in triplicate. A dilution series of Ivermectin (40–0.3 ng/mL; Sigma Aldrich) was used as positive control. A compound concentration was considered 'active' if >85 worms were dead. The assay was incubated for 48 h at 23 ± 3 °C. The live-dead ratio was assessed by stereo microscopy. Ivermectin showed activity at 10 ng/mL. FE011, and Ionomycin (Cayman Chemicals, Ann Arbor, MI, USA) were dissolved in DMSO to get 10 mM stock solutions. Madin-Darby canine kidney (MDCK II) cells were kindly provided by Prof. Dr. Frieberthshäuser (University of Marburg). Cytotoxicity was assessed as described before.^[64] In brief, MDCK II cells were seeded in cell-culture treated 96-well microtiter plates. After reaching a confluence of 90%, cells were treated with FE011 and Ionomycin (100 μ M per well) and with the DMSO control. The plate was incubated at 37 °C and 5% CO₂ for 24 h. The cell viability was assessed by measuring the ATP content using the CellTiter-Glo Luminescent Cell Viability assay (Promega GmbH, Walldorf, Germany) according to the manufacturer's protocol. Luminescence was measured using a black 96-well plate (Greiner Bio-One GmbH, Frickenhausen, Germany) in a Synergy H4 microplate reader (Biotek [now Agilent], Bad Friedrichshall, Germany). Relative light units (RLU) were normalized to the DMSO control and set to 100%. Measurements were done with three replicates and the standard deviations were calculated using Graphpad Prism 9.1.2 (226) (GraphPad Software, LLC, San Diego, CA, USA).

Acknowledgements

This work was funded by the Hessian State Ministry of Higher Education, Research and the Arts (HMWK) via the state initiative for the development of scientific and economic excellence (LOEWE center for Insect Biotechnology and Bioresources). Sanofi-Aventis Deutschland GmbH and Evotec International GmbH financially supported this work in the framework of the Sanofi-Fraunhofer Natural Products Center and its follow up, the Fraunhofer-Evotec Natural Products Center of Excellence. The authors thank Pascal Geisler, Franziska Warnke, Jennifer Kuhn, Nadine Zucchetto, Hamid Keyvani Hafshejani, Christine Wehr, Judith Haerter, Mona Abdullahi, Kirsten Susann Bommersheim, and Christoph Hartwig (all Fraunhofer) and Yvonne de Laval (BAM) for technical support, Prof. Dr. Rudy Plarre and Prof. Dr. Dino P. McMahon (both BAM), Prof. Dr. Thomas Degenkolb, Prof. Dr. Hans Brückner (both JLU) for valuable discussions, and Dr. Heike Hausmann (JLU) for NMR support and the NMR department of the Justus-Liebig-University Giessen for technical assistance. The authors thank Prof. Dr. Eva Frieberthshäuser (University of Marburg) for kindly providing MDCK II cells. All authors read and agreed on the final version of the manuscript. Open Access funding enabled and organized by Projekt DEAL.

Conflict of Interest

L. Toti, M. Kurz and P. E. Hammann are or have been Sanofi employees and may hold shares and/or stock options in the company. P. E. Hammann and J. Glaeser are or have been employed by Evotec International GmbH.

Data Availability Statement

The data that support the findings of this study are openly available in NCBI BioProject (PRJNA) at <https://www.ncbi.nlm.nih.gov/bioproject/PRJNA788263>, reference number 788263.

Keywords: *Coptotermes testaceus* · fungal pentapeptides · insect mycobiome · metabolomics · trichoderma

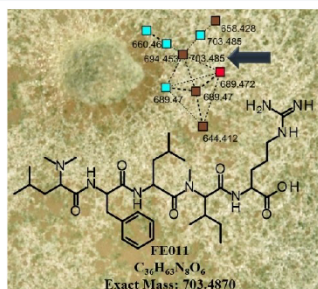
- [1] E. Mevers, T. Chouvenec, N.-Y. Su, J. Clardy, *J. Chem. Ecol.* **2017**, *43*, 1078–1085.
- [2] T. Větrovský, P. Soukup, P. Stiblík, K. Votýpková, A. Chakraborty, I. O. Larrañaga, D. Sillam-Dussès, N. Lo, T. Bourguignon, P. Baldrian, et al., *Fungal Ecol.* **2020**, *48*, 100991.
- [3] T. Chouvenec, P. Bardunias, C. A. Efstathion, S. Chakrabarti, M. L. Elliott, R. Giblin-Davis, N.-Y. Su, *Ann. Entomol. Soc. Am.* **2013**, *106*, 771–778.
- [4] T. Chouvenec, C. A. Efstathion, M. L. Elliott, N.-Y. Su, *Proc. Biol. Sci.* **2013**, *280*, 20131885.
- [5] T. Chouvenec, N.-Y. Su, A. Robert, *J. Invertebr. Pathol.* **2009**, *101*, 130–136.
- [6] a) I. Stefanini, *Yeast* **2018**, *35*, 315–330; b) D. Zhang, A. R. Lax, B. Henrissat, P. Coutinho, N. Katiya, W. C. Nierman, N. Fedorova, *Insect Mol. Biol.* **2012**, *21*, 235–245.
- [7] C. Wen, H. Xiong, J. Wen, X. Wen, C. Wang, *Front. Microbiol.* **2020**, *11*, 653.
- [8] V. Gouli, S. Gouli, J. A. P. Marcelino, M. Skinner, B. L. Parker, *Insects* **2013**, *4*, 631–645.
- [9] J. D. Rogers, Y.-M. Ju, J. Lehmann, *Mycologia* **2005**, *97*, 914–923.
- [10] M.-F. Li, G.-H. Li, K.-Q. Zhang, *Metabolites* **2019**, *9*, 58.
- [11] Z. Liu, Y. Sun, M. Tang, P. Sun, A. Wang, Y. Hao, Y. Wang, Y. Pei, *J. Nat. Prod.* **2020**, *83*, 3635–3641.
- [12] A. Iida, M. Sanekata, S. Wada, T. Fujita, H. Tanaka, A. Enoki, G. Fuse, M. Kanai, K. Asami, *Chem. Pharm. Bull.* **1995**, *43*, 392–397.
- [13] S. Wada, A. Iida, N. Akimoto, M. Kanai, N. Toyama, T. Fujita, *Chem. Pharm. Bull.* **1995**, *43*, 910–915.
- [14] T. Degenkolb, R. Dieckmann, K. F. Nielsen, T. Gräfenhan, C. Theis, D. Zafari, P. Chaverri, A. Ismaiel, H. Brückner, H. von Döhren, et al., *Mycol. Pro.* **2008**, *7*, 177–219.
- [15] H. A. Contreras-Cornejo, L. Macías-Rodríguez, E. del-Val, J. Larsen in *Reference Series in Phytochemistry* (Eds.: J.-M. Mérillon, K. G. Ramawat), Springer, Cham, **2020**.
- [16] J. F. d. S. Daniel, E. R. Filho, *Nat. Prod. Rep.* **2007**, *24*, 1128–1141.
- [17] X. Niu, N. Thaochan, Q. Hu, *J. Fungi* **2020**, *6*, 61.
- [18] M. Oberpaul, C. M. Zumkeller, T. Culver, M. Spohn, S. Mihajlovic, B. Leis, S. P. Glaeser, R. Plarre, D. P. McMahon, P. Hammann, et al., *Front. Microbiol.* **2020**, *11*, 597628.
- [19] a) B. J. Enagbonma, C. F. Ajillogba, O. O. Babalola, *Arch. Microbiol.* **2020**, *202*, 2697–2709; b) Q.-L. Chen, H.-W. Hu, Z.-Z. Yan, C.-Y. Li, B.-A. T. Nguyen, A.-Q. Sun, Y.-G. Zhu, J.-Z. He, *Soil Biol. Biochem.* **2021**, *152*, 108073.
- [20] K. R. Clarke, *Austral. Ecol.* **1993**, *18*, 117–143.
- [21] A. A. Visser, V. I. D. Ros, Z. W. de Beer, A. J. M. Debets, E. Hartog, T. W. Kuyper, T. Laessøe, B. Slippers, D. K. Aanen, *Mol. Ecol.* **2009**, *18*, 553–567.
- [22] K. Becker, M. Stadler, *J. Antibiot.* **2021**, *74*, 1–23.
- [23] G. T. Kirker, T. L. Wagner, S. V. Diehl, *Int. Biodeterior. Biodegrad.* **2012**, *72*, 18–25.
- [24] C. Beemelmans, H. Guo, M. Rischer, M. Poulsen, *Beilstein J. Org. Chem.* **2016**, *12*, 314–327.
- [25] A. P. M. Duarte, D. Attili-Angelis, N. C. Baron, L. C. Forti, F. C. Pagnocca, *Antonie van Leeuwenhoek* **2014**, *106*, 465–473.
- [26] B. J. F. d. S. Lima, M. F. Voidaleski, R. R. Gomes, G. Fornari, J. M. B. Soares, A. Bombassaro, G. X. Schneider, B. S. Da Soley, C. M. P. E. S. de Azevedo, C. Menezes, et al., *Fungal Biol.* **2020**, *124*, 194–204.
- [27] J. Kaur, R. Kaur, R. Datta, S. Kaur, A. Kaur, *J. Appl. Microbiol.* **2018**, *125*, 1455–1465.
- [28] G. Zimmermann, *Biol. Control* **2008**, *18*, 865–901.
- [29] C. A. Dunlap, M. A. Jackson, M. S. Wright, *Biocontrol. Sci. Technol.* **2007**, *17*, 513–523.
- [30] a) M. A. Jackson, S. Cliquet, L. B. Iten, *Biocontrol. Sci. Technol.* **2003**, *13*, 23–33; b) M. S. Wright, W. J. Connick, Jr., M. A. Jackson (The United States of America as represented by The Secretary of Agriculture), WO2003043417 A3, **2003**; c) S. Wraight, R. Carruthers, S. Jaronski, C. Bradley, C. Garza, S. Galaini-Wraight, *Biol. Control* **2000**, *17*, 203–217.
- [31] C. C. Staats, A. Junges, R. L. M. Guedes, C. E. Thompson, G. L. de Moraes, J. T. Boldo, L. G. P. de Almeida, F. C. Andreis, A. L. Gerber, N. Sbaraini, et al., *BMC Genomics* **2014**, *15*, 822.
- [32] M. del C. H. Rodríguez, H. C. Evans, L. M. de Abreu, D. M. de Macedo, M. K. Ndacnou, K. B. Bekele, R. W. Barreto, *Sci. Rep.* **2021**, *11*, 5671.
- [33] a) L.-H. Chen, Y.-Q. Cui, X.-M. Yang, D.-K. Zhao, Q.-R. Shen, *Australas. Plant Pathol.* **2012**, *41*, 239–245; b) R. A. A. Khan, S. Najeeb, S. Hussain, B. Xie, Y. Li, *Microorganisms* **2020**, *8*, 817.
- [34] P. K. Mukherjee, J. F. Hurley, J. T. Taylor, L. Puckhaber, S. Lehner, I. Druzhinina, R. Schumacher, C. M. Kenerley, *Biochem. Biophys. Res. Commun.* **2018**, *505*, 606–611.
- [35] J. S. Moffatt, J. D. Bu'Lock, T. H. Yuen, *J. Chem. Soc. D* **1969**, 839a–839a.
- [36] Q. Huang, Y. Tezuka, T. Kikuchi, Y. Momose, *Eur. J. Pharmacol.* **1994**, *271*, R5–R6.
- [37] W.-L. Shi, X.-L. Chen, L.-X. Wang, Z.-T. Gong, S. Li, C.-L. Li, B.-B. Xie, W. Zhang, M. Shi, C. Li, et al., *J. Exp. Bot.* **2016**, *67*, 2191–2205.
- [38] P. F. Andersson, S. B. K. Johansson, J. Stenlid, A. Broberg, *For. Pathol.* **2010**, *40*, 43–46.
- [39] E. T. Reese, *Biotechnol. Bioeng. Symp.* **1976**, 9–20.
- [40] H. Laatsch, *AntiBase: The Natural Compound Identifier*, Wiley-VCH, Weinheim, **2017**.
- [41] M. C. Pedras, L. I. Zaharia, D. E. Ward, *Phytochemistry* **2002**, *59*, 579–596.
- [42] K. S. Sree, V. Padmaja, Y. L. N. Murthy, *Pest Manage. Sci.* **2008**, *64*, 119–125.
- [43] C. Dumas, P. Robert, M. Pais, A. Vey, J.-M. Quiot, *Comp. Biochem. Physiol. Part C* **1994**, *108*, 195–203.
- [44] B. Junker, A. Walker, N. Connors, A. Seeley, P. Masurekar, M. Hesse, *Biotechnol. Bioeng.* **2006**, *95*, 919–937.
- [45] E. Matabaro, H. Kaspar, P. Dahlin, D. L. V. Bader, C. E. Murar, F. Staubli, C. M. Field, J. W. Bode, M. Künzler, *Sci. Rep.* **2021**, *11*, 3541.
- [46] J. Chatterjee, C. Gilon, A. Hoffman, H. Kessler, *Acc. Chem. Res.* **2008**, *41*, 1331–1342.
- [47] J. Chatterjee, F. Rechenmacher, H. Kessler, *Angew. Chem. Int. Ed.* **2013**, *52*, 254–269; *Angew. Chem.* **2013**, *125*, 268–283.
- [48] A. T. Bockus, J. A. Schwochert, C. R. Pye, C. E. Townsend, V. Sok, M. A. Bednarek, R. S. Lokey, *J. Med. Chem.* **2015**, *58*, 7409–7418.
- [49] A. K. Mukherjee, A. Sampath Kumar, S. Kranthi, P. K. Mukherjee, *3 Biotech* **2014**, *4*, 275–281.
- [50] R. H. Scheffrahn, T. F. Carrijo, J. Křeček, N.-Y. Su, A. L. Szalanski, J. W. Austin, J. A. Chase, J. R. Mangold, *Arthropod Syst. Phylogeny* **2015**, *73*, 333–348.
- [51] H. S. Gweon, A. Oliver, J. Taylor, T. Booth, M. Gibbs, D. S. Read, R. I. Griffiths, K. Schonrogge, *Methods Ecol. Evol.* **2015**, *6*, 973–980.
- [52] V. Robert, D. Vu, A. B. H. Amor, N. van de Wiele, C. Brouwer, B. Jabas, S. Szoke, A. Dridi, M. Triki, S. Ben Daoud, et al., *IMA Fungus* **2013**, *4*, 371–379.
- [53] Ø. Hammer, D. A. T. Harper, P. D. Ryan, *Palaeontol. Electron.* **2001**, *1*, 1–9.
- [54] M. Marner, M. A. Patras, M. Kurz, F. Zubeil, F. Förster, S. Schuler, A. Bauer, P. Hammann, A. Vilcinskas, T. F. Schäberle, et al., *J. Nat. Prod.* **2020**, *83*, 2607–2617.
- [55] K. Panzer, P. Yilmaz, M. Weiß, L. Reich, M. Richter, J. Wiese, R. Schmaljohann, A. Labes, J. F. Imhoff, F. O. Glöckner, et al., *PLoS One* **2015**, *10*, e0134377.
- [56] M. C. Chambers, B. Maclean, R. Burke, D. Amodei, D. L. Ruderman, S. Neumann, L. Gatto, B. Fischer, B. Pratt, J. Egerton, et al., *Nat. Biotechnol.* **2012**, *30*, 918–920.
- [57] J. Y. Yang, L. M. Sanchez, C. M. Rath, X. Liu, P. D. Boudreau, N. Bruns, E. Glukhov, A. Wodtke, R. de Felicio, A. Fenner et al., *J. Nat. Prod.* **2013**, *76*, 1686–1699.
- [58] F. Allen, R. Greiner, D. Wishart, *Metabolomics* **2015**, *11*, 98–110.

- [59] M. Oberpaul, S. Brinkmann, M. Marner, S. Mihajlovic, B. Leis, M. A. Patras, C. Hartwig, A. Vilcinskas, P. E. Hammann, T. F. Schäberle et al., *Microb. Biotechnol.* **2021**, *15*, 415–430.
- [60] a) N. A. Reisdorph, S. Walmsley, R. Reisdorph, *Metabolites* **2019**, *10*, 8; b) L. W. Sumner, A. Amberg, D. Barrett, M. H. Beale, R. Beger, C. A. Daykin, T. W.-M. Fan, O. Fiehn, R. Goodacre, J. L. Griffin et al., *Metabolomics* **2007**, *3*, 211–221.
- [61] P. Shannon, A. Markiel, O. Ozier, N. S. Baliga, J. T. Wang, D. Ramage, N. Amin, B. Schwikowski, T. Ideker, *Genome Res.* **2003**, *13*, 2498–2504.
- [62] R. Bhushan, H. Brückner, *Amino Acids* **2004**, *27*, 231–247.
- [63] T. Stiernagle, *Maintenance of C. elegans* (February 11, **2006**). *WormBook* (Ed.: The *C. elegans* Research Community), WormBook, Available online: <http://www.wormbook.org> (accessed on 25 January 2022).
- [64] J. Krämer, T. Lüddecke, M. Marner, E. Maiworm, J. Eichberg, K. Hards, T. F. Schäberle, A. Vilcinskas, R. Predel, *Toxin Rev.* **2022**, *14*, 58.

Manuscript received: December 22, 2021
Revised manuscript received: March 16, 2022
Accepted manuscript online: March 17, 2022
Version of record online: ■■■, ■■■■

RESEARCH ARTICLE

Metabolic opportunities from an infected termite nest: Isolation and structural analysis by NMR spectroscopy and MS/MS revealed a novel pentapeptide (FE011) and five derivatives produced by a strain of *Trichoderma* enriched in and isolated from an infected nest of the wood-feeding termite *Coptotermes testaceus*.



M. Oberpaul, S. Brinkmann, Dr. M. S. Spohn, Dr. S. Mihajlovic, Dr. M. Marner, Dr. M. A. Patras, Dr. L. Toti, Dr. M. Kurz, Prof. Dr. P. E. Hammann, Prof. Dr. A. Vilcinskas, Dr. J. Glaeser*, Prof. Dr. T. F. Schäberle*

1 – 11

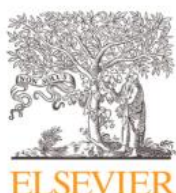
Trichoderma-Derived Pentapeptides from the Infected Nest Mycobiome of the Subterranean Termite *Coptotermes testaceus*



**MANUSCRIPT 5: TWO-STEP GENERATION OF
MONODISPERSE AGAROSE-SOLIDIFIED
DOUBLE EMULSIONS (W/W/O)
EXCLUDING AN INNER OIL BARRIER**

Status: accepted and available online on 2/11/2021

Author's contributions: method validation, data analysis and interpretation,
contribution to figure design, manuscript revision



Contents lists available at ScienceDirect

MethodsX

journal homepage: www.elsevier.com/locate/mex

Method Article

Two-step generation of monodisperse agarose-solidified double emulsions (w/w/o) excluding an inner oil barrier



Stephan Brinkmann^a, Markus Oberpaul^a, Jens Glaeser^{a,b,*},
Till F. Schäberle^{a,c,*}

^a Fraunhofer Institute for Molecular Biology and Applied Ecology (IME), Branch for Bioresources, 35392 Giessen, Germany

^b Evotec International GmbH, Göttingen 37079, Germany

^c Institute for Insect Biotechnology, Justus-Liebig-University of Giessen, Giessen 35392, Germany

A B S T R A C T

Miniaturization of biomedical and chemical research areas is performed using microfluidic techniques. Droplet-based microfluidic applications are of high interest for various applications, e.g., high-throughput screening assays. Many of them are based on simple water-in-oil (w/o) or oil-in-water (o/w) emulsions that are easily to produce. More complex assays based on separate compartments require the use of multiple emulsions, such as water-in-oil-in-water (w/o/w) or oil-in-water-in-oil (o/w/o) emulsions. In this study an easy, fast to establish method to generate agarose-solidified (w/w/o) double emulsions with $\sim 55 \mu\text{m}$ in diameter, in which both agarose-phases are not separated by a surfactant stabilized oil is described. An off-chip emulsion-breaking and washing step of the inner agarose droplets based on density gradient centrifugation was designed, offering new possibilities for high-throughput assays on picoliter scale. In brief, this paper reports:

- the protocol to generate agarose-solidified (w/w/o) double emulsions non-separated by surfactant stabilized oil;
- an off-chip washing protocol of agarose-solidified emulsions based on density gradient centrifugation.

© 2021 The Authors. Published by Elsevier B.V.

This is an open access article under the CC BY license (<http://creativecommons.org/licenses/by/4.0/>)

A R T I C L E I N F O

Method name: Two-step generation of monodisperse agarose-solidified double emulsions (w/w/o) excluding an inner oil barrier

Keywords: Droplet-based microfluidics, Water-in-water-in-oil emulsion, Microreactor, Microencapsulation, Microdroplet, High-throughput assay

Article history: Received 15 August 2021; Accepted 28 October 2021; Available online 2 November 2021

* Corresponding authors at: Fraunhofer Institute for Molecular Biology and Applied Ecology (IME), Branch for Bioresources, 35392 Giessen, Germany.

E-mail addresses: jens.glaeser@evotec.com (J. Glaeser), till.f.schaerberle@agr.uni-giessen.de (T.F. Schäberle).

<https://doi.org/10.1016/j.mex.2021.101565>

2215-0161/© 2021 The Authors. Published by Elsevier B.V. This is an open access article under the CC BY license (<http://creativecommons.org/licenses/by/4.0/>)

Specifications table

Subject Area:	Materials Science
More specific subject area:	Microfluidic double emulsion
Method name:	Two-step generation of monodisperse agarose-solidified double emulsions (w/w/o) excluding an inner oil barrier
Name and reference of original method:	Combination of high-throughput Microfluidics and FACS technologies to leverage the numbers game in natural product discovery http://doi.org/10.1111/1751-7915.13872
Resource availability:	Microfluidic hardware/software: https://www.dolomite-microfluidics.com/microfluidic-systems/%C2%B5encapsulator/

Background

The field of microfluidics set new standards in miniaturization of biomedical and chemical research areas. Droplet-based microfluidics is used as a tool for small scale single-cell or cell culture analysis, chemical synthesis as well as high-throughput screening [1]. Achieved by dispersions of stabilized liquids within continuous immiscible fluids, thousands of emulsions are generated within minutes, which subsequently are used as micro compartments suitable for such experiments [2]. Beside simple water-in-oil (w/o) or oil-in-water (o/w) emulsions, more complex ones, carrying single or multiple emulsions that represent more compartments, enable the build-up of systems with higher complexity. However, the latter are more difficult to generate. Widely used are water-in-oil-in-water (w/o/w) and oil-in-water-in-oil (o/w/o) emulsions, which can be employed for applications such as drug delivery vehicles, cell carriers, barcoding of droplets, microscale sensors, and more [3]. Other combinations of phases such as w/w and w/w/w are challenging, however applicable using aqueous phases of different properties, e.g., density, viscosity, and refractive index [4,5]. With millions of emulsions generated within minutes, powerful high-throughput analysis and sorting tools are required to retrieve events of interest. Optofluidic setups [6,7], fluorescence-activated droplet sorter (FADS) [8,9] or commercially available multichannel fluorescence-activated cell sorter (FACS) [10,11] are such tools. They differ in the analyzable emulsion-types, sample throughput and sorting capabilities, assay readout, and biocompatibility.

In this protocol (Fig. 1), we demonstrate the generation of agarose-solidified (w/w/o) double emulsions (diameter: $\sim 55 \mu\text{m}$, volume: $\sim 87 \text{ pL}$) building on agarose-solidified (w/o) emulsions (first phase; diameter: $\sim 40 \mu\text{m}$, volume: $\sim 33.5 \text{ pL}$) that are produced beforehand with the same microfluidic setup. The workflow includes an emulsion-breaking step of the first phase that results in the release of all compartments of the first phase into an aqueous phase. This is followed by a density-gradient washing step thereof to wash the first phase droplets and while working with e.g., cell cultures or bacteria to separate them from motile cells that did not get stuck within the agarose droplets. Subsequently, a second phase of liquid agarose is added. This procedure enables that both agarose phases are not compartmentalized by the fluorocarbon oil (NovecTM 7500), which is stabilized with a surfactant (Pico-SurfTM 1), necessary for emulsion stability. The emulsion-breaking step is essential, since the oil and surfactant are known to function as a barrier, which however is not completely understood until today, for several molecules with slow diffusion properties [12,13]. Moreover, with no diffusion barrier and the second phase to be added any time after incubation of the first phase, this method allows various applications for e.g., two-layer high-throughput cell culture

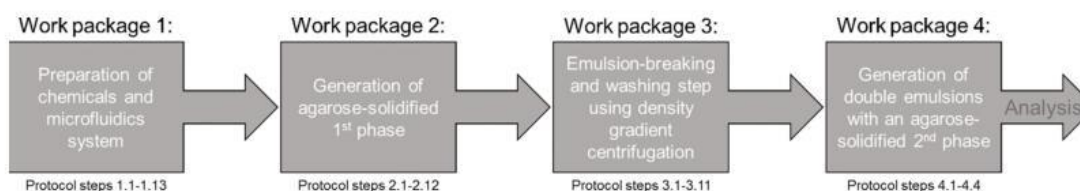


Fig. 1. Overview of the complete workflow to generate agarose-solidified (w/w/o) double emulsions.

and screening assays that rely on an intermediate washing step. This is supported by the use of a low-melting agarose that allows operations at low temperatures feasible for cell culture experiments. Applicable for e.g., fluorescence-activated cell sorting (FACS)-based technologies, a variable high-throughput readout of an envisaged assay, based on such double emulsions, is given. To the best of our knowledge, this is the first report of successful generated agarose-solidified double emulsions not separated by an inner oil barrier. Designated to run on the commercially available microfluidic ' μ Encapsulator System' (Dolomite Microfluidics, Royston, UK), trained microfluidic users can easily implement this method in any lab.

Overview of the method

Fig. 1 depicts the general procedure to generate agarose-solidified (w/w/o) double emulsion using the commercially available microfluidic ' μ Encapsulator System' (Dolomite Microfluidics), including solution and microfluidics system preparation (work package 1), generation of agarose-solidified (w/o) emulsion (first phase, work package 2), an emulsion-breaking and washing step of the first phase (work package 3), and the generation of the final agarose-solidified (w/w/o) double emulsions (work package 4). Work package 3 is critical for this application, especially while working with cell cultures. The emulsion of the solidified agarose and the fluorocarbon oil Novec™ 7500 stabilized with Pico-Surf™ 1 (first phase) needs to be de-emulsified, since otherwise in the end both agarose phases would be separated by a diffusion barrier not fully understood [12,13]. The emulsion-breaking results in release of the first phase content into the aqueous phase that did not get stuck within the agarose, e.g., still motile cells. As a solution to separate agarose-solidified droplets of the first phase from other compartments, we designed a washing step based on density gradient centrifugation using Nycodenz®.

Materials

Chemicals

- Pico-Surf™ 1 (5% (w/w) in Novec™ 7500) (Sphere Fluidics, Cambridge, UK, prod. no. C022)
- Novec™ 7500 (Iolitec Ionic Liquids Technologies GmbH, Heilbronn, GER, prod. no. FL-0004-HP)
- Pico-Break™ 1 – Emulsion Breaking Solution (Sphere Fluidics, Cambridge, UK, prod. no. C081)
- SeaPrep agarose (Lonza, Basel, Switzerland, prod. no. 50,302)
- Nycodenz® (Axis-Shield Poc AS, Oslo, Norway, prod. no. 1,002,424)
- 2-Propanol (Honeywell International Inc., Morristown, New Jersey, US, prod. no. 34,965)

Equipment

- Temperature control unit, Meros TCU-100 (TCU, Dolomite Microfluidics, Royston, UK, prod. no. 3,200,428)
- μ Encapsulator Top Interface (Dolomite Microfluidics, Royston, UK, prod.no. 3,200,569)
- Linear Connector (Dolomite Microfluidics, Royston, UK, prod. no. 3,000,024)
- μ Encapsulator 1 Sample Reservoir Chip (Dolomite Microfluidics, Royston, UK, prod. no. 3,200,444)
- μ Encapsulator 1 - 2 Reagent Droplet Chip (50 μ m etch depth), fluorophilic, (Dolomite Microfluidics, Royston, UK, prod. no. 3,200,445)
- Pressure pumps, Mitos P-Pump (Dolomite Microfluidics, Royston, UK, prod. no. 3,200,176)
 - Mitos Flow Rate Sensor (Dolomite Microfluidics, Royston, UK, prod. no. 3,200,098, 3,200,099)
 - Mitos Sensor Interfaces (Dolomite Microfluidics, Royston, UK, prod. no. 3,200,200)
- Four-way connector (Dolomite Microfluidics, Royston, UK, prod. no. 3,200,454)
- Air compressor Fengda AS-189
- High-speed CMOS camera PL-D721CU (Navitar Inc., Rochester, NY, USA)
- Stereomicroscope Stemi SV 11 (Carl Zeiss, Oberkochen, Germany)

- Halogen light source KL 2500 LCD (Schott AG, Mainz, Germany)
- Fluorescence microscope DM2000 LED equipped with a DFC450 C camera (Leica Microsystems, Wetzlar, Germany)
- Centrifuge 5810 R (Eppendorf AG, Hamburg, Germany)
- Centrifuge 5424 R (Eppendorf AG, Hamburg, Germany)
- Fridge
- Neubauer chambers (0.1 mm depth, Paul Marienfeld GmbH & CO. KG, Lauda-Königshofen, Germany)
- Adjustable 10, 100 and 1000 μ L pipettes

Consumables

- 1 mL NORM-JECT syringes (Henke-Sass, Wolf GmbH, Tuttlingen, Germany prod. no. 4010.200V0)
- 30 mL syringes (Becton, Dickinson and Company, Franklin Lakes, New Jersey, US, prod. no. 309,650)
- Needles – Sterican® Gr. 14, G 23 \times 1 1/4" / \varnothing 0,60 \times 30 mm, blue (B. Braun SE, Melsungen, Germany, prod. no. 4,657,640)
- 15 mL centrifuge tubes (Greiner Bio-One International GmbH, Frickenhausen, Germany, prod. no. 188,261)
- 0.2 μ m CA syringe filter (Corning Inc., Corning, NY, USA, prod. no. 431,224)
- 1.5 mL reaction tubes (SARSTEDT AG & Co. KG, Nümbrecht, Germany)
- Sterile pipette tips
- Microorganisms used as showcases in this study:
 - Environmental microorganisms isolated in our previous study [13]
 - *E. coli* DH5 α pFU95 (expressing *gfp_{mut3.1}*)
 - *E. coli* DH5 α pFU96 (expressing *dsRed2*)

Software

- Dolomite Flow Control Center (Dolomite UK, prod. no. 3,200,475)
- Pixelink Capture Software (Navitar Inc., Rochester, NY, USA)
- Leica Application Suite v4.8.0 (Leica Microsystems CMS GmbH, Heerbrugg, Switzerland)

Experimental protocol

In this section each work package and therein the individual tasks (protocol steps) are described step-wise and in detail.

1. Work package – Preparation of chemicals and microfluidic system

The commercially available microfluidic 'µEncapsulator System' (Dolomite Microfluidics) is very user-friendly (Fig. 2). The assembly of all parts, the cleaning and sterilization of chips as well as the troubleshooting of blockages is described in the 'µEncapsulator System User Manual' (<https://www.dolomite-microfluidics.com/support/downloads/>). Prior to each experiment, prepare and perform the following chemicals and steps:

- 1.1 Prepare 20 mL Novec™ 7500 containing 1% (w/w) Pico-Surf™ 1 (mix 4 mL Pico-Surf™ 1 5% (w/w) in Novec™ 7500 with 16 mL Novec™ 7500).
- 1.2 Prepare 40 mL water.
- 1.3 Prepare 3% (w/v) SeaPrep agarose in water (3 g SeaPrep in 100 mL water) and autoclave. **NOTE** Add a magnetic stirrer because after autoclaving the agarose is not dissolved well. Stir it at 60 °C until a homogeneous solution is obtained.
- 1.4 Prepare 20% and 30% (w/v) Nycodenz® solution in water (10 g and 15 g Nycodenz® in 50 mL water each).
- 1.5 Prepare 70% isopropanol (HPLC grade).

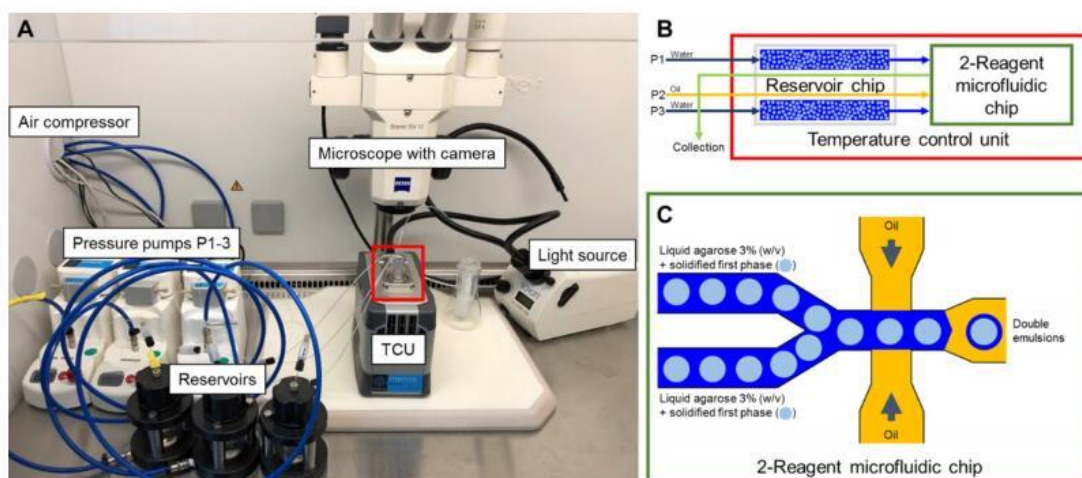


Fig. 2. Overview of the hardware setup (a), the temperature control unit (b) and the 2-Reagent microfluidic chip (c) used for the generation of the agarose-solidified 1st and 2nd phase.

Important Filter all solvents through 0.2 μm CA syringe filters to prevent blockage of microfluidic channels.

Microfluidic system (Fig. 2a):

- 1.6 Fill reservoirs with water (pump 1 and 3) and NovecTM 7500 with 1% (w/w) Pico-SurfTM 1 (pump 2).
- 1.7 Turn on the air compressor for pressure supply and operate it at 500–700 kPa.
- 1.8 Turn on all three pressure pumps, the TCU (temperature control unit), light source, and computer.
- 1.9 Open the Flow Control Center (FCC) Software (Dolomite Microfluidics) and Pixelink Capture Software (Navitar).

IMPORTANT The FCC software needs to be opened after the hardware is switched on to ensure connection.

- 1.10 Set the temperature of the TCU to 30 $^{\circ}\text{C}$ to prevent solidification of the low-melting agarose during encapsulation.
- 1.11 Priming the system (Fig. 2b) is done with the Linear Connector connected to the reservoir chip. Apply flow rates of 5 $\mu\text{L}/\text{min}$ on each channel for 5 min. This is necessary to prime all channels with their respective fluids and to push e.g., air bubbles out of the system.
- 1.12 Set the flow rates to 0 $\mu\text{L}/\text{min}$ and disconnect the Linear Connector. **NOTE** This ensures no backflow of fluids into their reservoirs without using valves.
- 1.13 Empty both sample reservoirs on the sample reservoir chip.

→ The system is now ready to be used for the generation of the first phase or for the generation of double-emulsions in the second step.

2. Work package – Generation of agarose-solidified 1st phase

We previously used the following protocol steps for encapsulation and cultivation of environmental microorganisms [13]. To obtain the here described agarose-solidified (w/w/o) double emulsions, it was necessary to use SeaPrep agarose instead of the previously used SeaPlaque one. Agarose-solidified (w/w/o) double emulsions were not possible to be obtained from a first phase produced with SeaPlaque agarose, probably due to different material properties.

2.1. Prepare the loading suspension to obtain a first phase of 1.5% (w/v) agarose droplets in a 1.5 mL reaction tube as following:

- 200 μ L 3% (w/v) SeaPrep in water
- 200 μ L water

NOTE Working with cell cultures, the water can be exchanged with the cells in their specific medium and other components. It is also possible to prepare the agarose with medium in advance to prevent dilution after mixing the liquid agarose and the water phase (cells + medium).

2.2 Vortex the solution for 10 s.

2.3 Load \sim 90 μ L into each reservoir of the reservoir chip.

2.4 Pipet 5 μ L of NovecTM 7500 post each loaded sample. **NOTE** This keeps the loaded sample separated from the water pushing it towards the 2-Reagent Droplet Chip (Fig. 2c).

2.5 Close the lid and connect the Linear Connector.

2.6 Set the flow rates for both pumps 1 and 3 supplying the loaded sample towards the 2-Reagent microfluidic chip to 2 μ L/min and the flow rate for the oil (pump 2) to 40 μ L/min. **NOTE** The pressure of the oil pump will be in the range of 350–550 mbar and of the water pumps between 550 and 800 mbar. A single pump should not exceed 1200 mbar, otherwise the channel of this pump is blocked. For the troubleshooting of blockages see the ' μ Encapsulator System User Manual' (<https://www.dolomite-microfluidics.com/support/downloads/>).

2.7 Wait 2–3 min for pressures to stabilize and then start to collect the generated droplets in a 1.5 mL reaction tube for about 25 min. **NOTE** A pressure drop indicates an emptied reservoir and therefore the end of the encapsulation.

2.8 Set the flow rate of all three pumps to 0 μ L/min.

2.9 Incubate the first phase at 8 $^{\circ}$ C for 20 min to solidify the liquid agarose-in-oil emulsions.

2.10 Disconnect the Linear Connector and empty both reservoirs of the reservoir chip.

2.11 Clean and sterilize the reservoir chip and the 2-Reagent microfluidic chip as following:

- To solve remaining residues pipet water up and down in each reservoir a few times followed by 70% isopropanol.
- Load both reservoirs with 70% isopropanol.
- Close the lid and connect the Linear Connector.
- Set all pumps to 7 μ L/min and run the system for 10 min.
- Load both reservoirs with water.
- Close the lid and connect the Linear Connector.
- Set all pumps to 7 μ L/min and run the system for 10 min.

2.12 After cleaning and sterilization, stop the flow of all three pumps. **NOTE** For long term storage all channels are dried/emptied.

→ At this point the microfluidic system is on hold. A shut down can be done by disconnecting the power of all individual parts, releasing the pressure from the air compressor and shutting down the computer.

3. Work package – Emulsion-breaking and washing step using density gradient centrifugation

The generation of agarose-solidified double emulsions with both agarose phases not separated by the surfactant (Pico-SurfTM 1) stabilized fluorocarbon oil (NovecTM 7500) requires an emulsion-breaking step of the first phase. Otherwise, both agarose phases are oil-separated – a barrier probably unwanted for some high-throughput assays, since diffusion properties for several molecules are not completely understood today [12,13]. The emulsion-breaking step is performed using Pico-BreakTM 1, according to the manufacturer's instruction with minor adaptations (https://spherfluidics.com/wp-content/uploads/2019/03/Pico-Break_User-Guide-March-2019.pdf).

This results in non-oil/surfactant-separated agarose-solidified droplets in an aqueous phase. Separated environments are still preserved, e.g., for cell cultures, or as in our case bacteria, that have been encapsulated and got stuck in the solidified agarose of the first phase. However, while working

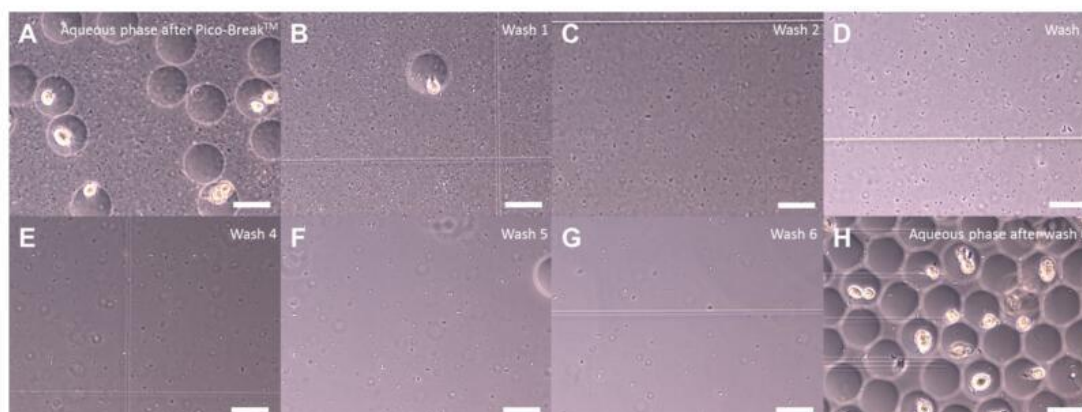


Fig. 3. Aqueous phase before (a), in-between (b-g) and after six washing steps consisting of centrifugation and supernatant exchange. Scale bar: 40 μ m.

with bacteria, we observed a huge problem of free swimming non-agarose-attached cells in the aqueous phase after emulsion-breaking (Fig. 3a). Applying this mixed aqueous phase to the second encapsulation to add the outer agarose layer, resulted in cross contamination of all solidified droplet-compartments by free swimming cells. A simple washing step by centrifugation and supernatant exchange resulted in a reduction of free swimming cells (Fig. 3b-g); however, even after six repetitions a few of them were observed in the aqueous phase (Fig. 3h). Therefore, a density gradient centrifugation protocol based on Nycodenz® (Figs. 4, 5a-i) was established to completely separate the free swimming cells (Fig. 5h) from the agarose-solidified droplets (Fig. 5i) containing non-motile cells with the following protocol steps:

- 3.1 Take the 1.5 mL reaction tube containing the first phase (agarose-solidified droplets and oil, Fig. 5f) and remove as much of the Pico-Surf™ 1 oil (bottom layer) as possible using a standard pipet. **NOTE** This reduces the amount of Pico-Break™ 1 necessary to break the w/o-emulsion.
- 3.2 The droplet layer has a volume of approximately 100 μ L. Add 250 μ L Pico-Break™ 1 and gently agitate the mixture by inverting. **NOTE** The solution turns orange and starts to disperse.
- 3.3 Centrifuge the sample at $1000 \times g$ for 1 min to disperse the aqueous (clear) and fluoruous (orange) phase.
- 3.4 Tilt 1.5 mL reaction tube to an angle of 45° and remove most of the orange fluoruous phase using a standard pipet.

Add 500 μ L water to the remaining solution in the 1.5 mL reaction tube and transfer it to a 15 mL centrifuge tube. **NOTE** While working with cell cultures, the water can be exchanged with specific medium and other components.

- 3.5 Carefully pipet 2 mL 20% Nycodenz® solution underneath this aqueous phase.
- 3.6 Carefully pipet 1 mL 30% Nycodenz® solution underneath the 20% Nycodenz® solution. Fig. 5a depicts how the solution should look like at this step.
- 3.7 Centrifuge at $2000 \times g$ for 1 min. **IMPORTANT** Do not centrifuge at higher speed or elongate this step, otherwise the cell-layer will not be separated from the droplet-layer (Fig. 5b).
- 3.8 To extract the droplet-layer, place a needle on top of a 1 mL syringe, pierce slowly through the centrifuge tube beneath the droplet-layer, which is situated on top of the 30% Nycodenz® solution, and pull out the droplets (Fig. 5c).
- 3.9 Transfer the clear content to a fresh 1.5 mL reaction tube.
- 3.10 Centrifuge the solution at $1000 \times g$ for 1 min and discard the supernatant until 200 μ L remain. **NOTE** The droplet-layer is hard to spot in a clear solution (Fig. 5d).
- 3.11 Wash the droplet-layer by adding 1000 μ L water (or medium), centrifugation at $1000 \times g$ for 1 min (Fig. 5e) and discard the supernatant until 100 μ L are left.

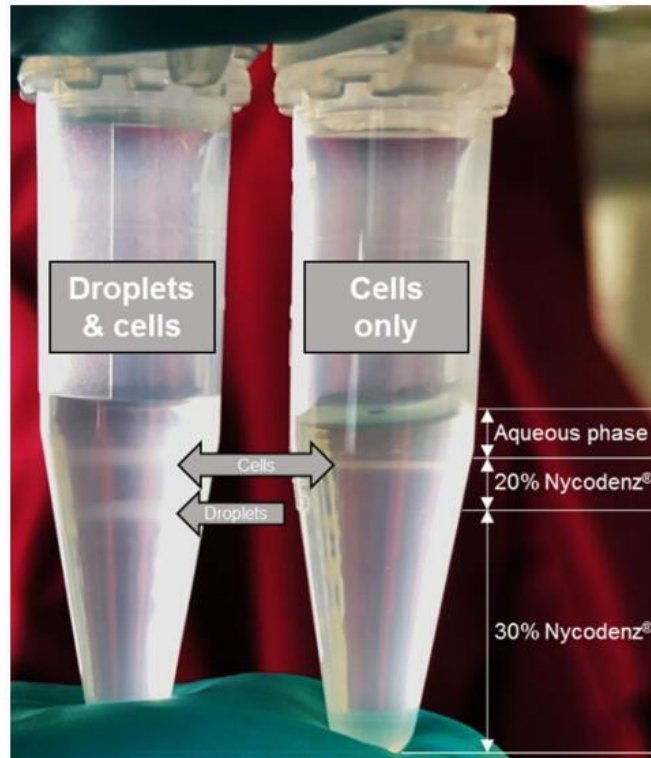


Fig. 4. Successful separation of free-swimming cells and agarose-solidified droplets of the first phase using density gradient centrifugation based on Nycodenz®.

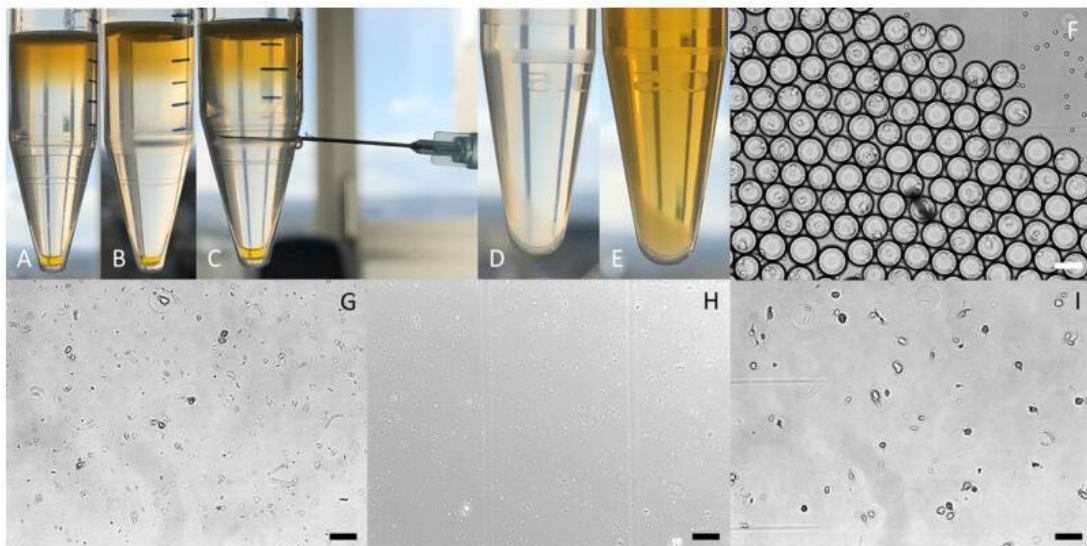


Fig. 5. Droplet-layer extraction after density gradient centrifugation (before (a) and after (b) centrifugation, pierced needle on droplet-layer level (c), milky droplet pellet in water (d), milky droplet pellet in medium (e)). Microscopic picture of the w/o emulsion of the first phase before (f) and after Pico-Break™ 1 treatment (g), the cell-layer (h) and the droplet-layer (i) after density gradient centrifugation. Scale bar: 40 μm .

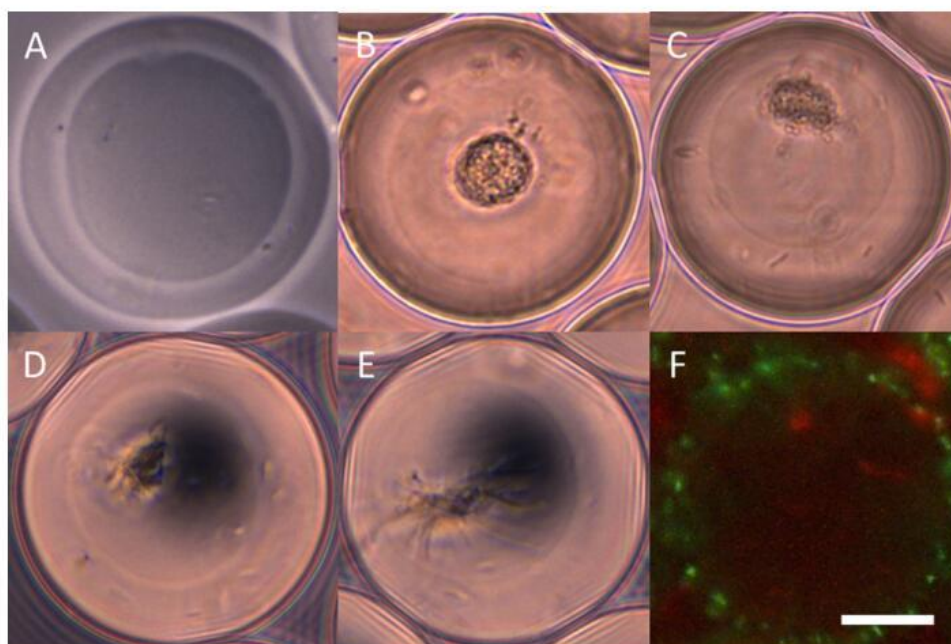


Fig. 6. Examples of agarose-solidified double emulsions with both phases empty (a), first phase carrying a microcolony of *E. coli* DH5 α derived from a single cell (b–e), and one with dsRed producing *E. coli* DH5 α pFU96 cells in the first phase and GFP producing *E. coli* DH5 α pFU95 cells in the outer layer (f). Scale Bar: 20 μ m.

→ At this point, the emulsion of the first phase is broken, the droplet-layer is washed and potentially free-swimming cells are discarded. The droplet-layer can now directly be used to be encapsulated a second time to add the second agarose layer.

4. Work package – Generation of double emulsions with an agarose-solidified 2nd phase

This work package is highly similar to the second one, since the same system and chips are used. The main difference for the production of double emulsions is that a different flow rate on the oil pump (pump 2) is applied.

4.1 Prepare the loading suspension to obtain double emulsions in a 1.5 mL reaction tube as following:

- 100 μ L 3% (w/v) SeaPrep in water
- ~100 μ L droplet-layer of the first phase after work package 3 (oil-free and washed)

4.2 Perform the previously described protocol Steps 2.2 to 2.5.

4.3 Set the flow rates for both pumps 1 and 3 supplying the loaded sample towards the 2-Reagent microfluidic chip to 2 μ L/min and the flow rate for the oil (pump 2) to 15 μ L/min. **NOTE** The pressure of the oil pump will be in the range of 450–650 mbar and of the water pumps between 800 and 1100 mbar. A single pump should not exceed 1400 mbar, otherwise the channel of this pump is blocked. For the troubleshooting of blockages see the ' μ Encapsulator System User Manual' (<https://www.dolomite-microfluidics.com/support/downloads/>).

4.4 Perform the previously described protocol Steps 2.7 to 2.12.

→ At this point, agarose-solidified double emulsions (w/w/o) without an inner oil barrier are generated and can be analyzed, e.g., using FACS, as previously described for agarose-solidified droplets of the first phase [13].

Method validation

Some agarose-solidified double emulsion examples are shown in Fig. 6. They are $\sim 55 \mu\text{m}$ in diameter with a volume of $\sim 87 \text{ pL}$ and they can be empty (Fig. 6a) or e.g., carry bacteria. In our case we did experiments with first phases carrying single *E. coli* DH5 α cells, incubated for a few hours and engulfed with a second agarose layer (Fig. 6b–e). An encapsulation of dsRed producing *E. coli* DH5 α pFU96 cells in the first phase and GFP producing *E. coli* DH5 α pFU95 cells in the outer layer (Fig. 6f) shows how cells are distributed in both compartments. Usually the microfluidics setup and all chemicals are prepared within half an hour. A single encapsulation generating the first or second phase takes with preparation about 45 min. To save time between experiments, the emulsion-breaking and washing step on the next sample can be applied while the microfluidics system runs with another sample. Therefore, several encapsulation are possible on one day.

Acknowledgments

This work was financially supported by the Hessen State Ministry of Higher Education, Research and the Arts (HMWK) via the state initiative for the development of scientific and economic excellence for the LOEWE Center for Insect Biotechnology and Bioresources. Sanofi-Aventis Deutschland GmbH and Evotec International GmbH contributed in the framework of the Sanofi-Fraunhofer Natural Products Center of Excellence/Fraunhofer-Evotec Natural Products Center of Excellence.

Declaration of Competing Interest

J.G. is employed at Evotec International GmbH. All authors declare no competing interests.

The authors declare that they have no known competing financial interests or personal relationships that could have appeared to influence the work reported in this paper.

References

- [1] L. Shang, Y. Cheng, Y. Zhao, Emerging droplet microfluidics, *Chem. Rev.* 117 (2017) 7964–8040, doi:[10.1021/acs.chemrev.6b00848](https://doi.org/10.1021/acs.chemrev.6b00848).
- [2] N. Convery, N. Gadegaard, 30 years of microfluidics, *Micro Nano Eng.* 2 (2019) 76–91, doi:[10.1016/j.mne.2019.01.003](https://doi.org/10.1016/j.mne.2019.01.003).
- [3] T.Y. Lee, T.M. Choi, T.S. Shim, R.A.M. Frijns, S.H. Kim, Microfluidic production of multiple emulsions and functional microcapsules, *Lab Chip* 16 (2016) 3415–3440, doi:[10.1039/c6lc00809g](https://doi.org/10.1039/c6lc00809g).
- [4] H. Cheung Shum, J. Varnell, D.A. Weitz, Microfluidic fabrication of water-in-water (w/w) jets and emulsions, *Biomicrofluidics* 6 (2012) 12808–128089, doi:[10.1063/1.3670365](https://doi.org/10.1063/1.3670365).
- [5] A. Sauret, Forced generation of simple and double emulsions in all-aqueous systems, *Appl. Phys. Lett.* 100 (2012) 154106, doi:[10.1063/1.3702434](https://doi.org/10.1063/1.3702434).
- [6] M. Tovar, S. Hengoju, T. Weber, L. Mahler, M. Choudhary, T. Becker, M. Roth, One sensor for multiple colors: fluorescence analysis of microdroplets in microbiological screenings by frequency-division multiplexing, *Anal. Chem.* 91 (2019) 3055–3061, doi:[10.1021/acs.analchem.8b05451](https://doi.org/10.1021/acs.analchem.8b05451).
- [7] S. Hengoju, S. Wohlfeil, A.S. Munser, S. Boehme, E. Beckert, O. Shvydkiv, M. Tovar, M. Roth, M.A. Rosenbaum, Optofluidic detection setup for multi-parametric analysis of microbiological samples in droplets, *Biomicrofluidics* 14 (2020) 24109, doi:[10.1063/1.5139603](https://doi.org/10.1063/1.5139603).
- [8] D. Vallejo, A. Nikoomanzar, B.M. Paegel, J.C. Chaput, Fluorescence-activated droplet sorting for single-cell directed evolution, *ACS Synth. Biol.* 8 (2019) 1430–1440, doi:[10.1021/acssynbio.9b00103](https://doi.org/10.1021/acssynbio.9b00103).
- [9] L. Mahler, K. Wink, R.J. Beulig, K. Scherlach, M. Tovar, E. Zang, K. Martin, C. Hertweck, D. Belder, M. Roth, Detection of antibiotics synthesized in microfluidic picolitre-droplets by various actinobacteria, *Sci. Rep.* 8 (2018) 13087, doi:[10.1038/s41598-018-31263-2](https://doi.org/10.1038/s41598-018-31263-2).
- [10] A. Zinchenko, S.R.A. Devenish, B. Kintsjes, P.Y. Colin, M. Fischlechner, F. Hollfelder, One in a million: flow cytometric sorting of single cell-lysate assays in monodisperse picolitre double emulsion droplets for directed evolution, *Anal. Chem.* 86 (2014) 2526–2533, doi:[10.1021/ac403585p](https://doi.org/10.1021/ac403585p).
- [11] J.C. Baret, Surfactants in droplet-based microfluidics, *Lab Chip* 12 (2012) 422–433, doi:[10.1039/c1lc20582j](https://doi.org/10.1039/c1lc20582j).
- [12] P. Gruner, B. Riechers, L.A. Chacón Orellana, Q. Brosseau, F. Maes, T. Beneyton, D. Pekin, J.C. Baret, Stabilisers for water-in-fluorinated-oil dispersions: key properties for microfluidic applications, *Curr. Opin. Colloid Interface Sci.* 20 (2015) 183–191, doi:[10.1016/j.cocis.2015.07.005](https://doi.org/10.1016/j.cocis.2015.07.005).
- [13] M. Oberpaul, S. Brinkmann, M. Marner, S. Mihajlovic, B. Leis, M.A. Patras, C. Hartwig, A. Vilcinskas, P.E. Hammann, T.F. Schäberle, M. Spohn, J. Glaeser, Combination of high-throughput microfluidics and FACS technologies to leverage the numbers game in natural product discovery, *Microb. Biotechnol.* (2021), doi:[10.1111/1751-7915.13872](https://doi.org/10.1111/1751-7915.13872).

3. SUMMARY OF CHAPTER 1

- i) The successful cultivation of new representatives of Acidobacteria were facilitated by applying the herein established method. Briefly, an adapted nycodenz density gradient protocol facilitated the segregation of viable cells from the termite nest matrix. The core microbiome of the termites *Coptotermes* spp. was defined by evaluating its stability over 2 years and in the presence of a fungal infection. The study additionally revealed a shift of the abundance of *Streptomyces* spp. along with Acidobacteria during the spread of the fungal infection. *Streptomyces* spp. are supposed to maintain colony health during fungal nest infections (Chouvenc *et al.*, 2013), but this phenomenon has yet to be explored for Acidobacteria. The implementation of a microplate-based high-throughput cultivation approach enabled the selective isolation of two new species in the genera *Terracidiphilus* and *Acidobacterium*, both belonging to the phylum Acidobacteria from an underexplored bioresource. Based on the comparison of 16S rRNA gene sequences, FHG110202 was found to be most closely related to *Acidobacterium ailaai*^T (97.7%) and FHG110214 to *Terracidiphilus gabretensis*^T (97.1%). Both strains were stored in the Fraunhofer IME strain collection and are currently a subject of further investigation.

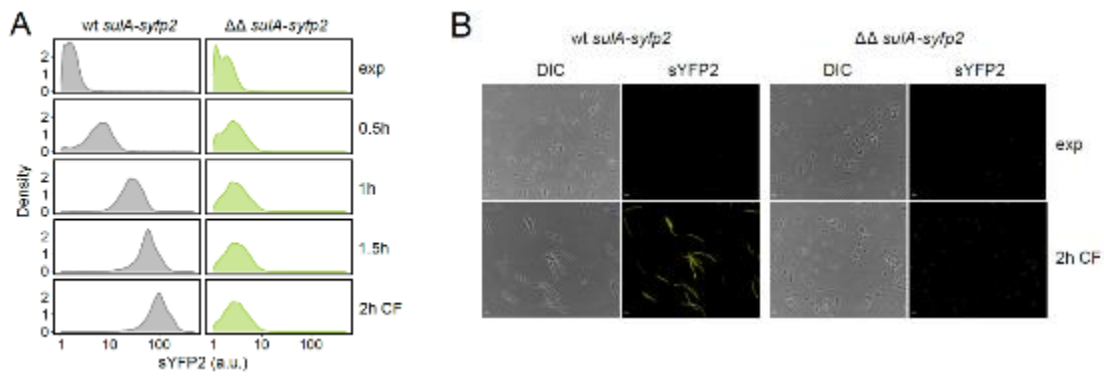
- ii) In brief, methods of i) were further developed by the sophisticated coupling of high-throughput microfluidics cultivation and flow cytometry with subsequent screening, which demonstrated the functionality of rapid prospection 'from bioresources to compounds'. Culture-independent methods were applied to the bulk of droplets, which received one single environmental cell. The evaluation of these data have revealed that by choosing the appropriate media, the chance is high that diverse microbes can be cultured in agarose-solidified microspheres. After running through the herein established cultivation pipeline, the cultivation of environmental cells in droplets in a prior step led to the isolation of a broad diversity. This was proven by the identification of 1071 cultures in 96-deep-well microplates, which affiliated to five phyla and 57 genera. One highlight

was the isolation of a member of the phylum Acidobacteria: FHG110552 was most closely related to *Edaphobacter modestus* (98.8%). The successful isolation of scarcely-cultured Proteobacteria (*Ancylobacter*, *Buttiauxella*, *Inquilinus*, *Kaistia*, *Labrys*, *Luteibacter*, *Polaromonas*, *Reyranella* and *Variovorax*) is also notable. Furthermore, the streamlined setup of a bioactivity-guided OSMAC approach, coupled with cosine-similarity analysis and metabolomics, led to the identification of six derivatives of serratamolide A produced by *Erwinia* sp. FHG110488. Although transcription factors controlling serrawettin biosynthesis have been reported, this is the first proof of an environmental *Erwinia* sp. producing serratamolide A. Unfortunately, no new natural product was identified, but further derivatives of known bioactive natural products such as macrotetrolides, massetolides, and cyclic lipopeptides were proposed by molecular networking. This successful and flexible platform will further facilitate the cultivation of microbial dark matter and will allow the rapid extraction of its chemical repertoire, when applied to other bioresources.

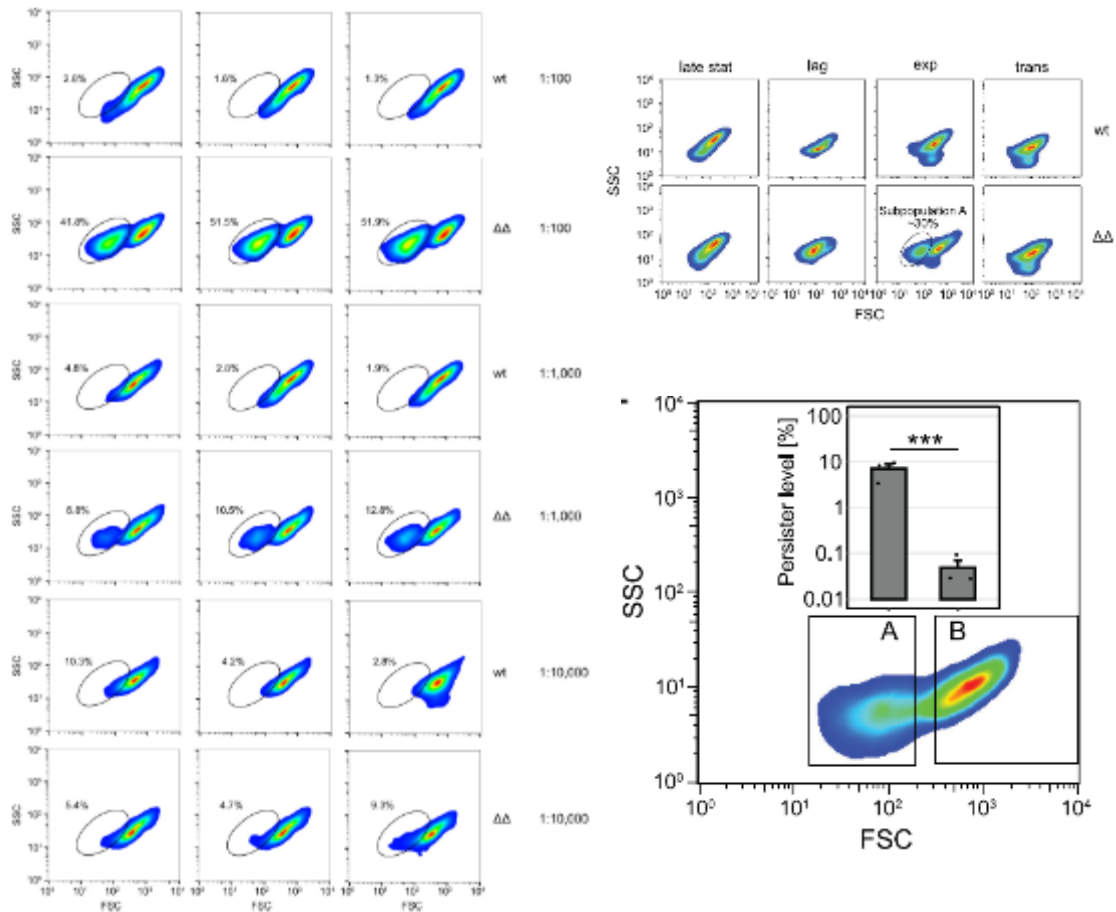
- iii) The hitherto uncultured representative FHG000416, which is most closely related to *Olivibacter domesticus* DSM 18733 (94.5%), was isolated from the termite nest of *C. gestroi* by using the technique from i). This supported the discovery of two novel lipoamino acids, which are analogs of the known Lipid 430. Two of the LAAs isolated from strain FHG000416 showed a valuable bioactivity with a minimal inhibitory concentration (MIC) of 8-16 µg/mL and the LPE 16 µg/mL against the Gram-negative pathogenic bacterium *Moraxella catarrhalis* ATCC 25238.
- iv) The analysis of the mycobiome of a termite nest from i), which was suffering from a spreading fungal infection, revealed a high abundance of *Trichoderma* spp. compared to the healthy colony. Strain FHG000513 was therefore isolated and screened for known and new natural products by applying metabolomic methods. One unknown pentapeptide namely FE011 was identified, then isolated and dereplicated by NMR spectroscopy. Furthermore, five derivatives thereof were predicted by MS/MS analysis.

Unfortunately, the peptide showed no activity against the tested screening panel, and its biological role thus requires further investigation.

- v) The conversion of the established microfluidics setup from ii) to a two-step double emulsion method was successful. This enables ultrahigh-throughput screening in droplets for natural product research, such as the screening of large clone libraries or targeted screening for novel antibiotics or enzymes.



CHAPTER 2: HIGH-THROUGHPUT *E. COLI* PERSISTER PHENOTYPING



4. AIMS OF CHAPTER 2

Environmental factors such as alarmones, bacteriostatic agents, and DNA damage lead to persister formation – a bet-hedging strategy of bacterial subpopulations to ensure the survival of the whole population. A hallmark of persister cells is their tolerance towards high concentrations of antibiotics. This includes the induction of the SOS response, which in turn lowers the susceptibility towards antibiotics. This can lead to relapse and therapeutic treatment failure during hospital-acquired infections (Lewis, 2010). Artificial high persister phenotypes are used in laboratories to dismantle all cascades leading to persistence, and only a few *hip* phenotypes have been investigated thus far (Kaldalu *et al.*, 2020). Due to the dynamic heterogeneous nature of persister cells (Balaban *et al.*, 2004), methods based on whole population measurements are inappropriate to display these cells as their signal becomes indistinct in the bulk (Goormaghtigh and van Melderen, 2019). Two options are either to use high-persistent mutants or flow cytometry to tackle this challenge. Both options should be combined herein.

- (i) Stationary phase *E. coli* cells undergo a phenotypical change by shriveling and changing from a rod-shaped to a coccoid morphology (Nyström, 2004). Persisters, which are drug-induced - e.g. by fluoroquinolone antibiotics - tend to change the morphology (Uzoечи and Abu-Lail, 2020; Wong *et al.*, 2021). These phenomena should be exploited to characterize the *hip* phenotype of *E. coli* on a single-cell level via flow cytometry. To this end, time series of flow cytometry scattering and cell sorting was applied to investigate the tightly regulated mechanisms of the type I toxin-antitoxin system TisB and its dependency on SOS induction. This was additionally enhanced by using the high persister model *E. coli* $\Delta 1-41 \Delta \text{ist-R}$ (Berghoff *et al.*, 2017) at different stages of the bacterial life cycle.
- (ii) Wild-type *E. coli* persister are dependent on the SOS response following DNA damage caused by fluoroquinolone antibiotics, which enhances persister formation during the early growth resumption phase (Völzing and Brynildsen, 2015; Mok and Brynildsen, 2018; Goormaghtigh and van Melderen, 2019). An ectopic fluorescence reporter for the activation of

the SOS response (*sulA-syfp2*) should be used to further investigate the SOS dependency with a special emphasis on the susceptibility of the *hip* phenotype of *E. coli* $\Delta 1-41$ $\Delta ist-R$ to DNA-damaging antibiotics (e.g. Mitomycin D).

**MANUSCRIPT 6: POST-TRANSCRIPTIONAL
DEREGULATION OF THE *TISB/ISTR-1*
TOXIN-ANTITOXIN SYSTEM PROMOTES
SOS-INDEPENDENT PERSISTENT
FORMATION IN *ESCHERICHIA COLI*.**

Status: published on 04/03/2021

Author's contributions: method validation, flow cytometry and cell concentration, data analysis of flow cytometry measurements, figure design, method writing, manuscript revision

Brief Report

Post-transcriptional deregulation of the *tisB/istR-1* toxin–antitoxin system promotes SOS-independent persister formation in *Escherichia coli*

Daniel Edelmann,¹ Markus Oberpaul,^{1,3}
Till F. Schäberle^{1,2,3,4} and Bork A. Berghoff^{1*}

¹Institute for Microbiology and Molecular Biology, Justus Liebig University Giessen, Giessen, 35392, Germany.

²Institute for Insect Biotechnology, Justus Liebig University Giessen, Giessen, 35392, Germany.

³Fraunhofer Institute for Molecular Biology and Applied Ecology (IME), Branch for Bioresources, Giessen, 35392, Germany.

⁴German Centre for Infection Research (DZIF), Partner Site Giessen-Marburg-Langen, Giessen, 35392, Germany.

Summary

Bacterial dormancy is a valuable strategy to endure unfavourable conditions. The term ‘persister’ has been coined for cells that tolerate antibiotic treatments due to reduced cellular activity. The type I toxin–antitoxin system *tisB/istR-1* is linked to persistence in *Escherichia coli*, because toxin TisB depolarizes the inner membrane and causes ATP depletion. Transcription of *tisB* is induced upon activation of the SOS response by DNA-damaging drugs. However, translation is repressed both by a 5′ structure within the *tisB* mRNA and by RNA antitoxin IstR-1. This tight regulation limits TisB production to SOS conditions. Deletion of both regulatory RNA elements produced a ‘high persistence’ mutant, which was previously assumed to depend on stochastic SOS induction and concomitant TisB production. Here, we demonstrate that the mutant generates a subpopulation of growth-retarded cells during late stationary phase, likely due to SOS-independent TisB accumulation. Cell sorting experiments revealed that the stationary phase-derived subpopulation contains most of the persister cells. Collectively our data show that deletion of the

regulatory RNA elements uncouples the persister formation process from the intended stress situation and enables the formation of TisB-dependent persisters in an SOS-independent manner.

Introduction

Bacteria have evolved so-called bet-hedging strategies to survive in fluctuating environments: some cells undergo a phenotypic change, which is commonly associated with the cost of strong growth retardation. While the majority of cells continue growing and contribute to the expansion of the population, the growth-retarded subpopulation is highly tolerant to multiple stress factors and ensures survival on the population level in case of fatal situations (Kussell and Leibler, 2005; Veening *et al.*, 2008; Ackermann, 2015). A prominent example for a successful bet-hedging strategy is the formation of persister cells (Balaban *et al.*, 2004; Harms *et al.*, 2016; Van den Bergh *et al.*, 2017). Persister cells were discovered in the 1940s, as they survived penicillin treatments (Hobby *et al.*, 1942; Bigger, 1944). In fact, a hallmark of persister cells is their ability to tolerate high concentrations of many different antibiotics and to re-establish growing populations upon treatment termination. Therefore, they are associated with therapeutic failure and infection relapse (Lewis, 2010).

Spontaneous persister formation as a bet-hedging strategy is not the prevailing mode of persister formation. In many cases, persistence is triggered by stress and other environmental stimuli (Balaban *et al.*, 2019; Kaldalu *et al.*, 2020). For example, alarmone (p)ppGpp is produced in response to different stresses and in turn triggers persistence (Korch *et al.*, 2003), which can be explained by (p)ppGpp-dependent ribosome dimerization (Song and Wood, 2020). Further environmental factors that trigger persistence include bacteriostatic agents (Kwan *et al.*, 2013), low magnesium levels (Pontes and Groisman, 2019), host immune cells (Helaine *et al.*, 2014) and DNA damage (Dörr *et al.*, 2009). In laboratory cultures, persister levels typically reach a

Received 3 September, 2020; accepted 11 December, 2020. *For correspondence. E-mail bork.a.berghoff@mikro.bio.uni-giessen.de; Tel. +49 641 99 35558; Fax +49 641 99 35549.

© 2020 The Authors. *Environmental Microbiology Reports* published by Society for Applied Microbiology and John Wiley & Sons Ltd. This is an open access article under the terms of the Creative Commons Attribution-NonCommercial License, which permits use, distribution and reproduction in any medium, provided the original work is properly cited and is not used for commercial purposes.

maximum during the stationary phase (Keren *et al.*, 2004; Harms *et al.*, 2017), because persister formation is triggered by starvation. This type of persistence has been termed 'stationary-phase-induced persistence' (Balaban *et al.*, 2019). Depending on culturing conditions, these stationary-phase persisters can 'contaminate' exponentially growing cultures, which has to be considered with caution when studying persistence in exponential phase (Balaban *et al.*, 2004; Harms *et al.*, 2017).

Studying the persister state is often complicated by the small size of persister fractions in culture samples. Large fractions of model persisters have been generated, e.g. by controllable expression of bacterial toxins or treatment with bacteriostatic agents (Kwan *et al.*, 2013; Mok *et al.*, 2015; Kim *et al.*, 2018a; Kim *et al.*, 2018b). Alternatively, mutants with an increased persister fraction, also called 'high persistence' (*hip*) mutants, have been employed as valuable systems for persister research. For example, kinase HipA is the toxin moiety from the type II toxin-antitoxin (TA) system HipAB (Black *et al.*, 1991, 1994), and the high persistence *hipA7* mutant (Moyed and Bertrand, 1983) was regularly used to study persistence in *Escherichia coli* (Korch *et al.*, 2003; Balaban *et al.*, 2004; Keren *et al.*, 2004). However, since HipA7 is non-toxic and has a different kinase activity compared with wild-type HipA (Korch *et al.*, 2003; Semanjski *et al.*, 2018), it remains doubtful whether the enriched persister fraction in *hipA7* cultures is evidence for toxin-mediated persistence in wild-type cultures.

In case of type II TA systems, there is an ongoing controversy concerning the direct link between toxins and persistence (Kim and Wood, 2016; Goormaghtigh *et al.*, 2018). By contrast, toxins from type I TA systems are potential persistence factors due to their ability to affect membrane potential and intracellular ATP levels (Dörr *et al.*, 2010; Gurnev *et al.*, 2012; Verstraeten *et al.*, 2015; Berghoff *et al.*, 2017; Wilmaerts *et al.*, 2018). In type I TA systems, the antitoxin is an RNA that prevents toxin production on the post-transcriptional level via sequestration of the toxin mRNA. Moreover, primary toxin mRNAs are translationally inert due to secondary structures that preclude ribosome binding (Berghoff and Wagner, 2019; Masachis and Darfeuille, 2018). A well-studied type I TA system is *tisB/listR-1* in *E. coli*. Toxin gene *tisB* is induced upon DNA damage as part of the SOS response, and transcription clearly depends on the SOS master regulator, LexA (Fernandez De Henestrosa *et al.*, 2000; Vogel *et al.*, 2004). Importantly, *tisB* is linked to persistence, since deletion of *tisB* reduces persister levels ~10-fold under DNA-damage conditions (Dörr *et al.*, 2010; Berghoff *et al.*, 2017). The primary *tisB* transcript (+1 mRNA) is translationally inert due to a secondary structure within the 5' untranslated region (Darfeuille *et al.*, 2007). A processing step removes the first

41 nucleotides from the 5' end, which produces the translationally active +42 mRNA. Under growth-promoting conditions, antitoxin IstR-1 is in excess and efficiently sequesters the +42 mRNA, which triggers its degradation (Vogel *et al.*, 2004; Darfeuille *et al.*, 2007). However, when +42 mRNA accumulates upon DNA damage, TisB production is favoured and contributes to drug-induced persistence (Dörr *et al.*, 2010; Berghoff *et al.*, 2017; Balaban *et al.*, 2019). Deletion of the two regulatory RNA elements (5' structure in *tisB* +1 mRNA and antitoxin IstR-1) produced a mutant ($\Delta 1-41 \Delta istR$) with a *hip* phenotype, which was tentatively explained by stochastic SOS induction and production of toxin TisB throughout growth (Berghoff *et al.*, 2017). TisB is a small hydrophobic protein that is located in the cytoplasmic membrane and causes breakdown of the proton motive force, which leads to membrane depolarization, ATP depletion and subsequent persister formation (Unoson and Wagner, 2008; Gurnev *et al.*, 2012; Berghoff *et al.*, 2017).

In the current study, we demonstrate that the *hip* phenotype of the deregulated mutant $\Delta 1-41 \Delta istR$ is based on LexA-independent *tisB* expression. Hence, post-transcriptional deregulation of the *tisB* gene has uncoupled the persister formation process from SOS induction.

Results and discussion

Persisters in the deregulated mutant originate from stationary phase

In this study, *E. coli* K-12 wild-type MG1655 and corresponding mutant strains were grown to late stationary phase, which was defined as 20 h after inoculating single colonies into liquid LB medium. Upon dilution of late stationary-phase cultures into fresh medium, lag phase was extended by approximately 60 min in $\Delta 1-41 \Delta istR$ (from now on $\Delta\Delta$) compared with wild-type cultures, as inferred from optical density (Fig. 1A) and validated by total cell counts (Supporting Information Fig. S1). Ectopic overexpression of antitoxin IstR-1 restored the wild-type phenotype, verifying that TisB production was responsible for the observed growth delay (Fig. 1A). Doubling times during exponential growth were not statistically different between strains (31.1 ± 0.9 min for wild type, 32.2 ± 0.5 min for $\Delta\Delta$ and 31.5 ± 0.2 for $\Delta\Delta$ plstR-1), demonstrating that the TisB-dependent effect was limited to initial growth resumption. Determination of single-cell lag times revealed that the median lag time of $\Delta\Delta$ cells was approximately 30 min longer (Supporting Information Figs S2A and S2B). These results indicated that other factors contributed to the extended lag phase in bulk experiments.

We applied light scattering in flow cytometry experiments to analyse cells at different growth stages.

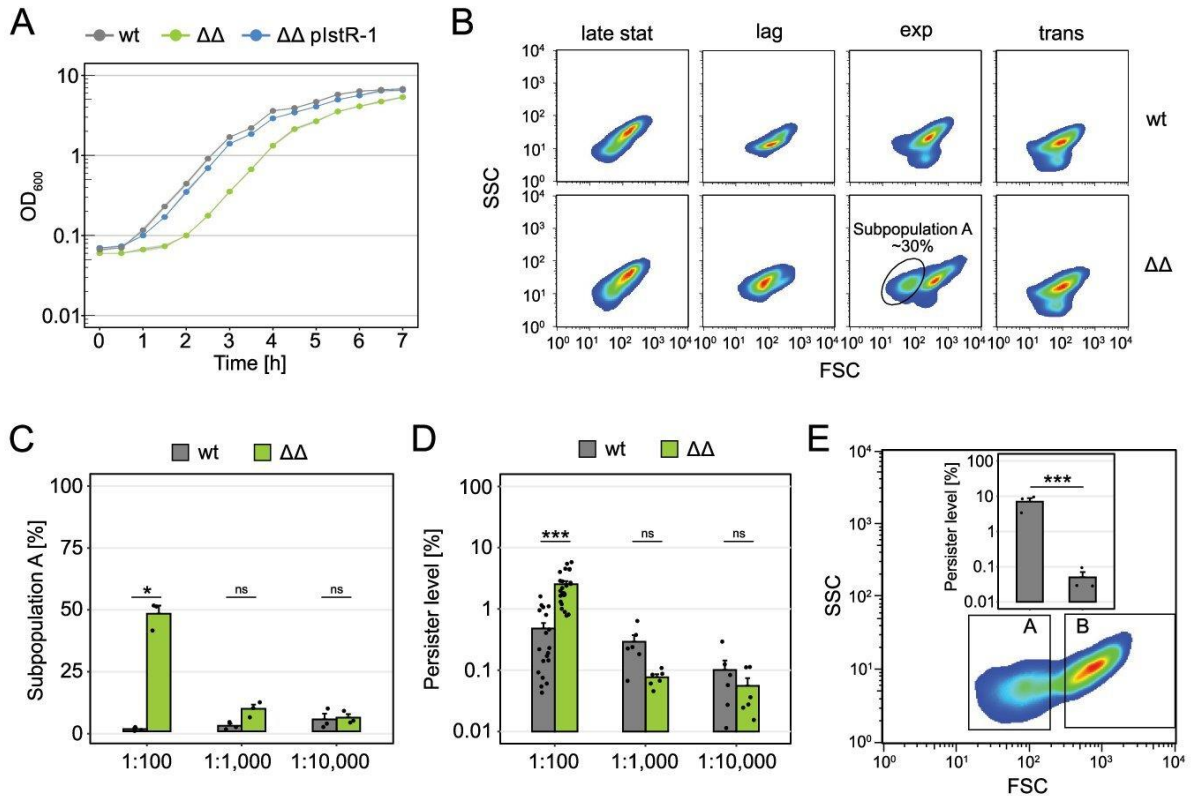


Fig. 1. Persisters of mutant $\Delta 1-41 \Delta istR$ originate from late stationary phase. **A.** Growth curves (OD_{600}) of late stationary-phase cultures diluted 1:100 into fresh LB medium. Lines indicate the mean and grey ribbons indicate the standard error of the mean (SEM; $n = 3$). In most instances, SEMs are too small to be visible. **B.** Flow cytometry analysis at various growth stages. Events were depicted as heat maps in scatter plots (FSC: forward scatter; SSC: side scatter). A representative experiment of biological triplicates is shown. The circle indicates the location of subpopulation A, which is absent in wt cultures. Percentage of subpopulation A is relative to all cells ($n > 3$). (late stat: late stationary phase, 20 h after inoculation; lag: 30 min after 100-fold dilution into fresh medium; exp: exponential phase, OD_{600} of 0.4; trans: transition phase, OD_{600} of 2.0). **C.** The size of subpopulation A was determined by flow cytometry at an OD_{600} of 0.4 after different dilutions of late stationary-phase cultures. Bars represent the mean (\pm SEM; $n = 3$). Black points represent the results of individual biological experiments. Original data can be found in Supporting Information Fig. S6. **D.** Influence of dilution on persister levels. Late stationary-phase cultures were diluted into fresh LB medium and grown until an OD_{600} of 0.4 was reached. Colony counts were determined before and after 6 h of CF treatment ($1 \mu\text{g ml}^{-1}$; $100\times$ MIC) to calculate persister levels. Bars represent the mean (\pm SEM; $n \geq 6$). Black points indicate the results of individual biological experiments. **E.** Gates for cell sorting are depicted. 500 000 events were sorted for subpopulations A and subpopulation B of the $\Delta\Delta$ mutant. Samples for sorting were from exponential phase (OD_{600} of 0.4). Colony counts were determined in sorted subpopulations before and after 6 h of CF treatment ($1 \mu\text{g ml}^{-1}$; $100\times$ MIC) to calculate persister levels. Bars represent the mean (\pm SEM; $n = 3$). Black points indicate the results of individual biological experiments. If applicable, pairwise *t*-tests were performed ($***P < 0.001$, $*P < 0.05$, ns: not significant). (wt: wild type MG1655; $\Delta\Delta$: $\Delta 1-41 \Delta istR$; plstR-1: *lstR-1* overexpression plasmid).

Population profiles of wild-type and $\Delta\Delta$ cultures were very similar in late stationary phase (Fig. 1B). However, in lag phase (30 min after dilution), slight differences occurred, and in exponential phase, population profiles were quite different. In $\Delta\Delta$ cultures, only two-thirds of the population resembled the profile of exponentially growing wild-type cells. Approximately one-third was more similar to stationary-phase cells with regard to cell length as judged from the forward scatter (subpopulation A; Fig. 1B). Under our experimental conditions, we did never observe such a subpopulation in exponential wild-type cultures. It is known that *E. coli* cells shrink during

stationary phase and adopt a coccoid morphology (Nyström, 2004). Indeed, light microscopy validated that $\Delta\Delta$ cultures retained a subpopulation of cells with a length similar to stationary-phase cells (Supporting Information Fig. S3). This subpopulation likely represented cells that had not fully proceeded to growth resumption. Upon continuous cultivation, the subpopulation disappeared, and wild-type and $\Delta\Delta$ cultures were finally indistinguishable in transition phase (Fig. 1B). Accordingly, the *hip* phenotype of the $\Delta\Delta$ mutant was only evident during lag and exponential phase, but persister levels were comparable to wild type in transition phase

(Supporting Information Fig. S4A). For persister assays, cultures were treated with the DNA-damaging fluoroquinolone ciprofloxacin (CF) at a concentration of 100× MIC (minimum inhibitory concentration) for 6 h. Biphasic kill curves revealed the existence of persisters and demonstrated that the 6-h time point was a good representation of persister levels in both wild-type and $\Delta\Delta$ cultures (Supporting Information Fig. S5A). In contrast to recent reports (Harms *et al.*, 2017), we did not observe major differences between CF at 100× and 1000× MIC (Supporting Information Fig. S5B). We, therefore, used CF at 100× MIC for 6 h in all subsequent persister assays.

To validate that subpopulation A in $\Delta\Delta$ cultures originated from stationary-phase cells, the number of inoculated cells from stationary-phase cultures was reduced to allow more cells to resume growth until a defined optical density was reached. More precisely, late stationary-phase cultures were diluted 1:100, 1:1000 or 1:10 000, and grown until an optical density at 600 nm (OD_{600}) of 0.4 (exponential phase) was reached. As expected, the size of subpopulation A decreased with the number of inoculated cells (Fig. 1C and Supporting Information Fig. S6). We assume that subpopulation A mainly contains non-growing cells and that extended cultivation enables growth resumption of these cells, but this needs further investigation. The observed features were reminiscent of stationary-phase persisters (Balaban *et al.*, 2004), and we speculated that the *hip* phenotype in $\Delta\Delta$ cultures was linked to the existence of subpopulation A. The dilution experiment was repeated, and cultures were treated directly with CF when an OD_{600} of 0.4 (exponential phase) was reached. In wild-type cultures, persister levels decreased with the number of inoculated cells, indicating the elimination of stationary-phase persisters (Balaban *et al.*, 2004; Keren *et al.*, 2004). Likewise, the *hip* phenotype of the $\Delta\Delta$ mutant was completely lost upon strong dilution (Fig. 1D). To directly prove that subpopulation A has an enriched persister fraction, subpopulations A and B were sorted based on their specific light scattering characteristics in flow cytometry experiments (Fig. 1E). Both subpopulations were subsequently treated with CF. As expected, subpopulation A contained approximately 200-fold more persisters than subpopulation B (Fig. 1E).

Live–dead cell viability assay was applied to reveal cells with damaged membranes, as indicated by strong staining with propidium iodide in relation to SYTO 9 stain (Supporting Information Fig. S7A). Subpopulation A had an increased proportion of cells with a damaged membrane in comparison to subpopulation B (7.3% versus 1.9% respectively). However, for 92.7% of cells staining did not indicate major damage (Supporting Information Fig. S7B). We conclude that subpopulation A mainly

contains cells with an intact membrane, many of which are persisters that originate from stationary phase.

Deregulation of tisB reduces cell viability in late stationary phase

Bacterial cultures exhibit increasing levels of persister cells during stationary phase due to triggered formation of stationary-phase (type I) persisters (Balaban *et al.*, 2004; Keren *et al.*, 2004; Jöers *et al.*, 2010; Harms *et al.*, 2017). However, persister levels in $\Delta\Delta$ cultures were surprisingly low during late stationary phase (Supporting Information Fig. S4A), which is counterintuitive, since we have shown that the *hip* phenotype of the mutant during exponential phase originates from stationary-phase cells (Fig. 1). Interestingly, the $\Delta\Delta$ mutant formed approximately 16-fold less colonies than the wild type when late stationary-phase cultures were plated on regular LB agar plates (Fig. 2A), even though total cell counts were comparable (Fig. 2B). We recently reported a plating defect for the $\Delta\Delta$ mutant during exponential phase when the oxidative stress regulator gene *soxS* was deleted. The plating defect was counteracted by addition of thiourea to LB agar plates, which is a scavenger of reactive oxygen species (Edelmann and Berghoff, 2019). Thiourea and the hydrogen peroxide-degrading enzyme catalase counteract the plating defect of a *Shewanella oneidensis* strain deleted for *oxyR*, encoding another important oxidative stress regulator (Shi *et al.*, 2015), and the same was observed here for an *E. coli oxyR* deletion strain (Supporting Information Fig. S8). However, neither thiourea nor catalase in LB agar plates improved culturability of $\Delta\Delta$ cultures (Supporting Information Fig. S8), indicating that a plating defect cannot account for the observed reduction in colony counts (Fig. 2A). Alternatively, $\Delta\Delta$ cultures might have a reduced number of viable cells. Indeed, when late stationary-phase cultures were serially diluted and cultivated in liquid LB medium, an at least fourfold reduction in viability was observed (Supporting Information Fig. S2C). Together, these data clearly suggested that $\Delta\Delta$ cultures contained more non-viable cells than wild-type cultures. The increased fraction of non-viable cells likely contributed to the extended lag phase of the $\Delta\Delta$ mutant (Fig. 1A). Live–dead cell viability assay revealed that most $\Delta\Delta$ cells had an intact membrane (96.4%; Supporting Information Fig. S7C), which is in agreement with previous results showing that *E. coli* cells retain an intact membrane, even when they lose viability upon extended nutrient limitation (Kim *et al.*, 2018a). The increased fraction of non-viable cells was still apparent in the early lag phase but largely disappeared in exponential and transition phase due to proliferation of viable cells (Fig. 2A), which was also confirmed by strong dilution

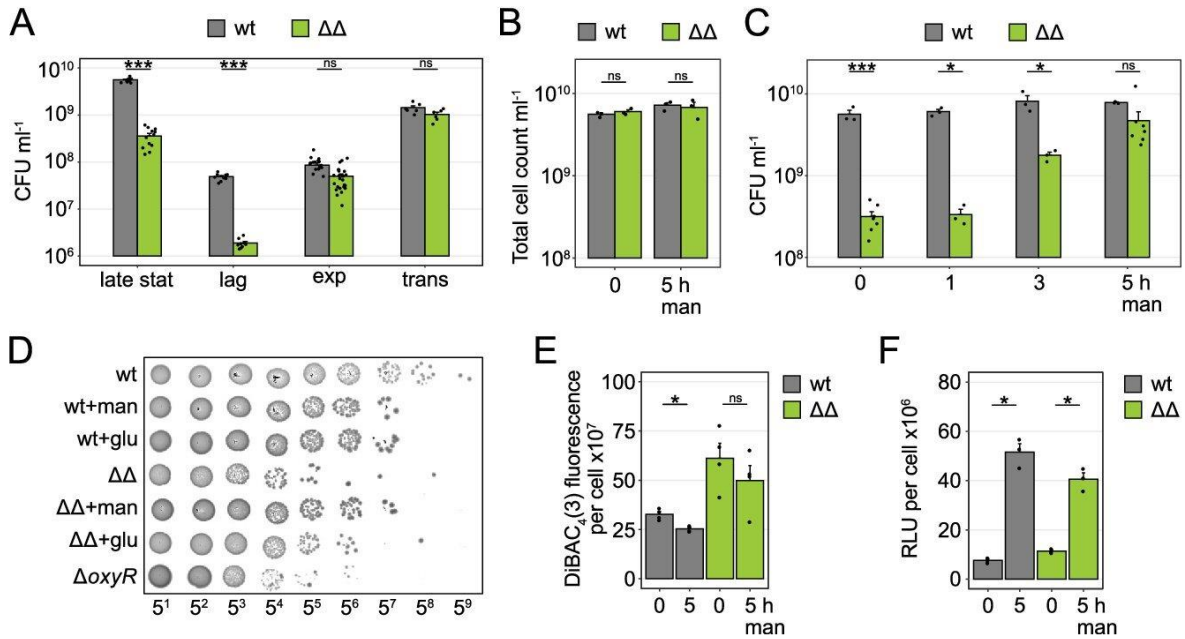


Fig. 2. Viability of mutant $\Delta 1-41 \Delta istR$ is reduced in late stationary phase. Cultures of wild-type MG1655 (wt) or $\Delta 1-41 \Delta istR$ ($\Delta\Delta$) were analysed at different growth stages. Liquid cultures were treated with 10 mM mannitol (man) for the indicated time periods before late stationary phase was reached (20 h after inoculation). Bars represent the mean (\pm SEM) and black points indicate results of individual biological experiments. A. Viable cell counts were determined at different growth stages (late stat: late stationary phase, 20 h after inoculation; lag: 30 min after 100-fold dilution into fresh medium; exp: exponential phase, OD_{600} of 0.4; trans: transition phase, OD_{600} of 2.0; $n \geq 6$). B. Total cell counts of late stationary-phase cultures were determined by microscopy using a counting chamber ($n = 3$). C. Serial dilutions of cultures at late stationary phase were plated on LB agar to determine viable cell counts ($n \geq 3$). D. Cultures were treated with 10 mM mannitol (man) or 10 mM glucose (glu) for 5 h before late stationary phase was reached. Serial dilutions (as indicated at the bottom) were spotted on LB agar plates. A full scan can be found in Supporting Information Fig. S8. E. Cellular depolarization of late stationary-phase cultures was determined by staining with the potential-sensitive probe DiBAC₄(3). Fluorescence values were normalized to total cell counts ($n = 3$). F. Cellular ATP levels were determined in late stationary phase using luminescence assays. Relative light units (RLU) were normalized to total cell counts ($n = 3$). If applicable, pairwise *t*-tests were performed ($***P < 0.001$, $*P < 0.05$, ns: not significant).

and extended incubation of late stationary-phase cultures (Supporting Information Fig. S9).

We assumed that reduced viability was caused by *TisB* expression during late stationary phase and impaired membrane functioning due to *TisB*-dependent depolarization of the inner membrane (Gurnev *et al.*, 2012; Berghoff *et al.*, 2017). It is known that membranes can be repolarized by metabolic stimuli, e.g. addition of mannitol (Allison *et al.*, 2011; Verstraeten *et al.*, 2015). Therefore, we tested whether viability was restored by adding mannitol to late stationary-phase cultures. While the wild type was not affected by mannitol, colony counts of the $\Delta\Delta$ mutant on LB agar plates transiently increased upon prolonged duration of the mannitol treatment. When liquid cultures were treated with mannitol for 5 h before late stationary phase was reached, light scattering patterns in flow cytometry experiments did not change (Supporting Information Fig. S10), but colony counts of the $\Delta\Delta$ mutant nearly reached wild-type levels (Fig. 2C). Since total cell counts were largely unaffected by mannitol (Fig. 2B), we conclude that mannitol restores viability of the $\Delta\Delta$ mutant

in late stationary phase. In line with this, lag phase of the $\Delta\Delta$ mutant in liquid cultures was shorter after mannitol treatment (Supporting Information Fig. S11). We tested whether another fermentable sugar, such as glucose, could restore viability of the $\Delta\Delta$ mutant. Indeed, glucose showed the same positive effect as mannitol when added to liquid cultures before late stationary phase was reached (Fig. 2D). As expected, when late stationary-phase cultures were left untreated and sugars were only added to LB agar plates, viability was not restored (Supporting Information Fig. S8).

We were curious whether mannitol would really affect membrane polarization (Allison *et al.*, 2011), and applied the potential-sensitive probe DiBAC₄(3). Since DiBAC₄(3) only enters cells with a depolarized membrane, high cellular DiBAC₄(3) fluorescence indicates strong depolarization. As expected, the $\Delta\Delta$ mutant had a higher cellular DiBAC₄(3) fluorescence than the wild type in late stationary phase, indicating *TisB*-dependent depolarization. However, the addition of mannitol did not significantly decrease DiBAC₄(3) fluorescence (Fig. 2E). By

contrast, the addition of mannitol significantly increased cellular ATP levels in both wild-type and $\Delta\Delta$ cultures (Fig. 2F). Even though mannitol restored viability, it did not increase persister levels of the $\Delta\Delta$ mutant in late stationary phase (Supporting Information Fig. S4B), suggesting that depolarization alone is not sufficient to trigger persistence in $\Delta\Delta$ cultures. Further experiments are clearly needed to understand the nature of the reduced viability and its connection to persistence.

*The high persistence phenotype of the deregulated mutant depends on *tisB* expression*

Our data strongly indicate that post-transcriptional deregulation of the *tisB* gene generates multiple phenotypes related to growth and persistence. To validate that these phenotypes really depend on *tisB* expression, and are not due to secondary mutations or polar effects in the $\Delta\Delta$ mutant, we specifically impeded *tisB* expression by two different strategies: strong constitutive overexpression of anti-toxin *IstR-1* from a plasmid (strain $\Delta\Delta$ *plstR-1*) and deletion of the 90-bp *tisB* coding sequence (strain $\Delta\Delta\Delta*tisB*). Both strains lost the *hip* phenotype in exponential phase (Fig. 3A), but regained culturability in late stationary phase (Fig. 3B), clearly showing that *tisB* expression was responsible for the observed phenotypes.$

*The lack of regulatory RNA elements in the deregulated mutant enables SOS-independent persistence due to the accumulation of *TisB**

Transcription of the *tisB* gene is induced upon self-cleavage of the LexA repressor under DNA-damaging conditions (Little, 1991). The *lexA3* mutation generates the non-cleavable LexA3 variant (Fernandez De Henestrosa *et al.*, 2000), and avoids induction of the SOS response. Upon CF treatment during exponential phase, induction of *tisB* clearly depends on LexA (Supporting Information Fig. S12A). In exponential phase, wild-type persister levels severely declined due to the *lexA3* mutation (Fig. 4A), confirming previous results (Dörr *et al.*, 2009; Völzing and Brynildsen, 2015; Mok and Brynildsen, 2018). By contrast, the *hip* phenotype of the $\Delta\Delta$ mutant was not affected by the *lexA3* mutation (Fig. 4A), which indicates that persisters in the $\Delta\Delta$ mutant are generated in a LexA-independent manner before CF is administered.

Our physiological data suggest that, in the $\Delta\Delta$ mutant, toxin *TisB* accumulates during late stationary phase independent of LexA regulation. Indeed, we detected accumulation of *tisB* +42 mRNA and 3xFLAG-tagged *TisB* protein in the $\Delta\Delta$ mutant during late stationary phase (Fig. 4B). Transcriptional regulation of *tisB* was not accountable for the observed accumulation, since

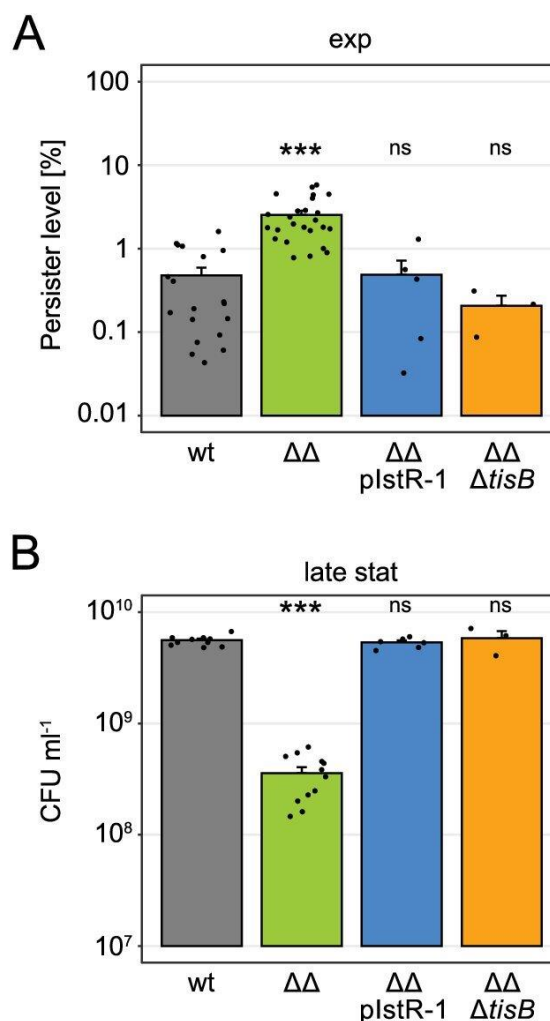


Fig. 3. Phenotypes of mutant Δ 1-41 Δ *istR* depend on *tisB* expression. Cultures of wild-type MG1655 (wt), Δ 1-41 Δ *istR* ($\Delta\Delta$), $\Delta\Delta$ with *IstR-1* overexpression plasmid ($\Delta\Delta$ *plstR-1*) and $\Delta\Delta$ with deletion of *tisB* ($\Delta\Delta\Delta$ *tisB*) were analysed. Bars represent the mean (\pm SEM; $n \geq 3$). Black points indicate the results of individual biological experiments. A. Late stationary-phase cultures (20 h after inoculation) were diluted 1:100 into fresh medium and grown to exponential phase (exp, OD₆₀₀ of 0.4). Colony counts were determined before and after 6 h of CF treatment (1 μ g ml⁻¹; 100 \times MIC) to calculate persister levels. B. Viable cell counts were determined by plating dilutions of late stationary-phase cultures (20 h after inoculation). Pairwise *t*-tests were performed in comparison to wt (****P* < 0.001, ns: not significant).

(i) *tisB* +1 mRNA did not accumulate in wild-type cultures, (ii) accumulation of *tisB* +42 mRNA in $\Delta\Delta$ cultures was not affected by the *lexA3* mutation (Fig. 4B) and (iii) a fluorescent fusion to the *tisB* promoter did not reveal an increased promoter activity (Supporting Information Fig. S12B). 3xFLAG-*TisB* was also detected in $\Delta\Delta$ cultures during exponential phase, even though

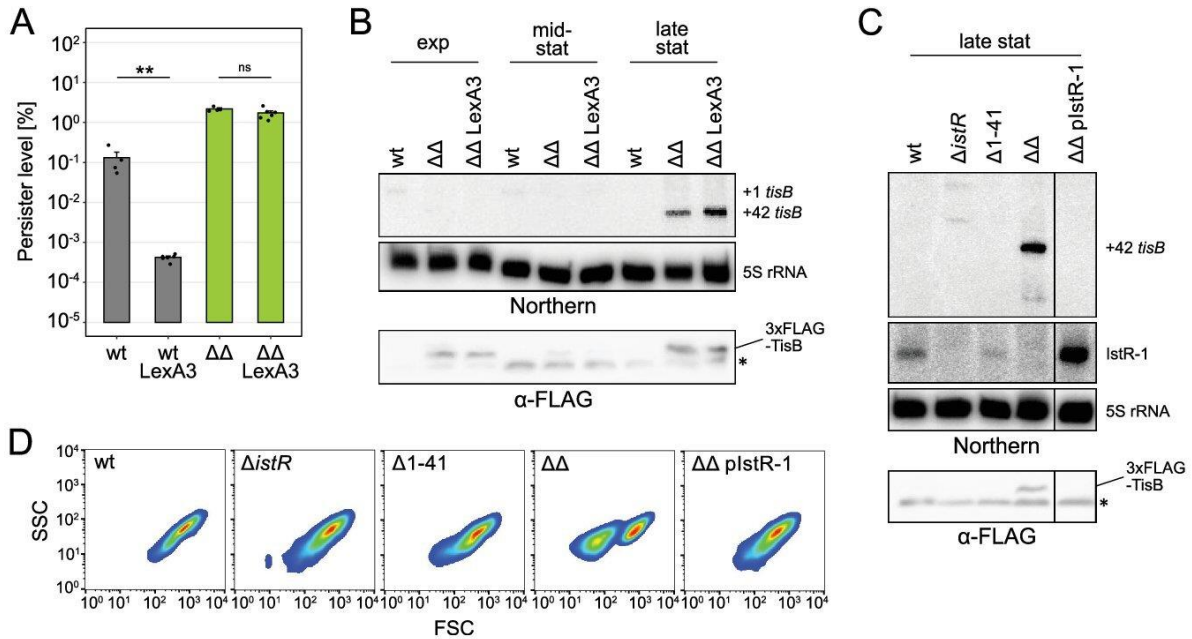


Fig. 4. Deregulation of *tisB* promotes SOS-independent TisB expression. **A.** Persister levels during exponential phase (OD_{600} of 0.4) after 6 h of CF treatment ($1 \mu\text{g ml}^{-1}$; $100\times$ MIC). Stationary-phase cultures (16 h after inoculation) were diluted 1:100 into fresh LB medium to obtain exponential-phase cultures. Bars represent the mean (\pm SEM; $n \geq 4$). Black points indicate the results of individual biological experiments. A pairwise *t*-test was performed (** $P < 0.01$, ns: not significant). **B.** Northern blot analysis of *tisB* mRNA and immunodetection of 3xFLAG-TisB at different growth stages. Samples were collected at exponential phase (exp, OD_{600} of 0.4), mid-stationary phase (mid-stat, OD_{600} of 4.0) and late stationary phase (late stat, 20 h after inoculation). Specific *tisB* mRNAs (+1 and +42) are indicated. 5S rRNA was probed as loading control. For immunodetection of TisB, only strains with chromosomally encoded 3xFLAG-TisB were subjected to Tricine-SDS-PAGE. 3xFLAG-TisB was detected using an anti-FLAG antibody. The asterisk indicates an unspecific band at approximately 10 kDa that serves as loading control for each growth condition. **C.** Northern blot analysis of *tisB* mRNA and antitoxin IstR-1, and immunodetection of 3xFLAG-TisB during late stationary phase (late stat, 20 h after inoculation). See (B) for explanation. For illustration purposes, one lane was omitted from the blots (indicated by a vertical line). **D.** Flow cytometry analysis during exponential phase (OD_{600} of 0.4). Events were depicted as heat maps in scatter plots (FSC: forward scatter; SSC: side scatter). A representative experiment of biological triplicates is shown. (wt: wild type MG1655; $\Delta\Delta$: $\Delta 1-41 \Delta istR$; plstR-1: IstR-1 overexpression plasmid).

tisB +42 mRNA levels were not increased (Fig. 4B). Control experiments showed that the 3xFLAG sequence itself had no major influence on +42 mRNA levels (Supporting Information Fig. S12C), and that the 3xFLAG-TisB protein detected in exponential phase was not simply a carryover from stationary phase (Supporting Information Fig. S12D). We suggest that constitutive expression of 3xFLAG-TisB in exponential phase is due to basal transcription of *tisB*, but we cannot exclude effects of the 3xFLAG on translation or protein stability.

We speculated that accumulation of 3xFLAG-TisB was due to the lack of post-transcriptional control by antitoxin IstR-1. Indeed, when IstR-1 was present (mutant $\Delta 1-41$ or mutant $\Delta\Delta$ with ectopic IstR-1 expression), neither *tisB* +42 mRNA nor 3xFLAG-TisB protein accumulated in late stationary phase (Fig. 4C). Accordingly, the distinct subpopulation was not observable during outgrowth experiments in strains that had a chromosomal *istR-1* copy or ectopically expressed IstR-1 (Fig. 4D). Since *tisB* +42 mRNA was quite stable (half-life of ~ 35 min) in

the $\Delta\Delta$ mutant during late stationary phase (Supporting Information Fig. S13), the lack of IstR-1 probably stabilizes the +42 mRNA and allows its accumulation in stationary-phase cells when turnover of mRNAs is generally low (Barnett *et al.*, 2007). This assumption is supported by half-life measurements for the small RNA RybB. In early stationary phase, RybB has a half-life of approximately 8 min (Vogel, 2003). By contrast, in late stationary phase, the half-life of RybB was more than 40 min (Supporting Information Fig. S13).

Conclusions

To date, only few *hip* phenotypes have been characterized in detail (Kaldalu *et al.*, 2020). In case of the $\Delta\Delta$ mutant, it was hypothesized that the *hip* phenotype is caused by stochastic DNA damage and activation of the SOS response, which would enable TisB production due to the lack of post-transcriptional repression (Pennington

and Rosenberg, 2007; Berghoff *et al.*, 2017; Berghoff and Wagner, 2019). Here, we show that the *hip* phenotype does not depend on SOS induction, and we also exclude other possibilities concerning transcriptional activation. We rather suggest that post-transcriptional deregulation of the *tisB* gene promotes TisB production during late stationary phase (when the translationally active *tisB* mRNA accumulates due to low RNA turnover) and during exponential phase (when only basal levels of translationally active *tisB* mRNA are present, but translation rate is high).

Our data suggest that TisB production in exponential phase is not sufficient to generate the *hip* phenotype of the $\Delta\Delta$ mutant. Instead, we observed that TisB production generates a subpopulation of stationary-phase cells, which exhibit a delayed growth resumption (as shown by single-cell lag times), and that this subpopulation is responsible for the occurrence of a high persister fraction in the $\Delta\Delta$ mutant. TisB-dependent persister formation in wild-type cultures has been denoted drug-induced persistence (Balaban *et al.*, 2019), since the drug itself (i.e. a DNA-damaging antibiotic) triggers TisB production and subsequent persister formation (Dórr *et al.*, 2010). Persister cells in the $\Delta\Delta$ mutant match the criteria for stationary-phase (type I) persisters (Balaban *et al.*, 2004), since (i) they represent a pre-existing subpopulation of cells, (ii) the number of inoculated cells is proportional to the number of persister cells and (iii) they resume growth with an extended lag phase. Using metabolic labeling and mass spectrometry analysis, we have observed recently that ampicillin-enriched persisters from $\Delta\Delta$ cultures show enhanced synthesis of RpoS and several RpoS-dependent proteins with functions during stationary phase (Spanka *et al.*, 2019). These findings further underscore the notion that TisB persisters in $\Delta\Delta$ cultures originate from stationary phase.

Type I persistence has also been denoted 'persistence by lag', since the prolonged lag phase is a hallmark of this persistence type (Brauner *et al.*, 2016). In theory, every event that increases the likelihood of single cells to adopt a prolonged growth-deficient state favours persistence by lag, which has, e.g. been observed upon diauxic shifts (Kotte *et al.*, 2014). When bacterial cultures are subjected to cyclic antibiotic treatments, persistence by lag might evolve due to mutations (Fridman *et al.*, 2014). In the $\Delta\Delta$ mutant, persistence by lag occurs due to post-transcriptional deregulation of a type I toxin gene and presumably elevated toxin levels (Rotem *et al.*, 2010; Berghoff *et al.*, 2017).

We note that persister levels in $\Delta\Delta$ cultures are surprisingly low at late stationary phase. The reduced viability of $\Delta\Delta$ cells cannot account for this observation, because mannitol increases viability but does not restore high persister levels. The *tisB* +42 mRNA still accumulated in the

presence of mannitol (Supporting Information Fig. S12E), and mannitol was not able to repolarize the membrane of $\Delta\Delta$ cells. We conclude that mannitol can neither avoid TisB accumulation nor reverse TisB-dependent depolarization. The mannitol-dependent increase in cellular ATP levels rather points to the possibility that mannitol, and probably other sugars like glucose, enter glycolysis and support fermentative processes to restore ATP levels by substrate-level phosphorylation. Hypothetically, elevated ATP levels maintain viable functions but avoid persister formation.

In the current study, we provide a thorough phenotypic characterization of the $\Delta\Delta$ mutant, which helps to appreciate its *hip* phenotype, and even though the high persister fraction in the $\Delta\Delta$ mutant might not reflect the wild-type situation, it provides a framework to study TisB-dependent persistence. Importantly, the *hip* phenotype of the $\Delta\Delta$ mutant is not based on an impaired toxin variant, as in the case of HipA7 (Korch *et al.*, 2003; Semajski *et al.*, 2018), but rather on increased expression of a wild-type toxin.

Finally, our data help to explain why type I toxins are tightly regulated by RNA elements. If these regulatory elements are absent, cells might inadvertently enter a deep state of toxin-induced dormancy, from which it is difficult to recover. It is generally assumed that strains with an extended lag phase or *hip* phenotype have a fitness cost due to their impaired growth (Fridman *et al.*, 2014; Stepanyan *et al.*, 2015). However, depending on the frequency and duration of stressful events, they might out-compete wild-type strains due to their increased stress tolerance, but this advantage would certainly represent a trade-off, and fitness costs might exceed impaired growth. It can be expected that the $\Delta\Delta$ mutant would suffer from oxidative stress (Edelmann and Berghoff, 2019), membrane perturbations and possibly other disruptive effects due to elevated toxin levels. These fitness costs have likely favoured tight control of type I toxins, which is typically achieved by regulatory RNA elements in wild-type strains (Berghoff and Wagner, 2017).

Acknowledgements

We thank Alisa Rizvanovic, Cédric Romilly and Gerhart Wagner (Uppsala University) for providing strains. We are grateful to Elena Evguenieva-Hackenberg (University of Giessen) for critical reading of the manuscript. We thank Gerrit Eichner (University of Giessen) for helpful comments regarding statistical analysis. We are grateful to John Hook (University of Giessen) for assistance with microscopy. This research was funded by the German Research Council (DFG) in the framework of the SPP 2002 (BE 5210/3-1 to B.A.B.). Work at the Schäberle labs was funded by the Hesse State Ministry for Higher Education, Research and the Arts through the LOEWE program. Open Access funding enabled and organized by ProjektDEAL.

References

- Ackermann, M. (2015) A functional perspective on phenotypic heterogeneity in microorganisms. *Nat Rev Microbiol* **13**: 497–508.
- Allison, K.R., Brynildsen, M.P., and Collins, J.J. (2011) Metabolite-enabled eradication of bacterial persisters by aminoglycosides. *Nature* **473**: 216–220.
- Balaban, N.Q., Helaine, S., Lewis, K., Ackermann, M., Aldridge, B., Andersson, D.I., et al. (2019) Definitions and guidelines for research on antibiotic persistence. *Nat Rev Microbiol* **17**: 441–448.
- Balaban, N.Q., Merrin, J., Chait, R., Kowalik, L., and Leibler, S. (2004) Bacterial persistence as a phenotypic switch. *Science* **305**: 1622–1625.
- Barnett, T.C., Bugrysheva, J.V., and Scott, J.R. (2007) Role of mRNA stability in growth phase regulation of gene expression in the group A *Streptococcus*. *J Bacteriol* **189**: 1866–1873.
- Berghoff, B.A., Hoekzema, M., Aulbach, L., and Wagner, E.G.H. (2017) Two regulatory RNA elements affect TisB-dependent depolarization and persister formation. *Mol Microbiol* **103**: 1020–1033.
- Berghoff, B.A., and Wagner, E.G.H. (2017) RNA-based regulation in type I toxin–antitoxin systems and its implication for bacterial persistence. *Curr Genet* **63**: 1011–1016.
- Berghoff, B.A., and Wagner, E.G.H. (2019) Persister formation driven by TisB-dependent membrane depolarization. In *Persister Cells and Infectious Disease*. Lewis, K. (ed). Cham: Springer International Publishing, pp. 77–97.
- Bigger, J.W. (1944) Treatment of staphylococcal infections with penicillin by intermittent sterilisation. *Lancet* **244**: 497–500.
- Black, D.S., Irwin, B., and Moyed, H.S. (1994) Autoregulation of *hip*, an operon that affects lethality due to inhibition of peptidoglycan or DNA synthesis. *J Bacteriol* **176**: 4081–4091.
- Black, D.S., Kelly, A.J., Mardis, M.J., and Moyed, H.S. (1991) Structure and organization of *hip*, an operon that affects lethality due to inhibition of peptidoglycan or DNA synthesis. *J Bacteriol* **173**: 5732–5739.
- Brauner, A., Fridman, O., Gefen, O., and Balaban, N.Q. (2016) Distinguishing between resistance, tolerance and persistence to antibiotic treatment. *Nat Rev Microbiol* **14**: 320–330.
- Darfeuille, F., Unoson, C., Vogel, J., and Wagner, E.G.H. (2007) An antisense RNA inhibits translation by competing with standby ribosomes. *Mol Cell* **26**: 381–392.
- Dörr, T., Lewis, K., and Vulic, M. (2009) SOS response induces persistence to fluoroquinolones in *Escherichia coli*. *PLoS Genet* **5**: e1000760.
- Dörr, T., Vulic, M., and Lewis, K. (2010) Ciprofloxacin causes persister formation by inducing the TisB toxin in *Escherichia coli*. *PLoS Biol* **8**: e1000317.
- Edelmann, D., and Berghoff, B.A. (2019) Type I toxin-dependent generation of superoxide affects the persister life cycle of *Escherichia coli*. *Sci Rep* **9**: 14256.
- Fernandez De Henestrosa, A.R., Ogi, T., Aoyagi, S., Chafin, D., Hayes, J.J., Ohmori, H., and Woodgate, R. (2000) Identification of additional genes belonging to the LexA regulon in *Escherichia coli*. *Mol Microbiol* **35**: 1560–1572.
- Fridman, O., Goldberg, A., Ronin, I., Shosh, N., and Balaban, N.Q. (2014) Optimization of lag time underlies antibiotic tolerance in evolved bacterial populations. *Nature* **513**: 418–421.
- Goormaghtigh, F., Fraikin, N., Putrinš, M., Hallaert, T., Hauryliuk, V., Garcia-Pino, A., et al. (2018) Reassessing the role of type II toxin–antitoxin systems in formation of *Escherichia coli* type II persister cells. *MBio* **9**: e00640-18.
- Gumev, P.A., Ortenberg, R., Dörr, T., Lewis, K., and Bezrukov, S.M. (2012) Persister-promoting bacterial toxin TisB produces anion-selective pores in planar lipid bilayers. *FEBS Lett* **586**: 2529–2534.
- Harms, A., Fino, C., Sørensen, M.A., Semsey, S., and Gerdes, K. (2017) Prophages and growth dynamics confound experimental results with antibiotic-tolerant persister cells. *MBio* **8**: e01964-17.
- Harms, A., Maisonneuve, E., and Gerdes, K. (2016) Mechanisms of bacterial persistence during stress and antibiotic exposure. *Science* **354**: aaf4268.
- Helaine, S., Cheverton, A.M., Watson, K.G., Faure, L.M., Matthews, S.A., and Holden, D.W. (2014) Internalization of *Salmonella* by macrophages induces formation of non-replicating persisters. *Science* **343**: 204–208.
- Hobby, G.L., Meyer, K., and Chaffee, E. (1942) Observations on the mechanism of action of Penicillin. *Proc Soc Exp Biol Med* **50**: 281–285.
- Jöers, A., Kaldalu, N., and Tenson, T. (2010) The frequency of persisters in *Escherichia coli* reflects the kinetics of awakening from dormancy. *J Bacteriol* **192**: 3379–3384.
- Kaldalu, N., Hauryliuk, V., Turnbull, K.J., La Mensa, A., Putrinš, M., and Tenson, T. (2020) *In vitro* studies of persister cells. *Microbiol Mol Biol Rev* **84**: e00070-20.
- Keren, I., Kaldalu, N., Spoering, A., Wang, Y., and Lewis, K. (2004) Persister cells and tolerance to antimicrobials. *FEMS Microbiol Lett* **230**: 13–18.
- Kim, J., Yamasaki, R., Song, S., Zhang, W., and Wood, T.K. (2018b) Single cell observations show persister cells wake based on ribosome content. *Environ Microbiol* **20**: 2085–2098.
- Kim, J.-S., Chowdhury, N., Yamasaki, R., and Wood, T.K. (2018a) Viable but non-culturable and persistence describe the same bacterial stress state. *Environ Microbiol* **20**: 2038–2048.
- Kim, J.-S., and Wood, T.K. (2016) Persistent persister misperceptions. *Front Microbiol* **7**: 2134.
- Korch, S.B., Henderson, T.A., and Hill, T.M. (2003) Characterization of the *hipA7* allele of *Escherichia coli* and evidence that high persistence is governed by (p)ppGpp synthesis. *Mol Microbiol* **50**: 1199–1213.
- Kotte, O., Volkmer, B., Radzikowski, J.L., and Heinemann, M. (2014) Phenotypic bistability in *Escherichia coli*'s central carbon metabolism. *Mol Syst Biol* **10**: 736.
- Kussell, E., and Leibler, S. (2005) Phenotypic diversity, population growth, and information in fluctuating environments. *Science* **309**: 2075–2078.
- Kwan, B.W., Valenta, J.A., Benedik, M.J., and Wood, T.K. (2013) Arrested protein synthesis increases persister-like cell formation. *Antimicrob Agents Chemother* **57**: 1468–1473.
- Lewis, K. (2010) Persister cells. *Annu Rev Microbiol* **64**: 357–372.

- Little, J.W. (1991) Mechanism of specific LexA cleavage: autodigestion and the role of RecA coprotease. *Biochimie* **73**: 411–422.
- Masachis, S., and Darfeuille, F. (2018) Type I toxin-antitoxin systems: regulating toxin expression via Shine-Dalgarno sequence sequestration and small RNA binding. In *Microbiol Spectr*: **6**(4). <https://dx.doi.org/10.1128/microbiolspec.RWR-0030-2018>.
- Mok, W.W.K., and Brynildsen, M.P. (2018) Timing of DNA damage responses impacts persistence to fluoroquinolones. *Proc Natl Acad Sci U S A* **115**: E6301–E6309.
- Mok, W.W.K., Park, J.O., Rabinowitz, J.D., and Brynildsen, M.P. (2015) RNA futile cycling in model persisters derived from MazF accumulation. *MBio* **6**: e01588-15.
- Moyed, H.S., and Bertrand, K.P. (1983) *hipA*, a newly recognized gene of *Escherichia coli* K-12 that affects frequency of persistence after inhibition of murein synthesis. *J Bacteriol* **155**: 768–775.
- Nyström, T. (2004) Stationary-phase physiology. *Annu Rev Microbiol* **58**: 161–181.
- Pennington, J.M., and Rosenberg, S.M. (2007) Spontaneous DNA breakage in single living *Escherichia coli* cells. *Nat Genet* **39**: 797–802.
- Pontes, M.H., and Groisman, E.A. (2019) Slow growth determines nonheritable antibiotic resistance in *Salmonella enterica*. *Sci Signal* **12**: eaax3938.
- Rotem, E., Loinger, A., Ronin, I., Levin-Reisman, I., Gabay, C., Shoshani, N., et al. (2010) Regulation of phenotypic variability by a threshold-based mechanism underlies bacterial persistence. *Proc Natl Acad Sci U S A* **107**: 12541–12546.
- Semanjski, M., Germain, E., Bratl, K., Kiessling, A., Gerdes, K., and Macek, B. (2018) The kinases HipA and HipA7 phosphorylate different substrate pools in *Escherichia coli* to promote multidrug tolerance. *Sci Signal* **11**: eaat5750.
- Shi, M., Wan, F., Mao, Y., and Gao, H. (2015) Unraveling the mechanism for the viability deficiency of *Shewanella oneidensis oxyR* null mutant. *J Bacteriol* **197**: 2179–2189.
- Song, S., and Wood, T.K. (2020) ppGpp ribosome dimerization model for bacterial persister formation and resuscitation. *Biochem Biophys Res Commun* **523**: 281–286.
- Spanka, D.-T., Konzer, A., Edelmann, D., and Berghoff, B.A. (2019) High-throughput proteomics identifies proteins with importance to postantibiotic recovery in depolarized persister cells. *Front Microbiol* **10**: 378.
- Stepanyan, K., Wenseleers, T., Duéñez-Guzmán, E.A., Muratori, F., Van den Bergh, B., Verstraeten, N., et al. (2015) Fitness trade-offs explain low levels of persister cells in the opportunistic pathogen *Pseudomonas aeruginosa*. *Mol Ecol* **24**: 1572–1583.
- Unoson, C., and Wagner, E.G.H. (2008) A small SOS-induced toxin is targeted against the inner membrane in *Escherichia coli*. *Mol Microbiol* **70**: 258–270.
- Van den Bergh, B., Fauvart, M., and Michiels, J. (2017) Formation, physiology, ecology, evolution and clinical importance of bacterial persisters. *FEMS Microbiol Rev* **41**: 219–251.
- Veening, J.-W., Smits, W.K., and Kuipers, O.P. (2008) Bistability, epigenetics, and bet-hedging in bacteria. *Annu Rev Microbiol* **62**: 193–210.
- Verstraeten, N., Knapen, W.J., Kint, C.I., Liebens, V., Van den Bergh, B., Dewachter, L., et al. (2015) Obg and membrane depolarization are part of a microbial bet-hedging strategy that leads to antibiotic tolerance. *Mol Cell* **59**: 9–21.
- Vogel, J. (2003) RNomics in *Escherichia coli* detects new sRNA species and indicates parallel transcriptional output in bacteria. *Nucleic Acids Res* **31**: 6435–6443.
- Vogel, J., Argaman, L., Wagner, E.G.H., and Altuvia, S. (2004) The small RNA IstR inhibits synthesis of an SOS-induced toxic peptide. *Curr Biol* **14**: 2271–2276.
- Völzing, K.G., and Brynildsen, M.P. (2015) Stationary-phase persisters to ofloxacin sustain DNA damage and require repair systems only during recovery. *MBio* **6**: e00731-15.
- Wilmaerts, D., Bayoumi, M., Dewachter, L., Knapen, W., Mika, J.T., Hofkens, J., et al. (2018) The persistence-inducing toxin HokB forms dynamic pores that cause ATP leakage. *MBio* **9**: e00744–e00718.

Supporting Information

Additional Supporting Information may be found in the online version of this article at the publisher's web-site:

Fig. S1. Total cell counts during lag phase.

Fig. S2. Single-cell lag time determination.

Fig. S3. Length distribution of wt and $\Delta\Delta$ cells during late stationary and exponential phase.

Fig. S4. Persister levels at different growth stages.

Fig. S5. Verification of persister assay parameters.

Fig. S6. The size of subpopulation A is affected by dilution of pre-cultures.

Fig. S7. Live-dead cell viability assay.

Fig. S8. Analysis of viability using spot assays.

Fig. S9. Viable cell counts during exponential phase.

Fig. S10. Flow cytometry analysis of late stationary-phase cultures with mannitol.

Fig. S11. Mannitol counteracts the prolonged lag phase of the $\Delta\Delta$ mutant.

Fig. S12. Expression levels of *tisB* under various conditions.

Fig. S13. Half-life determination of *tisB* +42 mRNA at late stationary phase.

Table S1. Strains and plasmids used in this study.

Table S2. Oligodeoxyribonucleotides used in this study.

**MANUSCRIPT 7: ELEVATED EXPRESSION OF TOXIN TISB
PROTECTS PERSISTENT CELLS AGAINST
CIPROFLOXACIN BUT ENHANCES
SUSCEPTIBILITY TO MITOMYCIN C**

Status: published 27/04/2021

Author's contributions: method validation, flow cytometry and cell concentration, data analysis of flow cytometry measurements, figure design, method writing, manuscript revision



Article

Elevated Expression of Toxin TisB Protects Persister Cells against Ciprofloxacin but Enhances Susceptibility to Mitomycin C

Daniel Edelmann ¹, Florian H. Leinberger ¹ , Nicole E. Schmid ¹, Markus Oberpaul ² , Till F. Schäberle ^{2,3,4} and Bork A. Berghoff ^{1,*}

- ¹ Institute for Microbiology and Molecular Biology, Justus Liebig University Giessen, 35392 Giessen, Germany; Daniel.B.Edelmann@bio.uni-giessen.de (D.E.); Florian.Leinberger@mikro.bio.uni-giessen.de (F.H.L.); Nicole.E.Schmid@mikro.bio.uni-giessen.de (N.E.S.)
- ² Branch for Bioresources, Fraunhofer Institute for Molecular Biology and Applied Ecology (IME), 35392 Giessen, Germany; Markus.Oberpaul@ime.fraunhofer.de (M.O.); Till.F.Schaeberle@agrar.uni-giessen.de (T.F.S.)
- ³ Institute for Insect Biotechnology, Justus Liebig University Giessen, 35392 Giessen, Germany
- ⁴ Partner Site Giessen-Marburg-Langen, German Center for Infection Research (DZIF), 35392 Giessen, Germany
- * Correspondence: bork.a.berghoff@mikro.bio.uni-giessen.de; Tel.: +49-641-99-35558



Citation: Edelmann, D.; Leinberger, F.H.; Schmid, N.E.; Oberpaul, M.; Schäberle, T.F.; Berghoff, B.A. Elevated Expression of Toxin TisB Protects Persister Cells against Ciprofloxacin but Enhances Susceptibility to Mitomycin C. *Microorganisms* **2021**, *9*, 943. <https://doi.org/10.3390/microorganisms9050943>

Academic Editor:
Muhammad Kamruzzaman

Received: 7 April 2021
Accepted: 23 April 2021
Published: 27 April 2021

Publisher's Note: MDPI stays neutral with regard to jurisdictional claims in published maps and institutional affiliations.



Copyright: © 2021 by the authors. Licensee MDPI, Basel, Switzerland. This article is an open access article distributed under the terms and conditions of the Creative Commons Attribution (CC BY) license (<https://creativecommons.org/licenses/by/4.0/>).

Abstract: Bacterial chromosomes harbor toxin-antitoxin (TA) systems, some of which are implicated in the formation of multidrug-tolerant persister cells. In *Escherichia coli*, toxin TisB from the *tisB/istR-1* TA system depolarizes the inner membrane and causes ATP depletion, which presumably favors persister formation. Transcription of *tisB* is induced upon DNA damage due to activation of the SOS response by LexA degradation. Transcriptional activation of *tisB* is counteracted on the post-transcriptional level by structural features of *tisB* mRNA and RNA antitoxin IstR-1. Deletion of the regulatory RNA elements (mutant $\Delta 1-41 \Delta istR$) uncouples TisB expression from LexA-dependent SOS induction and causes a ‘high persistence’ (*hip*) phenotype upon treatment with different antibiotics. Here, we demonstrate by the use of fluorescent reporters that TisB overexpression in mutant $\Delta 1-41 \Delta istR$ inhibits cellular processes, including the expression of SOS genes. The failure in SOS gene expression does not affect the *hip* phenotype upon treatment with the fluoroquinolone ciprofloxacin, likely because ATP depletion avoids strong DNA damage. By contrast, $\Delta 1-41 \Delta istR$ cells are highly susceptible to the DNA cross-linker mitomycin C, likely because the expression of SOS-dependent repair systems is impeded. Hence, the *hip* phenotype of the mutant is conditional and strongly depends on the DNA-damaging agent.

Keywords: toxin-antitoxin systems; DNA damage; SOS response; fluoroquinolones; mitomycin C; persistence

1. Introduction

Bacteria are equipped with numerous systems to sense environmental stress factors and transduce the perceived stress signals into adequate responses. These stress responses aim to repair the stress-induced damages, maintain essential cellular functions, and adjust the physiological status to the stressful situation. However, if stress levels are elevated, regular stress responses might not be sufficient to maintain survival. For such fatal situations, bacteria have evolved survival strategies that are based on the formation of stress-tolerant cells through phenotypic variation [1,2]. The corresponding subpopulations sacrifice their own propagation for the survival of the whole population, thereby increasing the overall fitness of the genotype in unpredictable environments [3].

The formation of stress-tolerant cells is often enhanced or triggered by stress, which also applies to persister cells [4–6]. Persister cells were first described in the 1940s [7,8], and are probably present in every bacterial population. They represent phenotypic variants

with increased tolerance to high concentrations of stressors, including antibiotics. While an antibiotic rapidly kills the sensitive part of a population, persister cells endure the treatment for a prolonged period. Therefore, the presence of persister cells is revealed by a characteristic biphasic killing curve [4,9]. Even though persister subpopulations are very heterogeneous in terms of persister formation mechanisms [10,11], major cellular processes are typically inhibited in persister cells, resulting in growth retardation and inactivation of antibiotic targets, often referred to as dormancy [6]. However, complete dormancy is not necessary for persister formation, and persister cells might retain metabolic activity [12–14]. In *Escherichia coli*, it was even observed that persisters actively extrude β -lactam antibiotics by efflux pumps, rather than rely on passive dormancy for protection [15].

The persistence mechanism might also strongly depend on the specific action of an antibiotic. Quinolone antibiotics, for example, inhibit topoisomerase II (gyrase) and IV, thereby causing double-strand breaks (DSBs). Bacteria respond to DSBs by induction of the SOS response. The RecBCD enzyme complex binds to double-stranded DNA ends and produces single-stranded 3' tails to enable loading with recombinase RecA, which initiates DSB repair via homologous recombination [16]. RecA-nucleofilaments subsequently trigger self-cleavage of the LexA repressor, leading to activation of the SOS response [17]. LexA-regulated genes contain a 20-bp LexA-box sequence in their promoter regions. The heterology index (HI) indicates the similarity of a particular LexA-box to the consensus sequence [18]. Genes that have a LexA-box with a low HI are tightly repressed by LexA and, hence, strongly induced upon LexA cleavage [19–21]. LexA regulates many genes with a function in DNA repair, but also the progression of cell division. For example, SulA inhibits cell division to extend the time that is needed for DNA repair [22]. When *E. coli* cultures are treated with DNA-damaging fluoroquinolones, persistence clearly depends on a functional SOS response, including specific DNA repair proteins [23,24]. Furthermore, SOS pre-induction by low fluoroquinolone levels supports persistence when antibiotic concentrations are subsequently increased [23,25]. SOS induction also plays an important role in persister survival during the post-antibiotic recovery phase after fluoroquinolone treatments [26–28].

Toxin-antitoxin (TA) systems are implicated in several processes, including stress adaptation, genomic stabilization, and phage abortive infection [29–31]. They are classified into different types according to the mechanism by which the antitoxin controls its cognate toxin [32]. TA systems are also suspected to halt cell growth and directly favor persister formation under stress conditions. Indeed, the SOS-induced toxin gene *tisB* from the type I TA system *tisB/istR-1* was shown to influence persistence upon DNA damage in *E. coli* [25,33,34]. The LexA-box in the promoter region of *tisB* has a very low HI and transcription is, therefore, strongly induced under DNA-damaging conditions [35]. However, translation is tightly regulated by the 5' untranslated region (UTR) of *tisB* mRNA and RNA antitoxin IstR-1. The primary *tisB* transcript (+1 mRNA) is translationally inactive due to a 5' UTR structure, which sequesters a so-called ribosome standby site (RSS) and thus prevents pre-loading of the 30S ribosomal subunit [36]. Upon processing of the primary transcript to the +42 mRNA, the RSS becomes accessible for 30S binding, which is promoted by a pseudoknot at the +42 mRNA 5' end and ribosomal protein S1 [37,38]. However, under non-stress conditions, translation is counteracted by binding of antitoxin IstR-1 to the RSS. Upon IstR-1 binding, the RNA duplex is cleaved by RNase III, and the resulting +106 mRNA is translationally inactive [36,39]. The two regulatory RNA elements (5' UTR structure in *tisB* +1 mRNA and antitoxin IstR-1) clearly restrict TisB expression to stress conditions [25,40–42]. TisB is a small hydrophobic protein with a length of 29 amino acids. It is located in the cytoplasmic membrane and causes the breakdown of the proton motive force, which leads to membrane depolarization and ATP depletion [25,43,44]. Since ATP depletion favors persister formation [45,46], depolarization and subsequent ATP depletion tentatively explain TisB-dependent persistence upon ciprofloxacin (Cip) treatment [25,33].

In *E. coli* wild-type cultures, TisB-dependent depolarization was only observed after prolonged Cip treatment. However, deletion of the two regulatory RNA elements (mutant

$\Delta 1-41 \Delta istR$) increased the likelihood of depolarization, even when cultures were treated with low doses of Cip [25]. Furthermore, the $\Delta 1-41 \Delta istR$ mutant has a ‘high persistence’ (*hip*) phenotype for different antibiotics during the exponential phase [25,47,48]. We have recently observed that TisB expression is uncoupled from SOS induction in the $\Delta 1-41 \Delta istR$ mutant and that the *hip* phenotype originates from LexA-independent TisB expression during the late stationary phase [42]. Here, we show that elevated TisB levels impede the expression of SOS genes, likely due to global inhibition of cellular processes. Treatment with Cip is tolerated by preventing strong DNA damage. By contrast, treatment with the DNA cross-linker mitomycin C (MMC) efficiently eradicates persisters in $\Delta 1-41 \Delta istR$ cultures. Our study demonstrates that the *hip* phenotype is conditional, and that post-transcriptional regulation of *tisB* likely ensures maximal fitness under a variety of environmental conditions.

2. Materials and Methods

2.1. Growth Conditions

All strains used in this study were derived from *E. coli* K-12 wild type MG1655 (Table S1) and grown in lysogeny broth (LB) at 37 °C with orbital shaking (180 rpm). If applicable, selection makers were added at the following concentrations: 200 $\mu\text{g mL}^{-1}$ ampicillin, 50 $\mu\text{g mL}^{-1}$ kanamycin, 15 $\mu\text{g mL}^{-1}$ chloramphenicol, and 6 $\mu\text{g mL}^{-1}$ tetracycline. Inoculation was performed by transferring a single colony into a fresh medium and incubating overnight. Pre-cultures were diluted 100-fold into fresh LB medium. Optical density measurements at 600 nm (OD_{600}) were applied to monitor growth using a Cell density meter model 40 (Fisher Scientific, Schwerte, Germany).

2.2. Plasmid and Strain Construction

For the construction of pBAD-*syfp2*, the *syfp2* gene was PCR-amplified using primers *syfp2*-for-Eco and *syfp2*-rev-Hind. A modified pBAD vector [43] was amplified with primers *topo-fw-Hind* and *topo-rev-Eco*. PCR products were digested with EcoRI and HindIII (FastDigest; Thermo Fisher Scientific, Schwerte, Germany) and ligated using T4 DNA ligase (New England Biolabs, Ipswich, MA, USA). The final construct was confirmed by sequencing (Microsynth SeqLab, Göttingen, Germany). Chromosomal deletions and *syfp2* fusions were constructed using the heat-inducible λ red system as described in detail elsewhere [25,47,49,50]. If applicable, chromosomal deletions were moved to recipient strains using P1 transduction. Target-specific screening PCRs were performed to confirm chromosomal constructs. All primers for plasmid and strain construction are listed in Table S2.

2.3. Microplate Reader Experiments

Reporter strains containing chromosomal *syfp2* constructs were grown in LB medium and treated with Cip (0.1 $\mu\text{g mL}^{-1}$; 10 \times MIC) or MMC (4 \times MIC; MG1655: 2.5 $\mu\text{g mL}^{-1}$; $\Delta 1-41 \Delta istR$: 10 $\mu\text{g mL}^{-1}$) during the exponential phase (OD_{600} of ~0.4). sYFP2 expression from plasmid pBAD-*syfp2* was induced with 0.2% L-arabinose (L-ara) at indicated time points. For recovery experiments, Cip was removed by washing with 0.9% NaCl, and dilution of cells into a fresh medium. Cell numbers were adjusted to corresponding persister levels. Incubation was performed with continuous shaking at 37 °C in an Infinite M Nano⁺ microplate reader (Tecan, Männedorf, Switzerland) using transparent 96-well plates (Greiner Bio-One, Frickenhausen, Germany). sYFP2 fluorescence was monitored with excitation and emission wavelengths of 510 and 540 nm, respectively. The gain was set to 90 for chromosomal *syfp2* constructs, and to 50 for pBAD-*syfp2*. Optical density was measured at 600 nm. For chromosomal *syfp2* reporter strains, fluorescence values were background-corrected (LB auto-fluorescence) and normalized to OD_{600} . Fluorescence values from pBAD-*syfp2* expression experiments were normalized to OD_{600} .

2.4. Microscopy

Microscopy experiments were performed with a Leica DMI 6000 B inverse microscope (Leica Camera AG, Wetzlar, Germany) using an HCX PL APO 100×/1.4 differential interference contrast (DIC) objective. Images were recorded with a pco.edge sCMOS camera (PCO AG, Kelheim, Germany). For fluorescence images, a custom filter set (T495lpxr, ET525/50m; Chroma Technology, Bellows Falls, VT, USA) was applied. The VisiView software (Visitron Systems GmbH, Puchheim, Germany) was used for image recording and images were processed with the ImageJ-based Fiji tool (version 1.52p).

2.5. Flow Cytometry

Cell samples were withdrawn during the exponential phase (OD_{600} of ~0.4) and at indicated time points, washed with 1× PBS, fixed with paraformaldehyde (4% in 1× PBS) for 30 min on ice, and stored at 4 °C until measurements. Flow cytometry experiments were performed with a FACSCalibur (BD Bioscience, San Jose, CA, USA) using the CellQuest Pro 4.0.2 (BD) software. Samples were acquired using the forward scatter (Amp: 10^2 , Amp gain: 1.00), side scatter (500 V, Amp gain: 1.00) to exclude debris and a fluorescence detector FL1-H (excitation: 488 nm, emission: 530 nm, 500 V, Amp gain: 1.00) for the relative quantification of sYFP2 signals. Analysis was performed with normalized data sets (DownSample 2.0.0 plugin; 10,000 events) using FlowJo v. 10.6.2 (BD). R package *ggplot2* (version 3.3.2) with function *geom_density* and count variables was used to draw smoothed distribution plots.

2.6. Persister Assays

Pre-cultures for persister assays were incubated for 20 h in LB medium. If applicable, appropriate selection markers were added. Experimental cultures were prepared by 100-fold dilutions of overnight cultures into fresh LB medium without additives and incubated until the exponential phase was reached (OD_{600} of ~0.4). Treatments were performed with Cip at a final concentration of $1 \mu\text{g mL}^{-1}$ (100× MIC), or MMC at final concentrations of $10 \mu\text{g mL}^{-1}$ (4× MIC) for MG1655 or $2.5 \mu\text{g mL}^{-1}$ (4× MIC) for $\Delta 1-41 \Delta \text{istR}$ for six hours. Pre- and post-treatment samples were withdrawn and serial dilutions (in 0.9% NaCl) were plated on LB agar plates supplemented with 20 mM MgSO_4 . Colony counts were determined after 24 h and 40 h for pre- and post-treatment samples, respectively, in order to calculate persister levels.

2.7. ATP Measurements

ATP levels were determined as previously described [42] using the BacTiter-Glo Microbial Cell Viability Assay (Promega, Madison, WI, USA). Relative light units (RLU) were background-corrected (plain LB medium) and normalized to OD_{600} .

2.8. DNA Damage Assay

Strains harboring pBAD-*syfp2* plasmids were grown to the exponential phase (OD_{600} of ~0.4) and treated with Cip ($0.1 \mu\text{g mL}^{-1}$; 10× MIC) for two hours. Plasmid DNA from 20 mL culture was extracted using the NucleoSpin Plasmid purification kit (Macherey-Nagel, Düren, Germany) according to the manufacturer's instructions. Then, 200 ng DNA were linearized by HindIII (FastDigest; Thermo Fisher Scientific, Schwerte, Germany) digestion at 37 °C for four hours and separated on 0.7% agarose gels containing 1× TBE. GeneRuler 1 kb Plus DNA ladder (Thermo Fisher Scientific, Schwerte, Germany) was used as a size marker. DNA was detected by ethidium bromide staining.

2.9. RNA Methods

The hot acid-phenol method was applied to isolate total RNA as described [35]. The quality of ribosomal RNA was assessed on 1% agarose gels, containing 1× TBE and 25 mM guanidinium thiocyanate, followed by staining with ethidium bromide. For quantitative RT-PCR (qRT-PCR), DNA-free RNA was isolated using the NucleoSpin RNA kit according

to the manufacturer's protocol (Macherey-Nagel, Düren, Germany). The Brilliant III Ultra-Fast SYBR Green QRT-PCR Master Mix (Agilent Technologies, Santa Clara, CA, USA) was applied using DNA-free RNA in a final concentration of 1 ng μL^{-1} . The CFX Connect Real-Time System (Bio-Rad, Hercules, CA, USA) and the CFX Maestro Software (Bio-Rad) were used to determine cycle threshold (Ct) values. Relative transcript levels [51] were determined using either *hcaT* (exponential-phase samples) or *cysG* (Cip-treated samples) as reference for normalization [35,52]. Primers for qRT-PCR can be found in Table S2.

2.10. Western Blot Analysis

For immunodetection of 3 \times FLAG-TisB, cell samples were harvested by centrifugation (11,000 $\times g$, 3 min) and resuspended in SDS sample buffer. Samples were incubated at 95 °C for 5 min and subsequently subjected to Tricine-SDS-PAGE followed by semi-dry electroblotting [53]. Proteins were blotted onto PVDF membranes (Immobilon-P, 0.45 μm ; Merck, Darmstadt, Germany). 3 \times FLAG-tagged proteins were detected using a monoclonal ANTI-FLAG M2-Peroxidase (HRP) antibody (Merck, Darmstadt, Germany). Further details were described previously [42].

2.11. Statistical Analysis

Statistical analysis was performed using R statistical language (Version 3.6.0; <https://www.r-project.org/>; date accessed: 5 July 2019). Two-tailed Welch's *t*-test was performed on log₁₀-transformed data. Normality was assessed using the Shapiro–Wilk test. *p*-value adjustment was performed by pairwise comparison according to the Holm–Bonferroni method (*p*-values < 0.05 were considered as significant). For statistical analysis of flow cytometry data, Van der Waerden test with a post-hoc pairwise comparison was applied using package PMCMR (*p*-values < 0.001 were considered as significant).

3. Results

3.1. Persisters in Mutant $\Delta 1-41 \Delta istR$ Neither Experience Strong DNA Damage nor Rely on Double-Strand Break Repair upon Ciprofloxacin Treatment

We have recently observed that persister cells in exponential-phase cultures of mutant $\Delta 1-41 \Delta istR$ (from now on $\Delta\Delta$) are carried over from stationary phase, where they are formed due to SOS-independent TisB expression. Hence, the *hip* phenotype of this mutant does not depend on SOS induction through LexA degradation, as shown by experiments with the non-cleavable LexA variant LexA3 [42]. However, it was not addressed whether $\Delta\Delta$ persisters experience DNA damage or rely on DNA repair mechanisms. Since the *hip* phenotype of mutant $\Delta\Delta$ is best documented in the exponential phase [25,42,47,48], we performed Cip treatments when an optical density at 600 nm (OD₆₀₀) of ~0.4 was reached. Mutant $\Delta\Delta$ was compared to its parental strain *E. coli* K-12 wild type MG1655. From *E. coli* wild-type persisters it is known that activation of the SOS response and repair of DNA damage is especially important for survival during the early recovery phase after fluoroquinolone treatments [26–28]. Therefore, we tested the activation of the SOS response in $\Delta\Delta$ cultures during post-antibiotic recovery by measuring a transcriptional *sulA-syfp2* reporter fusion, which is a valuable read-out for SOS induction [26,28]. Cells were treated with Cip for two hours, washed, diluted into a fresh medium, and transferred to microtiter plates to measure growth (OD₆₀₀) and sYFP2 fluorescence over time. Immediately after the transfer, wild-type cultures scored high fluorescence values of ~12,000 arbitrary units (a.u.). By contrast, fluorescence values in $\Delta\Delta$ cultures were quite low (<500 a.u.; Figure 1A). This considerable difference was due to high *sulA-syfp2* expression in wild-type cultures after two hours of Cip treatment (Figure S1). Shortly after the transfer, wild-type cultures exhibited a further increase in sYFP2 fluorescence, reaching ~34,000 a.u. after six hours of recovery. Maximum sYFP2 fluorescence preceded growth resumption by one hour, as judged from an increase in OD₆₀₀ at around seven hours recovery (Figure 1A). Upon growth resumption, sYFP2 fluorescence steadily declined over time. These findings were consistent with single-cell observations of *E. coli* wild-type persisters treated with the

fluoroquinolone ofloxacin during the exponential phase [28]. The $\Delta\Delta$ mutant showed a very different pattern. First, growth resumption after Cip treatment was clearly shifted to a later time point (from ~7 to ~13 h recovery; Figure 1A). We have recently observed that the lag phase after dilution of stationary-phase cultures was extended by ~60 min in mutant $\Delta\Delta$ compared to wild type [42]. The six-hour shift in growth resumption, as observed here (Figure 1A), clearly confirms the delayed post-antibiotic recovery of $\Delta\Delta$ cells [25,47,48]. Second, sYFP2 fluorescence stayed at a low level over the whole recovery period (Figure 1A). Hence, the $\Delta\Delta$ mutant did not induce the SOS response during recovery.

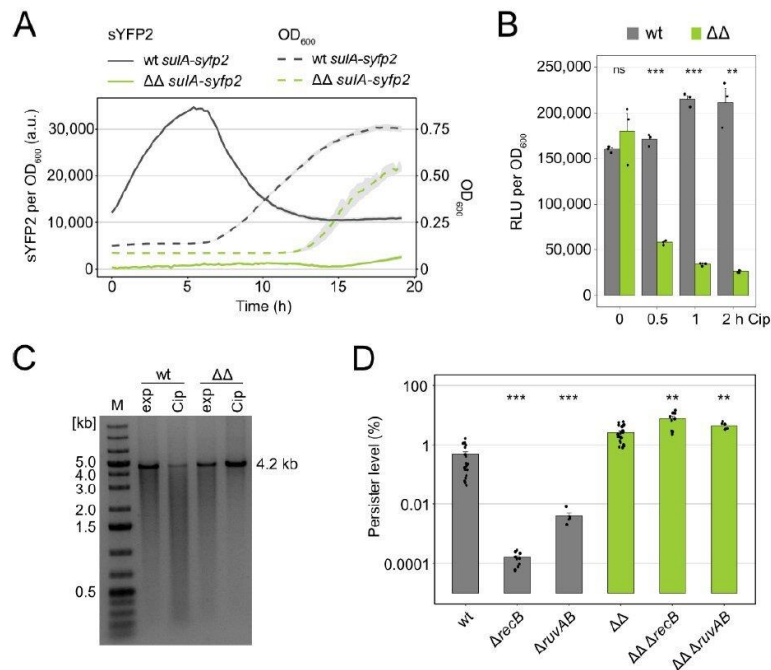


Figure 1. DSB repair is not crucial for persisters of mutant $\Delta 1-41 \Delta istR$. **(A)** SOS induction during recovery. Strains were treated with Cip ($0.1 \mu\text{g mL}^{-1}$; $10\times$ MIC) for two hours during the exponential phase (OD_{600} of ~ 0.4). Cip was removed by washing, cells were resuspended in a fresh medium and transferred to 96-well plates. Growth (dotted lines) and sYFP2 fluorescence from chromosomal *sulA-syfp2* fusions (solid lines) were monitored in a microplate reader. Fluorescence measurements were normalized to the corresponding OD_{600} measurements. Data represent the mean (colored lines) and SEM (grey ribbon; $n = 3$). **(B)** ATP levels were determined by a luciferase-based assay upon treatment with Cip ($0.1 \mu\text{g mL}^{-1}$; $10\times$ MIC). Relative light units (RLU) were background-corrected and normalized to OD_{600} . Bars represent the mean (\pm SEM; $n = 3$). A pairwise *t*-test was performed to compare wt and $\Delta\Delta$ at each time point (ns: not significant, $** p < 0.01$, $*** p < 0.001$). Black dots indicate the results of individual biological experiments. **(C)** Linearized plasmid DNA was analyzed on an agarose gel. Plasmid DNA was extracted from cultures in exponential phase (exp, OD_{600} of ~ 0.4) and after two hours of Cip treatment ($0.1 \mu\text{g mL}^{-1}$; $10\times$ MIC). A marker (M) in kb is shown on the left-hand side. **(D)** Colony counts were determined before and after six hours of Cip treatment ($1 \mu\text{g mL}^{-1}$; $100\times$ MIC) to calculate persister levels. Bars represent the mean (\pm SEM; $n \geq 6$). A pairwise *t*-test was performed to compare *recB* and *ruvAB* deletions to their parental strains ($** p < 0.01$, $*** p < 0.001$). (wt: wild type MG1655; $\Delta\Delta$: $\Delta 1-41 \Delta istR$). Black dots indicate the results of individual biological experiments.

Our observations raised the question of whether $\Delta\Delta$ persisters experienced strong DNA damage at all. TisB expression causes ATP depletion [43], and ATP depletion itself was shown to avoid Cip-induced DSBs [45]. We first assessed ATP levels by a luciferase-based assay. In wild-type cultures, ATP levels stayed stable or were even slightly increased (1.3-fold), during the first two hours of Cip treatment (Figure 1B). In $\Delta\Delta$ cultures, ATP levels dropped by ~3-fold already after 30 min and by ~7-fold after two hours (Figure 1B). These findings support the prevailing model that TisB-dependent depolarization leads to ATP depletion [25,33,43,44]. To assess the occurrence of DSBs, plasmid DNA was extracted from wild-type and $\Delta\Delta$ cells before and after two hours of Cip treatment. The integrity of linearized plasmids was analyzed on agarose gels. Wild-type cells had a clear reduction in full-length plasmids and an increased fraction of shorter fragments, indicative of Cip-induced DSBs (Figure 1C). By contrast, $\Delta\Delta$ cells mainly contained full-length plasmids (Figure 1C), suggesting that $\Delta\Delta$ cells did not experience strong DNA damage. However, a time-course experiment indicated that minor DNA damage might occur in $\Delta\Delta$ cells at least during the first 30 min of Cip treatment (Figure S2).

Together, the above data suggested that $\Delta\Delta$ persisters do not rely on DNA repair in order to survive a Cip treatment. To test this possibility, persister assays were performed with *recB* and *ruvAB* deletion strains. Both the RecBCD enzyme complex and the RuvAB Holliday junction complex are important components of DSB repair via homologous recombination. Deletion of *recB* and *ruvAB* in the wild-type background reduced persister levels upon Cip treatment by more than 3000-fold and 100-fold, respectively (Figure 1D). Similar results were already obtained in other studies [23,24]. By contrast, in the $\Delta\Delta$ background, persister levels even slightly increased due to the *recB* and *ruvAB* deletions (Figure 1D). These experiments demonstrated that $\Delta\Delta$ persisters do not rely on DSB repair. We note that the persister level of ~3% in $\Delta\Delta$ cultures (Figure 1D) does not reflect the population-wide protection against DNA damage (Figure 1C). We speculate that most $\Delta\Delta$ cells die due to Cip-induced TisB overexpression (see Discussion) but cannot exclude the involvement of other factors.

3.2. TisB Overexpression in Mutant $\Delta 1-41 \Delta istR$ upon Ciprofloxacin Treatment

The *tisB* promoter is very sensitive to DNA damage [21,35], and even minor DNA damage, as observed early during a Cip treatment (Figure S2), is expected to cause *tisB* transcription in $\Delta\Delta$ cells. Indeed, increased *tisB* +42 mRNA levels were observed in the $\Delta\Delta$ mutant upon Cip treatment [25]. Due to the lack of post-transcriptional *tisB* repression in mutant $\Delta\Delta$ (Figure 2A), increased TisB protein levels can be expected as well. Chromosomal insertion of a 3×FLAG sequence into the *tisB* gene (between codon 2 and 3) allowed us to detect 3×FLAG-TisB expressed from the $\Delta\Delta$ locus upon treatment with the DNA-damaging antibiotic Cip. Importantly, the N-terminal 3×FLAG-tag does not affect TisB localization or functionality [43]. Western blot analysis revealed that expression of 3×FLAG-TisB from the $\Delta\Delta$ locus was comparable to induction of 3×FLAG-TisB from plasmid p+42-3×FLAG-*tisB* [43] using L-arabinose (L-ara) as an inducer (Figure 2B). Hence, Cip treatment caused overexpression of TisB in the $\Delta\Delta$ mutant. Since ectopic overexpression of TisB causes rRNA degradation [43,47], we isolated total RNA from wild-type and $\Delta\Delta$ cultures. Progressive rRNA degradation was observed in $\Delta\Delta$ cultures after 60 min of Cip treatment, while rRNA remained intact for 180 min in wild-type cultures (Figure 2C). These data demonstrated that $\Delta\Delta$ cells were clearly affected by elevated levels of the membrane-targeting toxin TisB.

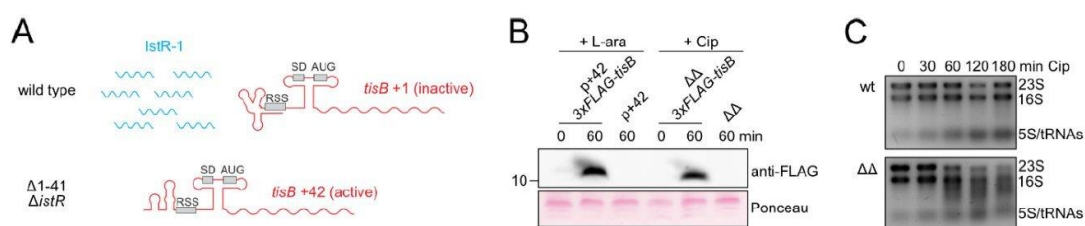


Figure 2. TisB overexpression in mutant $\Delta 1-41 \Delta istR$. (A) Graphical illustration of RNA species expressed from the *tisB/istR-1* system. In the wild type, RNA antitoxin IstR-1 and the translationally inactive *tisB +1* mRNA are present. In mutant $\Delta\Delta$, transcription from the LexA-dependent promoter produces the translationally active *tisB +42* mRNA. (B) Western blot analysis of 3 \times FLAG-TisB, either expressed from plasmid p+42-3 \times FLAG-*tisB* by addition of L-ara (0.2%), or from the $\Delta\Delta$ -3 \times FLAG-*tisB* locus by addition of Cip (0.1 $\mu\text{g mL}^{-1}$; 10 \times MIC) for 60 min. Total protein was separated by Tricine-SDS-PAGE. 3 \times FLAG-TisB was detected using an anti-FLAG antibody. Constructs without 3 \times FLAG sequence served as specificity controls. Western membranes were stained with Ponceau as a loading control. (C) Total RNA was isolated during exponential phase (OD_{600} of ~ 0.4) and at different time points during Cip treatment (0.1 $\mu\text{g mL}^{-1}$; 10 \times MIC). RNA quality was analyzed on agarose gels. rRNAs (23S, 16S, and 5S) and tRNAs are indicated. (wt: wild type MG1655; $\Delta\Delta$: $\Delta 1-41 \Delta istR$).

3.3. Major Cellular Processes Are Inhibited in Mutant $\Delta 1-41 \Delta istR$ upon Ciprofloxacin Treatment

It has been shown that ectopic overexpression of TisB causes rapid shutdown of major cellular processes, including transcription and translation [43], likely affecting global gene expression. Here, induction of the *syfp2* gene from plasmid pBAD-*syfp2* was monitored to evaluate gene expression in the $\Delta\Delta$ mutant upon Cip treatment. Cells were exposed to Cip and subsequently treated with L-ara to induce the *syfp2* gene at different time points during the Cip treatment. In wild-type cultures, the addition of L-ara caused an immediate increase in sYFP2 fluorescence, even after five hours of Cip treatment (Figure 3A). By contrast, when L-ara was added to $\Delta\Delta$ cultures at the beginning of the Cip treatment, the increase in sYFP2 fluorescence was clearly diminished (Figure 3B). More intriguingly, an increase in sYFP2 fluorescence was absent in $\Delta\Delta$ cultures when L-ara was added as early as 30 min after the onset of Cip treatment (Figure 3B).

To test whether this complete shutdown of gene expression already occurred on the level of transcription, mRNA levels of *syfp2* were monitored using quantitative RT-PCR. Under non-stress conditions, *syfp2* mRNA levels were strongly induced (~ 1370 -fold) by L-ara in both wild-type and $\Delta\Delta$ cultures (Figure 3C). By contrast, 60 min after Cip treatment, *syfp2* mRNA levels were not inducible at all in $\Delta\Delta$ cultures, while wild-type cultures still showed strong induction (~ 1160 -fold). We conclude that TisB overexpression either completely shuts down transcription or interferes with the uptake of L-ara, which seems plausible since uptake systems depend on either the proton gradient (AraE) or ATP (AraFGH), both of which are exhausted by the action of TisB [25,43,44]. In a control experiment, cultures were pre-treated with L-ara for 30 min, to enable maximum uptake of the inducer, and only subsequently exposed to Cip. Wild-type cultures exhibited a steadily increasing sYFP2 fluorescence. In $\Delta\Delta$ cultures, sYFP2 signals increased for ~ 75 min at a rate that was comparable to the wild type. Afterward, the increase in sYFP2 fluorescence was clearly reduced, but not completely abolished (Figure 3D). When $\Delta\Delta$ cells were treated with L-ara alone, sYFP2 fluorescence steadily increased over time, reaching maximum levels comparable to wild-type experiments (Figure 3D). Treatment with Cip alone did not cause an increase in sYFP2 fluorescence, demonstrating that Cip itself had no influence on the reporter (Figure 3D). In summary, we conclude that TisB overexpression in $\Delta\Delta$ cultures causes the shutdown of energy-dependent transport processes due to membrane depolarization and ATP depletion, which completely hinders L-ara uptake already after ~ 30 min of Cip treatment. Upon ongoing TisB overexpression (after ~ 75 min), gene expression is negatively affected, likely due to a shortage of ATP.

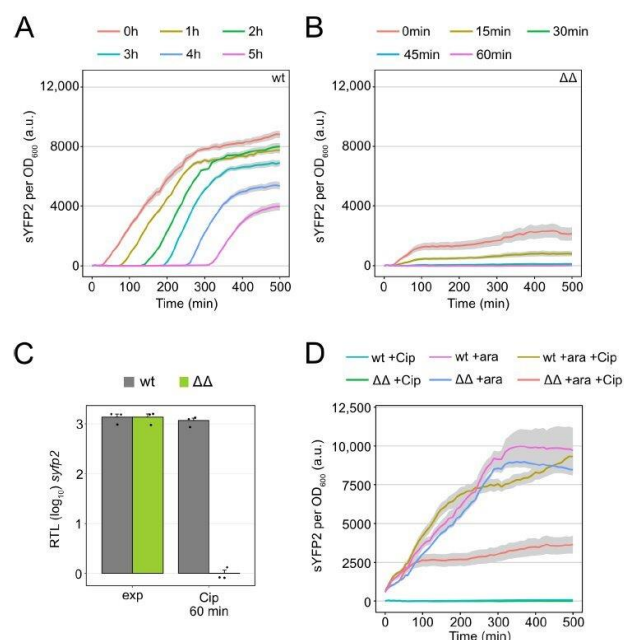


Figure 3. Gene expression is inhibited in mutant $\Delta 1-41 \Delta istR$ upon ciprofloxacin. (A,B) sYFP2 fluorescence from plasmid pBAD-*syfp2* was monitored in a microplate reader. Strains wt pBAD-*syfp2* (A) and $\Delta\Delta$ pBAD-*syfp2* (B) were treated with Cip ($0.1 \mu\text{g mL}^{-1}$; $10\times$ MIC) during the exponential phase (OD_{600} of ~ 0.4), which corresponds to time point 0 min. sYFP2 expression was induced by adding 0.2% L-Ara at the indicated time points during Cip treatment. Fluorescence measurements were normalized to the corresponding OD_{600} measurements. Data represent the mean (colored lines) and SEM (grey ribbons; $n = 3$). (C) Relative transcript levels (RTL, \log_{10}) were calculated by qRT-PCR to assess *syfp2* induction upon treatment with L-ara. RNA samples were collected before and 30 min after induction with 0.2% L-ara, either during the exponential phase (exp, OD_{600} of ~ 0.4) or after 60 min of Cip treatment ($0.1 \mu\text{g mL}^{-1}$; $10\times$ MIC). Bars represent the mean (\pm SEM; $n = 3$). Black dots indicate the results of individual biological experiments. (D) sYFP2 fluorescence from plasmid pBAD-*syfp2* was monitored in a microplate reader. sYFP2 expression was induced by 0.2% L-Ara (+ara) 30 min before treatment with Cip ($0.1 \mu\text{g mL}^{-1}$; $10\times$ MIC). Treatments with L-ara or Cip alone served as controls. Fluorescence measurements were normalized to the corresponding OD_{600} measurements. Data represent the mean (colored lines) and SEM (grey ribbons; $n = 3$). (wt: wild type MG1655; $\Delta\Delta$: $\Delta 1-41 \Delta istR$).

Conclusions drawn from toxin overexpression experiments might not directly apply to the wild-type situation. In order to show that the negative influence of TisB on gene expression also occurs in the wild type, a *tisB* deletion strain was investigated. Measurements with the inducible *syfp2* reporter system (plasmid pBAD-*syfp2*) demonstrated that the *tisB* deletion strain scored higher sYFP2 fluorescence values than the wild type, which was particularly evident after prolonged treatment with Cip (Figure S3). These data suggest that, in wild-type cells, increasing TisB amounts inhibit gene expression upon extended periods of DNA damage.

3.4. High TisB Levels Counteract Expression of SOS Genes

We have so far shown that the $\Delta\Delta$ mutant strongly produces TisB upon Cip treatment (Figure 2B), likely due to minor DNA damage (Figure S2), and that strong TisB production is linked to an overall reduction in gene expression (Figure 3). It remains, however, unknown to which extent other SOS genes are induced in the $\Delta\Delta$ mutant. In order to assess Cip-dependent SOS induction, the transcriptional *sulA-syfp2* reporter fusion was applied. A

steady, population-wide increase in sYFP2 fluorescence from the *sulA* locus was detected only in wild-type cultures, as revealed by flow cytometry (Figure 4A). After two hours of Cip treatment, the median sYFP2 fluorescence had increased significantly (~61-fold). These findings were supported by sYFP2 measurements with another SOS reporter construct (*dinB-syfp2*; Figure S1). The $\Delta\Delta$ mutant only exhibited a very slight, albeit significant, increase in sYFP2 fluorescence of ~2-fold during the first hour of Cip treatment, but median fluorescence values stayed stable afterward (Figure 4A). We note that the one-hour time frame of sYFP2 production from the *sulA-syfp2* reporter in $\Delta\Delta$ cells perfectly matches our observations with the inducible *syfp2* system (Figure 3). Furthermore, fluorescence microscopy revealed that Cip-induced and SulA-dependent cell filamentation [54,55] was absent in $\Delta\Delta$ cultures (Figure 4B). The filamentation phenotype was restored by ectopic overexpression of antitoxin IstR-1 in $\Delta\Delta$ (Figure S4), suggesting that lack of filamentation in $\Delta\Delta$ cultures was due to a TisB-dependent defect in SulA expression.

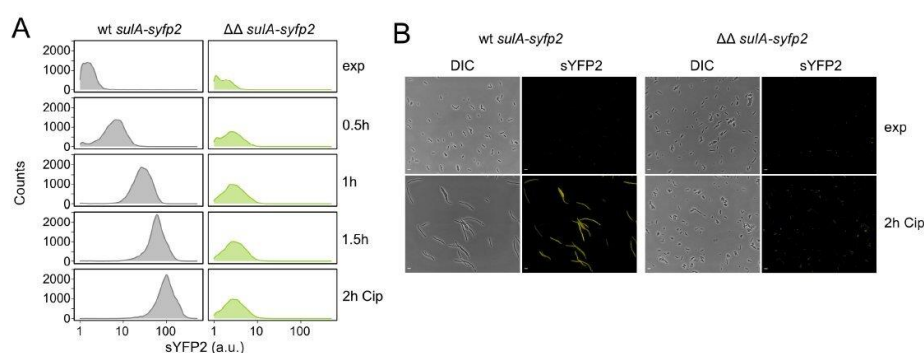


Figure 4. Inhibition of *sulA* expression in mutant $\Delta 1-41 \Delta \text{istR}$ upon ciprofloxacin. **(A)** Flow cytometry analysis of *sulA-syfp2* fusion strains treated with Cip. Cell samples were taken during the exponential phase (exp, OD_{600} of ~0.4) and at indicated time points of Cip treatment ($0.1 \mu\text{g mL}^{-1}$; $10\times$ MIC). Event counts were normalized to 10,000 events. **(B)** Differential interference contrast (DIC) and fluorescence (sYFP2) microscopy images of strains harboring chromosomal *sulA-syfp2* fusions during exponential phase (exp, OD_{600} of ~0.4) and after two hours of Cip treatment ($0.1 \mu\text{g mL}^{-1}$; $10\times$ MIC). Scale bars indicate $5 \mu\text{m}$. (wt: wild type MG1655; $\Delta\Delta$: $\Delta 1-41 \Delta \text{istR}$).

3.5. The Hip Phenotype of Mutant $\Delta 1-41 \Delta \text{istR}$ Is Lost upon Treatment with the DNA Cross-Linker Mitomycin C

Tolerance to Cip in $\Delta\Delta$ persisters does not depend on DSB repair due to the prevention of strong DNA damage (Figure 1). We were curious whether the *hip* phenotype of the $\Delta\Delta$ mutant would still occur when cells were treated with MMC. MMC is a potent DNA cross-linker, which is effective against persisters from different bacterial species [56]. The MIC for MMC was four-fold higher in the wild type compared to the $\Delta\Delta$ mutant ($2.5 \mu\text{g/mL}$ versus $0.625 \mu\text{g/mL}$, respectively; Figure S5). For persister assays, the MMC concentration was adjusted to $4\times$ MIC ($10 \mu\text{g/mL}$ for wild type and $2.5 \mu\text{g/mL}$ for $\Delta\Delta$). In both strains, MMC was more effective against persisters than Cip (Figure 5A). However, in $\Delta\Delta$ cultures, the persister level was ~15-fold lower than in wild-type cultures (0.004% versus 0.06%, respectively; Figure 5A), demonstrating that the $\Delta\Delta$ mutant was highly susceptible to MMC. Similar to what was observed upon Cip treatment, SOS induction (as measured by the *sulA-syfp2* reporter fusion) was largely suppressed in the $\Delta\Delta$ mutant upon MMC treatment (Figure 5B), and induction was also not observed in the post-antibiotic recovery phase (data not shown). Furthermore, inhibition of gene expression (as measured by pBAD-*syfp2*) occurred in MMC-treated $\Delta\Delta$ cells (Figure 5C). These data suggest that $\Delta\Delta$ persisters fail to survive an MMC treatment due to their inability to induce the SOS response. In this particular case, and in contrast to Cip (Figure 5A), $\Delta\Delta$ cells are even more likely to perish than wild-type cells.

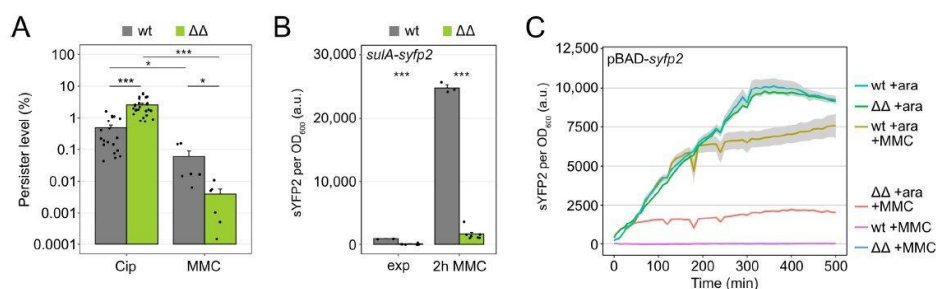


Figure 5. Mutant $\Delta 1-41 \Delta istR$ is highly susceptible to mitomycin C. (A) Colony counts were determined before and after six hours of Cip ($1 \mu\text{g mL}^{-1}$; $100\times$ MIC) or MMC treatment (wt: $10 \mu\text{g mL}^{-1}$; $\Delta\Delta$: $2.5 \mu\text{g mL}^{-1}$; $4\times$ MIC). Colony counts were used to calculate persister levels. Bars represent the mean (\pm SEM; $n \geq 6$). A pairwise *t*-test was performed to compare persister levels (* $p < 0.05$, *** $p < 0.001$). Black dots indicate the results of individual biological experiments. (B) sYFP2 fluorescence from a chromosomal *sulA-syfp2* fusion was monitored in a microplate reader. Reporter strains were analyzed during the exponential phase (exp, OD_{600} of ~ 0.4) and after two hours of MMC treatment (wt: $10 \mu\text{g mL}^{-1}$; $\Delta\Delta$: $2.5 \mu\text{g mL}^{-1}$; $4\times$ MIC). Fluorescence measurements were background-corrected and normalized to OD_{600} . Bars represent the mean (\pm SEM; $n \geq 3$). A pairwise *t*-test was performed to compare wt and $\Delta\Delta$ (*** $p < 0.001$). Black dots indicate the results of individual biological experiments. (C) sYFP2 fluorescence from plasmid pBAD-*syfp2* was monitored in a microplate reader. sYFP2 expression was induced by 0.2% L-Ara (+ara) 30 min before treatment with MMC (wt: $10 \mu\text{g mL}^{-1}$; $\Delta\Delta$: $2.5 \mu\text{g mL}^{-1}$; $4\times$ MIC). Treatments with L-ara or MMC alone served as controls. Fluorescence measurements were normalized to the corresponding OD_{600} measurements. Data represent the mean (colored lines) and SEM (grey ribbons; $n = 3$). (wt: wild type MG1655; $\Delta\Delta$: $\Delta 1-41 \Delta istR$).

4. Discussion

Persister cells are marked by their ability to tolerate high levels of antibiotics and resume growth after the antibiotic treatment has ceased. While dormancy is generally expected to favor persistence, it is not necessary for persistence to occur. Persister cells might retain metabolic activity or even actively extrude antibiotics [12,14,15]. However, inactivation of distinct cellular processes clearly supports persister formation, as exemplified by ribosome hibernation [57], reduced uptake of antibiotics [58], treatment with bacteriostatic agents [59], and expression of toxins from TA systems [60,61]. The small membrane-targeting toxins TisB, HokB, and GhoT have been implicated in bacterial persistence due to their ability to reduce the proton motive force and deplete cellular ATP levels [12,25,33,62–64]. While GhoT belongs to a type V TA system [63], TisB and HokB are toxins from type I TA systems. A hallmark of type I TA systems is tight regulation of toxin expression at the post-transcriptional level. Primary transcripts of toxin genes are translationally inert due to intrinsic secondary structures that prevent ribosome binding and translation initiation, which leads to transcription-translation uncoupling. Activation of primary transcripts involves a processing step that enables structural rearrangements and ribosome accessibility [36,65–68]. However, processed mRNAs are bound by cognate RNA antitoxins, which triggers degradation by RNase III. We refer the reader to recent reviews for more mechanistic details on post-transcriptional regulation in type I TA systems [41,69–72]. It is intuitive to assume that such sophisticated regulation serves a purpose, such as avoidance of toxin overexpression and concomitant side effects, some of which were revealed in the current study.

Past experiments have demonstrated that mutant $\Delta\Delta$ has a *hip* phenotype upon treatment with fluoroquinolones and β -lactams [25,47,48]. It was assumed that the regulatory mutant rapidly produces TisB upon DNA damage, which allows many cells to enter the persister state before detrimental DNA damage occurs [25]. However, we only recently observed that the regulatory mutant produces TisB during the late stationary phase in an SOS- and LexA-independent manner, and that stationary-phase expression of TisB gives rise to a subpopulation of growth-retarded cells that are likely to be scored as persisters

upon Cip treatment [42]. Here, we show that mutant $\Delta\Delta$ has strongly elevated TisB levels during the exponential phase upon Cip treatment (Figure 2B). We assume that all actively growing cells will quickly overproduce TisB in an SOS- and LexA-dependent manner, while the pre-existing and growth-retarded subpopulation is not prone to further TisB production. Even though all cells are expected to experience ATP depletion (Figure 1B), thereby preventing strong Cip-induced DNA damage (Figure 1C) [45], only the pre-existing subpopulation contributes to the *hip* phenotype [42]. Since ectopic overexpression of TisB reduces viable cell counts by at least 10-fold [43], it seems likely that the actively growing part of the population is not killed by Cip-induced DNA damage but rather Cip-induced TisB overexpression.

It appears that cell death occurs in mutant $\Delta\Delta$ due to strong TisB expression upon Cip treatment. It is known that ectopic overexpression of TisB causes rRNA degradation and shutdown of major cellular processes [43,47]. Here, the same was observed in the regulatory mutant after ~60 min of Cip treatment (Figures 2C and 3), indicating that a threshold of TisB protein was reached, beyond which most cellular processes are strongly impeded. The rRNA degradation is indicative of ribosome destabilization, which together with enhanced ATP depletion would largely explain the shutdown of protein biosynthesis. In *Helicobacter pylori*, ectopic expression of toxin AapA1 and concomitant rRNA degradation are correlated with cell death [65]. However, a direct causal link between rRNA degradation and cell death is lacking for mutant $\Delta\Delta$. On the contrary, we have indications that rRNA degradation does not affect survival (our unpublished data). We rather suggest that rRNA degradation is an unwanted side effect in the regulatory mutant, possibly contributing to a deeper state of dormancy and an extended period of post-antibiotic recovery of TisB-dependent persister cells.

Several studies have emphasized the importance of SOS induction and DNA repair during the post-antibiotic recovery phase after fluoroquinolone treatments [26–28]. According to this view, the persister phenotype depends on an active mechanism that follows the antibiotic treatment. Alternatively, the persister phenotype is established due to the inactivation of antibiotic targets, for example, by strong ATP depletion [45,46]. Fluoroquinolones cause DSBs by stabilizing DNA-cleavage complexes formed by topoisomerase II (gyrase) or IV. Accumulation of DSBs is largely avoided by ATP depletion and concomitant inactivation of topoisomerases [45]. TisB-induced persistence clearly conforms to the latter model, underscoring the importance of cellular inactivation for persistence.

Interestingly, our data indicate that strong TisB production impedes the expression of SOS genes (Figure 4), thereby corrupting the induction of DNA repair systems. However, when treated with Cip, this disadvantage is not apparent because strong DNA damage is prevented (Figure 1C). Hence, SOS induction and DSB repair systems are dispensable for persister survival in the particular case of the $\Delta\Delta$ mutant (Figure 1D). MMC, on the other hand, initiates crosslinking of opposing DNA strands after spontaneous reduction of the drug. Since TisB-producing cells are expected to maintain reducing power, as observed for HokB-expressing cells [12], crosslinking and DSBs cannot be avoided by the action of TisB. Now, induction of the SOS response and DNA repair systems are crucial to counteract and tolerate MMC. In this particular case, wild-type cells are better adapted, and the *hip* phenotype of mutant $\Delta\Delta$ converts into a highly susceptible phenotype (Figure 5A). These experiments demonstrate that *hip* phenotypes can be conditional and that an advantage under certain conditions easily turns into a disadvantage as soon as conditions change. If persister formation is understood as a bet-hedging strategy for survival [1,62], it is certainly a benefit to bet on diverse persister types.

Finally, sYFP2 fluorescence measurements suggest that translation is inhibited upon TisB expression in mutant $\Delta\Delta$ (Figure 3B,D), similar to what was observed for ectopic TisB expression [43]. Since protein synthesis is the most energy-consuming process in bacterial cells [73], TisB-dependent ATP depletion (Figure 1B) [43] is a satisfying explanation for the observed inhibition of translation. In addition, the import of sugars, such as L-ara, might be inhibited, as indicated by the lack of *sypf2* induction on the mRNA level (Figure 3C).

We assume that both depolarization and ATP depletion rapidly interfere with transport over the inner membrane but cannot exclude that TisB accumulation itself has a negative influence on transport systems. Reduced uptake of sugars might also contribute to the prolonged post-antibiotic recovery time that has been observed for TisB persisters [25,47]. Recovery was even further delayed when the *ompF* gene was deleted [48]. OmpF is an outer membrane porin that provides the sugar supply to the periplasm [74]. If *ompF* is deleted in mutant $\Delta\Delta$, cells likely struggle to provide the necessary resources for initiating growth due to limited uptake at both the inner and outer membrane. Further experiments are clearly needed to evaluate the TisB-dependent effect on sugar transport and its implication for recovery.

In summary, we revealed several side effects of TisB overexpression in mutant $\Delta\Delta$, ranging from rRNA degradation to inhibition of cellular process, including expression of SOS genes and probably membrane transport. Since mutant $\Delta\Delta$ is an engineered strain, it remains an important question whether similar TisB-dependent side effects also occur in wild-type cells upon DNA damage. Preliminary experiments, comparing wild type to a *tisB* deletion strain, indeed suggest that some effects also occur in wild-type cultures upon extended periods of DNA damage (Figure S3 and our unpublished data). Whether these secondary effects influence TisB-induced persistence remains an exciting question for future studies.

Supplementary Materials: The following are available online at <https://www.mdpi.com/article/10.3390/microorganisms9050943/s1>. Table S1: Strains and plasmids used in this study, Table S2: Oligodeoxyribonucleotides used in this study, Figure S1: Induction of SOS genes upon ciprofloxacin, Figure S2: Time course experiment for DNA damage analysis, Figure S3: sYFP2 expression upon prolonged ciprofloxacin treatment, Figure S4: Cell filamentation upon ciprofloxacin, Figure S5: MIC determination for ciprofloxacin and mitomycin C.

Author Contributions: Conceptualization, D.E. and B.A.B.; Validation, D.E.; Formal Analysis, D.E., F.H.L., N.E.S. and M.O.; Investigation, D.E., F.H.L., N.E.S. and M.O.; Writing—Original Draft Preparation, B.A.B.; Writing—Review and Editing, D.E. and B.A.B.; Visualization, D.E. and B.A.B.; Supervision, T.F.S. and B.A.B.; Project Administration, B.A.B.; Funding Acquisition, T.F.S. and B.A.B. All authors have read and agreed to the published version of the manuscript.

Funding: This research was funded by the German Research Council (DFG) in the framework of the SPP 2002 (BE 5210/3-1 to B.A.B.). Parts of the work were financially supported by the Hessen State Ministry of Higher Education, Research, and the Arts (HMWK) via a grant for the LOEWE Research Center Insect Biotechnology and Bioresources.

Data Availability Statement: The data presented in this study are available on request from the corresponding author.

Acknowledgments: Meike Schwan and Kai Thormann (University of Giessen) are acknowledged for help with fluorescence microscopy. We are grateful to Matthew McIntosh and Gabriele Klug (University of Giessen) for their support with microplate reader experiments. We want to thank Bahar Asian for the construction of plasmid pBAD-*syfp2*.

Conflicts of Interest: The authors declare no conflict of interest.

References

1. Veening, J.-W.; Smits, W.K.; Kuipers, O.P. Bistability, Epigenetics, and Bet-Hedging in Bacteria. *Annu. Rev. Microbiol.* **2008**, *62*, 193–210. [[CrossRef](#)] [[PubMed](#)]
2. Ackermann, M. A functional perspective on phenotypic heterogeneity in microorganisms. *Nat. Rev. Genet.* **2015**, *13*, 497–508. [[CrossRef](#)] [[PubMed](#)]
3. Kussell, E.; Leibler, S. Phenotypic Diversity, Population Growth, and Information in Fluctuating Environments. *Science* **2005**, *309*, 2075–2078. [[CrossRef](#)] [[PubMed](#)]
4. Balaban, N.Q.; Helaine, S.; Lewis, K.; Ackermann, M.; Aldridge, B.; Andersson, D.I.; Brynildsen, M.P.; Bumann, D.; Camilli, A.; Collins, J.J.; et al. Definitions and guidelines for research on antibiotic persistence. *Nat. Rev. Genet.* **2019**, *17*, 441–448. [[CrossRef](#)] [[PubMed](#)]

5. Kaldalu, N.; Hauryluk, V.; Turnbull, K.J.; La Mensa, A.; Putrinš, M.; Tenson, T. In Vitro Studies of Persister Cells. *Microbiol. Mol. Biol. Rev.* **2020**, *84*, e00070-20. [[CrossRef](#)] [[PubMed](#)]
6. Lewis, K. Persister Cells. *Annu. Rev. Microbiol.* **2010**, *64*, 357–372. [[CrossRef](#)] [[PubMed](#)]
7. Bigger, J. Treatment of staphylococcal infections with penicillin by intermittent sterilisation. *Lancet* **1944**, *244*, 497–500. [[CrossRef](#)]
8. Hobby, G.L.; Meyer, K.; Chaffee, E. Observations on the Mechanism of Action of Penicillin. *Exp. Biol. Med.* **1942**, *50*, 281–285. [[CrossRef](#)]
9. Brauner, A.; Fridman, O.; Gefen, O.; Balaban, N.Q. Distinguishing between resistance, tolerance and persistence to antibiotic treatment. *Nat. Rev. Genet.* **2016**, *14*, 320–330. [[CrossRef](#)] [[PubMed](#)]
10. Amato, S.M.; Brynildsen, M.P. Mechanisms of Stress-Activated Persister Formation in *Escherichia coli*. In *Stress and Environmental Regulation of Gene Expression and Adaptation in Bacteria*; John Wiley & Sons, Inc.: Hoboken, NJ, USA, 2016; pp. 446–453.
11. Allison, K.R.; Brynildsen, M.P.; Collins, J.J. Heterogeneous bacterial persisters and engineering approaches to eliminate them. *Curr. Opin. Microbiol.* **2011**, *14*, 593–598. [[CrossRef](#)]
12. Wilmaerts, D.; Bayoumi, M.; Dewachter, L.; Knapen, W.; Mika, J.T.; Hofkens, J.; Dedecker, P.; Maglia, G.; Verstraeten, N.; Michiels, J. The Persistence-Inducing Toxin HokB Forms Dynamic Pores That Cause ATP Leakage. *mBio* **2018**, *9*, e00744-18. [[CrossRef](#)]
13. Radzikowski, J.L.; Vedelaar, S.; Siegel, D.; Ortega, Á.D.; Schmidt, A.; Heinemann, M. Bacterial Persistence Is an Active σ^S Stress Response to Metabolic Flux Limitation. *Mol. Syst. Biol.* **2016**, *12*, 882. [[CrossRef](#)]
14. Orman, M.A.; Brynildsen, M.P. Dormancy Is Not Necessary or Sufficient for Bacterial Persistence. *Antimicrob. Agents Chemother.* **2013**, *57*, 3230–3239. [[CrossRef](#)]
15. Pu, Y.; Zhao, Z.; Li, Y.; Zou, J.; Ma, Q.; Zhao, Y.; Ke, Y.; Zhu, Y.; Chen, H.; Baker, M.A.; et al. Enhanced Efflux Activity Facilitates Drug Tolerance in Dormant Bacterial Cells. *Mol. Cell* **2016**, *62*, 284–294. [[CrossRef](#)]
16. Dillingham, M.S.; Kowalczykowski, S.C. RecBCD Enzyme and the Repair of Double-Stranded DNA Breaks. *Microbiol. Mol. Biol. Rev.* **2008**, *72*, 642–671. [[CrossRef](#)]
17. Little, J. Mechanism of specific LexA cleavage: Autodigestion and the role of RecA coprotease. *Biochimie* **1991**, *73*, 411–421. [[CrossRef](#)]
18. Lewis, L.K.; Harlow, G.R.; Gregg-Jolly, L.A.; Mount, D.W. Identification of High Affinity Binding Sites for LexA which Define New DNA Damage-inducible Genes in *Escherichia coli*. *J. Mol. Biol.* **1994**, *241*, 507–523. [[CrossRef](#)]
19. De Henestrosa, A.R.F.; Ogi, T.; Aoyagi, S.; Chafin, D.; Hayes, J.J.; Ohmori, H.; Woodgate, R. Identification of additional genes belonging to the LexA regulon in *Escherichia coli*. *Mol. Microbiol.* **2002**, *35*, 1560–1572. [[CrossRef](#)]
20. Wade, J.T.; Reppas, N.B.; Church, G.M.; Struhl, K. Genomic Analysis of LexA Binding Reveals the Permissive Nature of the *Escherichia coli* Genome and Identifies Unconventional Target Sites. *Genes Dev.* **2005**, *19*, 2619–2630. [[CrossRef](#)]
21. Courcelle, J.; Khodursky, A.; Peter, B.; Brown, P.O.; Hanawalt, P.C. Comparative Gene Expression Profiles Following UV Exposure in Wild-Type and SOS-Deficient *Escherichia coli*. *Genetics* **2001**, *158*, 41–64.
22. Kreuzer, K.N. DNA Damage Responses in Prokaryotes: Regulating Gene Expression, Modulating Growth Patterns, and Manipulating Replication Forks. *Cold Spring Harb. Perspect. Biol.* **2013**, *5*, a012674. [[CrossRef](#)]
23. Dörr, T.; Lewis, K.; Vulić, M. SOS Response Induces Persistence to Fluoroquinolones in *Escherichia coli*. *PLoS Genet.* **2009**, *5*, e1000760. [[CrossRef](#)]
24. Theodore, A.; Lewis, K.; Vulić, M. Tolerance of *Escherichia coli* to Fluoroquinolone Antibiotics Depends on Specific Components of the SOS Response Pathway. *Genetics* **2013**, *195*, 1265–1276. [[CrossRef](#)]
25. Berghoff, B.A.; Hoekzema, M.; Aulbach, L.; Wagner, E.G.H. Two Regulatory RNA Elements Affect TisB-Dependent Depolarization and Persister Formation. *Mol. Microbiol.* **2017**, *103*, 1020–1033. [[CrossRef](#)]
26. Völzing, K.G.; Brynildsen, M.P. Stationary-Phase Persisters to Ofloxacin Sustain DNA Damage and Require Repair Systems Only during Recovery. *mBio* **2015**, *6*, e00731-15. [[CrossRef](#)]
27. Mok, W.W.K.; Brynildsen, M.P. Timing of DNA damage responses impacts persistence to fluoroquinolones. *Proc. Natl. Acad. Sci. USA* **2018**, *115*, E6301–E6309. [[CrossRef](#)]
28. Goormaghtigh, F.; Van Melderen, L. Single-cell imaging and characterization of *Escherichia coli* persister cells to ofloxacin in exponential cultures. *Sci. Adv.* **2019**, *5*, eaav9462. [[CrossRef](#)]
29. Van Melderen, L. Toxin–Antitoxin Systems: Why so Many, What For? *Curr. Opin. Microbiol.* **2010**, *13*, 781–785. [[CrossRef](#)]
30. Goeders, N.; Chai, R.; Chen, B.; Day, A.; Salmond, G.P. Structure, Evolution, and Functions of Bacterial Type III Toxin–Antitoxin Systems. *Toxins* **2016**, *8*, 282. [[CrossRef](#)]
31. Harms, A.; Brodersen, D.E.; Mitarai, N.; Gerdes, K. Toxins, Targets, and Triggers: An Overview of Toxin–Antitoxin Biology. *Mol. Cell* **2018**, *70*, 768–784. [[CrossRef](#)]
32. Page, R.; Peti, W. Toxin–antitoxin systems in bacterial growth arrest and persistence. *Nat. Chem. Biol.* **2016**, *12*, 208–214. [[CrossRef](#)] [[PubMed](#)]
33. Dörr, T.; Vulić, M.; Lewis, K. Ciprofloxacin Causes Persister Formation by Inducing the TisB toxin in *Escherichia coli*. *PLoS Biol.* **2010**, *8*, e1000317. [[CrossRef](#)] [[PubMed](#)]
34. Wagner, E.G.H.; Unoson, C. The Toxin–Antitoxin System TisB–IstR1: Expression, Regulation, and Biological Role in Persister Phenotypes. *RNA Biol.* **2012**, *9*, 1513–1519. [[CrossRef](#)] [[PubMed](#)]
35. Berghoff, B.A.; Karlsson, T.; Källman, T.; Wagner, E.G.H.; Grabherr, M.G. RNA-sequence data normalization through in silico prediction of reference genes: The bacterial response to DNA damage as case study. *BioData Min.* **2017**, *10*, 30. [[CrossRef](#)]

36. Darfeuille, F.; Unoson, C.; Vogel, J.; Wagner, E.G.H. An Antisense RNA Inhibits Translation by Competing with Standby Ribosomes. *Mol. Cell* **2007**, *26*, 381–392. [[CrossRef](#)]
37. Romilly, C.; Deindl, S.; Wagner, E.G.H. The ribosomal protein S1-dependent standby site in *tisB* mRNA consists of a single-stranded region and a 5' structure element. *Proc. Natl. Acad. Sci. USA* **2019**, *116*, 15901–15906. [[CrossRef](#)]
38. Romilly, C.; Lippegau, A.; Wagner, E.G.H. An RNA pseudoknot is essential for standby-mediated translation of the *tisB* toxin mRNA in *Escherichia coli*. *Nucleic Acids Res.* **2020**, *48*, 12336–12347. [[CrossRef](#)]
39. Vogel, J.; Argaman, L.; Wagner, E.H.; Altuvia, S. The Small RNA IstR Inhibits Synthesis of an SOS-Induced Toxic Peptide. *Curr. Biol.* **2004**, *14*, 2271–2276. [[CrossRef](#)]
40. Berghoff, B.A.; Wagner, E.G.H. Persister Formation Driven by TisB-Dependent Membrane Depolarization. In *Persister Cells and Infectious Disease*; Lewis, K., Ed.; Springer: Cham, Switzerland, 2019; pp. 77–97.
41. Berghoff, B.A.; Wagner, E.G.H. RNA-based regulation in type I toxin–antitoxin systems and its implication for bacterial persistence. *Curr. Genet.* **2017**, *63*, 1011–1016. [[CrossRef](#)]
42. Edelmann, D.; Oberpaul, M.; Schäberle, T.F.; Berghoff, B.A. Post-transcriptional Deregulation of the *tisB/istR-1* Toxin–Antitoxin System Promotes SOS-independent Persister Formation in *Escherichia coli*. *Environ. Microbiol. Rep.* **2021**, *13*, 159–168. [[CrossRef](#)]
43. Unoson, C.; Wagner, E.G.H. A small SOS-induced toxin is targeted against the inner membrane in *Escherichia coli*. *Mol. Microbiol.* **2008**, *70*, 258–270. [[CrossRef](#)]
44. Gunev, P.A.; Ortenberg, R.; Dörr, T.; Lewis, K.; Bezrukov, S.M. Persister-promoting bacterial toxin TisB produces anion-selective pores in planar lipid bilayers. *FEBS Lett.* **2012**, *586*, 2529–2534. [[CrossRef](#)]
45. Shan, Y.; Gandt, A.B.; Rowe, S.E.; Deisinger, J.P.; Conlon, B.P.; Lewis, K. ATP-Dependent Persister Formation in *Escherichia coli*. *mBio* **2017**, *8*, e02267-16. [[CrossRef](#)]
46. Conlon, B.P.; Rowe, S.E.; Gandt, A.B.; Nuxoll, A.S.; Donegan, N.P.; Zalis, E.A.; Clair, G.; Adkins, J.N.; Cheung, A.L.; Lewis, K. Persister formation in *Staphylococcus aureus* is associated with ATP depletion. *Nat. Microbiol.* **2016**, *1*, 1–7. [[CrossRef](#)]
47. Edelmann, D.; Berghoff, B.A. Type I toxin-dependent generation of superoxide affects the persister life cycle of *Escherichia coli*. *Sci. Rep.* **2019**, *9*, 1–10. [[CrossRef](#)]
48. Spanka, D.-T.; Konzer, A.; Edelmann, D.; Berghoff, B.A. High-Throughput Proteomics Identifies Proteins with Importance to Postantibiotic Recovery in Depolarized Persister Cells. *Front. Microbiol.* **2019**, *10*, 378. [[CrossRef](#)]
49. Datta, S.; Costantino, N.; Court, D.L. A set of recombineering plasmids for gram-negative bacteria. *Gene* **2006**, *379*, 109–115. [[CrossRef](#)]
50. Datsenko, K.A.; Wanner, B.L. One-step inactivation of chromosomal genes in *Escherichia coli* K-12 using PCR products. *Proc. Natl. Acad. Sci. USA* **2000**, *97*, 6640–6645. [[CrossRef](#)]
51. Livak, K.J.; Schmittgen, T.D. Analysis of Relative Gene Expression Data Using Real-Time Quantitative PCR and the 2^{(-Delta Delta C(T))}. *Method. Methods* **2001**, *25*, 402–408. [[CrossRef](#)]
52. Zhou, K.; Zhou, L.; Lim, Q.E.; Zou, R.; Stephanopoulos, G.; Too, H.-P. Novel reference genes for quantifying transcriptional responses of *Escherichia coli* to protein overexpression by quantitative PCR. *BMC Mol. Biol.* **2011**, *12*, 18. [[CrossRef](#)]
53. Schägger, H. Tricine-SDS-PAGE. *Nat. Protoc.* **2006**, *1*, 16–22. [[CrossRef](#)] [[PubMed](#)]
54. Bi, E.; Lutkenhaus, J. Cell division inhibitors SulA and MinCD prevent formation of the FtsZ ring. *J. Bacteriol.* **1993**, *175*, 1118–1125. [[CrossRef](#)] [[PubMed](#)]
55. Bos, J.; Zhang, Q.; Vyawahare, S.; Rogers, E.; Rosenberg, S.M.; Austin, R.H. Emergence of antibiotic resistance from multinucleated bacterial filaments. *Proc. Natl. Acad. Sci. USA* **2015**, *112*, 178–183. [[CrossRef](#)] [[PubMed](#)]
56. Kwan, B.W.; Chowdhury, N.; Wood, T.K. Combatting bacterial infections by killing persister cells with mitomycin C. *Environ. Microbiol.* **2015**, *17*, 4406–4414. [[CrossRef](#)]
57. McKay, S.L.; Portnoy, D.A. Ribosome Hibernation Facilitates Tolerance of Stationary-Phase Bacteria to Aminoglycosides. *Antimicrob. Agents Chemother.* **2015**, *59*, 6992–6999. [[CrossRef](#)]
58. Allison, K.R.; Brynildsen, M.P.; Collins, J.J. Metabolite-enabled eradication of bacterial persisters by aminoglycosides. *Nat. Cell Biol.* **2011**, *473*, 216–220. [[CrossRef](#)]
59. Kwan, B.W.; Valenta, J.A.; Benedik, M.J.; Wood, T.K. Arrested Protein Synthesis Increases Persister-Like Cell Formation. *Antimicrob. Agents Chemother.* **2013**, *57*, 1468–1473. [[CrossRef](#)]
60. Harms, A.; Maisonneuve, E.; Gerdes, K. Mechanisms of bacterial persistence during stress and antibiotic exposure. *Science* **2016**, *354*, aaf4268. [[CrossRef](#)] [[PubMed](#)]
61. Ronneau, S.; Helaine, S. Clarifying the Link between Toxin–Antitoxin Modules and Bacterial Persistence. *J. Mol. Biol.* **2019**, *431*, 3462–3471. [[CrossRef](#)] [[PubMed](#)]
62. Verstraeten, N.; Knapen, W.J.; Kint, C.I.; Liebens, V.; Bergh, B.V.D.; Dewachter, L.; Michiels, J.E.; Fu, Q.; David, C.C.; Fierro, A.C.; et al. O₂ and Membrane Depolarization Are Part of a Microbial Bet-Hedging Strategy that Leads to Antibiotic Tolerance. *Mol. Cell* **2015**, *59*, 9–21. [[CrossRef](#)] [[PubMed](#)]
63. Wang, X.; Lord, D.M.; Cheng, H.-Y.; Osbourne, D.O.; Hong, S.H.; Sanchez-Torres, V.; Quiroga, C.; Zheng, K.; Herrmann, T.; Peti, W.; et al. A new type V toxin-antitoxin system where mRNA for toxin GhoT is cleaved by antitoxin GhoS. *Nat. Chem. Biol.* **2012**, *8*, 855–861. [[CrossRef](#)]

64. Cheng, H.-Y.; Soo, V.W.C.; Islam, S.; McAnulty, M.J.; Benedik, M.J.; Wood, T.K. Toxin GhoT of the GhoT/GhoS toxin/antitoxin system damages the cell membrane to reduce adenosine triphosphate and to reduce growth under stress. *Environ. Microbiol.* **2014**, *16*, 1741–1754. [[CrossRef](#)]
65. Arnion, H.; Korkut, D.N.; Gelo, S.M.; Chabas, S.; Reignier, J.; Iost, I.; Darfeuille, F. Mechanistic insights into type I toxin antitoxin systems in *Helicobacter pylori*: The importance of mRNA folding in controlling toxin expression. *Nucleic Acids Res.* **2017**, *45*, 4782–4795. [[CrossRef](#)]
66. Kristiansen, K.I.; Weel-Sneve, R.; Booth, J.A.; Bjørås, M. Mutually exclusive RNA secondary structures regulate translation initiation of DinQ in *Escherichia coli*. *RNA* **2016**, *22*, 1739–1749. [[CrossRef](#)]
67. Wen, J.; Harp, J.R.; Fozo, E.M. The 5' UTR of the type I toxin ZorO can both inhibit and enhance translation. *Nucleic Acids Res.* **2017**, *45*, 4006–4020. [[CrossRef](#)]
68. Thisted, T.; Nielsen, A.; Gerdes, K. Mechanism of post-segregational killing: Translation of Hok, SrnB and Pnd mRNAs of plasmids R1, F and R483 is activated by 3'-end processing. *EMBO J.* **1994**, *13*, 1950–1959. [[CrossRef](#)]
69. Gerdes, K.; Wagner, E.G.H. RNA antitoxins. *Curr. Opin. Microbiol.* **2007**, *10*, 117–124. [[CrossRef](#)]
70. Wen, J.; Fozo, E.M. sRNA Antitoxins: More than One Way to Repress a Toxin. *Toxins* **2014**, *6*, 2310–2335. [[CrossRef](#)]
71. Masachis, S.; Darfeuille, F. Type I Toxin-Antitoxin Systems: Regulating Toxin Expression via Shine-Dalgarno Sequence Sequestration and Small RNA Binding. In *Regulating with RNA in Bacteria and Archaea*; American Society for Microbiology: Washington, DC, USA, 2019; Volume 6, pp. 173–190.
72. Brantl, S.; Jahn, N. sRNAs in bacterial type I and type III toxin-antitoxin systems. *FEMS Microbiol. Rev.* **2015**, *39*, 413–427. [[CrossRef](#)]
73. Szaflarski, W.; Nierhaus, K.H. Question 7: Optimized Energy Consumption for Protein Synthesis. *Orig. Life Evol. Biosphere* **2007**, *37*, 423–428. [[CrossRef](#)]
74. Nikaido, H. Molecular Basis of Bacterial Outer Membrane Permeability Revisited. *Microbiol. Mol. Biol. Rev.* **2003**, *67*, 593–656. [[CrossRef](#)] [[PubMed](#)]

5. SUMMARY OF CHAPTER 2

- (i) Comprehensive persister phenotyping revealed that the *hip* phenotype was not dependent on SOS induction. Rather more likely, post-transcriptional deregulation of *tisB* gene expression promotes membrane depolarization, thus ATP depletion, causing the stationary-phase *hip* phenotype. Moreover, deletion of the regulatory RNA elements uncoupled TisB toxin expression from LexA-dependent SOS induction and the formation of the *hip* phenotype following treatment with antibiotics. In summary, the work presented herein provides a stationary-phase model to study TisB-dependent persistence, which is – most importantly – not based on an impaired toxin variant (Semanjski *et al.*, 2018), but rather on the increased expression of a wild-type toxin.

- (ii) The SOS response and its involvement in persister formation was further dismantled by introducing the non-cleavable variant LexA3, which is important in respect of proper SOS response caused by DNA damage. By using the stationary phase persister model *E. coli* $\Delta 1-41$ $\Delta ist-R$ from i), it was proven that depolarization due to the depletion of ATP, avoids fatal DNA damage after ciprofloxacin treatment. An elevated level of the toxin TisB therefore maximizes the survival of persister in the presence of ciprofloxacin in an SOS/LexA-independent manner, while enhancing susceptibility to the DNA cross-linking agent mitomycin C. This was most probably caused by the suppression of the SOS response in the $\Delta\Delta$ background, and thus the dsDNA repair system. In summary, this is in agreement with the indication that a diverse persister strategy is favored (Balaban *et al.*, 2004), which maximizes the survival rate of the whole population by optimally balancing the advantages and disadvantages of each strategy.

6. DISCUSSION

Environmental microorganisms and the NPs they synthesize are a major source of inspiration for drug development. An estimated 50–70% of all drugs on the market are derived from NPs (Newman and Cragg, 2020). Historically, the introduction of the Waksman cultivation pipeline facilitated the cultivation of numerous Actinobacteria, many of which synthesize drugs or precursors thereof, which are still used today (Baltz, 2008; Newman and Cragg, 2020). Following the golden era of antibiotics, the rediscovery rate of known bacteria and respective NPs grew steadily (Schäberle and Hack, 2014). Ultimately, this led to a lack of novel structures suitable as drug candidates (Ventola, 2015). The field of NP discovery must therefore gain access to the so-called microbial dark matter to exploit its metabolic capabilities (Lok, 2015). As a consequence, new cultivation approaches must be developed, to leverage this numbers game, which in turn promotes NP discovery campaigns dramatically (Lewis, 2020). This is necessary because the likelihood of finding novel NPs is higher in untapped bacterial taxa (Hoffmann *et al.*, 2018; Lewis, 2020). These adapted approaches will provide more inspiration for new chemical entities in the bacterial kingdom by facilitating their isolation using new cultivation strategies, such as microfluidics cultivation (Quigley *et al.*, 2020; Matilla, 2021). Depending on the library, an estimation claims that 5,000 – 10,000 drug-like compounds tested only one drug will reach the market (Matthews *et al.*, 2016), which is even lower for NPs, hence their discovery has become a numbers game.

Therefore, the application of ultrahigh-throughput approaches such as combined microfluidics cultivation and metabolomics-guided screening pipelines are one inevitable option to leverage the numbers game in natural products discovery.

2.1.1 Ultrahigh-throughput microfluidics expands the cultivability of microbial dark matter

To access the chemical repertoire of the microbial dark matter, one of the best options is to cultivate the elusive bacteria in the laboratory. This opens the door for OSMAC approaches in bioprospecting campaigns, which are still more promising than cloning libraries (Bode *et al.*, 2002; Harbers, 2008; Nora *et al.*,

2019). Even so, only ~1% of known bacteria have been cultivated successfully thus far (Lok, 2015; Hug *et al.*, 2016). What are the candidates for NP research, which have not been extensively researched today? One example of an underexplored phylum is represented by Acidobacteria (Kielak *et al.*, 2016). They are ubiquitous, and many representatives possess biosynthetic gene cluster in the same amount as the well-characterized NP producing Actinobacteria (Crits-Christoph *et al.*, 2021). Only a few Acidobacteria have been cultured (Kaeberlein *et al.*, 2002) and were prospected for their chemical potential (Eichorst *et al.*, 2018). We therefore adapted a flexible high-throughput cultivation technique to selectively meet Acidobacteria-specific growth conditions (Oberpaul *et al.*, 2020), which are responsible for the limited number of representatives cultured thus far (Kielak *et al.*, 2017; Sikorski *et al.*, 2022). Illumina amplicon sequencing applied to different nest levels and individuals of the termite genus *Coptotermes* revealed a stable core microbiome and that termite nests contain abundant Acidobacteria (up to 10%). Their overall abundance in the nest material was observed in all samples that were evaluated over a timeframe of 2 years. Interestingly, abundance of Acidobacteria spp. increased over time during a fungal infection as well as *Streptomyces* spp. It was proposed that they were recruited by termites and defend the colony against fungal intruders, thus maintain the colonies health (Chouvenc *et al.*, 2013). This leads to the assumption that Acidobacteria may also help to maintain colony health, but this hypothesis has to be addressed in detail in future investigations. The selective microplate-based high-throughput approach led to the isolation of new representatives (Oberpaul *et al.*, 2020), which are still under investigation to characterize their NPs. This research may shed light on their ecological and/or biological roles in xylophagous lower termites. This knowledge could also be used to get an inspiration for strategies to control these pests, for example by interfering with their core microbiome, which might be essential for homeostasis.

The above-mentioned microplate-based high-throughput approach was successful in terms of targeted cultivation. However, some problems that occur in all microplate-based cultivation campaigns should be addressed in the following setup. One major issue is the distribution of single cells into microplate wells as well as the fact that the size ratio of one well of a 96-well microplate to the single cell is enormous. Thus, microfluidic cultivation should be exploited to implement a step, which lowers this ratio dramatically, before cells are distributed to

microplates. The idea behind is that encapsulation in agarose-solidified microspheres influences the growth of single cells positively due to the miniaturization. It also allows automation and even higher throughput (Mahler *et al.*, 2021). Briefly, an existing ultrahigh-throughput microfluidics cultivation approach was modified to improve the obtained microbial diversity. This was confirmed using single cells obtained by the Nycodenz gradient method described herein from sludge obtained from forest soil. Individual cells were counted by FACS and distributed into approx. every tenth of five millions of agarose-solidified microspheres. First it was assessed, which factors e.g. C-source, C:N ratio and pH value influences the cultured microbial diversity positively. Thus, Illumina amplicon sequencing was used to visualize the diversity within the bulk of droplets of eight different media. This led to three modified media, which were used for the encapsulation to increase the cultured diversity. All droplets containing grown colonies originating from a single cell were identified by staining with a membrane potential dye and FACS. Then arrayed into a 384-well microplates. The stepwise scale-up from the microsphere to the cavities of a 384-well and then 96-deepwell microplate should improve the successful isolation of cultures (e.g. dependent on their own growth mediation factors). Based on the turbidity cultures were up-scaled. Then after repeated fermentation the culture broth was split up for an OSMAC approach, and was used as the inoculum for a fermentation in a miniaturized 96-well system (Duetz, 2007). This resulted in >6000 extracts, retrieved from 1071 cultures (57 genera out of 5 phyla in total), sufficient for several antimicrobial and antifungal assays, thus leading to a high probability of finding undescribed natural products. The modulation of media components (C-sources) and especially pH significantly enhanced the cultivated diversity, ultimately resulted in the isolation of strains from underexplored phyla such as Acidobacteria, and other genera including *Ancylobacter*, *Buttiauxella*, *Inquilinus*, *Kaistia*, *Labrys*, *Luteibacter*, *Polaromonas*, *Reyranella* and *Variovorax* (Oberpaul *et al.*, 2021). Genetic fingerprinting and metabolomics were applied to all cultured strains for their phylogenetic and chemical classification, to reduce redundancy in downstream processing, e.g. due to one overrepresented strain (as observed for *Penicillium* sp. herein). Known bioactive molecules were automatically annotated using a metabolomics pipeline (Märner *et al.*, 2020). This facilitated the quick dereplication of three chosen bioactive extracts into hitherto unknown bioactive derivatives of known NPs. Derivatives are interesting in many ways: i) they were

overlooked previously, thus unpublished (Marner *et al.*, 2020), ii) they comprise bioactivities that are not true for the initially described compound (Bill *et al.*, 2021) and iii) they have different physicochemical properties, which e.g. influences their stability, solubility or membrane permeability (Chatterjee *et al.*, 2013; Bockus *et al.*, 2015). The latter was exemplified with GE81112A, whereas for the proposed structure no antibacterial effect was observed even though its configuration only differed in only one position. On the other hand, its corresponding epimer was turning active against *E. coli* (Jürjens *et al.*, 2018), which was even further improved by derivatization of the pharmacophores (Zwick *et al.*, 2021). This was also proven recently with a new colistin derivative biphenyl-macolacin, but on the other hand emphasizes the necessity for novel antibiotics, since colistin (and derivatives thereof) can cause severe nephrotoxicity (Zheng *et al.*, 2020).

Even though only new derivatives were found by applying our setup, this is the first report of Serrawettin A produced by an *Erwinia* species, although its ability to produce serratamolides is suggested (Tanikawa *et al.*, 2006). Moreover, the application of the microfluidics cultivation pipeline established herein was used for a cultivation campaign to obtain microbial diversity from the carton nest of *C. testaceus*. This facilitated the cultivation of a *Gemmata* sp. – a member of the phylum Planctomycetes (unpublished data). They are supposed to have promising genetic potential (Wiegand *et al.*, 2018; Kallscheuer and Jogler, 2021) regarding NP research and this represents the first *Gemmata* spp. isolated from a termite nest.

To prove the idea that lower xylophagous termites provide a rich source of novel microorganisms producing new NPs, strains isolated from the latter were fermented and prospected for chemical novelty. *Olivibacter* sp. FHG000416 was found to produce derivatives of known lipids, and new pentapeptides produced by *Trichoderma* sp. FHG000531 were isolated and characterized. Strain FHG000416 was isolated from the carton nest of *C. gestroi* and shared a sequence identity of 94.5% to *Olivibacter domesticus* DSM 18733, thus leading to the assumption that it represents a new species within the genus *Olivibacter*. It also produced a derivative of the known lysophosphatidylethanolamine (LPE) 451 (Woznica *et al.*, 2016) and derivatives of Lipid 430 (Sohlenkamp and Geiger, 2016). Both inhibited the growth of the Gram-negative human pathogen *Moraxella catarrhalis* ATCC 25238 comprising valuable MICs (MICs: 8 and 16 µg/mL) (Bill *et al.*, 2021). Strain FHG000531 was isolated from a nest infected with fungi. We exploited this unique

situation to characterize the mycobiome of the infected nest, already proven to undergo a microbiome shift (Oberpaul *et al.*, 2020). Illumina amplicon sequencing was applied, revealing a high abundance of *Trichoderma* spp in the nest material. They were also highly abundant in the samples associated with infected termite individuals, but not the healthy ones. Hence, the strain was isolated and its metabolic repertoire was analyzed by applying an OSMAC approach, which was followed by molecular networking of the methanolic extracts. This revealed many known toxic and insecticidal compounds and derivatives thereof, as well as one cluster containing six hitherto unknown pentapeptides (including the isolation and characterization of one of them by NMR spectroscopy and MS/MS). The novel pentapeptide featured an unusual *N,N*-dimethyl-leucine residue, that is poorly described (Junker *et al.*, 2006). However, it did not show any bioactivity when tested against a broad panel of pathogenic bacteria and fungi, nor was it toxic toward the plant *Brassica rapa* susp. *rapa* and the invertebrate *Caenorhabditis elegans* (Oberpaul *et al.*, 2022). Despite the lack of activity in these assays, the concept of finding chemical novelty in uncultured strains from underexplored bioresources using the herein established setups was proven. However, the role of the mycobiome (and microbiome) of lower termites needs further investigation towards the interaction with the termites and colony health status as described for higher termites (Beemelmans *et al.*, 2016; Benndorf *et al.*, 2018; Klassen *et al.*, 2019).

In summary, this platform facilitates sample selection for miniaturized and largely automated NP discovery campaigns. It offers a strategy to reduce complex environmental samples to a diverse range of axenic cultures, which in turn facilitates the integration of the arrayed strains into various bioprospecting campaigns supported by OSMAC approaches. The combination of these techniques, all of which are easily accessible, increases the throughput, simultaneously decreases the workload and the timespan from sampling to bioassays by limiting the number of lab generations (around 3-4) required to generate axenic cultures. This relatively low number is an advantage in respect of the unwanted effect that the bacteria adapt too far to the lab environment and cultivation conditions. Thus, probably leading to downregulation of genes related to antibiotics resistance and likewise their production, which is poorly understood (Jahn *et al.*, 2017; Maeda *et al.*, 2020). The microfluidics cultivation approach established herein will interest scientists seeking to exploit microbial diversity not

strictly limited to NP discovery. There are no limitations in terms of bioresources, organism type, cultivation parameters (e.g., temperature, pH, carbon source, shaking, and oxygen availability) or screenings. Given the low cost per extract from axenic cultures, the high throughput (>1000 cultures per week), standardized formats (ANSI microplate), and automated steps (robotics, annotation of known NPs) this setup is a great example of a standardized pipeline suitable for the interface between academia and industry.

In summary, rapid cultivation in microspheres to leverage the isolation of hitherto uncultured bacteria was therefore successfully proven, and should be applied to additional underexplored bioresources to further expand the diversity of the microbial cultures accessible for bioprospecting campaigns.

To take the success of cultivation to the next level, we established a so-called 'droplet-in-droplet' process using the devices described above (Brinkmann *et al.*, 2021b). This enabled the introduction of a second shell, which nestles around the solidified inner agarose sphere, to facilitate the compartmentalization of spatially non-separated droplets described before (Skhiri *et al.*, 2012). The transport of small molecules between the compartments is still possible, but the exchange of bacteria is hindered (Mahler *et al.*, 2021). This was confirmed by the encapsulation of *E. coli* dh5 α strains labeled with green fluorescent protein (GFP) in the inner sphere and red fluorescent protein (dsRed) in the outer shell, respectively. The labeled bacteria remained in their respective layers. However, motile microorganisms - *E. coli* dh5 α lacks pili for locomotion (Wood *et al.*, 2006) - may have the ability to break through this barrier, although this possibility was not addressed experimentally herein. So-called 'helper strains' or rather 'helper molecules' such as siderophores or quorum sensing molecules promote the growth of bacteria (Whitehead *et al.*, 2001; D'Onofrio *et al.*, 2010; Verbeke *et al.*, 2017). This would be helpful in the following context: In the first step, environmental bacteria are individually encapsulated in an agarose-solidified droplet containing a specified growth medium. In a second step, a second layer is introduced around the first droplet, containing a defined number of bacteria functioning as helper strains. Additionally, to promote growth an extract is prepared and added to the medium (e.g. soil extract). Importantly, the second layer must not be solidified. After the desired incubation time and conditions are imposed, the second shell containing the helper strain could be released by an emulsion breaker and removed by FACS. This co-cultivation might promote the

growth of encapsulated single bacteria, allowing them to form a more robust colony that grows the next-largest format (e.g. 384-well microplates), which might not be the case if the bacteria were diluted on an agar plate (Staley and Konopka, 1985). Indeed, this method facilitates all kinds of co-encapsulation experiments and could even enable the observation of certain bacterial consortia. For example, the introduction of even more layers could be used to assemble synthetic consortia for stepwise bioprocessing applications (Shong *et al.*, 2012). Microfluidics cultivation is not widely used to date, and is usually limited to oral and soil microbiota (Zengler *et al.*, 2002; Mahler *et al.*, 2018; Mahler *et al.*, 2021; Oberpaul *et al.*, 2021).

Most of the low-hanging fruits from the Waksman pipeline have already been harvested. However, examination of underexplored bioresources, novel cultivation approaches, computational technologies in drug discovery and combinations thereof have already uncovered novel natural products such as darobactin (Imai *et al.*, 2019), teixobactin (Ling *et al.*, 2015), lugdunin (Zipperer *et al.*, 2016), abyssomycin (Riedlinger *et al.*, 2004), and halicin (Stokes *et al.*, 2020). Each of these techniques has advantages and disadvantages, but their sophisticated combination, ultrahigh-throughput potential and high degree of automation are clearly favorable.

In conclusion, the results presented in this chapter highlight the use of such techniques to accelerate the cultivation of hitherto uncultured microorganisms from underexplored bioresources, ultimately resulting in the discovery of novel chemical entities.

2.1.2 High-throughput persister phenotyping

Relapsing infections caused by bacterial persister cells pose a severe threat to patients (Lewis, 2013). Persister cells exist in a dormant state, where most broad-spectrum antibiotics, which target active cellular processes, become ineffective. Incorrect dosing of antibiotics can promote persister formation and the cells tend to 'wake up' with even stronger resistance to the perceived antibiotic. Given our incomplete understanding of persister formation, *hip* phenotypes have been established in the laboratory (Korch *et al.*, 2003). One example is the TisB-dependent *hip* phenotype $\Delta\Delta$ discussed herein (Edelmann *et al.*, 2021b). Persister formation is a stochastically driven process (Manuse *et al.*, 2021), so high-

throughput methods such as flow cytometry strongly support the experimental analysis of the heterogeneity of persister phenotypes (Mohiuddin *et al.*, 2020). In Chapter 2, this technique supports the research on the toxin-antitoxin system *tisB/istR-1*. This facilitated the statistical evaluation of an observed subpopulation, which otherwise might have been overlooked (Edelmann *et al.*, 2021b). Light scattering revealed that nearly 75% of the population resembled exponentially growing wild-type cells, whereas the remaining 25% was more akin to the shape and size of stationary-phase cells. This was confirmed by light microscopy and a dilution experiment, suggesting that subpopulation A was linked to the *hip* phenotype of the $\Delta\Delta$ mutant. A sorting experiment confirmed the hypothesis – persister cells were 200-fold more abundant in the smaller population. The study therefore established a stationary-phase persister model to understand TisB-dependent persistence. Noteworthy, the model is not based on an impaired toxin variant (Semanjski *et al.*, 2018), but reflects the amplified expression of a wild-type toxin. Moreover, the SOS cascade in *E. coli* was uncovered in more detail by introducing the non-cleavable variant LexA3. This regulates many of the genes involved in DNA repair and the cell division cascade, for example by interfering with Sula. This was confirmed by the enhanced susceptibility of the $\Delta\Delta$ mutant to the DNA cross-linking agent mitomycin C, and was observed by flow scattering along with a live/dead staining.

It is noteworthy that the first persister-related gene *hipA* was found by using a microfluidics setup for persister screening (Balaban *et al.*, 2004). In that setup, the use of membrane potential dyes facilitated the analysis of ATP-dependent persister cells. To observe and characterize this population in terms of the stochastic recurrence of single persister cells, they could be arrayed into droplets as described in Chapter 1. This could also help to further characterize the efficacy of several antibiotics or combinations thereof. A colony derived from a single persister cell could thus provide information about the viability of the whole persister population on a single-cell level. This is comparable to the so-called ScanLag method (Levin-Reisman *et al.*, 2010), but is rather more convincing because it is compatible with cell staining and has a higher throughput and thus higher statistical power. Moreover, this could be combined with the introduction of compounds to screen for triggering agents, which can promote the recurrence of persister cells or even dormant cells (Song and Wood, 2021), or in contrast can inhibit recurrence.

In summary, the $\Delta\Delta$ mutant does not express SOS genes, and is therefore more susceptible to DNA cross-linking agents such as mitomycin C, probably due to the impeded SOS response (Edelmann *et al.*, 2021a). The $\Delta\Delta$ mutant and other introduced mutations combined with high-throughput phenotyping will therefore provide more detailed insight into persister formation in *E. coli*, and will help to identify and characterize potential targets for antimicrobials or other treatment options for relapsing infections. Furthermore, it would be interesting to evaluate a combination of the herein established microfluidics setup with the *hip* phenotype in terms of stochastic analysis and to uncover further aspects of persister formation on a single-cell level.

7. FUTURE PERSPECTIVE

It has been proposed that there are no more broad-spectrum compounds left to be discovered and novel antibiotics against gram-negative bacteria are even more difficult to find (Lewis 2020). It is therefore a good option to optimize screenings towards specific drug applicable targets. For example, pathogenic bacteria expressing reporter genes provide an easy readout in high-throughput assays, which led to the discovery of e.g. platensymycin (Wang *et al.*, 2006). The concept behind such screens is to focus the screening on certain drug applicable targets, in this particular case on type II fatty acid synthesis (FASII), which is essential and exclusive for bacteria (Kodali *et al.*, 2005). To this end the comprehensive *E.coli* fluorescent reporter library introduced by Zaslaver and co-workers could be used (Zaslaver *et al.*, 2006). This comprehensive library consist of several plasmids, whereas a transcription of a gene is linked with the production of gfp, e.g. *recA*. Combined with the before-mentioned microfluidics setup, this displays an option to specifically search for antimicrobials targeting the expression of genes or proteins involved therein. Due to the versatility of the microfluidics setup, it would be possible to screen encapsulated environmental bacteria or huge cDNA libraries (Klaus *et al.*, 2021), which increases the probability of success by increasing the throughput and separating the events of interest for downstream processing.

A further possibility is the 'integrated cultivation and screening' in droplets featuring a single shell or a 'droplet-in-droplet' process (Glaeser *et al.*, 2018). As well as abiotic factors, several biological parameters can be exchanged in such a

setup. For example: environmental strains or heterologous cDNA libraries are sources of antimicrobials that could be encapsulated to prospect for natural products. Pathogenic bacteria, the comprehensive *E. coli* library, persister cells or protein substrates could be used as targets. Moreover, an integrated cultivation and screening could also be used to prospect for predatory microbes, which could be co-encapsulated with GFP-producing screening strains to provide a simple readout suitable for high-throughput screening and sorting. This would support the discovery of antimicrobials, because predatory bacteria such as *Myxococcales* tend to produce a plethora of antibacterials (Matthijs *et al.*, 2014; Herrmann *et al.*, 2017; Bhat *et al.*, 2021).

In conclusion, these highly versatile ultrahigh-throughput methods offer a general screening strategy for bioactive compounds or proteins, as well as the cultivation of unknown microbes, microbial interaction studies, and bacterial phenotyping on a single-cell level. Moreover, they will support the discovery of new antibiotics in many different ways, thus helping the research community to outpace the increasing threat of the antimicrobial resistance crisis.

8. REFERENCES

- Akselband, Y., Cabral, C., Castor, T.P., Chikarmane, H.M., and McGrath, P. (2006) Enrichment of slow-growing marine microorganisms from mixed cultures using gel microdrop (GMD) growth assay and fluorescence-activated cell sorting. *Journal of Experimental Marine Biology and Ecology* **329** (2): 196–205.
- Andrei, S., Droc, G., and Stefan, G. (2019) FDA approved antibacterial drugs: 2018-2019. *Discoveries (Craiova)* **7** (4): e102.
- Auld, D.S., Coassin, P.A., Coussens, N.P. Hensley, P., Klumpp-Thomas, C., Michael, S., Sittampalam, G.S., et al. (2020) Microplate Selection and Recommended Practices in High-throughput Screening and Quantitative Biology **2020** (n: Markossian S, Grossman A, Brimacombe K, et al., editors. Assay Guidance Manual [Internet]. Bethesda (MD): Eli Lilly & Company and the National Center for Advancing Translational Sciences; 2004-.).
- Bachmann, B.O., van Lanen, S.G., and Baltz, R.H. (2014) Microbial genome mining for accelerated natural products discovery: is a renaissance in the making? *J Ind Microbiol Biotechnol* **41** (2): 175–184.
- Balaban, N.Q., Merrin, J., Chait, R., Kowalik, L., and Leibler, S. (2004) Bacterial persistence as a phenotypic switch. *Science* **305** (5690): 1622–1625.
- Balty, C., Guillot, A., Fradale, L., Brewee, C., Boulay, M., Kubiak, X., et al. (2019) Ruminococcin C, an anti-clostridial sactipeptide produced by a prominent member of the human microbiota Ruminococcus gnavus. *J Biol Chem* **294** (40): 14512–14525.
- Balty, C., Guillot, A., Fradale, L., Brewee, C., Lefranc, B., Herrero, C., et al. (2020) Biosynthesis of the sactipeptide Ruminococcin C by the human microbiome: Mechanistic insights into thioether bond formation by radical SAM enzymes. *J Biol Chem* **295** (49): 16665–16677.
- Baltz, R.H. (2008) Renaissance in antibacterial discovery from actinomycetes. *Curr Opin Pharmacol* **8** (5): 557–563.
- Baret, J.-C., Miller, O.J., Taly, V., Ryckelynck, M., El-Harrak, A., Frenz, L., et al. (2009) Fluorescence-activated droplet sorting (FADS): efficient microfluidic cell sorting based on enzymatic activity. *Lab Chip* **9** (13): 1850–1858.
- Beemelmans, C., Guo, H., Rischer, M., and Poulsen, M. (2016) Natural products from microbes associated with insects. *Bellstein J Org Chem* **12**: 314–327.
- Benndorf, R., Guo, H., Sommerwerk, E., Weigel, C., Garcia-Altare, M., Martin, K., et al. (2018) Natural Products from Actinobacteria Associated with Fungus-Growing Termites. *Antibiotics (Basel)* **7** (3): 83.
- Berghoff, B.A., Hoekzema, M., Aulbach, L., and Wagner, E.G.H. (2017) Two regulatory RNA elements affect TisB-dependent depolarization and persister formation. *Molecular Microbiology* **103** (6): 1020–1033.
- Bhat, M.A., Mishra, A.K., Bhat, M.A., Banday, M.I., Bashir, O., Rather, I.A., et al. (2021) Myxobacteria as a Source of New Bioactive Compounds: A Perspective Study. *Pharmaceutics* **13** (8).
- Bill, M.-K., Brinkmann, S., Oberpaul, M., Patras, M.A., Leis, B., Marner, M., et al. (2021) Novel Glycerophospholipid, Lipo- and N-acyl Amino Acids from Bacteroidetes: Isolation, Structure Elucidation and Bioactivity. *Molecules* **26** (17).
- Binnenkade, L., Kreienbaum, M., and Thormann, K.M. (2018) Characterization of ExeM, an Extracellular Nuclease of *Shewanella oneidensis* MR-1. *Front Microbiol* **9**: 1761.
- Bitschar, K., Sauer, B., Focken, J., Dehmer, H., Moos, S., Konnerth, M., et al. (2019) Lugdunin amplifies innate immune responses in the skin in synergy with host- and microbiota-derived factors. *Nat Commun* **10** (1): 2730.
- Bockus, A.T., Schwochert, J.A., Pye, C.R., Townsend, C.E., Sok, V., Bednarek, M.A., and Lokey, R.S. (2015) Going Out on a Limb: Delineating The Effects of β -Branching, N-Methylation, and Side Chain Size on the Passive Permeability, Solubility, and Flexibility of Sanguinamide A Analogues. *J Med Chem* **58** (18): 7409–7418.
- Bode, H.B., Bethe, B., Höfs, R., and Zeeck, A. (2002) Big Effects from Small Changes: Possible Ways to Explore Nature's Chemical Diversity. *ChemBioChem* **3** (7): 619.
- Boitard, L., Cottinet, D., Bremond, N., Baudry, J., and Bibette, J. (2015) Growing microbes in millifluidic droplets. *Eng. Life Sci.* **15** (3): 318–326.
- Bowler, P., Murphy, C., and Wolcott, R. (2020) Biofilm exacerbates antibiotic resistance: Is this a current oversight in antimicrobial stewardship? *Antimicrob Resist Infect Control* **9** (1): 162.
- Brauner, A., Fridman, O., Gefen, O., and Balaban, N.Q. (2016) Distinguishing between resistance, tolerance and persistence to antibiotic treatment. *Nat Rev Microbiol* **14** (5): 320–330.
- Brinkmann, S., Kurz, M., Patras, M.A., Hartwig, C., Marner, M., Leis, B., et al. (2021a) Genomic and chemical decryption of the *Bacteroidetes* phylum for its potential to biosynthesize natural products.
- Brinkmann, S., Oberpaul, M., Glaeser, J., and Schäberle, T.F. (2021b) Two-step generation of monodisperse agarose-solidified double emulsions (w/w/o) excluding an inner oil barrier. *MethodsX* **8**: 101565.
- Brinkrolf, K., Shukla, S.P., Griep, S., Rupp, O., Heise, P., Goesmann, A., et al. (2021) Genomic analysis of novel *Yarrowia*-like yeast symbionts associated with the carrion-feeding burying beetle *Nicrophorus vespilloides*. *BMC Genomics* **22** (1): 323.
- Brogi, S. (2019) Computational Approaches for Drug Discovery. *Molecules* **24** (17).
- Brower, K.K., Carswell-Crumpton, C., Klemm, S., Cruz, B., Kim, G., Calhoun, S.G.K., et al. (2020) Double emulsion flow cytometry with high-throughput single droplet isolation and nucleic acid recovery. *Lab Chip* **20** (12): 2062–2074.
- Bruns, A., Hoffelner, H., and Overmann, J. (2003) A novel approach for high throughput cultivation assays and the isolation of planktonic bacteria. *FEMS Microbiol Ecol* **45** (2): 161–171.
- Bryant, D.A., Costas, A.M.G., Maresca, J.A., Chew, A.G.M., Klatt, C.G., Bateson, M.M., et al. (2007) *Candidatus Chloracidobacterium thermophilum*: an aerobic phototrophic Acidobacterium. *Science* **317** (5837): 523–526.
- Butler, M.S. (2004) The role of natural product chemistry in drug discovery. *J. Nat. Prod.* **67** (12): 2141–2153.
- Butler, M.S., and Buss, A.D. (2006) Natural products--the future scaffolds for novel antibiotics? *Biochem Pharmacol* **71** (7): 919–929.
- Caballero-Aguilar, L.M., Duchib, S., Quigley, A., Onofriolo, C., Di Bellab, C., and Moultona, S.E. (2021) Microencapsulation of Growth Factors by microfluidic system. *MethodsX*: 101324.
- Cao, J., Hafermann, L., and Köhler, J.M. (2017) Stochastically reduced communities-Microfluidic compartments as model and investigation tool for soil microorganism growth in structured spaces. *Eng. Life Sci.* **17** (7): 792–800.
- Chahine, E.B., Dougherty, J.A., Thornby, K.-A., and Guirguis, E.H. (2021) Antibiotic Approvals in the Last Decade: Are We Keeping Up With Resistance? *Ann Pharmacother*: 10600280211031390.
- Challinor, V.L., and Bode, H.B. (2015) Bioactive natural products from novel microbial sources. *Ann. N.Y. Acad. Sci.* **1354** (1): 82–97.
- Chatterjee, J., Rechenmacher, F., and Kessler, H. (2013) N-methylation of peptides and proteins: an important element for modulating biological functions. *Angew Chem Int Ed Engl* **52** (1): 254–269.
- Chevrette, M.G., Carlson, C.M., Ortega, H.E., Thomas, C., Ananiev, G.E., Barns, K.J., et al. (2019) The antimicrobial potential of *Streptomyces* from insect microbiomes. *Nat Commun* **10** (1): 516.
- Chevrette, M.G., and Currie, C.R. (2019) Emerging evolutionary paradigms in antibiotic discovery. *J Ind Microbiol Biotech* **46** (3-4): 257–271.
- Chouvenc, T., Efstathion, C.A., Elliott, M.L., and Su, N.-Y. (2013) Extended disease resistance emerging from

- the faecal nest of a subterranean termite. *Proc. R. Soc. B.* **280** (1770): 20131885.
- Clatworthy, A.E., Pierson, E., and Hung, D.T. (2007) Targeting virulence: a new paradigm for antimicrobial therapy. *Nat Chem Biol* **3** (9): 541–548.
- Connon, S.A., and Giovannoni, S.J. (2002) High-throughput methods for culturing microorganisms in very-low-nutrient media yield diverse new marine isolates. *Appl Environ Microbiol* **68** (8): 3878–3885.
- Corinaldesi, C. (2015) New perspectives in benthic deep-sea microbial ecology. *Front. Mar. Sci.* **2**.
- Crits-Christoph, A., Diamond, S., Al-Shayeb, B., Valentin-Alvarado, L., and Banfield, J.F. (2021) A widely distributed genus of soil Acidobacteria genomically enriched in biosynthetic gene clusters. *bioRxiv* (doi: 10.1101/2021.05.10.443473).
- Crits-Christoph, A., Diamond, S., Butterfield, C.N., Thomas, B.C., and Banfield, J.F. (2018) Novel soil bacteria possess diverse genes for secondary metabolite biosynthesis. *Nature* **558** (7710): 440–444.
- Cully, M. (2018) Deal watch: Roche taps potential antibiotics mine with Warp Drive Bio. *Nat Rev Drug Discov* **17** (1): 8–9.
- Da Rocha, U.N., van Overbeek, L., and van Elsas, J.D. (2009) Exploration of hitherto-uncultured bacteria from the rhizosphere. *FEMS Microbiol Ecol* **69** (3): 313–328.
- Dafale, N.A., Srivastava, S., and Purohit, H.J. (2020) Zoonosis: An Emerging Link to Antibiotic Resistance Under "One Health Approach". *Indian J Microbiol* **60** (2): 139–152.
- Demarque, D.P., Dusi, R.G., Sousa, F.D.M. de, Grossi, S.M., Silvério, M.R.S., Lopes, N.P., and Espindola, L.S. (2020) Mass spectrometry-based metabolomics approach in the isolation of bioactive natural products. *Sci Rep* **10** (1): 1051.
- Díaz-Pascual, F., Hartmann, R., Lempp, M., Vidakovic, L., Song, B., Jeckel, H., et al. (2019) Breakdown of Vibrio cholerae biofilm architecture induced by antibiotics disrupts community barrier function. *Nat Microbiol* **4** (12): 2136–2145.
- Díaz-Aguilar, M., Ekkelenkamp, M., Morosini, M.-I., Huertas, N., Del Campo, R., Zamora, J., et al. (2021) Anti-biofilm activity of murepavadin against cystic fibrosis Pseudomonas aeruginosa isolates. *J Antimicrob Chemother* **76** (10): 2578–2585.
- D'Onofrio, A., Crawford, J.M., Stewart, E.J., Witt, K., Gavrish, E., Epstein, S., et al. (2010) Siderophores from neighboring organisms promote the growth of uncultured bacteria. *Chem Biol* **17** (3): 254–264.
- Dörr, T., Lewis, K., and Vulić, M. (2009) SOS response induces persistence to fluoroquinolones in Escherichia coli. *PLoS Genet* **5** (12): e1000760.
- Dörr, T., Vulić, M., and Lewis, K. (2010) Ciprofloxacin causes persister formation by inducing the TisB toxin in Escherichia coli. *PLoS Biol* **8** (2): e1000317.
- Duetz, W.A. (2007) Microtiter plates as mini-bioreactors: miniaturization of fermentation methods. *Trends Microbiol* **15** (10): 469–475.
- Duetz, W.A., Rüedi, L., Hermann, R., O'Connor, K., Büchs, J., and Witholt, B. (2000) Methods for Intense Aeration, Growth, Storage, and Replication of Bacterial Strains in Microtiter Plates. *Appl. Environ. Microbiol.* **66** (6): 2641–2646.
- Dunny, G.M., and Winans, S.C. (1999) *Cell-cell signaling in bacteria*. Washington, D.C.: ASM Press.
- ECDC/EFSA/EMA 2021 ECDC/EFSA/EMA third joint report on the integrated analysis of the consumption of antimicrobial agents and occurrence of antimicrobial resistance in bacteria from humans and food-producing animals (JIACRA III) **2021**.
- Eckmann, C. (2014) Wirksamkeit von Ceftarolin bei komplizierten Haut- und Weichgewebeeinfektionen. *Dtsch Med Wochenschr* **139 Suppl 3**: S87-8.
- Edelmann, D., and Berghoff, B.A. (2019) Type I toxin-dependent generation of superoxide affects the persister life cycle of Escherichia coli. *Sci Rep* **9** (1): 14256.
- Edelmann, D., Leinberger, F.H., Schmid, N.E., Oberpaul, M., Schäberle, T.F., and Berghoff, B.A. (2021a) Elevated Expression of Toxin TisB Protects Persister Cells against Ciprofloxacin but Enhances Susceptibility to Mitomycin C. *Microorganisms* **9** (5).
- Edelmann, D., Oberpaul, M., Schäberle, T.F., and Berghoff, B.A. (2021b) Post-transcriptional deregulation of the tisB/istR-1 toxin-antitoxin system promotes SOS-independent persister formation in Escherichia coli. *Environ Microbiol Rep* **13** (2): 159–168.
- Eichorst, S.A., Trojan, D., Roux, S., Herbold, C., Rattei, T., and Wobken, D. (2018) Genomic insights into the Acidobacteria reveal strategies for their success in terrestrial environments. *Environ Microbiol* **20** (3): 1041–1063.
- Etienne, G., Vian, A., Biočanin, M., Deplancke, B., and Amstad, E. (2018) Cross-talk between emulsion drops: how are hydrophilic reagents transported across oil phases? *Lab Chip* **18** (24): 3903–3912.
- Fiedler, H.-P. (2021) Abyssomicins-A 20-Year Retrospective View. *Mar Drugs* **19** (6).
- Foxman, B. (2010) The epidemiology of urinary tract infection. *Nat Rev Urol* **7** (12): 653–660.
- Frost, I., Kapoor, G., Craig, J., Liu, D., and Laxminarayan, R. (2021) Status, challenges and gaps in antimicrobial resistance surveillance around the world. *J Glob Antimicrob Resist* **25**: 222–226.
- Gao, W., Navaroli, D., Naimark, J., Zhang, W., Chao, S., and Meldrum, D.R. (2013) Microbe observation and cultivation array (MOCA) for cultivating and analyzing environmental microbiota. *Microbiome* **1** (1): 4.
- Gavrish, E., Sit, C.S., Cao, S., Kandror, O., Spoering, A., Peoples, A., et al. (2014) Lassomycin, a ribosomally synthesized cyclic peptide, kills mycobacterium tuberculosis by targeting the ATP-dependent protease ClpC1P1P2. *Chem Biol* **21** (4): 509–518.
- Ghose, A.K., Viswanadhan, V.N., and Wendoloski, J.J. (1999) A knowledge-based approach in designing combinatorial or medicinal chemistry libraries for drug discovery. 1. A qualitative and quantitative characterization of known drug databases. *J Comb Chem* **1** (1): 55–68.
- Glaeser, J., Spohn, M., Oberpaul, M., Marner, M., Leis, B., Vilcinskis, A., and Hammann, P. (2018): Plugging in Microfluidics/FACS technologies in industrial discovery processes to exploit invertebrate microbiomes for new Gram negative antibiotics. *3rd European Conference On Natural Products 2018*. Frankfurt am Main, Germany. https://dechema.de/Veranstaltungen/Archiv/2018/3rd+ECNP+2018+_02_05_09/Programme/_/_neu_Programm_ECNP_2018.pdf [Access date: 16.04.2022].
- Gödeke, J., Paul, K., Lassak, J., and Thormann, K.M. (2011) Phage-induced lysis enhances biofilm formation in Shewanella oneidensis MR-1. *ISME J* **5** (4): 613–626.
- Goldstein, S.L., and Klassen, J.L. (2020) Pseudonocardia Symbionts of Fungus-Growing Ants and the Evolution of Defensive Secondary Metabolism. *Front Microbiol* **11**: 621041.
- Goormaghtigh, F., and van Melderen, L. (2019) Single-cell imaging and characterization of Escherichia coli persister cells to ofloxacin in exponential cultures. *Sci. Adv.* **5** (6): eaav9462.
- Hacker, J., and Kaper, J.B. (2000) Pathogenicity islands and the evolution of microbes. *Annu. Rev. Microbiol.* **54** (1): 641–679.
- Harbers, M. (2008) The current status of cDNA cloning. *Genomics* **91** (3): 232–242.
- Heine, D., Holmes, N.A., Worsley, S.F., Santos, A.C.A., Innocent, T.M., Scherlach, K., et al. (2018) Chemical warfare between leafcutter ant symbionts and a co-evolved pathogen. *Nat Commun* **9** (1): 2208.
- Heise, P., Liu, Y., Degenkolb, T., Vogel, H., Schäberle, T.F., and Vilcinskis, A. (2019) Antibiotic-Producing Beneficial Bacteria in the Gut of the Burying Beetle *Nicrophorus vespilloides*. *Front Microbiol* **10**: 1178.
- Hengoju, S., Tovar, M., Man, D.K.W., Buchheim, S., and Rosenbaum, M.A. (2020) Droplet Microfluidics for Microbial Biotechnology. *Adv Biochem Eng Biotechnol.*
- Herrmann, J., Fayad, A.A., and Müller, R. (2017) Natural products from myxobacteria: novel metabolites and bioactivities. *Nat. Prod. Rep.* **34** (2): 135–160.

- Hirsch, R., Wiesner, J., Marker, A., Pfeifer, Y., Bauer, A., Hammann, P.E., and Vilcinskas, A. (2019) Profiling antimicrobial peptides from the medical maggot *Lucilia sericata* as potential antibiotics for MDR Gram-negative bacteria. *J Antimicrob Chemother* **74** (1): 96–107.
- Hoffmann, T., Krug, D., Bozkurt, N., Duddela, S., Jansen, R., Garcia, R., et al. (2018) Correlating chemical diversity with taxonomic distance for discovery of natural products in myxobacteria. *Nat Commun* **9** (1): 803.
- Høiby, N., Bjarnsholt, T., Givskov, M., Molin, S., and Ciofu, O. (2010) Antibiotic resistance of bacterial biofilms. *International Journal of Antimicrobial Agents* **35** (4): 322–332.
- Høiby, N., Ciofu, O., Johansen, H.K., Song, Z., Moser, C., Jensen, P.Ø., et al. (2011) The clinical impact of bacterial biofilms. *Int J Oral Sci* **3** (2): 55–65.
- Huemer, M., Mairpady Shambat, S., Brugger, S.D., and Zinkernagel, A.S. (2020) Antibiotic resistance and persistence—Implications for human health and treatment perspectives. *EMBO Rep* **21** (12): e51034.
- Hug, L.A., Baker, B.J., Anantharaman, K., Brown, C.T., Probst, A.J., Castelle, C.J., et al. (2016) A new view of the tree of life. *Nat Microbiol* **1**: 16048.
- Hutchings, M.I., Truman, A.W., and Wilkinson, B. (2019) Antibiotics: past, present and future. *Curr Opin Microbiol* **51**: 72–80.
- Iglesias, A., Latorre-Pérez, A., Stach, J.E.M., Porcar, M., and Pascual, J. (2020) Out of the Abyss: Genome and Metagenome Mining Reveals Unexpected Environmental Distribution of Abyssomicins. *Front Microbiol* **11**: 645.
- Imai, Y., Meyer, K.J., Iinishi, A., Favre-Godal, Q., Green, R., Manuse, S., et al. (2019) A new antibiotic selectively kills Gram-negative pathogens. *Nature* **576** (7787): 459–464.
- Jahn, L.J., Munck, C., Ellabaan, M.M.H., and Sommer, M.O.A. (2017) Adaptive Laboratory Evolution of Antibiotic Resistance Using Different Selection Regimes Lead to Similar Phenotypes and Genotypes. *Front Microbiol* **8**: 816.
- Janashia, I., Choiset, Y., Rabesona, H., Hwanhlem, N., Bakuradze, N., Chanishvili, N., and Haertlé, T. (2016) Protection of honeybee *Apis mellifera* by its endogenous and exogenous lactic flora against bacterial infections. *Ann Agr Sci* **14** (3): 177–181.
- Janion, C. (2008) Inducible SOS response system of DNA repair and mutagenesis in *Escherichia coli*. *Int. J. Biol. Sci.* **4** (6): 338–344.
- Jiang, C.-Y., Dong, L., Zhao, J.-K., Hu, X., Shen, C., Qiao, Y., et al. (2016) High-Throughput Single-Cell Cultivation on Microfluidic Streak Plates. *Appl Environ Microbiol* **82** (7): 2210–2218.
- Junker, B., Walker, A., Connors, N., Seeley, A., Masurekar, P., and Hesse, M. (2006) Production of indole diterpenes by *Aspergillus alliaceus*. *Biotechnol Bioeng* **95** (5): 919–937.
- Jürjens, G., Schuler, S.M.M., Kurz, M., Petit, S., Couturier, C., Jeannot, F., et al. (2018) Total Synthesis and Structural Revision of the Antibiotic Tetrapeptide GE81112A. *Angew Chem Int Ed Engl* **57** (37): 12157–12161.
- Kaeberlein, T., Lewis, K., and Epstein, S.S. (2002) Isolating "uncultivable" microorganisms in pure culture in a simulated natural environment. *Science* **296** (5570): 1127–1129.
- Kaldalu, N., Haurlyiuk, V., Turnbull, K.J., La Mensa, A., Putrinš, M., and Tenson, T. (2020) In Vitro Studies of Persister Cells. *Microbiol Mol Biol Rev* **84** (4).
- Kallscheuer, N., and Jogler, C. (2021) The bacterial phylum Planctomycetes as novel source for bioactive small molecules. *Biotechnol Adv* **53**: 107818.
- Kästner, B., Hengoju, S., Svensson, C.-M., Figge, M.T., and Rosenbaum, M.A. (2021) Mit Tropfenmikrofluidik zu Hochgeschwindigkeits-Biotechnologie. *Biospektrum* **27** (3): 260–262.
- Katz, L., and Baltz, R.H. (2016) Natural product discovery: past, present, and future. *J Ind Microbiol Biotech* **43** (2–3): 155–176.
- Kielak, A.M., Barreto, C.C., Kowalchuk, G.A., van Veen, J.A., and Kuramae, E.E. (2016) The Ecology of Acidobacteria: Moving beyond Genes and Genomes. *Front Microbiol* **7**: 744.
- Kielak, A.M., Castellane, T.C.L., Campanharo, J.C., Colnago, L.A., Costa, O.Y.A., Da Corradi Silva, M.L., et al. (2017) Characterization of novel Acidobacteria exopolysaccharides with potential industrial and ecological applications. *Sci Rep* **7**: 41193.
- Klassen, J.L., Lee, S.R., Poulsen, M., Beemelmans, C., and Kim, K.H. (2019) Efmomyins K and L From a Termite-Associated *Streptomyces* sp. M56 and Their Putative Biosynthetic Origin. *Front Microbiol* **10**: 1739.
- Klaus, M., Zurek, P.J., Kaminski, T.S., Pushpanath, A., Neufeld, K., and Hollfelder, F. (2021) Ultrahigh-Throughput Detection of Enzymatic Alcohol Dehydrogenase Activity in Microfluidic Droplets with a Direct Fluorogenic Assay. *ChemBioChem*.
- Klugman, K.P., and Black, S. (2018) Impact of existing vaccines in reducing antibiotic resistance: Primary and secondary effects. *Proc Natl Acad Sci USA* **115** (51): 12896–12901.
- Klugman, K.P., Madhi, S.A., Huebner, R.E., Kohberger, R., Mbelle, N., and Pierce, N. (2003) A trial of a 9-valent pneumococcal conjugate vaccine in children with and those without HIV infection. *N Engl J Med* **349** (14): 1341–1348.
- Kodali, S., Galgoci, A., Young, K., Painter, R., Silver, L.L., Herath, K.B., et al. (2005) Determination of selectivity and efficacy of fatty acid synthesis inhibitors. *J Bio Chem* **280** (2): 1669–1677.
- Korch, S.B., Henderson, T.A., and Hill, T.M. (2003) Characterization of the *hipA7* allele of *Escherichia coli* and evidence that high persistence is governed by (p)ppGpp synthesis. *Molecular Microbiology* **50** (4): 1199–1213.
- Krug, D., and Müller, R. (2014) Secondary metabolomics: the impact of mass spectrometry-based approaches on the discovery and characterization of microbial natural products. *Nat. Prod. Rep.* **31** (6): 768–783.
- Kumpitsch, C., Koskinen, K., Schöpf, V., and Moissl-Eichinger, C. (2019) The microbiome of the upper respiratory tract in health and disease. *BMC Biol* **17** (1): 87.
- Lackner, G., Peters, E.E., Helfrich, E.J.N., and Piel, J. (2017) Insights into the lifestyle of uncultured bacterial natural product factories associated with marine sponges. *Proc Natl Acad Sci USA* **114** (3): E347–E356.
- Lakemeyer, M., Zhao, W., Mandl, F.A., Hammann, P., and Sieber, S.A. (2018) Thinking Outside the Box—Novel Antibacterials To Tackle the Resistance Crisis. *Angew Chem Int Ed Engl* **57** (44): 14440–14475.
- Laxminarayan, R. (2021) 2020: The year of the microbe. *Indian J Med Microbiol* **39** (1): 140–141.
- Lechevalier, H.A., and Corke, C.T. (1953) The replica plate method for screening antibiotic-producing organisms. *Appl Microbiol* **1** (2): 110–112.
- Lee, S.-H., Ka, J.-O., and Cho, J.-C. (2008) Members of the phylum Acidobacteria are dominant and metabolically active in rhizosphere soil. *FEMS Microbiol Letters* **285** (2): 263–269.
- Leman, M., Abouakil, F., Griffiths, A.D., and Tabeling, P. (2015) Droplet-based microfluidics at the femtolitre scale. *Lab Chip* **15** (3): 753–765.
- Levin-Reisman, I., Gefen, O., Fridman, O., Ronin, I., Shwa, D., Sheftel, H., and Balaban, N.Q. (2010) Automated imaging with ScanLag reveals previously undetectable bacterial growth phenotypes. *Nat Methods* **7** (9): 737–739.
- Lewis, K. (2007) Persister cells, dormancy and infectious disease. *Nat Rev Microbiol* **5** (1): 48–56.
- Lewis, K. (2010) Persister cells. *Annu. Rev. Microbiol.* **64** (1): 357–372.
- Lewis, K. (2013) Platforms for antibiotic discovery. *Nat Rev Drug Discov* **12** (5): 371–387.
- Lewis, K. (2021) The Science of Antibiotic Discovery. *Cell* **181** (1): 29–45.
- Ling, L.L., Schneider, T., Peoples, A.J., Spoering, A.L., Engels, I., Conlon, B.P., et al. (2015) A new antibiotic kills pathogens without detectable resistance. *Nature* **517** (7535): 455–459.
- Lipinski, C.A., Lombardo, F., Dominy, B.W., and Feeney, P.J. (2001) Experimental and computational

- approaches to estimate solubility and permeability in drug discovery and development settings PII of original article: S0169-409X(96)00423-1. The article was originally published in *Advanced Drug Delivery Reviews* 23 (1997) 3–25. 1. *Advanced Drug Delivery Reviews* **46** (1-3): 3–26.
- Lok, C. (2015) Mining the microbial dark matter. *Nature* **522** (7556): 270–273.
- Lucien, M.A.B., Canarie, M.F., Kilgore, P.E., Jean-Denis, G., Fénélon, N., Pierre, M., *et al.* (2021) Antibiotics and antimicrobial resistance in the COVID-19 era: Perspective from resource-limited settings. *Int J Infect Dis* **104**: 250–254.
- Ma, F., Xu, S., Tang, Z., Li, Z., and Zhang, L. (2021) Use of antimicrobials in food animals and impact of transmission of antimicrobial resistance on humans. *Biosafety and Health* **3** (1): 32–38.
- Maeda, T., Iwasawa, J., Kotani, H., Sakata, N., Kawada, M., Horinouchi, T., *et al.* (2020) High-throughput laboratory evolution reveals evolutionary constraints in *Escherichia coli*. *Nat Commun* **11** (1): 5970.
- Mahler, L., Niehs, S.P., Martin, K., Weber, T., Scherlach, K., Hertweck, C., *et al.* (2021) Highly parallelized droplet cultivation and prioritization of antibiotic producers from natural microbial communities. *eLife* **10**.
- Mahler, L., Wink, K., Beulig, R.J., Scherlach, K., Tovar, M., Zang, E., *et al.* (2018) Detection of antibiotics synthesized in microfluidic picolitre-droplets by various actinobacteria. *Sci Rep* **8** (1): 13087.
- Manuse, S., Shan, Y., Canas-Duarte, S.J., Bakshi, S., Sun, W.-S., Mori, H., *et al.* (2021) Bacterial persisters are a stochastically formed subpopulation of low-energy cells. *PLoS Biol* **19** (4): e3001194.
- Marner, M., Patras, M.A., Kurz, M., Zubeil, F., Förster, F., Schuler, S., *et al.* (2020) Molecular Networking-Guided Discovery and Characterization of Stechlisins, a Group of Cyclic Lipopeptides from a *Pseudomonas* sp. *J. Nat. Prod.* **83** (9): 2607–2617.
- Mason, D.J., Power, E.G., Talsania, H., Phillips, I., and Gant, V.A. (1995) Antibacterial action of ciprofloxacin. *Antimicrob Agents Chemother* **39** (12): 2752–2758.
- Matilla, M.A. (2021) Facing crises in the 21st century: microfluidics approaches for antibiotic discovery. *Microb Biotechnol.*
- Matthews, H., Hanison, J., and Nirmalan, N. (2016) "Omics"-Informed Drug and Biomarker Discovery: Opportunities, Challenges and Future Perspectives. *Proteomes* **4** (3): 28.
- Matthijs, S., Vander Wauven, C., Cornu, B., Ye, L., Cornelis, P., Thomas, C.M., and Ongena, M. (2014) Antimicrobial properties of *Pseudomonas* strains producing the antibiotic mupirocin. *Res Microbiol* **165** (8): 695–704.
- Medema, M.H., Rond, T. de, and Moore, B.S. (2021) Mining genomes to illuminate the specialized chemistry of life. *Nat Rev Genet* **22** (9): 553–571.
- Mohiuddin, S.G., Kavousi, P., and Orman, M.A. (2020) Flow-cytometry analysis reveals persister resuscitation characteristics. *BMC Microbiol* **20** (1): 202.
- Mok, W.W.K., and Brynildsen, M.P. (2018) Timing of DNA damage responses impacts persistence to fluoroquinolones. *Proc Natl Acad Sci USA* **115** (27): E6301–E6309.
- Mølbak, K. (2004) Spread of resistant bacteria and resistance genes from animals to humans--the public health consequences. *J Vet Med Series B* **51** (8-9): 364–369.
- Morel, C.M., Alm, R.A., Årdal, C., Bandera, A., Bruno, G.M., Carrara, E., *et al.* (2020) A one health framework to estimate the cost of antimicrobial resistance. *Antimicrob Resist Infect Control* **9** (1): 187.
- Mulani, M.S., Kamble, E.E., Kumkar, S.N., Tawre, M.S., and Pardesi, K.R. (2019) Emerging Strategies to Combat ESKAPE Pathogens in the Era of Antimicrobial Resistance: A Review. *Front Microbiol* **10**: 539.
- Nakamura, K., Yamazaki, Y., Shiraishi, A., Kobayashi, S., Harada, M., Yoshiyama, M., *et al.* (2016) Virulence Differences among *Melicoccoccus plutonius* Strains with Different Genetic Backgrounds in *Apis mellifera* Larvae under an Improved Experimental Condition. *Sci Rep* **6** (1): 33329.
- Navarrete, A.A., Kuramae, E.E., Hollander, M. de, Pijl, A.S., van Veen, J.A., and Tsai, S.M. (2013) Acidobacterial community responses to agricultural management of soybean in Amazon forest soils. *FEMS Microbiol Ecol* **83** (3): 607–621.
- Newman, D.J., and Cragg, G.M. (2020) Natural Products as Sources of New Drugs over the Nearly Four Decades from 01/1981 to 09/2019. *J Nat Prod* **83** (3): 770–803.
- Nge, P.N., Rogers, C.I., and Woolley, A.T. (2013) Advances in microfluidic materials, functions, integration, and applications. *Chem. Rev.* **113** (4): 2550–2583.
- Nichols, D., Cahoon, N., Trakhtenberg, E.M., Pham, L., Mehta, A., Belanger, A., *et al.* (2010) Use of ichip for high-throughput in situ cultivation of "uncultivable" microbial species. *Appl Environ Microbiol* **76** (8): 2445–2450.
- Nichols, W.W., Newell, P., Critchley, I.A., Riccobene, T., and Das, S. (2018) Avibactam Pharmacokinetic/Pharmacodynamic Targets. *Antimicrob Agents Chemother* **62** (6).
- Nonin-Lecomte, S., Fermon, L., Felden, B., and Pinel-Marie, M.-L. (2021) Bacterial Type I Toxins: Folding and Membrane Interactions. *Toxins* **13** (7): 490.
- Nora, L.C., Westmann, C.A., Martins-Santana, L., Alves, L.d.F., Monteiro, L.M.O., Guazzaroni, M.-E., and Silva-Rocha, R. (2019) The art of vector engineering: towards the construction of next-generation genetic tools. *Microb Biotechnol* **12** (1): 125–147.
- Nouioui, I., Carro, L., García-López, M., Meier-Kolthoff, J.P., Woyke, T., Kyrpides, N.C., *et al.* (2018) Genome-Based Taxonomic Classification of the Phylum Actinobacteria. *Front Microbiol* **9**: 2007.
- Nyström, T. (2004) Stationary-phase physiology. *Annu. Rev. Microbiol.* **58** (1): 161–181.
- Oberpaul, M., Brinkmann, S., Marner, M., Mihajlovic, S., Leis, B., Patras, M.A., *et al.* (2021) Combination of high-throughput microfluidics and FACS technologies to leverage the numbers game in natural product discovery. *Microb Biotechnol.*
- Oberpaul, M., Spohn, M.S., Brinkmann, S., Mihajlovic, S., Marner, M., Patras, M.A., *et al.* (2022) Trichoderma-derived pentapeptides from the infected nest mycobiome of the subterranean termite *Coptotermes testaceus*. *ChemBioChem*: e202100698.
- Oberpaul, M., Zumkeller, C.M., Culver, T., Spohn, M., Mihajlovic, S., Leis, B., *et al.* (2020) High-Throughput Cultivation for the Selective Isolation of Acidobacteria From Termite Nests. *Front Microbiol* **11**: 597628.
- Orman, M.A., and Brynildsen, M.P. (2016) Persister formation in *Escherichia coli* can be inhibited by treatment with nitric oxide. *Free Radic Biol Med* **93**: 145–154.
- Palazzotto, E., and Weber, T. (2018) Omics and multi-omics approaches to study the biosynthesis of secondary metabolites in microorganisms. *Curr Opin Microbiol* **45**: 109–116.
- Panter, F., Bader, C.D., and Müller, R. (2021) Synergizing the potential of bacterial genomics and metabolomics to find novel antibiotics. *Chem. Sci.* **12** (17): 5994–6010.
- Pendleton, J.N., Gorman, S.P., and Gilmore, B.F. (2013) Clinical relevance of the ESKAPE pathogens. *Expert Review of Anti-infective Therapy* **11** (3): 297–308.
- Pintado, V., Ruiz-Garabajosa, P., Escudero-Sanchez, R., Gioia, F., Herrera, S., Vizcarra, P., *et al.* (2022) Carbapenemase-producing Enterobacterales infections in COVID-19 patients. *Infect Dis (Lond)* **54** (1): 36–45.
- Pye, C.R., Bertin, M.J., Lokey, R.S., Gerwick, W.H., and Lington, R.G. (2017) Retrospective analysis of natural products provides insights for future discovery trends. *Proc Natl Acad Sci USA* **114** (22): 5601–5606.
- Quigley, J., Peoples, A., Sarybaeva, A., Hughes, D., Ghiglieri, M., Achorn, C., *et al.* (2020) Novel Antimicrobials from Uncultured Bacteria Acting against *Mycobacterium tuberculosis*. *mBio* **11** (4).
- Quinn, G.A., Banat, A.M., Abdelhameed, A.M., and Banat, I.M. (2020) Streptomycetes from traditional medicine:

- sources of new innovations in antibiotic discovery. *Journal of Medical Microbiology* **69** (8): 1040–1048.
- Rangseekaew, P., and Pathom-Aree, W. (2019) Cave Actinobacteria as Producers of Bioactive Metabolites. *Front Microbiol* **10**: 387.
- Rawson, T.M., Wilson, R.C., and Holmes, A. (2021) Understanding the role of bacterial and fungal infection in COVID-19. *Clin Microbiol Infect* **27** (1): 9–11.
- Reiter, S., Cahn, J.K.B., Wiebach, V., Ueoka, R., and Piel, J. (2020) Characterization of an Orphan Type III Polyketide Synthase Conserved in Uncultivated "Entotheonella" Sponge Symbionts. *ChemBioChem* **21** (4): 564–571.
- Riedlinger, J., Reicke, A., Zähler, H., Krismer, B., Bull, A.T., Maldonado, L.A., et al. (2004) Abyssomicins, inhibitors of the para-aminobenzoic acid pathway produced by the marine *Verrucospora* strain AB-18-032. *J Antibiot (Tokyo)* **57** (4): 271–279.
- Riyanti, Marner, M., Hartwig, C., Patras, M.A., Wodi, S.I.M., Rieuwpassa, F.J., et al. (2020) Sustainable Low-Volume Analysis of Environmental Samples by Semi-Automated Prioritization of Extracts for Natural Product Research (SeaPEPR). *Mar Drugs* **18** (12): 649.
- Sadaka, C., Ellsworth, E., Hansen, P.R., Ewin, R., Damborg, P., and Watts, J.L. (2018) Review on Abyssomicins: Inhibitors of the Chorismate Pathway and Folate Biosynthesis. *Molecules* **23** (6): 1371.
- Sakula, A. (1988) Selman Waksman (1888–1973), discoverer of streptomycin: A centenary review. *British Journal of Diseases of the Chest* **82**: 23–31.
- Sanseverino, I., Navarro Cuenca, A., Loos, R., Marinov, D., and Lettieri, T. (2019) *State of the Art on the Contribution of Water to Antimicrobial Resistance*.
- Schäberle, T.F., and Hack, I.M. (2014) Overcoming the current deadlock in antibiotic research. *Trends Microbiol* **22** (4): 165–167.
- Schatz, A., Bugle, E., and Waksman, S.A. (1944) Streptomycin, a Substance Exhibiting Antibiotic Activity Against Gram-Positive and Gram-Negative Bacteria*. *Experimental Biology and Medicine* **55** (1): 66–69.
- Scherlach, K., and Hertweck, C. (2021) Mining and unearthing hidden biosynthetic potential. *Nat Commun* **12** (1): 3864.
- Schmidt, E.W., Obratsova, A.Y., Davidson, S.K., Faulkner, D.J., and Haygood, M.G. (2000) Identification of the antifungal peptide-containing symbiont of the marine sponge *Theonella swinhoei* as a novel δ -proteobacterium, "Candidatus Entotheonella palauensis". *Marine Biology* **136** (6): 969–977.
- Schmidt, S., Kildgaard, S., Guo, H., Beemelmans, C., and Poulsen, M. (2021) The chemical ecology of the fungus-farming termite symbiosis. *Nat. Prod. Rep.*
- Schneider, Y.K. (2021) Bacterial Natural Product Drug Discovery for New Antibiotics: Strategies for Tackling the Problem of Antibiotic Resistance by Efficient Bioprospecting. *Antibiotics (Basel)* **10** (7).
- Semanjski, M., Germain, E., Bratl, K., Kiessling, A., Gerdes, K., and Macek, B. (2018) The kinases HipA and HipA7 phosphorylate different substrate pools in *Escherichia coli* to promote multidrug tolerance. *Sci. Signal.* **11** (547).
- Shan, Y., Brown Gandt, A., Rowe, S.E., Deisinger, J.P., Conlon, B.P., and Lewis, K. (2017) ATP-Dependent Persister Formation in *Escherichia coli*. *mBio* **8** (1).
- Shirley, M. (2018) Ceftazidime-Avibactam: A Review in the Treatment of Serious Gram-Negative Bacterial Infections. *Drugs* **78** (6): 675–692.
- Shong, J., Jimenez Diaz, M.R., and Collins, C.H. (2012) Towards synthetic microbial consortia for bioprocessing. *Curr Opin Biotechnol* **23** (5): 798–802.
- Sikorski, J., Baumgartner, V., Birkhofer, K., Boeddinghaus, R.S., Bunk, B., Fischer, M., et al. (2022) The Evolution of Ecological Diversity in Acidobacteria. *Front Microbiol* **13**.
- Skhiri, Y., Gruner, P., Semin, B., Brosseau, Q., Pekin, D., Mazutis, L., et al. (2012) Dynamics of molecular transport by surfactants in emulsions. *Soft Matter* **8** (41): 10618.
- Sköld, O. (2000) Sulfonamide resistance: mechanisms and trends. *Drug Resist Updat* **3** (3): 155–160.
- Sohlenkamp, C., and Geiger, O. (2016) Bacterial membrane lipids: diversity in structures and pathways. *FEMS Microbiol Rev* **40** (1): 133–159.
- Song, S., and Wood, T.K. (2021) 'Viable but non-culturable cells' are dead. *Environ Microbiol* **23** (5): 2335–2338.
- Srinivas, N., Jetter, P., Ueberbacher, B.J., Werneburg, M., Zerbe, K., Steinmann, J., et al. (2010) Peptidomimetic antibiotics target outer-membrane biogenesis in *Pseudomonas aeruginosa*. *Science* **327** (5968): 1010–1013.
- Staley, J.T., and Konopka, A. (1985) Measurement of in situ activities of nonphotosynthetic microorganisms in aquatic and terrestrial habitats. *Annu. Rev. Microbiol.* **39** (1): 321–346.
- Stokes, J.M., Yang, K., Swanson, K., Jin, W., Cubillos-Ruiz, A., Donghia, N.M., et al. (2020) A Deep Learning Approach to Antibiotic Discovery. *Cell* **180** (4): 688–702.e13.
- Stork, N.E. (2018) How Many Species of Insects and Other Terrestrial Arthropods Are There on Earth? *Annu. Rev. Entomol.* **63** (1): 31–45.
- Tacconelli, E., Carrara, E., Savoldi, A., Harbarth, S., Mendelson, M., Monnet, D.L., et al. (2018) Discovery, research, and development of new antibiotics: the WHO priority list of antibiotic-resistant bacteria and tuberculosis. *The Lancet Infectious Diseases* **18** (3): 318–327.
- Tanikawa, T., Nakagawa, Y., and Matsuyama, T. (2006) Transcriptional downregulator hexS controlling prodigiosin and serrawettin W1 biosynthesis in *Serratia marcescens*. *Microbiol Immunol* **50** (8): 587–596.
- Tegtmeier, D., Hurka, S., Mihajlovic, S., Bodenschatz, M., Schlimbach, S., and Vilcinskis, A. (2021) Culture-Independent and Culture-Dependent Characterization of the Black Soldier Fly Gut Microbiome Reveals a Large Proportion of Culturable Bacteria with Potential for Industrial Applications. *Microorganisms* **9** (8).
- Terekhov, S.S., Smirnov, I.V., Stepanova, A.V., Bobik, T.V., Mokrushina, Y.A., Ponomarenko, N.A., et al. (2017) Microfluidic droplet platform for ultrahigh-throughput single-cell screening of biodiversity. *Proc Natl Acad Sci USA* **114** (10): 2550–2555.
- Thomas, C.M., and Nielsen, K.M. (2005) Mechanisms of, and barriers to, horizontal gene transfer between bacteria. *Nat Rev Microbiol* **3** (9): 711–721.
- Tommasi, R., Brown, D.G., Walkup, G.K., Manchester, J.I., and Miller, A.A. (2015) ESKAPEing the labyrinth of antibacterial discovery. *Nat Rev Drug Discov* **14** (8): 529–542.
- Tortorella, E., Tedesco, P., Palma Esposito, F., January, G.G., Fani, R., Jaspars, M., and Pascale, D. de (2018) Antibiotics from Deep-Sea Microorganisms: Current Discoveries and Perspectives. *Mar Drugs* **16** (10).
- U.S. Centers for Disease Control and Prevention (2013) *Antibiotic resistance threats in the United States, 2013: Accessed September 15, 2021.* <https://www.cdc.gov/drugresistance/biggest-threats.html>.
- U.S. Centers for Disease Control and Prevention (2019) *Antibiotic resistance threats in the United States, 2019: Accessed August 25, 2021.* <https://www.cdc.gov/drugresistance/biggest-threats.html>.
- Uzoechi, S.C., and Abu-Lail, N.I. (2020) Variations in the Morphology, Mechanics and Adhesion of Persister and Resister *E. coli* Cells in Response to Ampicillin: AFM Study. *Antibiotics (Basel)* **9** (5).
- van Arnam, E.B., Ruzzini, A.C., Sit, C.S., Horn, H., Pinto-Tomás, A.A., Currie, C.R., and Clardy, J. (2016) Selvamycin, an atypical antifungal polyene from two alternative genomic contexts. *Proc Natl Acad Sci USA* **113** (46): 12940–12945.
- van Boeckel, T.P., Brower, C., Gilbert, M., Grenfell, B.T., Levin, S.A., Robinson, T.P., et al. (2015) Global trends in antimicrobial use in food animals. *Proc Natl Acad Sci USA* **112** (18): 5649–5654.
- van Moll, L., Smet, J. de, Cos, P., and van Campenhout, L. (2021) Microbial symbionts of insects as a source of

- new antimicrobials: a review. *Crit Rev Microbiol* **47** (5): 562–579.
- Vekemans, J., Hasso-Agopsowicz, M., Kang, G., Hausdorff, W.P., Fiore, A., Tayler, E., *et al.* (2021) Leveraging Vaccines to Reduce Antibiotic Use and Prevent Antimicrobial Resistance: a WHO Action Framework. *Clinical Infectious Diseases*.
- Ventola, C.L. (2015) The antibiotic resistance crisis: part 1: causes and threats. *PT* **40** (4): 277–283.
- Verbeke, F., Craemer, S. de, Debunne, N., Janssens, Y., Wynendaele, E., van de Wiele, C., and Spiegeleer, B. de (2017) Peptides as Quorum Sensing Molecules: Measurement Techniques and Obtained Levels In vitro and In vivo. *Front Neurosci* **11**: 183.
- Volpatti, L.R., and Yetisen, A.K. (2014) Commercialization of microfluidic devices. *Trends Biotechnol* **32** (7): 347–350.
- Völzing, K.G., and Brynildsen, M.P. (2015) Stationary-Phase Persisters of Ofloxacin Sustain DNA Damage and Require Repair Systems Only during Recovery. *mBio* **6** (5): e00731-15.
- Waksman, S.A. (1943) Production and Activity of Streptomycin. *J Bacteriol* **46** (3): 299–310.
- Waksman, S.A. (1947) Microbial Antagonisms and Antibiotic Substances. *Arch Intern Med* **80** (3): 418.
- Waksman, S.A. (1950) Streptomycin and neomycin: an antibiotic approach to tuberculosis. *Br Med J* **2** (4679): 595–600.
- Waksman, S.A. (1960) The actinomycins and their importance. *Ann. N.Y. Acad. Sci.* **89**: 484–485.
- Waksman, S.A., Horning, E.S., and Spencer, E.L. (1942) THE PRODUCTION OF TWO ANTIBACTERIAL SUBSTANCES, FUMIGACIN AND CLAVACIN. *Science* **96** (2487): 202–203.
- Waksman, S.A., and Lechevalier, H.A. (1949) Neomycin, a New Antibiotic Active against Streptomycin-Resistant Bacteria, including Tuberculosis Organisms. *Science* **109** (2830): 305–307.
- Wang, J., Soisson, S.M., Young, K., Shoop, W., Kodali, S., Galgocsi, A., *et al.* (2006) Platensimycin is a selective FabF inhibitor with potent antibiotic properties. *Nature* **441** (7091): 358–361.
- Whitehead, N.A., Barnard, A.M., Slater, H., Simpson, N.J., and Salmond, G.P. (2001) Quorum-sensing in Gram-negative bacteria. *FEMS Microbiol Rev* **25** (4): 365–404.
- Wiegand, S., Jogler, M., and Jogler, C. (2018) On the maverick Planctomycetes. *FEMS Microbiol Rev* **42** (6): 739–760.
- Wilson, M.C., Mori, T., Rückert, C., Uria, A.R., Helf, M.J., Takada, K., *et al.* (2014) An environmental bacterial taxon with a large and distinct metabolic repertoire. *Nature* **506** (7486): 58–62.
- Wink, J., Mohammadipanah, F., and Hamed, J. (ed.) (2017) *Biology and Biotechnology of Actinobacteria*. Cham: Springer International Publishing.
- Wohlleben, W., Bera, A., Mast, Y., and Stegmann, E. (2017) Regulation of Secondary Metabolites of Actinobacteria. In *Biology and Biotechnology of Actinobacteria*. Wink, J., Mohammadipanah, F., and Hamed, J. (ed.). Cham: Springer International Publishing, pp. 181–232.
- Wohlleben, W., Mast, Y., Stegmann, E., and Ziemert, N. (2016) Antibiotic drug discovery. *Microb Biotechnol* **9** (5): 541–548.
- Wong, F., Stokes, J.M., Cervantes, B., Penkov, S., Friedrichs, J., Renner, L.D., and Collins, J.J. (2021) Cytoplasmic condensation induced by membrane damage is associated with antibiotic lethality. *Nat Commun* **12** (1): 2321.
- Wood, T.K., González Barrios, A.F., Herzberg, M., and Lee, J. (2006) Motility influences biofilm architecture in *Escherichia coli*. *Appl Microbiol Biotechnol* **72** (2): 361–367.
- World Health Organization 2019 The 2019 WHO AWaRe classification of antibiotics for evaluation and monitoring of use.
- Woznica, A., Cantley, A.M., Beemelmans, C., Freinkman, E., Clardy, J., and King, N. (2016) Bacterial lipids activate, synergize, and inhibit a developmental switch in choanoflagellates. *Proc Natl Acad Sci USA* **113** (28): 7894–7899.
- Wright, G. (2015) Antibiotics: An irresistible newcomer. *Nature* **517** (7535): 442–444.
- Wu, N., He, L., Cui, P., Wang, W., Yuan, Y., Liu, S., *et al.* (2015) Ranking of persister genes in the same *Escherichia coli* genetic background demonstrates varying importance of individual persister genes in tolerance to different antibiotics. *Front Microbiol* **6**: 1003.
- Zaslaver, A., Bren, A., Ronen, M., Itzkovitz, S., Kikoin, I., Shavit, S., *et al.* (2006) A comprehensive library of fluorescent transcriptional reporters for *Escherichia coli*. *Nat Methods* **3** (8): 623–628.
- Zendo, T., Ohashi, C., Maeno, S., Piao, X., Salminen, S., Sonomoto, K., and Endo, A. (2020) Kunkecin A, a New Nisin Variant Bacteriocin Produced by the Fructophilic Lactic Acid Bacterium, *Apilactobacillus kunkeei* FF30-6 Isolated From Honey Bees. *Front Microbiol* **11**: 571903.
- Zengler, K., Toledo, G., Rappe, M., Elkins, J., Mathur, E.J., Short, J.M., and Keller, M. (2002) Cultivating the uncultured. *Proc Natl Acad Sci USA* **99** (24): 15681–15686.
- Zha, L., Pan, L., Guo, J., French, N., Villanueva, E.V., and Tefsen, B. (2020) Effectiveness and Safety of High Dose Tigecycline for the Treatment of Severe Infections: A Systematic Review and Meta-Analysis. *Adv Ther* **37** (3): 1049–1064.
- Zhang, J., Li, B., Qin, Y., Karthik, L., Zhu, G., Hou, C., *et al.* (2020) A new abyssomicin polyketide with anti-influenza A virus activity from a marine-derived *Verrucosipora* sp. MS100137. *Appl Microbiol Biotechnol* **104** (4): 1533–1543.
- Zhang, W., Ding, W., Li, Y.-X., Tam, C., Bougouffa, S., Wang, R., *et al.* (2019) Marine biofilms constitute a bank of hidden microbial diversity and functional potential. *Nat Commun* **10** (1): 517.
- Zheng, E.J., Stokes, J.M., and Collins, J.J. (2020) Eradicating Bacterial Persisters with Combinations of Strongly and Weakly Metabolism-Dependent Antibiotics. *Cell Chem Biol* **27** (12): 1544–1552.e3.
- Zinchenko, A., Devenish, S.R.A., Kintses, B., Colin, P.-Y., Fischlechner, M., and Hollfelder, F. (2014) One in a million: flow cytometric sorting of single cell-lysate assays in monodisperse picolitre double emulsion droplets for directed evolution. *Anal. Chem.* **86** (5): 2526–2533.
- Zipperer, A., Konnerth, M.C., Laux, C., Berscheid, A., Janek, D., Weidenmaier, C., *et al.* (2016) Human commensals producing a novel antibiotic impair pathogen colonization. *Nature* **535** (7613): 511–516.
- Zwick, C.R., Sosa, M.B., and Renata, H. (2021) Modular Chemoenzymatic Synthesis of GE81112 B1 and Related Analogues Enables Elucidation of Its Key Pharmacophores. *J Am Chem Soc* **143** (3): 1673–1679.

9. SUPPORTING INFORMATION

Table S1: All marketed antibiotic classes at this time, a well-known example, origin and mechanism of action. NP = NP origin (Fungi or Bacterium); S = synthetic; (Butler, 2004; Butler and Buss, 2006; Lakemeyer *et al.*, 2018). B = bacterial origin; F = fungal origin); BB = broad-spectrum, G+ = Gram-positive; G- = Gram-negative.

No	Antibiotic class	Example	Origin	First microorganism	Mechanism of action	Target
1	Aminoglycosides	Kanamycin	NP	B (<i>Streptomyces kanamyceticus</i>)	30S ribosomal subunit	BS
2	Tetracyclines	Oxytetracycline	NP	B (<i>Streptomyces aureofaciens/rimosus</i>)	30S ribosomal subunit	BS
3	Chloramphenicol	Chloramphenicol	NP	B (<i>Streptomyces venezuelae</i>)	50S ribosomal subunit	BS
4	Fusidic acid	Fusidic acid	NP	F (<i>Fusidium coccineum</i>)	50S ribosomal subunit	G+
5	Lincosamides	Lincomycin	NP	B (<i>Streptomyces lincolnensis</i>)	50S ribosomal subunit	BS
6	Macrolides	Erythromycin	NP	B (<i>Saccharopolyspora erythraea</i>)	50S ribosomal subunit	BS
7	Streptogramins	Pristinamycin	NP	B (<i>Streptomyces pristinaespiralis</i>)	50S ribosomal subunit	G+
8	Glycopeptides	Vancomycin	NP	B (<i>Amycolatopsis orientalis</i>)	Cell wall synthesis (D-Ala-D)	G+
9	Quinolones	Ciprofloxacin	S	synthetic	DNA-Gyrase + unknown mechanism supposed	BS
10	Aminopyrimidines	Trimethoprim	S	synthetic	Folic acid metabolism	BS

No	Antibiotic class	Example	Origin	First microorganism	Mechanism of action	Target
11	Sulfonamides	Prontosil	S	synthetic	Folic acid metabolism	G+
12	Oxazolidinone	Linezolid	S	synthetic	<i>N</i> -formylmethionyl-tRNA-ribosome-mRNA complex	BS
13	Nitro-heterocycles	Nitrofurantoin	S	synthetic	Nucleic acid synthesis (formation of toxic compounds)	BS
14	Lipopeptides	Daptomycin	NP	B (<i>Streptomyces roseosporus</i>)	Pore formation (Depolarization)	G+
15	Polypeptides	e.g Colistin	NP	B (e.g. <i>Bacillus colistinus</i>)	Pore formation (Depolarization)	G-
16	Carbapenems	Thienamycin	NP	B (<i>Streptomyces cattleya</i>)	Transpeptidase (Cell wall)	BS
17	Cephalosporins	Cephalosporin C	NP	F (<i>Acremonium chrysogenum</i>)	Transpeptidase (Cell wall)	BS
18	Monobactams	Aztreonam	NP	B (<i>Chromobacterium violaceum</i>)	Transpeptidase (Cell wall)	G-
19	β -lactams	Penicillin	NP	F (<i>Penicillium notatum</i>)	Transpeptidase (Cell wall)	BS
20	Fosfomycin	Fosfomycin	NP	B (<i>Streptomyces viridochromogenes</i>)	UDP-N-acetylglucosamine 1-carboxyvinyltransferase	BS
21	Ansamycines	Rifamycin	NP	B (<i>Amycolatopsis rifamycinica</i>)	β -subunit of DNA-dependent RNA-Polymerase	BS

10. DANKSAGUNGEN

Zunächst möchte ich Prof. Dr. Till Schäberle für den freundschaftlichen Umgang und die positive Arbeitsatmosphäre herzlich danken, und dafür, dass er die Betreuung und das Erstgutachten dieser Arbeit übernommen hat, sowie für die Hilfe beim Einstieg in das neue Projekt.

Besonderer Dank gilt PD Dr. Jens Glaeser, aber auch Prof. Dr. Peter Hamann und Prof. Dr. Andreas Vilcinskas für die Initiierung des Projektes, die freundliche Einführung in die Projektgruppe und besonders für die Ermöglichung, im industrienahen Umfeld zu arbeiten. Prof. Dr. Andreas Vilcinskas möchte ich zusätzlich für die Bereitschaft danken, das Zweitgutachten zu übernehmen und dass er uns Doktoranden fortwährend den Rücken gestärkt hat. Ein riesiges Dankeschön gilt Dr. Luigi Toti, der unseren Laboralltag um ein Vielfaches erleichtert hat und uns stets für fachliche Diskussionen bereitstand. Zusätzlich möchte ich mich bei Dr. Armin Bauer, Dr. Alberto Plaza und Dr. Sören Schuler für die fachlichen Diskussionen in Bezug auf meine Projekte bedanken.

Ein ganz besonderer Dank gilt Marius, da er unentwegt die angefertigten Arbeiten und Korrekturen der Manuskripte unterstützt hat und natürlich auch, weil ich mit deiner Hilfe so viele Herausforderungen meistern konnte!

Bene, Micha, Stephan, Celine, Daniel und Bork möchte ich für die vielen unvergesslichen Erlebnisse aus dem Kabinett der Kuriositäten und die vielen Motivationsschübe danken! Ganz herzlicher Dank gilt Kornelia und Micha für die Korrekturen und Formatierungstipps zu dieser Arbeit! Danke an Egbert für das Beantworten von tiefgründigen Fragen zu Physik und Stochastik und an Günter ohne „h“, den Excelkünstler.

Herzlichen Dank an Rolf, Tanja, Steffi, Micha, Jochen, Mai und Gerrit, für die interessanten fachlichen und privaten Gespräche und kulinarischen Ausflüge der besonderen Art beim „Käffchen“ (Stichwort: Thunfischquark), die Unterstützung im Labor und die Freizeitaktivitäten fernab davon.

Prof. Dr. Dino McMahon und Prof. Dr. Rudy Plarre möchte ich dafür danken, dass sie unser „Termitenprojekt“ an der Bundesanstalt für Materialforschung und –prüfung (BAM) unterstützt haben, sowie für die Hilfe beim Sammeln der Proben und den Zugewinn der Arbeiten durch rege fachliche Diskussionen.

Ich möchte mich bei allen Mitarbeitenden, die ich während meiner Zeit kennen lernen durfte, herzlich bedanken, da ich fortwährend eine positive Arbeitsatmosphäre und Hilfsbereitschaft erfahren durfte! Besonders möchte ich dem „Team Termiten“ bestehend aus Jenny, Kirsten, Christine, Mareike und Hamid danken, die mich im Labor immer tatkräftig unterstützt haben.

Danke an alle für die vielen lebenserhaltenden Kuchen und Törtchen!

Vielen Dank an meine Familie und Freunde, die mich in jeder Lage unterstützt und bestärkt haben!

Der größte Dank aber gilt Julia! Danke, dass du mir so oft und so lange den Rücken freigehalten hast und immer für mich da warst! Ohne dich hätte ich es nicht geschafft diesen Berg zu bezwingen!

11. LISTE AUSGEWÄHLTER WISSENSCHAFTLICHER BEITRÄGE

Primärliteratur, die Teil der vorliegenden Arbeit ist:

- Oberpaul M**, Spohn M, Brinkmann S, Mihajlovic S, Marner M, Patras MA, Toti L, Kurz M, Vilcinskas A, Glaeser J*, Schäberle TF*.
- 8 Trichoderma-derived pentapeptides isolated from the nest mycobiome of the subterranean termite *Coptotermes testaceus*
ChemBioChem (2022) Mar 17; e202100698. doi: 10.1002/cbic.202100698
-
- Brinkmann S, **Oberpaul M**, Glaeser J*, Schäberle TF*.
- 7 Two-step generation of monodisperse agarose-solidified double emulsions (w/w/o) excluding an inner oil barrier
Methods X (2021) 8: 101565 doi: 10.1016/j.mex.2021.101565
-
- Bill MK#, Brinkmann S#, **Oberpaul M**, Patras MA, Leis B, Marner M, Maitre MP, Hammann PE, Vilcinskas A, Schuler SMM*, Schäberle TF*.
- 6 Novel Glycerophospholipid, Lipo- and N-acyl Amino Acids from Bacteroidetes: Isolation, Structure Elucidation and Bioactivity.
Molecules (2021) Aug 27;26(17):5195. doi: 10.3390/molecules26175195
-
- Oberpaul M**#, Brinkmann S#, Marner M, Mihajlovic S, Leis B, Patras MA, Hartwig C, Vilcinskas A, Hammann PE, Schäberle TF*, Spohn M*, Glaeser J*.
- 5 Combination of high-throughput microfluidics and FACS technologies to leverage the numbers game in NP discovery.
Microb. Biotechnol. (2021) Jun 24. doi: 10.1111/1751-7915.13872
-
- Edelmann D, Leinberger FH, Schmid NE, **Oberpaul M**, Schäberle TF, Berghoff BA*.
- 4 Elevated Expression of Toxin TisB Protects Persister Cells against Ciprofloxacin but Enhances Susceptibility to Mitomycin C.
Microorganisms (2021) Apr 27;9(5):943. doi: 10.3390/microorganisms9050943
-
- Edelmann D, **Oberpaul M**, Schäberle TF, Berghoff BA*.
- 3 Post-transcriptional deregulation of the *tisB/istR-1* toxin-antitoxin system promotes SOS-independent persister formation in *Escherichia coli* Environmental Microbiology
Environ. Microbiol. Rep. (2021) Apr;13(2):159-168. doi: 10.1111/1758-2229.12919
-
- Oberpaul M**, Zumkeller CM, Culver T, Spohn M, Mihajlovic S, Leis B, Glaeser SP, Plarre R, McMahon DP, Hammann PE, Schäberle TF*, Glaeser J*, Vilcinskas A*.
- 2 High-Throughput Cultivation for the Selective Isolation of Acidobacteria From Termite Nests
Front. Microbiol. (2020) 11:597628. doi: 10.3389/fmicb.2020.597628

Primärliteratur, die nicht Teil der vorliegenden Arbeit ist:

-
- Eichmann J, **Oberpaul M**, Weidner T, Gerlach D, Czermak P*.
- 1 Selection of High Producers From Combinatorial Libraries for the Production of Recombinant Proteins in *Escherichia coli* and *Vibrio natriegens*.
Front. Bioeng. Biotechnol. (2019) 7:254. doi: 10.3389/fbioe.2019.00254

diese Autoren haben gleichberechtigt an der Publikation mitgewirkt

* korrespondierende Autoren

Tagungsbeiträge:

- Oberpaul M**, Spohn M, Brinkmann S, Leis B, Mihajlovic S, Patras M, McMahon DP, Hammann P, Schäberle TF, Vilcinskis A, Glaeser J.
7 High-throughput cultivation and screening platform for natural product discovery from environmental bioresources
International VAAM Workshop (2019). Biology of Microorganisms Producing Natural Products, Jena, Germany.
-
- Oberpaul M**, Spohn M, Brinkmann S, Patras M, Fracowiak J, Plarre R, McMahon DP, Hammann P, Vilcinskis A, Glaeser J.
6 Combined microfluidics/FACS platform for antibiotic drug discovery of insect-associated microorganisms.
INSECTA (2018). 2nd Symposium for Insect Biotechnology & Bioresources, Gießen, Germany.
-
- Glaeser J, Spohn M, **Oberpaul M**; Marner M, Leis B, Vilcinskis A, Hammann P.
5 Plugging in Microfluidics/FACS technologies in industrial discovery processes to exploit invertebrate microbiomes for new Gram negative antibiotics.
ECNP (2018). 3rd European Conference on Natural Products, Frankfurt am Main, Germany.
-
- Oberpaul M**, Brinkmann S, Marner M, Spohn M, Leis B, Hammann P, Vilcinskis A, Glaeser J.
4 A high throughput platform using a combined Microfluidics / FACS setup for antibiotic drug discovery of termite nest-associated microorganisms
ECNP (2018). 3rd European Conference on Natural Products, Frankfurt am Main, Germany.
-
- Oberpaul M**, Spohn M, Fracowiak J, Plarre R, McMahon DP, Hammann P, Vilcinskis A, Glaeser J.
3 Exploiting termite nest microbiomes for antibiotic discovery by using an ultra-high throughput Microfluidics/FACS driven pipeline combined with a microtiter plate based cultivation strategy
VAAM Annual Conference (2018). Wolfsburg, Germany.
-
- Oberpaul M**, Nguyen M, Fracowiak J, Zubeil F, Plarre R, Hammann P, Vilcinskis A, Glaeser J.
2 Exploiting termite nest microbiomes for antibiotic drug discovery using an integrated high throughput Microfluidics/FACS Pipeline
32nd International Workshop of VAAM Section of "Biology of Bacteria Producing Natural Products" (2017). Tübingen, Germany.
-
- Glaeser J, **Oberpaul M**; Nguyen M, Stadler T, Fracowiak J, Plarre R, Hammann P, Vilcinskis A.
1 Exploiting termite nest microbiomes for antibiotic discovery by using an ultra-high throughput Microfluidics/FACS driven pipeline
5th Joint conference of the DGHM & VAAM (2017). VAAM Annual Conference, Würzburg, Germany.
-

12. CURRICULUM VITAE

(only in printed version)